NOTTINGHAM
TRENT UNIVERSITY

Condition Monitoring of Water Leakage Detection in Buried Pipes Using Sensor Fusion Systems

Bubaker H. Shakmak

A thesis submitted in partial fulfilment of the requirements of Nottingham Trent University of the degree of Doctor of Philosophy

May 2016

DECLARATION

The thesis is submitted to Nottingham Trent University (NTU) for the degree of PhD.

I declare that the work in this thesis was carried out in accordance with the regulations of NTU, its original except where indicated by specific reference in text. I further declare that no part of the thesis has been submitted in support of another degree or qualification of this or any other education institution in the United Kingdom or overseas. Any views expressed in the thesis are those of the author and in no way represent those of the University.

Signed:.. (Candidate), Date: ....

Acknowledgements

Praise be to Allah

Abstract:

Water is significantly lost within water networks in most countries with an estimates of 30% would be lost due to leaks in water pipelines. Water leaks are one of the major factors facing the world, from waste water for no appropriate reason other than a lack of sustainable management programmes. This research work will investigates several sensor techniques and image/signal processing methods to detect water leaks within buried pipeline system. A sensor fusion method for the detection of water leakage in pipes, which consists of two or more sensory systems, is proposed in this research work. The suggested sensor fusion system will investigate a combination of transient signals of several direct types, such as flow and pressure, and non-direct types such as acoustic signals and infrared images. The sensors will identify signals inside the pipeline system and will detect any acoustic or transient signals. This might happen as a result of a leakage while the thermal imager will look outside the pipeline system for any leakage signs. This is by way of detecting the contrast in temperature and humidity of the soil surrounding the leakage point. The data has been collected using software that can read and store the required signal data with the infrared image data as required. The collected data is subjected to processing using the Matlab software and based on the results a computer algorithm which has been developed to be used in detection, locating and identifying the leaks using artificial intelligence techniques. The methodology of this research work includes constructing a test rig of a pipeline equipped with necessary instrumentations for data acquiring purposes. As such, data acquisition device, pressure sensors, acoustic sensors, temperature sensors, infrared camera, normal visual camera and any other necessary equipment for water flow control. A series of experiments have been conducted with the test rig in the laboratory and a field experimental work has been conducted in Libya with the results having been highlighted within this report.

The expected contribution to knowledge would include significant technical and theoretical aspects of the experimental work and analysis. The contribution includes the comparison between the high and low-resolution infrared cameras. Additionally, an application of a novel approach to using a combination of infrared technology and visual images with a sensory fusion system of acoustic emission and transient signal to detect water leaks in pipeline systems. The work requires building a test rig to develop the

experimental work as well as carrying out field works. The contribution to knowledge also includes the developing of an artificial intelligence algorithm for detecting water leakage in pipelines, which would determine the best times of detection when estimating and quantifying the leakage amount.

Publications

Shakmak, B. and Al-Habaibeh, A., 2015, November. Detection of water leakage in buried pipes using infrared technology; a comparative study of using high and low-resolution infrared cameras for evaluating distant remote detection. In *Applied Electrical Engineering and Computing Technologies (AEECT), 2015 IEEE Jordan Conference on* (pp. 1-7). IEEE.

Fanshawe, S., Al-Habaibeh, A. and Shakmak, B., 2015, November. An innovative design and evaluation of a stratified hot water storage system-the Water Snake. In Applied Electrical Engineering and Computing Technologies (AEECT), 2015 IEEE Jordan Conference on (pp. 1-6). IEEE.

Abbreviations

AE: Acoustic Emission

ANN: Artificial Neural Network.

AO: Orthogonal Arrays.

ASM: Associated Matrix.

ASPS: Automated Sensor and Signal Processing Selection Approach.

CMS: Condition Monitoring System.

CMS: Condition Monitoring System.

CPM: Computational Pipeline Monitoring.

DWT: Discrete Wavelet transform.

EMD: Empirical Mode decomposition.

FRD: Frequency Response Diagram.

GMRP: Great Man-made River Project.

GPR: Ground Penetrating Radar.

GUI: Graphical User Interface.

IR: Infrared Red.

ITA: Inverse-Transient Analysis.

ITA: Inverse-Transient Analysis.

LVQ: Learning Vector Quantisation.

MAD: Mean Absolute Deviation

MCMD: Million cubic meters per day.

NDT: Non-Destructive Testing.

NTU: Nottingham Trent University.

PCCP: Pre-stressed Concrete Cylinder Pipe.

ROI: Region Of Interest.

RASM: Resultant Associated Matrix.

SCADA: Supervisory Control and Data Acquisition.

SCFs: Sensory Characteristic Features

SM: Stability Matrix

STD: Standard Deviation

TDR: Time Domain Reflectometry.

VDM: Virtual Distortion Method.

WDS: Water Distribution System.

WT: Wavelet transform.

Contents

List of Figures:

List of Tables

Chapter 1. Introduction:

1.1. Water leakage

Water resources are a concern all over the world and a high standard of water management is highly required everywhere to save vital consumption of those resources. Leaks are one of the major problems that the world suffers from as it waste water for no apparent reason other than a lack of sustainable management [1].

Leak or leakage can be defined as an untimed and unexpected escape of a fluid from its original or designated transfer or holding system at any location on that system. Economically, leaks are a considerable cost in addition to wasting water resources; it consumes significant power usage to treat water or to transfer it from one point to another.

Some global studies showed that the losses are ranging from 10% to 40% around the world [2] and in some urban areas reach up to 50% [3, 4]. Canada loses on average 13% of water, which is withdrawn by water suppliers before it reaches the final consumers [5]. In Saudi Arabia, the average water loss due to leakage reaches 30% and varied from 1% to 80% [6]. The water losses in Poland are estimated to exceed 18.6% and the actual percentage could be over 20% [7]. The leakage from the water distribution systems in most cities of India is 45-50% [8].

In addition to water losses, water leakage can create environmental problems, especially when it causes water contamination and subsequently creates further distillation and damage to nearby areas at the leaking point [9]. Leaks are the main reason for water pipeline failures. The 'US Department of Transportation Pipeline and Hazardous Materials Safety Administration' (PHMSA) have reported that leaks are responsible for 25% of pipeline failures [10]. In the past, water leakages are ignored when the cost of the energy was quite significantly low, however, since the 1980s the considerations for water leakage have changed for both economic and environmental reasons [6].

Water pipeline failures and its subsequent effects are a complex process. The mechanism that causes these failures are complex and cannot be explained in leman terms simply [11]. Water distribution systems are vulnerable to accidents and could cause hazards to human life and contribute to the wider health and safety and environmental impact that can cause health related issues [12]. Ingress of containment to pipeline system occurs due

to transient pressure caused by a leak [9]. Human life and properties would be at risk due to leaks [13].

Leaks in water pipelines are unavoidable and can unexpectedly happen at any time for various reasons such as old/rusty pipeline systems, pipe material defects, incorrect installation works, construction works nearby the pipeline and internal or external deterioration of the pipe walls [14].
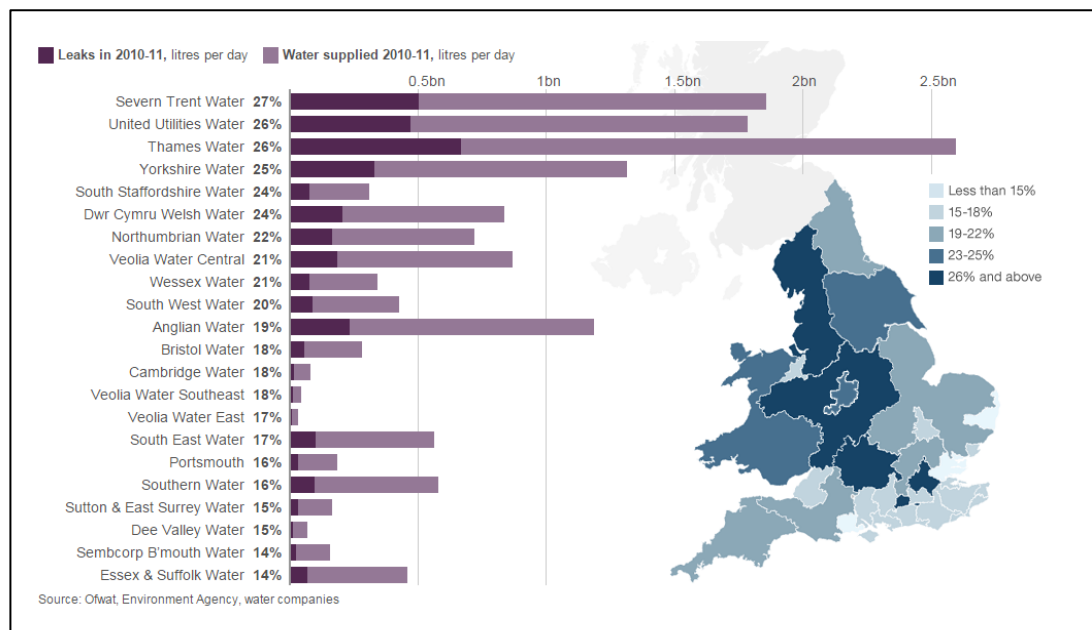
Figure 1.1: Major water companies in England and Wales ranked by the percentage of their supply that is lost in leaks [Source: Ofwat, Environment Agency, water companies].

A recent study issued by BBC on 5th April 2012 from OFWAT, Environment Agency, showed that the water industry in England and Wales is losing about 3.6 billion cubic litres per day which are enough to supply 22 million people per day.

The report says that this amount of lost water 35% is lower than mid of 1990s which means that the problem of water leakage is still a serious problem despite all provisions taken by the water companies to improve their pipeline systems. Figure 1.1 shows the percentage of lost water by each company in England and Wales which ranges between 14% to 27% inclusively [15]. This huge amount of lost water in a developed country indicates how much the investigation in water leakage detection techniques is still needed.

1.2. Water leakage detection

Leaks have been classified to background losses and bursts (reported or unreported) [16]. Bursts are evident and can be immediately detected since they cause major interruption in the system. Background losses are the leaks from joints, fittings, small cracks, and holes. They are running slowly and for a long time before it is actual been detected because they do not lead to a quick and evident change in parameters such as pressure drop [16].

Detecting leaks as soon as they appear will save significant cost saving by consuming the water without significant losses, power consumption and the environment. Therefore, finding an efficient and low-cost leak detection system will surely reduce these losses. Furthermore, the early leak detection is essential for many reasons [17]. Early detecting of leaks in any water systems is a beneficial for both water suppliers and their customers. By enhancements in operational efficiency, lowering operational costs, reducing potential for contamination, extending the life of the facilities, reducing potential property damage, water system liability, and reducing water outage events [18]. Therefore, rather than spending more money on increasing water production which causes rapid consumption for water resources we should give all attention to water transportation pipelines and prevent leaks by maintaining water loss to the minimum.

The change in flow characteristic can be used to detect leakages as the performance of the system will be different from the typical operation characteristics [17, 19]. Detection methods can be applied internally inside the pipeline system and externally outside the pipeline system [20, 21].

The internal methods will look for any signals might be generated by the leak from inside the pipeline. In more details, the internal methods look for the change in flow parameters such as pressure, flow rate, velocity and temperature. For example, sensors could be placed inside the pipe such as hydrophones to listen to any signals inside the water or pressure transducers to detected pressure changes in the liquid. The main category of internal leak detection method is called computational pipeline monitoring (CPM) [20, 21].

The external methods will look for any signals or signs of the leak outside the pipeline. For example, the AE sensors such as accelerometers would be placed outside the pipeline to sense any vibrations emission [20, 22].

At the moment, the existing commercial techniques of the leak detection systems are varying from simple physical testing technique to advanced techniques such as acoustic emission. However, most of these methods are suffering from several limitations in the operation range as they will only detect leaks on certain ranges varies from one technique to another. These limitations in the range will require either numerous repeated tests to be done or installation of many sensors spaced at certain distances to cover the whole pipeline [2]. In other words, a lot of the available leak detection techniques appear capable of detecting leaks in a certain situation and not capable in some other situations and scenarios [23]. They may create false leak detection or detection with low fidelity. The easiest way to detect leaks is by monitoring the mass and the volume. They can detect the leaks and report their volume, however, they cannot determine the leak location [24]. There are limitations in availability of systematic leak detection techniques [25]. In addition to that, many techniques are still being performed manually to check the whole pipeline which means that: a) it will need significant manpower and material resources, b) it will not be able to monitor the general working conditions of the system, c) it will not detect any sudden leaks on time and consequently it will not be able to avoid any disastrous or damages that may happen [26]. It is said that a single method could detect leaks alone while in other cases would require a combination of methods to detect leaks [27]. Lots of the available detection methods are dedicated to some specified operating condition and leak characteristic [24]. In other words, none of the existing methods can detect leaks accurately alone as each of them have different detection accuracy [28]. Therefore, a sensory fusion system will be required to minimise such false alarms, the need of manual numerous repeated tests, and/or the use of large array or series of sensors.

In recent years, researchers around the world gave more attention to water leakage detection due to a shortage in water supply, increasing population and water distribution systems deterioration [29, 30]. The research on this subject is an attempt to address current problems in this area. It will investigate a combination of new approaches, techniques and methods using sensor fusion system using direct (e.g. flow, temperature, pressure, water level) and indirect sensory systems (e.g. acoustic emission). Direct

measurement methods of water level and flow rate will be used in verification and comparison of the results obtained to quantify water leakage. The approach will also use real data and compare it with a mathematically estimated flow data.

To avoid any false alarms that might occur using the previously mentioned sensory systems and to confirm the existence of any leakage, additional visual and thermal images will be introduced in this research work by utilising sensory fusion approach combined with artificial intelligence. During the literature review work on thermal imaging, it has been found that majority the current researches for leak detection are mainly focus on leak detection in gas and oil industry. It is also found that, most of the researches give more attention to the pipeline system rather than other components such as storage vessels [31].

The project will focus on small-scale lab environment to investigate a wide range of techniques including the selection of sensors, signal processing methods and artificial intelligence methods that could help in providing water leakage with potential scalability. Scalability is one of the objectives that will be investigated to identify which technique is dimension-independent and could be used on a pipe with different dimensions. Moreover, this study will investigate the use of the Automated Sensor and Signal Processing Selection (ASPS) approach which has been developed by Al-Habaibeh and Gindy, 2000, 2001 [32, 33] and Al-Habaibeh et al, 2002 [34] ,   and tested at NTU on turning and milling operations [35]. The approach is also adapted for Gearbox condition monitoring system [36]. The approach will be investigated and modified to be used in a monitoring system for water leak detection properly.   In addition, several artificial intelligent techniques will be tested including neural networks, fuzzy logic and novelty detection.

This proposal will highlight the domain and the context of the problem, previous researches in this area, the suggested methodology and expected contribution to knowledge.

1.3. Contribution to Knowledge

Water leakage of a significant nature will no doubt become a catastrophic event for areas of the world where this is a scares resource. Real time water leakage detection systems are required to save one of the most precious resources on earth (the water) which also

has a net effect upon the transportation. There would also be a significant impact upon the power necessary to pump the water and the environmental conurbation effect of a major leak. Failures to detect water leakage in real time, especially in large-scale projects, can lead to a catastrophic damage within a pipeline system. This may further imped on the nearby conurbation and such may create risk for the local inhabitants in a significant way. Therefore, the needs for automated detection system is vital. Current systems for water leakage detection suffer from limitations such as being time consuming and in part expensive. Moreover, most of them are using a singular technique, dedicated and designed to work for specific type of pipeline only (e.g. metal), which would cover a short distances of the pipeline, and are affected by external noises, such as traffic [37]. Even though, no singular technique can universally be applicable for all conditions, due to change in the pipeline system specification or parameters [38]. The use of an automated system as a condition monitoring of water leakage detection based on fusion system, contributes to reducing the limitations mentioned earlier which maintains high productivity of the water management systems. The successful and effective monitoring system for water leakage detection is the system that can detect leakages as early as possible before it cause subsequent complications. Those limitations in the existing water leakage detection techniques are summarised in the following points.

1. Detection range is limited and varies from one technique to another.

2. Requires threshold value to detect the leak.

3. Numerous repeated tests.

4. The number of sensors in some cases is high.

5. The detection ability changes with the change of the pipeline condition.

6. Applicable in one system and might not be applicable in another.

7. Most detection systems are able to detect leaks but cannot localise them or in some cases can localise the leak but with errors.

8. Most of the techniques are applied manually and need manpower.

9. Specialised techniques are high in cost.

10. Detection systems requires an assessment of the previous states of the pipeline system precisely, which is not possible in some cases.

1.3.1. Problems in developing condition monitoring systems for water leak detection

Designing a condition monitoring systems for water leakage detection system is suffering from some common problems such as selecting the appropriate sensor or group of sensors and selecting the best features that precisely describe the condition of the monitored system. Furthermore, selecting the right signal processing technique is an important issue as well. In some cases, the sensor acquires the signal as requested but if the used processing technique is not suitable, the monitoring system will fail. The successful condition monitoring system is based on the number and the type of the sensors (the hardware) which, affects the cost and the quality, and the acquired signals which have an impact on the efficiency and the speed of the system [32]. The following are the common limitations in developing proper condition monitoring systems for water leakage:

1. Selection of the appropriate sensor or a combination of a group of sensors.

    Deciding which is most appropriate either the signal or the image or them together as a sign of change in condition.

2. Extracting the best feature from the signal and/or the image using the appropriate signal or image processing techniques.

3. Designing an intelligent sensor fusion system using a combination of the images (thermal or visual) and signal.

4. Integrating the selected sensors and/or cameras to produce a successful system.

5. Finding the appropriate signal/image processing.

6. Extracting the required characteristic feature for any selected signal or image.

7. Estimating the fit time for detecting the leakage or the state of the monitored system.

8. Finding the leakage location using the proposed system.

9. Identifying the leak characteristic using the proposed system.

10. Designing a high-quality fusion system uses artificial intelligent techniques with low cost.

11. Using a fixed and continuous monitoring system for periodical inspection.

1.4. Aims and Objectives:

1.4.1.   The aim:

The project aims to overcome the current problems in water leakage detection systems by developing a more efficient and low-cost leak detection system. The suggested novel detection system is a sensor fusion system based on signal/image processing with artificial intelligence system.

1.4.2.   Objectives:

To achieve the aim, the Automated Sensor and Signal Processing Selection (ASPS) approach is applied and adapted for water leakage detection using signal/image processing method. The main objective of the research is presented as follows:

1. Selecting sensors for acquiring signal/image.

2. Investigating and selecting signal and image processing methods proper for designing the system.

3. Developing in-house software for signal and image acquisition.

4. Use in situ water leakage detection system.

5. Designing and erecting a test rig that simulates a real water system for experimental work.

6. Carrying out a fieldwork in order to examine the proposed system in a real environment.

7. Investigating the suitability of the selected sensors and signal processing techniques for dry environment.

8. Comparing the high-resolution and low-resolution thermal cameras to confirm the suitability of the low-resolution in detecting leakage.

9. Exploring best water leakage detection time using infrared based systems.

10. Investigating and developing image processing techniques for infrared thermal images.

11. Investigating the artificial intelligence techniques to be used.

12. Optimisation of the required combination of techniques and their scalabilities for the detection of water leakage.

1.5. Summary

The chapter started with introducing the problem of water leakage around the world. The leakage has been defined and percentage of water being lost around the world is presented. The percentages of water lost around the world is also highlighted. The rate of water loss becomes much more significant based on the volume of leakages reported. The international governments and water companies around the world are looking for higher management systems to detect and save water. The problems with current water leakage detection systems have been defined. The aim of the study is presented and the objectives have been listed and described.

Chapter 2. Literature Review

2.1. Condition monitoring systems:

Currently, intelligent condition monitoring systems are extremely requirement in all fields as they increase the productivity and improves the quality of the products. The term condition monitoring means the system that collects, analyse, and process a real-time data to extract useful information to automatically make the monitored system be aware of its stability awareness and process condition [33]. Monitoring and assessment of Water pipeline deterioration and its negative consequents are a complex process that requires the collection of data and information to determine the current status of the pipe condition or estimate the future condition. Pipeline condition monitoring and assessment or leak detection methods can be categorised to direct and indirect methods. In accordance to Liu & Kleiner (2013), the direct method is the direct pipeline inspection using visual, manual, automated and non-destructive testing while the indirect is the method related to flow audit [11]. Leak detection methods ranges from simple inspection such as visual inspection to complex methods in which advanced hardware and software are used [38]. In general, condition monitoring systems provide a systematic and fast method of monitoring. The condition monitoring system is based on sensors, acquired data (signal/images), processing method of the data and data classification stage [33].

2.1.1.   Leak detection methods as a monitoring system:

Leak detection methods varied and can be classified into multiple methods. The leak detection methods are classified based on the leak detection process to biological methods, hardware based methods and software based methods [39]. It can be also classified into external methods or internal methods. The external methods deal with evidence of the leak outside the pipeline. Whereas, the internal methods uses sensors to monitor flow parameters such pressure, flow rate, temperature, density [39]. In some literature, the leak detection methods have been categorised to hardware based methods and software based methods [40]. The leak detection system of the hardware based methods studied by the later reference is the Acoustic Devices, Cable Sensors, Fibre Optic Sensors, Soil Monitoring, Ultrasonic Flow Meters, and Vapour Monitoring System. While the software based methods are the Mass and Volume Balance, Real Time Transient Modelling, and the Pressure Point Analysis [14].

As revealed in the literature research work, there is a lack in designing a fusion system with a combination of signal and image (especially the thermal image) together with artificial intelligence. Apparently, a lot of the available research works use a single sensor or a single technique of signal or image processing. Therefore, the development of an artificial intelligent system and cost effective based on a fusion system is highly required. The system that uses the right data acquiring devices (sensor/cameras) for gathering an appropriate sensory data (signal and/or image) and extracting the sensitive features with the consideration of the cost. In this research, the proposed system considers this area and suggests the use of the ASPS approach as a novel method for designing fusion system for water leak detection.

The following sections present a review of some of the techniques used in monitoring pipe condition and leak detection that would be studied in this project work.

2.2. Thermal Imaging:

Thermal Imaging is an emerging high technology that can be utilised in a variety of fields including water leakage detection. As the temperature indicates the health of the mechanical systems where the faulty systems produce higher temperature, the thermal imaging based on emitted infrared has become an accepted and effective condition monitoring tool [41]. The infrared emitted from bodies are not visible to normal eyes however it becomes visible when converted to thermal image using thermal imaging devices such as thermal cameras [42]. The thermal imaging is a non-destructive testing technique (NDT) for sensing infrared radiated from the surface of any object [43]. It is detecting the infrared radiated from the tested body with the non-contact way [42, 43]. The thermography is a powerful tool for visualizing the target with the thermal gradient as it measures a large number of point temperature of the target and the surrounding [44] and it became increasingly used for leak detection and localization [31]. One of the main advantages of the thermal imaging it is the simplicity of use. It can be performed with the minimum required instrumentation which is only a camera and stand [41]. Another important advantage is that it will not alter the tested surface temperature as it is a non-contact technology [45]. With the improvement in technology and the appearance of high-tech thermal cameras, the thermal imaging became more precise, reliable, cost effective and friendly technology [42, 45].

The infrared is emitted from any object when its temperature is above the absolute zero (-273 °C) [11, 42, 45, 47]. The thermal image of any object is the result of the infrared radiation of the surface of that object which has been sensed using the thermal infrared camera. The thermal image is a visible image from which tested objects can be assessed based on their heat emission [11].

The thermal imaging is being used as a condition monitoring system in a wide range of application [41]. It has been utilised as a remote sensing technique to detect the temperature distribution on a surface [47]–[49]. The thermal imaging devices have become standard equipment in identifying victim/survivors in rescue robots [50]. The thermal images which are the product of the thermal imaging devices are defined as a temperature measurement technique that detects temperature variation of the measured surface [51]. It detects the infrared emitted from the target and the background when there is a contrast between the target and the background [52]. Water leakages are indeed affect the temperature of the vicinity soil which usually become not consistent with the surroundings and detectable [47]. In other words, the leakage changes the thermal characteristics of the soil close to the leak point and makes it more effective heat sink comparative to the dry soil away from the leak [22]. The concept of using the variation in temperature (i.e. as a result of evaporation or change in humidity as a result of a leak) will be investigated in this research work.

In this research work, thermal imaging method will play an important role in maintaining the pipeline system performance without being interrupted. The captured thermal images will be subjected to processing and will be utilised to check the existence of the leak in any suspected leak point. For more clarification, the system will take a thermal image for that point and subject it to processing to either confirm the existence of the leak or not. This step would be useful in the fluid transportation industry to avoid any sudden shutdown or any extra investigation or excavation works due to any false alarm that might be raised because of abnormal signals.

2.2.1.   Principle of heat transfer from/to the pipeline system

Heat is one form of energy. The heat transfers from higher temperature to a lower temperature in three modes known as conduction, convection, and radiation [53]. Thermal

conductivity is the rate of heat transferred through the pipe material [54]. The Thermal conductivity of some common material is shown in Table 2-1 below.

Table 2-1: Thermal conductivity of some common tubing materials [54]

Piping	Material	W/mK
Steel	Carbon Steel Copper	54
Copper	Copper	401
PEX	Cross-linked High-density Polyethylene	0.51
CPVC	Chlorinated Polyvinyl Chloride	0.14
PE	Polyethylene	0.38
PVC	Polyvinyl Chloride	0.19

When solar radiation falls on any surface of a material, part of this radiation is reflected on the surface and the rest is absorbed. The energy generated by the absorbed radiation will increase the temperature of the surface of the material. The difference in temperature between the surface and the material underneath will create heat flow from hotter part to the cooler part. The heat in soil transfers from one layer to another by conduction.
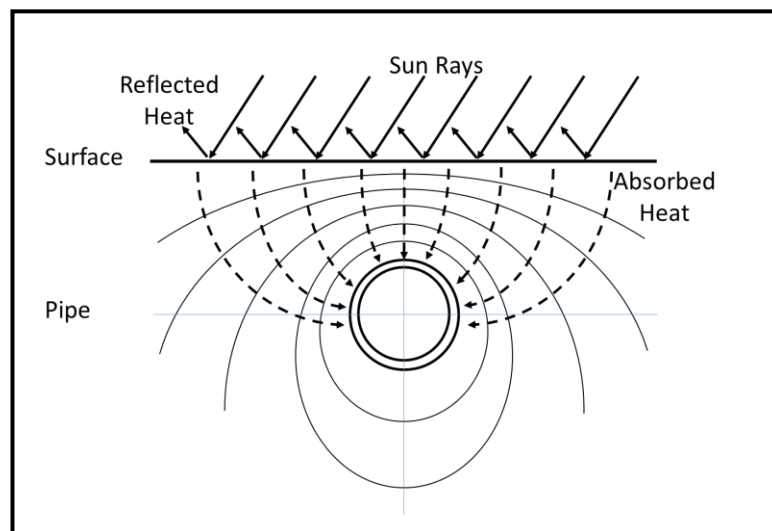
Figure 2.1: Example of heat flow from surface to pipe

Heat flow direction is moving from the hotter point to the cooler point. The rate of heat flow will depend on the conductivity of the material and the amount of temperature difference. The temperature of the surface above the buried pipeline depends on the surrounding, the soil properties, and the environment. The pipe below the surface as a

part of the surrounding to the surface plays a role in heat transfer [55]. Figure 2.1 above illustrates the direction of heat flow from surface to the pipeline. Usually, the pipeline is cooler than the surrounding areas even when there is no leak. This depends on the temperature of the fluid transported and some other factors such as the conductivity of the material of the pipe, diameter, and the thickness of the pipe wall. However, when the leak happens, the adjacent area to the pipeline becomes much cooler than the surrounding and more heat will transfer to it and then causes a remarkable change in the temperature of the surface above it. In this research work, the pipe material is plastic which known as less conductive material as indicated by Vlachopoulos & Strutt, 2002 [53].

2.2.2.   The principle of the thermal imaging in leak detection

The amount of radiation emitted by any object is based on its temperature and emissivity [44]. The amount of the emitted infrared radiation increased with temperature [56]. When there is a leak in the pipeline, the leaked water will definitely affect the temperature of the soil surrounding the leak point by spreading moisture in the vicinity nearby the leakage. Consequently, the temperature of the soil surface above the leakage point will be influenced by the change in the temperature of the soil underneath due to the moisture. Accordingly, the surface at that point will become incompatible with the surrounding surface. As a result of this variation in temperature, it is possible to detect the leakage point using the infrared thermal camera as it will capture a thermal image of the soil surface above the leak point. The temperature is measured by calibrating a relationship between the infrared and the true temperature where the surface near the leak point is considered a black-body as the wet surface absorbs the infrared radiation [39, 49]. Fahmy et al. (2010) and Inagaki & Okamoto (1997) investigated this area in a simple lab environment however, more research is still needed. In some cases the temperature variations might not be detectable using the infrared radiation as some of the thermography devices has a limitation in detecting temperature differences less than 0.2 °C [47]. The thermal imagers would visualise the leaks only if the leaked fluid and the background are not in thermal equilibrium [52]. To avoid these situations it is proposed that an extra heating or cooling might be used to generate a detectable temperature difference [11]. Both heating of the surface and/or cooling of the fluid will be investigated in this research work to increase the detectability of the leakages.

Thermal imaging can be produced using either the passive thermography or the active thermography. In the passive thermography, the temperature between the target and the background is based on the natural existing body temperature. While, in the active thermography, an external source of thermal energy has to be used to enhance the contrast between the target and the background [44].

2.2.3.   Emissivity

The emissivity is an important factor that has to be understood in order to read the correct temperature of an object using the thermal camera. Without taking the emissivity in consideration, the thermal camera will give false temperature reading. Some objects could be seen hotter or cooler than they actually are.

The right emissivity for any object have to be set up correctly because the thermal camera captures the emitted radiation from an object and the reflected radiation as well. The reflected radiation from surroundings will affect the real temperature of the object [45]. The emissivity of any object is measured compared to the blackbody. As the blackbody does not reflect infrared radiation form the surrounding bodies, its emissivity is considered to be 1.0 and other objects' emissivity is less than 1.0 and greater than or equal to 0.0 [46].

Emissivity of objects varies with the type of material and the condition of the object such as its temperature and the angle of view. The material emissivity has already been categorised and can be found in emissivity tables (See appendix I). However, the tables should be used as a guide only whereas the precise emissivity value varies from those tables due the object condition [57] . The good thing in using thermal camera is that the emissivity value can be set and adjusted even after taking the image by using image processing techniques.

As this research work is about finding the water leakage in a buried pipeline underneath a soil, the soil emissivity has been searched and found to be 0.92, 0.93 and 0.95 for dry, frozen and saturated with water soil. And for concrete, dry concrete and rough concrete found to be .92, 0.95, and 0.92-0.97 consequently.

2.3. Transient-based Leak Detection System:

In water transfer or distribution systems, the change in the physical condition creates a transient wave. One of the well-known techniques for leak detection is the transient-based leak detection system which totally depends on the change of the physical conditions of the pipeline system. The occurrence of a leak or any physical change in the pipeline system will vary the properties of the flow from the typical condition while the system is completely intact [58]. The leak itself is assumed to be a hydraulic phenomenon that creates a transient wave inside the pipeline. The transient wave signal transmits with it all necessary leak parameters such as its location and size which could be extracted by analysing and processing that wave signal [59]. The created wave travels to both terminals (inlet and outlet) of the pipeline in acoustic velocity causing changes in the pressure (negatively and positively) at the both terminals [14].

The leak causes pressure discontinuities and consequently it has been said that it would increase the damping rate of the transient signal [60]. In general as a sum of the above, the idea of using the transient wave as a leak detection technique is built on capturing the pressure signals created by the transient wave and then processing and analysing the signal to extract all necessary information. The process is carried out by a computer algorithm that gives the exact location and size of the leak by comparing the new conditions with the intact system condition taking in consideration the deviation of the intact system from its initial condition. However, this idea still suffers from many drawbacks such that it might not be able to detect small leaks [61]. Conversely, if this method is improved and enhanced the system is expected to be able to find the location of the leak and defines its size in a robust and reliable way as earliest as possible when it happens. Through capturing any deviation in pressure, the system can detect relatively smaller leaks in a short time [62]. This is can be achieved by comparing the pressure signal captured through the monitoring devices with the pressure signal that has been recorded when the system has no leak at all. Although the transient-based leak detection methodologies are expected to detect leaks with less costly instrumentation, do not cause shutdown or interruption of pipeline operation and do not require that the whole pipeline network is surveyed [23], there are still several limitations in the reliability and the confidence in the system for real industrial applications. Moreover, some researchers

believe that this method requires a huge amount of data and hence high computation costs which make it not adoptable [3].

2.3.1.   Basic concept of the Transient-based Leak Detection System

In order to highlight the basic concept of transient-based leak detection system, the following two examples show how the leak affects the transient signal. The first example Figure 2.2 is for a reservoir-pipe-valve system where the signal measured at the valve boundary when the valve is closed from initial open state to generate transient signals in both intact and leak conditions [2].
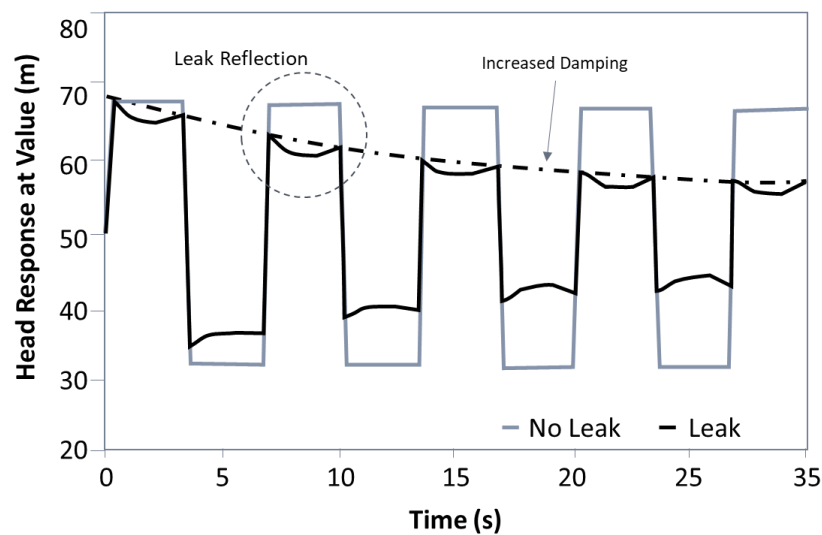
Figure 2.2: Comparison of transients in intact and leaking pipelines [2].

Figure 2.2 above compares the transient signal in both conditions of the leak and no leak. As clearly can be seen in the figure, the reflected signal is damping when there is a leak. This damping or the changing difference between the two conditions can be exploited to achieve leak detection. Wang et al, (2002) concluded that this process is capable of detecting leaks of 0.1% of the pipeline's cross-sectional area or even smaller [63]. However, no confirmation has been found about this from another researchers.

The second example, Figure 2.3 is a pipe system of 2000 meters long for which the transient signal generated by a sudden closure of side discharge valve located at a known distance from the upstream boundary. The measurement has been taken when the system was intact and when a leak was located at a known distance as well. Figure 2.3 also shows

the results of this example where the leaks have affected the signal and caused additional reflections in the transient trace.
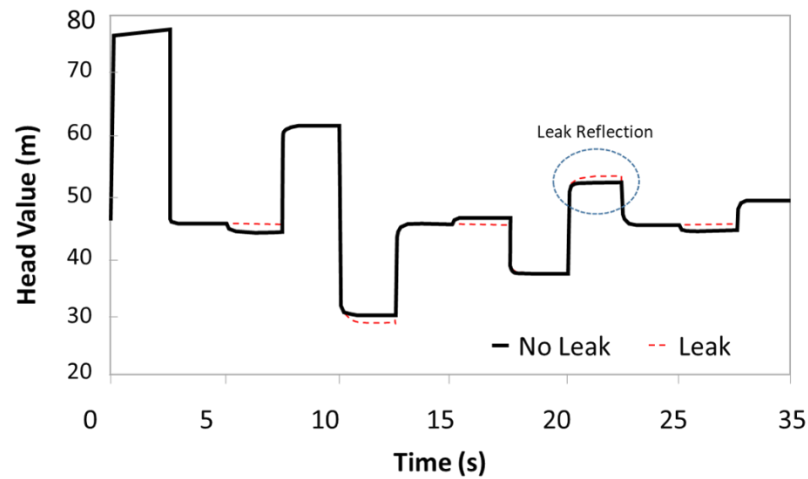
Figure 2.3: Numerical comparison of transient traces from leaking and intact pipes. (this chart has been extracted from [2])

In accordance with the two examples mentioned above, the leak has affected the transient signal by increasing its damping rate and creating reflected signal in the summation of the pressure residue. Identification and quantification of these effects are the basis of all transient leak detection techniques.

Figure 2.4 simply illustrates how the negative pressure wave generated by the leak can be utilised to determine its location. When a leak occurs, a negative pressure wave is generated and travels to both ends of the pipeline system (downstream and upstream) [39]. The signal of the negative pressure wave is captured by two sensors bracketing the leak location. The arrival time of the signal to each sensor can be calculated as follows [26]:
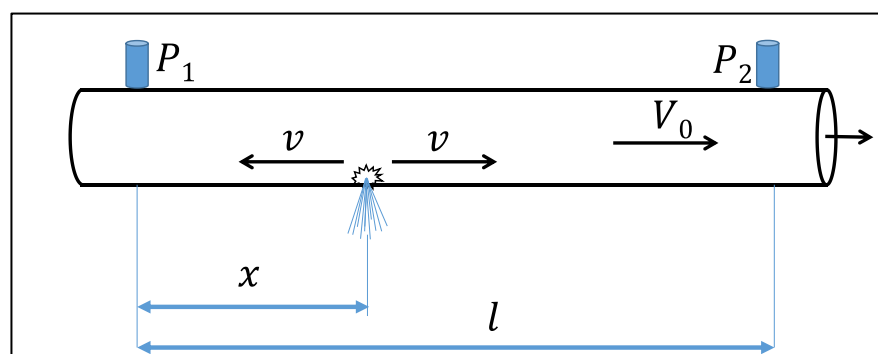
Figure 2.4: Locating leaks using transient wave

P_1 and P_2 are the pressure sensors.

x= distance between leak and downstream pressure sensor (leak location).

l= distance between the two sensors.

V_0= speed of water.

v= speed of negative pressure wave.

t_1: travel time of the signal to the downstream side

$$t1 = \frac{x}{v - V_0}$$ **(2-1)**

t_2: travel time of the signal to the upstream side

$$t1 = \frac{l - x}{v + V_0}$$ **(2-2)**

$$\Delta t = t_1 - t_2$$ **(2-3)**

$$\Delta t = \frac{x}{v - V_0} - \frac{l - x}{v + V0}$$ (2-4)

v is very high and V_0 is negligible.

The leak location (x) can be calculated by:

$$x = \frac{l + v * \Delta t}{2}$$ (2-5)

The speed of negative pressure wave (v), m/s, in water can be calculated based on known factors such as the density of water(ρ), Kg/m^3, the elastic modulus of water (K), Pa, the diameter of pipeline (D), m, the thickness of pipeline (e), m, the elastic modulus of the pipe material E, Pa, and the correction coefficient about constraints of pipeline C

$$v = (\frac{(\frac{K}{\rho})}{1 + (K/E)(D/e)C})^{1/2} \qquad (2\text{-}6)$$

In accordance to Colombo et al. (2009), to date, the thoughts related to the utilisation of these effects are divided into three schools of thought. The first school compares the inverse calibration of a numerical system model with the observed transient data. The process is known as the inverse-transient method which utilizes the transient signal in the time domain. Alternatively, the second school of thought presumes, that the frequency response of the system is changing with the existence of the leak, and thus it becomes possible to detect the changes in the system response. The third school of thoughts is by separating the effects in the pressure trace that occurred due to leaks. The process seeks to directly expose singularities in the signal induced by the leak. A number of varied techniques fall under this latter category and, for the purpose of nomenclature; these techniques are explained in the following subsections.

2.3.2.   Inverse-Transient Analysis (ITA)

This technique is dependable on the known parameters of the system such as pressure, the demands, and flow. These parameters are recorded during the transient event and then compared with the ones recorded earlier when the system is free of a leak. The results then are subjected to numerical analysis until the pressure traces are satisfactory matched to each other in both states and then any singularities such as a leak can be identified and quantified. This method has successfully detected and located single and multiple leaks but it requires that all boundary conditions and system properties have to be well defined [64]. However, it has been reported that the method might not be able to accurately detect smaller leaks and its successful is highly depend on the sensitivity of the analysis and the time in which it has been carried on [61].

2.3.3.   Frequency domain techniques

This technique utilises a periodically actuated device for transient generation and analysis the system's response as a whole rather than monitoring the transient response from a variety of locations along the pipeline system. In accordance with Lee et al. (2005), the technique of the frequency response diagram (FRD) needs neither the comparison

between intact and leak situation nor the extent of system friction [60]. However, it has been reported that the frequency response method is designed for a single pipeline only which make it impractical [65].

2.3.4.   Direct transient analysis

The previous techniques require the attention to all details of the system parameters, alternative approaches that do not require such attention have been searched and implemented. In this respect, there are few approaches exploiting this idea.

1.   Time-domain reflectometry (TDR)

When initial wave arrives at the leak, part of its energy will divert to form a new reflected signal. Calculating the arrival time of this reflected signal, the location of the leak can be determined [2]

2.   Advanced reflection techniques

This approach exploits the interpretation of pressure signals by applying an extension of the cross-correlations analysis. The approach calls for plotting a second derivative of the cross-correlations in order to uncover the signals impeded in a more complex pattern of the transient wave. The differentiated cross-correlations graph has revealed a clear peak corresponding to the leak and used to determine its actual location [2, 61].

3.   Transient damping methods

As the leakage can be discovered by exploiting the pressure attenuation property, its size and location can be analytically determined by Fourier analysis. The relationship between the damping rate of various signal frequencies is found using Fourier analysis. The transient signals contain a different damping rate of each frequency for a leaking pipeline when compared to intact pipeline [63].

2.4. Acoustic Emission (AE):

The AE is one of the most commonly used techniques in finding the hidden leaks [66]. The AE is non-destructive testing method that detects noise released from active source such as leaks [67]. It is an excellent tool for detecting and locating leaks especially in buried pipes [68]. The AE can be used to detect the noise created by the escape of fluid

from the pipeline [50]. It does not require shutdown of the system and can be used in pinpointing the leaks [40]. The leak is considered a physical change which generates a high-velocity jet when water escapes through the pipe wall from a hole or fracture and consequently creates a sound signal. The generated noise is liable to water pressure, pipe characteristics and leak size and shape [69]. The leaks generate a continuous AE signal which transfers and propagates through the fluid or the pipeline itself and the surrounding [59, 69]. The method is based on capturing these sound signals that have generated by the leak by placing two sensors at two different locations bracketing the suspected leak point or at the two ends of any section of the pipe system. To pinpoint any leak, the transmission time lagging is calculated for the two captured sound signals at each sensor and with a simple algebraic relationship the leak location can be determined [4, 29]. One drawback that the technology will need high-speed data acquisition systems. Another drawback, the sound signal usually is weak and fades quickly and the operation environment is full of noise which makes it not easy to capture that required sound signal [71, 72].

Figure 2.5 shows a simple sketch of leak detecting method using AE sensors located at a known distance (l) between them. By calculating the time when the signal arrives each sensor, the distances (l_1 & l_2) can be calculated and the leak can be detected. The Acoustic Emission method is found to be more effective and satisfactory for metallic pipes than the plastic pipes as the plastic pipes are quieter than the metallic ones [29]. The acoustical characteristics of the leak signal are significantly differing between metallic and plastic pipes [69]. Dissimilar to the metallic pipes, the signals in the plastic pipe does not transmit effectively. The use of the AE in the plastic pipes requires more consideration as the problems of signal interference and attenuation are more detrimental in the metallic pipes [4]. However, the use of continuous wave sensors (CW) could overcome the problem of pipeline material where the leaks generate very low Doppler frequency shift [73].
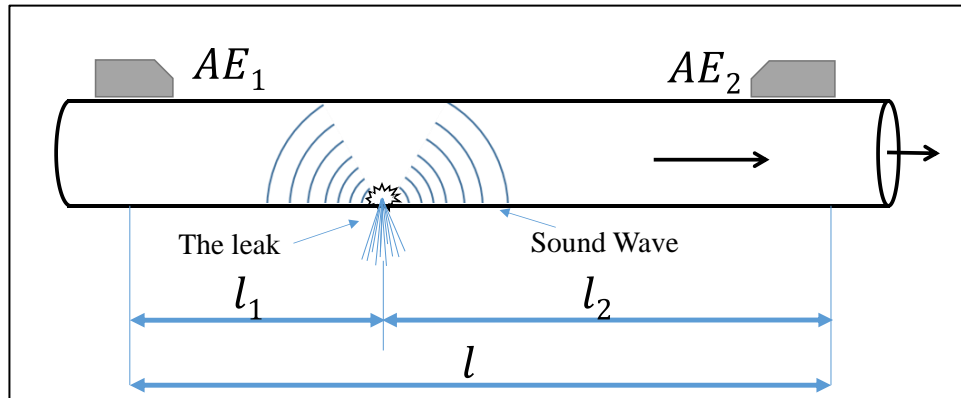
Figure 2.5: Detecting leaks using AE sensor.

In a study case, Anastasopoulos et al. (2009) have claimed that the effectiveness of the AE has been verified [68]. In their experiment they have placed four sensors and found that the signal has first reached to sensor 3 then to sensors 2 & 4 at the same time and then located the leak which was closer to sensor 3 and in the middle distance between 2 & 4 as shown in Figure 2.6. However, in this study they could only detect leaks in broader location rather than one exact point which made them to search for the suspected point by excavation up to 7 m length.
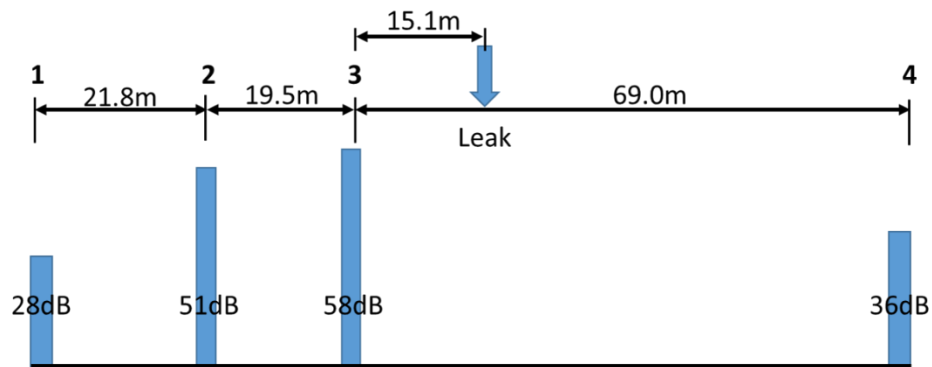
Figure 2.6: Detecting leak using AE sensors [68]

There are several techniques for acoustic emission method that have been used for detecting pipe defects and leaks. These techniques have been classified by Liu & Kleiner. (2013), in the following few paragraphs.

2.4.1.   Sonar Profiling System

This technique provides information from within the pipe especially for the parts submerged under the water line. The system travels in the pipe to scan the inner side of the pipe and sends pulses each 1.5 seconds to provide information about the cross section

of the pipe. One of the main features of this system is that it can scan both clear and non-clear water (e.g. sewer water). However, its cost seems to be high and depends on the size of pipe inspected [11].

2.4.2. Impact Echo:

This technique uses time domain and frequency domain by recording the impact generated wave. It is performed by hitting the tested pipe by a small impulse hammer to create an echo and then record the reflected wave of echo using accelerometer sensor in touch with the pipe adjacent to impact [11]. The impact echo equation is

$$T = \frac{V}{2F_p} \qquad\qquad\qquad \textbf{2-7}$$

Where: T is thickness, V is Wave speed, Fp is Peak Frequency.

2.4.3. Smart Ball

Smart Ball is a device in the shape of ball encompasses multiple sensors such as acoustic, pressure, temperature and accelerometer. The device transmits all necessary information while it navigates inside the pipeline with the flow direction (upstream to downstream). It is able to detect, locate and estimate the magnitude of the leak and report it to the external receiver [74].

2.4.4. Leak Finder RT

The technique is based on an enhanced cross-correlation function which presents a finer resolution for the narrow leak signal. The leak finder RT is composed of acoustic sensors, wireless signal transmission and a computer. The acoustic sensors are either accelerometer which is sensitive to background noise or hydrophones which are sensitive to leak noise. The acoustic sensors are located and attached to two ends of the tested pipeline section. The leak location can be estimated by calculating the arrival time of the signal to the two sensors. According to Liu & Kleiner (2013), the leak finder RT can process the signal in few minutes under most circumstances and the results are continuously displayed and updated on a screen while leak signals are being recorded [11].

2.5. Issues affecting system's reliability and performance:

There are some factors that might negatively or positively affect the leak detection in the available leak detection methods and consequently affecting the exact detection of the leak or might cause false alarms. In fact, The typical parameters of the pipeline and instruments change with aging of the pipeline system [75]. When these parameters change the detection of the leak might not be possible again. It is said that the band of the signal is affected by the state of the pipeline (size, material, pressure) and the surroundings (pipeline media, ambient temperature, etc.) [76]. The following paragraphs outline these factors and categorise them based on the liquid, the pipe, the leak, the season, and external factors.

2.5.1.   Liquid Parameters

   1. Flow Rate

The flow of the fluid itself in the normal situation of steady state has a low noise and produces a low-frequency signal but when a change in the flow rate happens is will be accompanied by a significant change in the signal amplitude [77].

   2. Flow Direction

The direction of flow has some effect on signal when it travels in the direction of the flow or against it. Wassef et al. (1985) found that the flow direction modulates the velocity of sound waves [77].

   3. Pressure

The increase in water pressure makes the signal much audible and detectable where the pressure increases the flow rate through a fixed size leak point and consequently produces higher amplitude leak signal [70, 79]. The higher pressure increases the propagation velocity of the signal [22]. However, the system should be able to detect leakage reliably at normal pressures since higher pressure could cause further problems and defects in the pipe.

4. Liquid purity

The existence of solid particle or gas bubbles in the liquid is significantly enhancing the acoustic emission from pipeline leaks. In pure water, the amplitude of the acoustic emission signal is very low and detected with difficulty. The solid particle and gas bubbles are important and can be utilised to enhance the acoustic emission. However the solid particles could clog the pinholes and therefore no leaks could be detected [79].

2.5.2.   Pipe Metrics

1. Pipe Diameter

Pipe diameter has a significant influence on signal transfer whereas, in small pipe diameters (≤ 300 mm), the signal travels longer distances especially when the material of the pipe is a metallic material [80]. While other researchers said that the attenuation of the signal in small diameter pipes will be higher and therefore, the sensors have to be located in shorter distances [68].

2. Pipe thickness

The thickness of the pipe wall in the pipeline system is affecting the signal transfer. The velocity of the wave depends on the frequency and the thickness of the pipe [67].

3. Pipeline Depth

Anastasopoulos et al. (2009), have denoted that the signal attenuation changes when the pipeline placed at different depths due to the thickness of soil layer above the pipeline [68]. With respect to the thermal image and temperature transfer, the depth of pipe affects the variation in temperature of the surface whereas in shallow depths present higher variation than the deeper one [37].

4. Medium Surrounding the Pipe:

Detectability of a signal in a pipe differs when the surrounding material of the pipe system differs. It has been frequently reported that the signal is clearly detectable when the pipe passes through a soil and the same signal will be no longer detectable when the pipe passes through water such as river or lake [81]. The wave speed highly depends on surrounding medium [29].

5. Pipe Friction

Steady-state friction and unsteady-state friction are thought to be factors that have an impact on the transient signal. Lee et al. (2005), has indicated that both frictions have minimal impact and negligible impedance, however, Wang et al. (2002) stated that transients in the pipeline are damped by both friction and leaks whereas, it is known that over time the friction factor increases [61, 64]. The deposition of minerals and oxides on the pipe surface is expected to influence the behaviour of the system over time [64].

6. Pipe Material

The pipe material can considerably affect the signal attenuation. In plastic pipes, the signal will attenuate faster than in metal pipes [80], the frequency content of measured leak signal is found small (<50 Hz), and signal amplitude at higher frequency is also found small [22]. Leak detection has been found to be more successful in lower frequencies signals where, in plastic pipes, the leak noise energy concentrated at frequencies below 100Hz [29]. However, Bimpas et al. (2010), have claimed that their system overcomes this problem and can detect leakage regarding what is the pipeline material [73].

2.5.3. Leak Parameters

1. Leak Hole Size

Leaks generally generate noise when they escape from pipe [58], however, this noise depends on the size of the hole. A small hole with a high pressure produces higher noise while large hole with low pressure produces weak noise [82].

2. Leak Hole Geometry

The geometrical shape of leak point has a significant effect on the leak detection system. In a mathematical model research work carried by Baghdadi & Mansy (1988), they stated that the hole geometry had an effect on the results. The leak hole of a rectangular shape has given slight error results for the leak location than the leak hole of a circular shape [83].

3. Leak path length

When the leak occurs, at the same pressure, in the pipe joints (e.g. through the gasket of the flange or pipe thread) or through a pinhole in the pipe body, the flow rate of the leak from the joint is much slower than the leak from the pinhole [79].

4. Leak location

Baghdadi & Mansy (1988), have stated that the error in calculating the distance of the leak from the input side was smaller when leak hole was far from the input while the error was bigger when the hole was closer [83].

2.5.4. Sensors

1. Sensors Location:

Leak's distance from the AE sensors is affects the detection of the leak based on the media (fluid or the pipe) that the signal transfers through it [68]

2. Sensitivity of Sensors:

High sensitivity sensors are required when the frequency is at higher attenuation otherwise, the signal cannot be detected (e.g. in a plastic pipe) [22]. Thus, the selection of the proper sensor that can detect the required signal is mandatory in detecting leaks.

2.5.5. Season

The signal transfer is affected differently by seasons. In winter, when the soil above the pipeline is frozen, the signal can have fewer high frequency components than the signal measured in summer [22]. The natural climatic condition has an effect in captured thermal images [84]. The rate of temperature change in winter is less than in summer [37]. Atef et al. (2016), in as a study carried out in Doha, have claimed that their investigation work was successful in both summer and winter with minor error [85]. This could be due to the fact that Doha is in a hot region.

2.5.6. External Noise (Background Noise):

Background noise, in a complex system, can arise from many sources such as vibration caused by pumps and traffic, all of which can complicate the separation of the leak signal

from a vast range of other disturbances and events [82]. Some leak detection loggers have been developed to work at night time to avoid the daytime background noise and when the demand for water is at its lowest [25].

2.6. Reliability of Systems and Selection of sensors and signal processing methods (ASPS)

The key issue in this research work is to improve the general reliability of the system given all the above parameters and factors. From the condition monitoring point of view, there is still a need to select the correct sensors and signal processing methods for an enhanced leakage detection system. The Automated Sensory and Signal Processing Selection System (ASPS) approach is to investigate and evaluate the best combination of sensors and signal processing methods combined with artificial intelligence techniques such as the Artificial Neural Network (ANN) to detect the water leakage in the suitable way whilst ensuring cost is minimised to enable further investments.

The Automated Sensory and Signal Processing Selection System (ASPS) aims to design an effective Condition Monitoring System (CMS). The approach is proposed to design an experimental work to select the appropriate number and type of sensors required for a successful monitoring system.[32, 34].

The ASPS approach is an engineering optimisation method for designing and improving the quality by implementing a systematic application of design and analysis of the experiments in order to produce a high quality and low-cost system. The successful monitoring system can be identified as the system that has the ability to identify any singularities and can response on a reasonable time with the correct decision and proper action. In addition to this, the monitoring system can be considered a successful system when it can facilitate the job with less number of the selected sensors which means that the successful system is also dependent on the number and type of the sensors as they will have a direct impact on the overall cost. [32, 88].

The ASPS approach has been proposed to overcome the traditional methods of designing a Condition Monitoring System in which the design is based on repeated processes of trial and error method. The traditional method of trial and error is based on matching the abnormal condition with the normal condition until the minimum error condition

monitoring system is reached. Those traditional methods are time-consuming since they need long repetitive tests to reach the best configuration for the monitoring system [32]. In traditional methods, when the number of process parameters increases, a number of required experiments will significantly increase as well making the method too complex [87]. Al-Habaibeh & Parkin (2004) have confirmed the effectiveness of the proposed ASPS approach [86].

The approach is based on extracting sensitive sensory characteristic features (SCFs) related to the process condition for each obtained signal and uses the average dependency values obtained from Taguchi's Orthogonal Arrays as indicator to determine the useful combination of sensors or sensory characteristics features in predicting process faults. "the higher dependence the more appropriate a sensor is in predicting a fault" [32]. The SCFs are the key value for determining the faults where it can be defined as the sensory value that can be extracted from a signal using specific signal processing method using mathematical functions or statistical methods such as average and standard deviation [34].

Taguchi's method is known as a powerful tool aiding in developing a high quality and low-cost product. However, it has been designed to handle only a single performance [88]. Even though the ASPS is using Taguchi's Orthogonal Arrays, but it is more accurate in defining the factors and the results where it is defining the process parameters and faults as "factors" while defining the sensory characteristic features obtained from signals as "results" [34].

Al-Habaibeh et al. 2002 have shown that the approach can reduce the cost and complexity of monitoring system and a number of sensors used in a milling process and said that the approach can be used in a different process with minimum modifications [34]. According to the brief explanation shown in this section, the ASPS will be used to design the monitoring system for water leakage detection.

2.7. State of the art in water leakage detection

A large number of researchers are working on leak detection in water distribution systems. However, as revealed by the literature review, most of the researches are focusing on a single technique or mainly two techniques at any one time. It has been noted

that most researched techniques are based on the signal analysis (1D). Image technique (2D) is not common in monitoring systems of water leakage detection if compared to signal based techniques.

Table 2-2: Summary of some latest publications related to water leak detection.

No	Ref	Type or Research				Data Source & Technique			
		Theory	Case Study	Lab	Field Test	Simulation Model	Signal	Image	Fusion
1	Guo et al. (2016)	×					AE		
2	Ostapkowicz (2016)			×			Pressre		
3	Lai et al. (2016)			×				GPR	
4	Atef et al. (2016)				×			GPR/IR	
5	Tian et al. (2016)			×			Pressre		
6	Ranginkaman et al. (2016)			×			Pressre		
7	Moser et al. (2015)		×		×	Flow parameters			
8	Sousa et al. (2015)		×			Level & Pressure			
9	Nejjari et al. (2015)	×			×	Pressure			
10	Meseguer et al. (2015)		×			Flow and Pressure			
11	Martini et al. (2015)				×		AE		
12	(Anjana et al. (2015)		×				Pressre		
13	Sala and Kolakowski (2014)			×			Pressre		
14	Adachi et al. (2014)	×				Flow parameters			
15	Creaco and Pezzinga (2014)	×				Flow parameters			
16	Ayala-Cabrera et al. (2014)			×				GPR	
17	Gao et al. (2014)			×		pressure			
18	Gao, Qi, Wu, Han, et al. (2014)	×		×				GPR	
19	Agapiou et al. (2014)				×			GIS	
20	Demirci et al. (2012)				×	Flow parameters			
21	Wan et al. (2012)			×			AE		
22	Brunone et al. (2011)			×			Pressre		

Majority of the researchers who used image techniques in their research work did not include it as a part of an automated system. Some researchers have classified the thermal imagers as manual detection devices [89]. In this work the thermal camera or imager forms an important part of the proposed automated monitoring system. The literature review has revealed that the fusion system that combines 1D and 2D techniques has not been given any attention. There are few researchers who have implement two or more techniques in their research work, however, they have employed each technique independently not as a fusion system. Table 2-2 shows a comparison summary of some of the recent published researches which has been carried out for water leakage detection in the past few years. The table has been organised on the basis of the type of the research carried out and the techniques used in monitoring the pipeline and leakage detection. The table shows that maximum number of the researchers are working on one technique for pipeline monitoring and leakage detection.

The following paragraphs presents a brief for the papers in Table 2-2. The papers classified based on the data source and the technology used in water leak detection.

2.7.1. Signal based research work

Gua et al. 2016 [76] proposed an adaptive noise cancellation method based on Empirical Mode Decomposition (EMD). They used the EMD to decompose the signal to multiple intrinsic mode functions (IMF) then used the cross-correlation method to remove uncorrelated IMFs. The authors claim that this method does not require the identity of the signal characteristics which is required in the existing EMD. This is because the signal characteristics in water leakage detection are changeable with the change in the pipe status and makes the existing EMD difficult to apply.

Using pressure signal to detect water leak, Ostapkowicz (2016) carried an experimental work research and presented an algorithm applied to both negative pressure wave and gradient method to achieve a satisfactory level of single leak detection and diagnosis. For measuring the negative pressure wave they used standard and non-standard devices (pressure transducers and a conventional device called corrector) [24]. The experimental work involved sudden and slow leakage. The work claims that the experimental work has revealed that their algorithms, with the use of minimum number of standard devices and the help of non-standard devices, it is possible to efficiently detect the leaks. Tian et al.

(2016) also have utilised the pressure signal in pressurised liquid to detect and locate leaks. The leak is located using a proposed algorithm based on the pressure difference between the two sensors positioned before and after the leak point. The work has proposed the use of threshold value to detect the leak and claimed that their method proposed in the research is able to detect and locate the leak in 5 seconds [90].

The inverse transient analysis based research work is presented by Ranginkaman et al. (2016). The researchers have utilised the inverse frequency response analysis for a single and multi-leak detection and location with the help of particle swarm optimisation. The work carried out by fast closing an end valve to generate a transient state. The research has concluded that the frequency domain analysis is faster than time domain because there is no need for numerical computations. The leak in frequency diagram is more evident [91].

A signal from vibration and noise created by the leak is utilised in leak detection. In a field work, Martini et al. (2015) aimed to detect leaks from burst leakage on a real pipeline. The research utilised the vibration caused by the burst process of the leak to detect the leak. The performance of the proposed detection method has been weighed by using the standard deviation of the acceleration signal acquired from the vibration sensor [92]. In a study using Particle Filter approach, Anjana et al. (2015) have utilised the noisy information collected by the sensors. They said that the particle filter approach was able to estimate the flow values of the water distribution system. [8]. Sala & Kolakowski (2014) have utilised pressure measurements in estimating water leakage and controlling the water flow. The research has adapted the Virtual Distortion Method (VDM) for water leakage detection [7]. Brunone et al. (2011) used Impulse Response Function combined with wavelet analysis to improve the transient pressure signals by refining its shape to identify the peak points in the signal. the claimed that the leak localisation error has been reduced [93]. Wan et al. (2012) have used a wavelet transform technique to decompose the signal and used a classifier model for pipeline state recognition. They have enhanced the classification method by utilising bilinear search method to obtain the optimum model parameters for better recognition results. The leak location has been obtained using cross-correlation for each pair on either side of the leak. The authors claim that hierarchical leak detection and localisation method has improved the leak detection and localisation dramatically and facilitated the decision-making [94].

2.7.2.   Simulation Model based research work.

Moser et al. (2015) have investigated a reduction strategy with diagnosis methodology for water leak detection. They have utilised five categories such as the pipe diameter, the number of pipes, and the angle of the lateral pipe, the water demand, and a combination of the two of the previous to derive eleven reduction strategies to reduce the computation time in the network [95].

Sousa et al. (2015) have utilised water level and pressure at specific nodes for locating leaks using an optimisation technique. They have developed a computational methodology from linking a hydraulic model to optimisation model [13]. Nejjari et al. (2015) have carried out a strategy of optimal placement of sensors based on pressure sensitivity to reduce the number of used sensors, improve the leakage detection and maximise the performance of the available sensors. The study proposed an average worst leak expansion distance as a new performance measure for leak detection [96].

By comparing available flow and pressure parameters with simulated parameters differences due to faults in the distribution network can be revealed. Meseguer et al. (2015) have carried a study on this basis to optimise the sensor placement, detect leakage and localise it [97]. Another study carried out by Adachi et al. (2014) has proposed a method that requires minimal parameters than the previous studies. And also can be performed with a minimum number of sensors for leak estimation. This study ran a simulation of water distribution system divided to three virtual areas with three leakage scenarios [98]. Creaco & Pezzinga (2014) have developed an algorithm for leakage reduction by controlling the valves. The developed algorithm enables optimal location for the control valve and determines the isolation valves required to be closed in order to minimise the leakage and reduces the costs [99]. Demirci et al. (2012) said that by using the leakage control model through optimising the pumping schedule of a multi-source distribution system, the power consumption has been reduced as well as the amount of leakage have been reduced. According to the study, by using this model in HD city, the leakage changed from 11% to 8.6% and the power consumption reduced by 32% [100]. A new thought of calculating water leakage based on the use of blind source theory to calculate the leakage have been proposed by Gao et al. (2014). The blind source theory is

the situation in which it is difficult to separate source signal from overlapping signal [101].

2.7.3.   Image based techniques

The GPR is used for water leakage detection because the leaked water is a good factor that would affect the travelled radar waves. Thus, the GPR can produce an image for the searched area. Lai et al. (2016) have utilised the ground penetrating radar GPR in leakage detection in buried water pipes. The detection process carried out on an orthogonal grid above the suspected leak area. They scan laterally stacked 1D data to construct a 2D image and then later construct a 3D model of sliced images of the area of the leak [102]. Atef et al. (2016) have utilised The GPR together with the infrared thermal Imager. It has been found that the work is able to detect the leak in a reliable way while the camera is 2m height [85]. A study for the ability of the GPR in monitoring water leakage and its evolution have been carried out by Ayala-Cabrera et al. (2014) [103]. An experimental work has been carried on shallowly buried plastic pipe in soil and outdoor condition to test the ability of the GPR in detecting water leakage. The results have revealed that the detection of leaks through voids in the image highly depends on the investigated medium and the radar parameters. The process could detect voids in homogenous medium but in inhomogeneous soil or moist may not be able to detect voids [104].

Remote sensing technology combined with field spectroscopy and GIS for water leak detection experimental work have been carried out by Agapiou et al. 2014. They applied a high-resolution and multi- temporal satellite images in their methodology. A threshold of Normalised Difference Vegetation index (NVDI) has been utilised to discriminate between soil and vegetation areas. The NVDI used for interpreting the remote satellite images in order to identify the existence of the leakage. The work has been carried out in two case study areas in Cyprus. Rainfall season affects the results, therefore, the dry season is preferred [105].

2.8. Summary

The chapter has introduced the condition monitoring system used in water distribution system (WDS) and how it is been categorised to direct and non-direct monitoring system. The chapter also showed that the leak detection methods are ranging from simple visual

inspection to more complex methods that require advanced hardware and software. The leak detection methods are classified into external or internal methods. Three different technologies for water leak detection have been introduced in this chapter. The three technologies are the thermal imaging, the transient-based leak detection, and acoustic emission method. These methods have been reviewed extensively and their principle of work have been clarified and explained. The chapter outlined important issues that affecting systems reliability and performance in details. These issues have been categorised into five categories such as liquid parameters, pipe metrics, leak parameters, sensors, and external noise.

The chapter has introduced the novel approach of the automated sensory and signal processing selection system (ASPS) and provided extensive information about the reliability of this system. Finally, the chapter clarified the state of the art in water leak detection techniques and showed that there is a lack in using fusion systems in water leak detection. The chapter reviewed some of the recent research works in the field of water leak detection and exposed that those recent research works are focusing only one or two techniques.

Chapter 3. Methodology

3.1. Introduction

This chapter explains the research methodology of this research work in detail. The project is an attempt to build a reliable monitoring system for water leakage detection. The system would be able to identify and quantify any water leaks that may occur in a transportation pipeline system using high quality and low-cost fusion system to overcome problems found with systems based on single sensory systems. The chapter introduces current problems in the field of water leakage detection. A proposed novel approach using sensor fusion systems to detect water leakage is described in this chapter. This approach is based on the novel approach of ASPS suggested by Al-Habaibeh, (2000). To implement the novel approach ASPS for water leak detection, an experimental test rig has been designed and constructed in the laboratory of the Nottingham Trent University (NTU). A set of sensors and cameras have been selected and installed on the rig and adapted to work with the in-house developed software. In addition to the laboratory work and for verification purposes, a field work has been carried out in a real environment in Libya as target place to apply the technology. Unfortunately, there was a plan to revisit Libya for further field work in different seasons, but because of the severe political conditions, the visits have been cancelled. Therefore, the decision was made to carry on with the experimental works inside the university laboratory.

The proposed monitoring approach uses a sensor or a combination of sensors that is sensitive to the required operation. Therefore, the selection of the sensors is a critical issue. The data acquired by those sensors is subjected to processing to extract the useful information (features) from them. Figure 3.1 shows the basic schematic diagram of the proposed monitoring system for water leakage detection using fusion sensory system.

The sensors (1D and 2D) will get data from the water system using data acquisition devices. The acquired data will be subjected to processing to extract useful information from it and then utilised to produce the correct decision using an artificial intelligent system such as the neural networks.
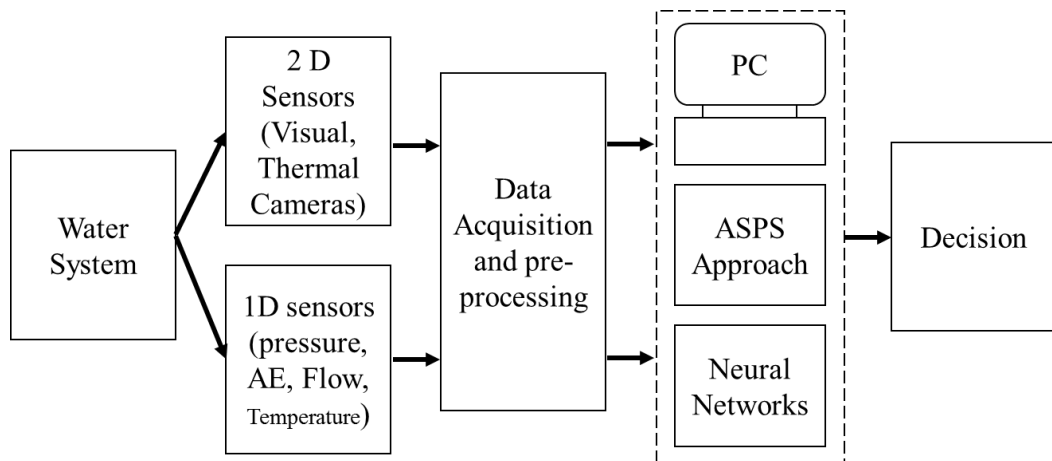
Figure 3.1: Schematic diagram of the proposed monitoring approach.

The proposed monitoring system is to monitor the system for any changes and detects the leaks once they occur   and locating the suspected point of the leak, confirming its existence and characterising the leakage. Figure 3.2 shows the sequence of the process from monitoring to confirming and characterising the leakage as follows:

1. Detecting the leakage using the right sensor or a combination of sensors. The sensors such as pressure, acoustic emission transducer, and a flow sensor can detect the leak once it happens.

2. Determining the location of the leakage. With an advanced signal processing techniques, and with the balance calculations, the location of the leakage could be determined. The thermal camera can detect the leakage and hence the exact location. Finding the location of the leakage using the thermal camera will not be immediate but after a period of time until the moisture from the leakage affects the temperature of the surface above the leakage.

3. Confirming the existence of the leakage. The thermal camera is used to confirm the existence of the leak where in some cases there would be a false alarm from the sensors.

4. Identifying the leakage characteristics (e.g. size). The size of the leakage spot could be used in defining the amount of the leak but it would be an estimation only.
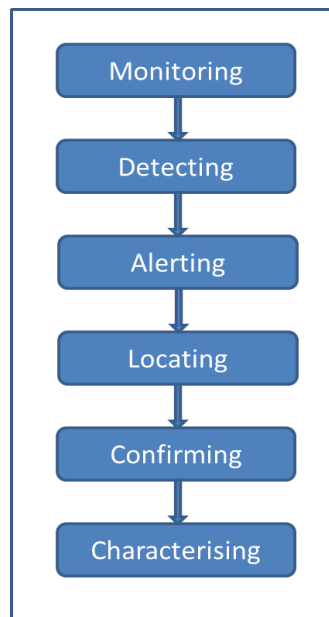
Figure 3.2: Process Sequence:

3.2. Experimental Pipeline system:

The pipeline system designed to be of an experimental scale inside the laboratory and part of it will be buried under a soil to represent actual situation. The used water pipe in the test rig is made of plastic material. Plastic pipe is selected because it is more difficult than the metal pipe to detect its leakage. The water runs in the system in a loop by pumping from the source tank through the pipe system to return to the same inlet tank. This will maintain the water level fixed if there is no leak. The water pipe is passing through a box filled with soil (the test section) where the leak will happen. An infrared light is used to heat the surface of the soil to simulate the sun. The next paragraph explains the design of experimental work pipeline in comparison with actual water pipeline such as the GMRP project pipeline. The experimental pipeline system is described in details in the next chapter.

3.2.1. Comparison between the actual pipeline and the experimental work pipeline.

In order to successfully apply the research project outcome in a real water transfer projects such as the GMRP (See appendix G), the experimental work designed to be with lowest efficient system parameters that might negatively affect leakage detection (e. g. pipe material, size of leak's hole, pipe depth, flow, pressure etc.). In the experimental work,

the used pipeline material (plastic) is one of the lowest conductive material. The pipe used in GMRP named Pre-stressed Concrete Cylinder Pipe (PCCP) is made of a steel cylinder lined and surrounded by concrete and pre-stressed wire. In addition, the experimental work the pipeline is buried at a depth of five times the pipe diameter while the cover depth of the PCCP pipeline is only half the pipe diameter only (See Figure 3.3). The pressure in GMRP pipeline system and the flow rate are high. In Phase two the flow reaches 2 Million Cubic Meters per Day (MCMD). The flow rate of the eastern branch only is 1.120 MCMD and the flow rate of the central branch is 0.8 MCMD [106]. The experimental pipeline flow is only 0.05 l/s. The simulated leak (the leaked water flow) has been made small as much as 0.0019 l/s. Table 3-1 and Table 3-2 show the average flow rate as calculated for the experimental rig and the leak.

Table 3-1: Calculated average flow rate in the experimental rig.

Trail No.	Elapsed Time (s)	Start Level (cm)	End Level (cm)	Level Drop (cm)	Length of the tank (cm)	Width of the tank (cm)	Volume (cm3)	Volume (Litre)	Flow Rate (l/s)
1	420	16.7	10.6	6.1	76	50.5	23411.8	23.412	0.056
2	420	16.65	10.8	5.85	76	50.5	22452.3	22.452	0.053
3	420	17.2	11.7	5.5	76	50.5	21109.0	21.109	0.050

Average Flow Rate (l/s)	**0.053**

Table 3-2: Calculated Average leak amount in litre per second

Trail No.	Elapsed Time (s)	Start Level (cm)	End Level (cm)	Level Drop (cm)	Length of the tank (cm)	widith of the tank (cm)	the leak volume (cm3)	Leak Volume (Litre)	Leak Rate (l/s)
1	60	21.5	21.24	0.26	76	50.5	997.9	0.998	0.017
2	60	19.95	19.7	0.25	76	50.5	959.5	0.960	0.016
3	60	19.15	18.81	0.34	76	50.5	1304.9	1.305	0.022
4	60	18.2	17.9	0.3	76	50.5	1151.4	1.151	0.019
5	60	17.3	16.98	0.32	76	50.5	1228.2	1.228	0.020
6	60	16.3	16.01	0.29	76	50.5	1113.0	1.113	0.019
7	60	15.35	15.35	0.27	76	50.5	1036.3	1.036	0.017

Average Leak Rate (l/s)	**0.019**

As the difference between the experimental pipeline parameters and the real pipeline parameters is notable, the amount of heat absorbed (or released) by the GMRP pipeline

is thought to be much more than the amount absorbed (or released) in the experimental pipeline.
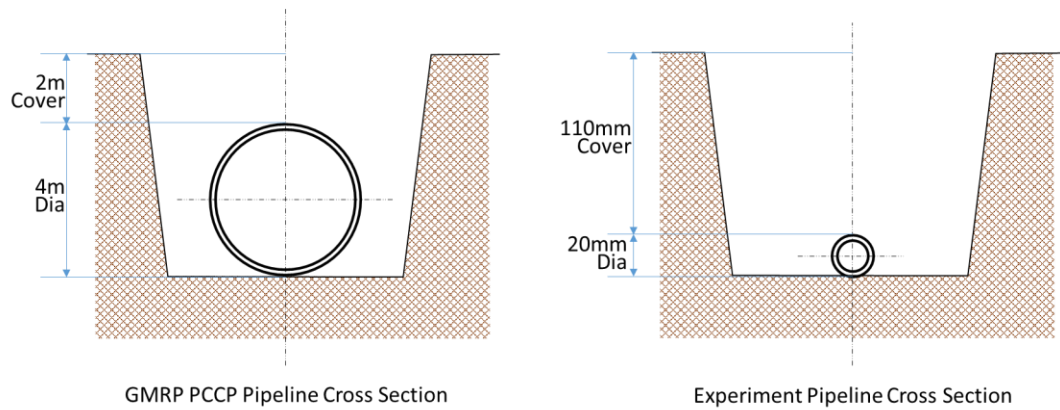
Figure 3.3: Comparison between the actual and experimental pipeline

3.2.2.   The initial design of the test rig:

The initial design of the experimental rig used to monitor the test section of the buried pipeline using two Infrared cameras (Flir 310A and IRISYS as a high and low-resolution thermal cameras) and monitored with other sensors (AE, pressure, flow sensors) as shown Figure 3.4. The rig consists of a pipeline with inlet/outlet water tank, water pump and valves to control water flow. The test area consists of a box filled with soil in which part of the pipeline is passing through it to simulate actual buried pipeline. The test area has been surrounded by polystyrene pieces to avert the heat effect of the surroundings in order to reduce heat loss and to have a more real simulation for the tested area. The pipeline is buried 110 mm deep under the surface which is about 5 times of the pipe diameter. The type of pipe material is a plastic material, which is known with less heat conductivity.

The pipeline system is consisting of water tanks and water pump plus several sensors and data acquisition devices, thermal cameras, and visual camera used. The buried section of the pipeline which is the section to be monitored contains a hole to resemble the leak point as shown in Figure 3.5 and Figure 3.6. The hole will be plugged and opened at random times to simulate sudden leak starts at an unidentified time. The pipeline is pressurised under the normal pressure of the water pump and the head available in the system. To control the pressure in the pipeline, a ball valve is installed at the end of the pipeline. The end control valve is used to increase the pressure to test the system in different pressure rates.
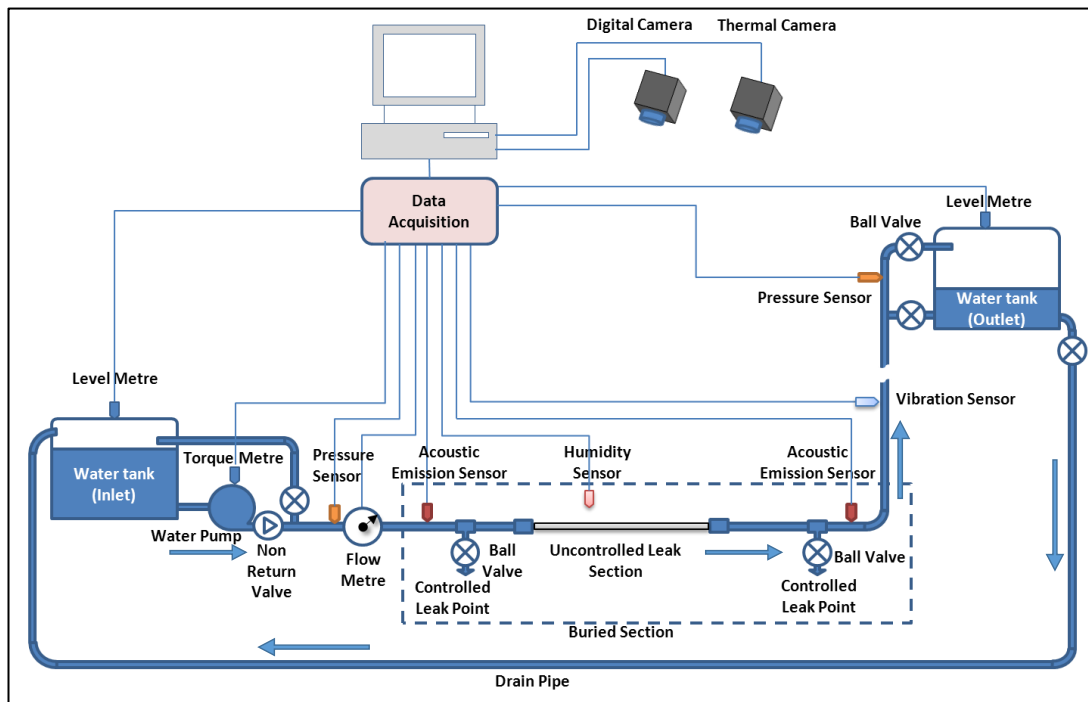
Figure 3.4: Concept Experimental Rig

The pipeline is tested for the leakage while it is buried in the soil with no asphalt or concrete slabs on the top. The second stage of the experimental work, which is the buried section is covered by concrete slabs above the buried section of the pipeline to simulate the condition where the pipeline passes under a road or a walkway.
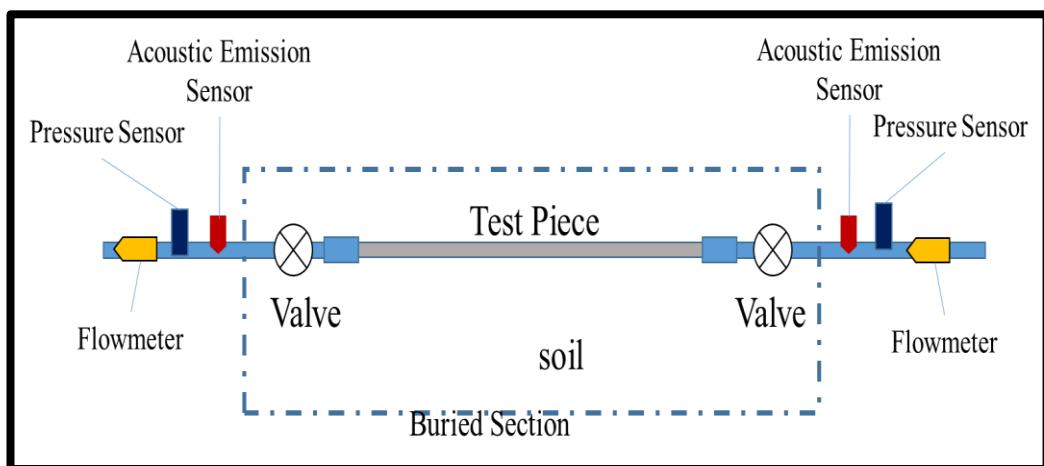
Figure 3.5: Buried test section.
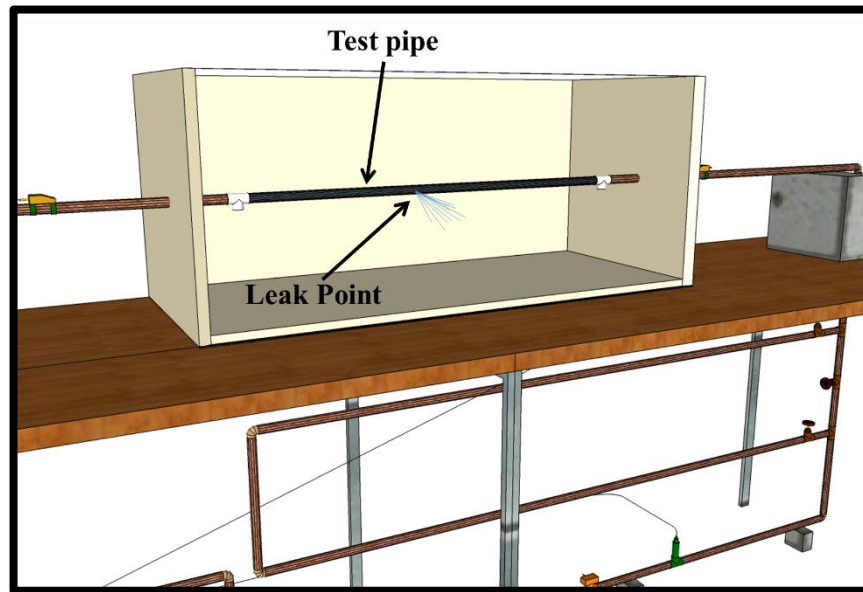
Figure 3.6: Buried section with leak point in 3D drawing

3.3. Experimental work scenarios

A number of experiments are carried out on the test rig. All the required parameters such as the acoustic emission, pressure, flow rate as well as thermal and visual images, are monitored continuously while the experiments are running. All required data (signals and images) is collected using the in-house made software.

For testing the thermal camera and use them in leak detection the rig equipped with an infrared light to simulate the day and night. First, few experiments used for verification and comparison purpose to examine the ability of the low-resolution camera in detecting the leakage compared to the high-resolution camera. For this purpose, a modern high-resolution camera used in-line with the low-resolution camera. The temperature of the water varied from very cold to average (warm) temperature.

For leak detection using sensors, the rig fitted with end control valve at the end side of the downstream section. The end control valve is used to control the pressure in the pipeline to produce a different situation of pressurised pipeline. Acoustic emission accelerometer, pressure sensors, flow sensor are installed to acquire the data during the operation of the system.

Leakage in the test area started at random times relative to the days in each experiment (for example, early morning, midday, early night, midnight and so on). A big number of the experiments ran with an uncovered plain soil to represent a situation similar to GMRP which is running in the Sahara (no concrete slab above it). In the last few experiments, a slab of concrete has been used to cover the test area to verify the ability of the thermal cameras in detecting the leakage through the concrete slab.

3.4. Thermal image processing for water leak detection.

On completion of the experimental work and collecting the required images, the images are subjected to processing in order to extract the useful information (features). The images are classified to no-leak and leak images as they are containing the information of the leak. Commonly, the raw images acquired by the cameras do not show much useful information. Images from both cameras need extra processing to ease the process of feature extraction. In the case of the no-leak condition, the images show either nothing (noisy image) or they show the pipeline traces. As mentioned in the previous paragraph 3.3, the result of the image processing is used to compare the low-resolution camera (IRISY) with the high-resolution camera (Flir 310A) to check the ability of the low-resolution camera in detecting leakages and pipeline traces as good as the high-resolution.

The processed image is used in detecting the leakage and deciding which best time of detection.

3.5. Field work

A field test is carried out in a real environment condition in Libya. The purpose of the field work is to investigate the ability of the thermal technology and the low-resolution camera (IRISYS) and to work in a real hot environment for water leak detection. The work carried out by digging a trench in an open area exposed to environmental conditions. A plastic water tube buried in the trench. The IRISYS camera located on one side of the trench. The experiment carried out during two complete cycles of day and night continually (48 hours). A large number of visual and thermal images is collected and subject to processing and analysis.

The equipment used in this work are the IRISYS thermal imager, Laptop with acquiring software, Water tube, and two electronic thermometers for monitoring water and environment temperatures.

3.6. Designing the suggested ASPS approach for water leak detection

The suggested ASPS for water leak detection system is designed based on the original ASPS approach which has been studied, designed, and confirmed earlier by Al-Habaibeh, (2000) [32]. As explained previously there are a lack of the use of the fusion systems for water leak detection as the available systems are based either on a single technique or multiple techniques without being used as a fusion system. The suggested new ASPS approach for water leak detection employs multiple sensors and cameras for acquiring signal and image as fusion system. The approach is carried out by extracting the best sensory characteristic features (SCFs) that indicate the state of the tested pipeline system for leak identification.

3.6.1.   Main structure of the ASPS approach:

The idea of the proposed ASPS approach is simple to understand but requires precise systematic steps to be performed successfully. Figure 3.7 shows the schematic diagram of the proposed approach for water leakage detection. The approach is based on getting the data from the available or selected standard devices such as sensors and cameras (1D & 2D sensors). Once the data is collected it is subjected to preparation (pre-processing) by determining the region of interest (ROI) to ease the extraction of the required information from it by removing any distracted or unwanted parts of either the image or the signal. The ROI can be automated to ease the processing of large numbers of images and signals. The process of selecting the ROI is explained in the signal and image processing section.

The prepared signals or images then subjected to processing using advanced techniques of signal and image processing such as Fast Fourier Transform and Discrete Wavelet Transform to extract the required features that can easily differentiate between the status of the monitored system before and after the searched event.
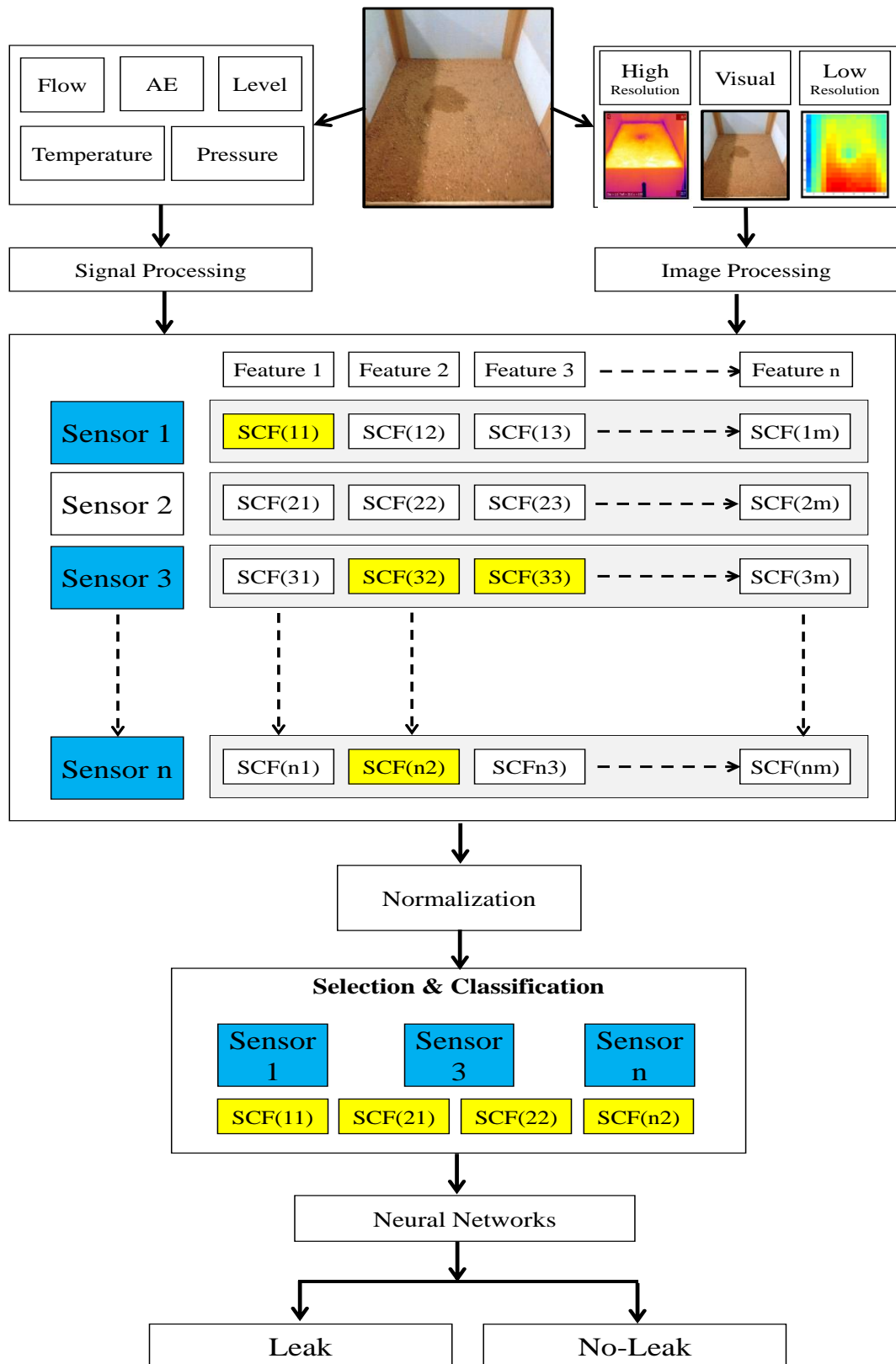
Figure 3.7: General schematic diagram for the proposed ASPS

On processing the data, a mathematical approach such as linear regression approach or a simple approach of calculating the difference in percentage along with statistical functions is used to differentiate between the two situations of the healthy condition and the unhealthy condition (No-leak and leak). The statistical functions such as mean, standard deviation, maximum, minimum, and so on are used to obtain a value for the both conditions. The magnitude of the slope or the percentage of the difference is the criteria that are used to select the sensitive feature of the sensors and cameras. This obtained feature is telling whether the sensor or the camera is able to detect any changes in the situation of the system. The extracted feature is also telling which best signal or image processing technique to be used as the different techniques give different results of the same signal or image. The selected features are ranked in ascending order from the best to the worst sensitivity then divided into groups called systems. Each group represents one complete system contains sensor(s) and processing techniques.

The information collected from the signals and images is tested with artificial intelligent techniques such as Neural Network to decide the condition of the designed system. The following step is to reduce the cost of the produced system by removing some sensors or cameras and choose which better combination of sensors and images can do the job without affecting the results. With this, the appropriate fusion system is designed.

3.6.2.   Linear Regression Analysis

The linear Regressing Analysis is a mathematical approach for modelling the relationship between dependent and independent variables. The parameters of the flowing water in the pipeline or the parameters in the area nearby the pipeline is changing once the leak occurs. This change in the parameters is affecting the sensory characteristic features SCFs values. As an example, the leak changes the pressure inside the pipeline system and the temperature of the soil in the area nearby the leak. The SCF value changes based on that change in the parameters. Some of these features (the SCFs) can change dramatically to a higher or lower value with the change in the parameters while others give a random change that cannot be used to judge the situation. The linear regression of the extracted SCFs is high in the first case and low in the second case. The SCF with higher linear regression value will be classified as high sensitive SCF and the one with low linear regression will be classified as low sensitive SCF. The slope value of the trend line is high

with the high sensitive SCF and low with the low sensitive SCF. The slope is a good indicator for the SCF sensitivity.

Figure 3.8 shows three examples of the extracted features. The figure explains the sensitivity of the SCF. The high sensitive SCF based on the value of the slope can be used to indicate the status of the tested items. The SCFs with a higher sensitivity is used in the designing stage of the best monitoring system and used later in the monitoring system as a part of the fusion system to be used for monitoring.
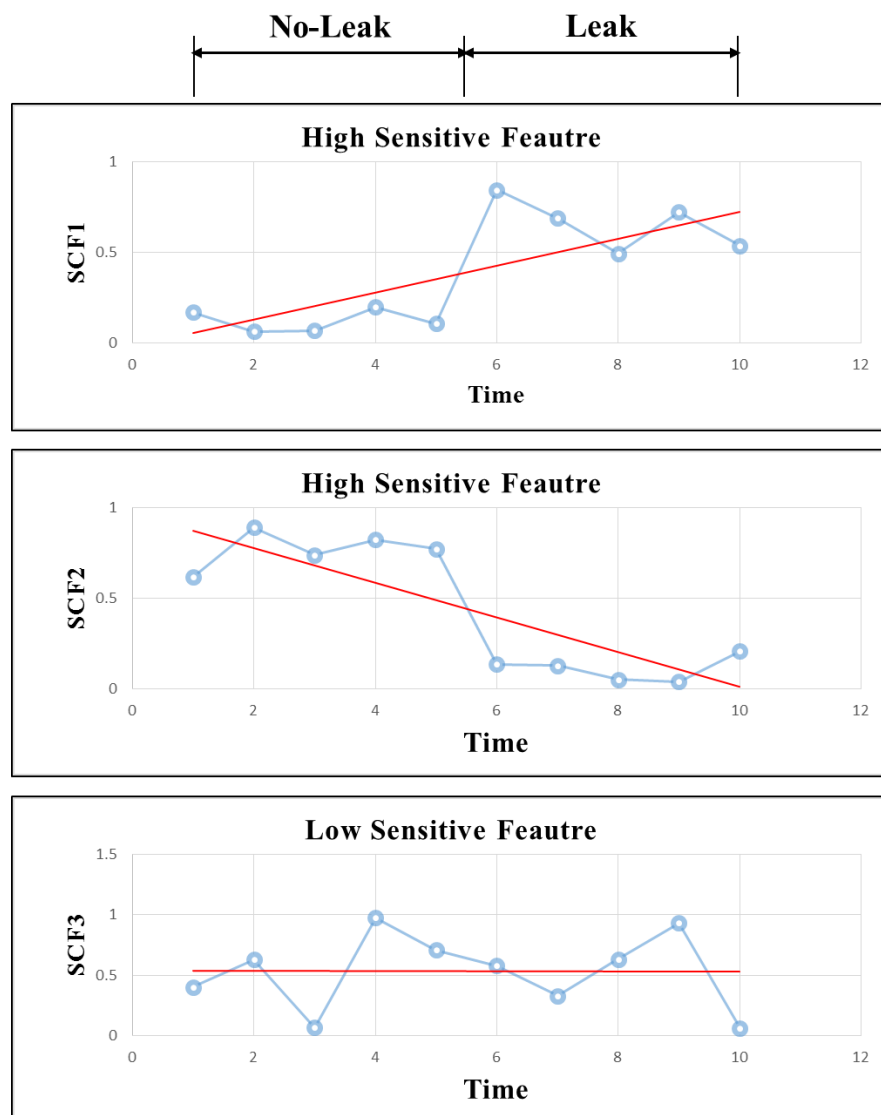
Figure 3.8: High and low sensitive features for leak detection

The selected SCFs is considered of high sensitivity when they produce a higher slope value if there is a change in the condition. The features are extracted from the raw data, and the processed data. Fast Fourier Transform and Discrete Wavelet Transform will be

used to process the raw data. In other words, each set of signals and images will be subjected to multiple forms of extracting useful features from them.

3.6.3.   Use of the percentage in calculating the sensitivity (%)

The change in the condition of the monitored system generates a difference in value between the old and the new condition. The sensitivity of the SCFs can be calculated using the percentage of the different (Delta) between the two situations. A higher percentage value is a higher sensitivity feature (SCF). The percentage is calculated by getting the absolute value of the difference divided by the maximum difference. The equation below is used to calculate the percentage. This method is precise in distinguishing the two conditions of the sample as it gives a readily normalised data ranging from 0 to 1.

$$\Delta = Max - Min \tag{3-1}$$

$$the\ percentage = |Max - Min|/Max\ diff \tag{3-2}$$

The maximum difference in equation $(3\text{-}1)$ is the maximum distance between the two peaks of the samples. There are three cases for to calculate the maximum difference. The cases are shown in the following figures.

The first case when both samples of data are positive. In this case, the maximum difference is the max value (Figure 3.9).
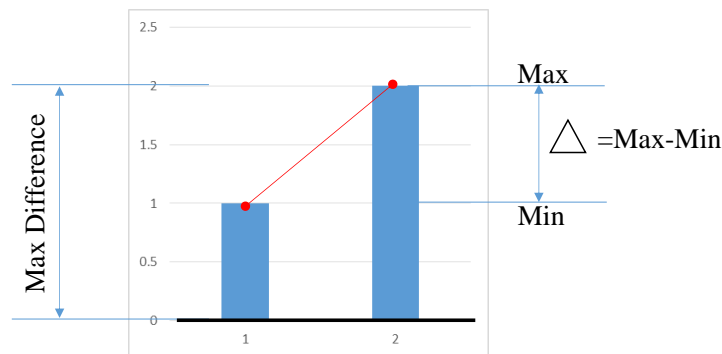
Figure 3.9: The maximum difference is equal to maximum value

The second case when the both samples are negative. The maximum difference, in this case, is equal to the absolute minimum (Figure 3.10).
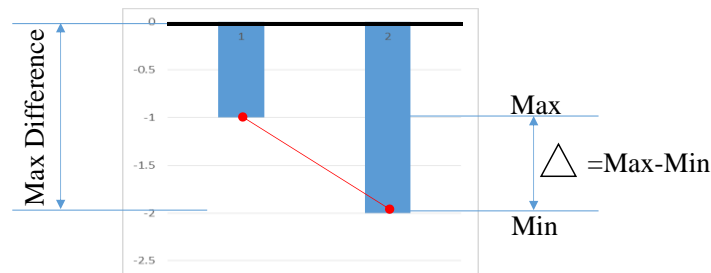
Figure 3.10: The maximum difference is equal to absolute minimum value

The third case is when two samples have different sign. In this case, the maximum difference is bigger than the maximum value and the absolute minimum and equal to delta which means the percentage of difference is at its peak value and equals to one (Figure 3.11).
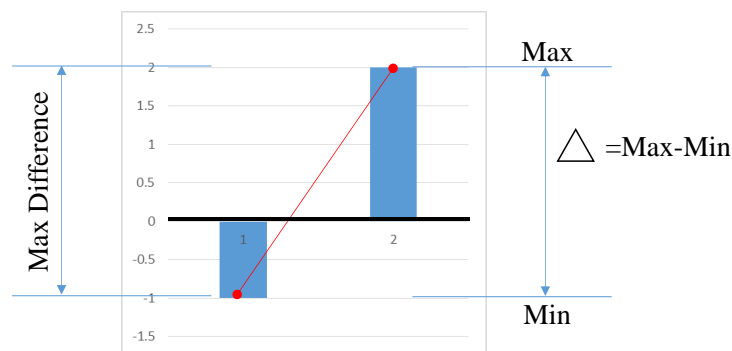
Figure 3.11: The maximum difference is equal to distance between the two peaks.

3.6.4.   Example of the sensitivity calculation in accordance to the ASPS approach

1- Get the processed data of the sensors for the both conditions (Before leak and After Leak)

Sensor 1		Sensor 1	
Before	After	Before	After
5.063005	7.330257	4.285821	4.379105
2.561379	2.108888	3.384286	1.28608
7.706492	2.294262	0.32684	4.04881
3.075871	10.33423	3.626808	0.393423
8.341151	6.731599	3.047946	1.930274

2- Get the features by calculating the percentage of delta of the data in each sensor

F1S1	0.3093
F2S1	0.176659
F3S1	0.702295
F4S1	0.702361
F5S1	0.192965

F1S2	0.021302
F2S2	0.619985
F3S2	0.919275
F4S2	0.891524
F5S2	0.366697

3- Join the features of all sensors to establish the associated matrix ASM.

Numerical ASM

F1	0.3093	0.021302
F2	0.176659	0.619985
F3	0.702295	0.919275
F4	0.702361	0.891524
F5	0.192965	0.366697
	S1	S2

Visual Representation ASM
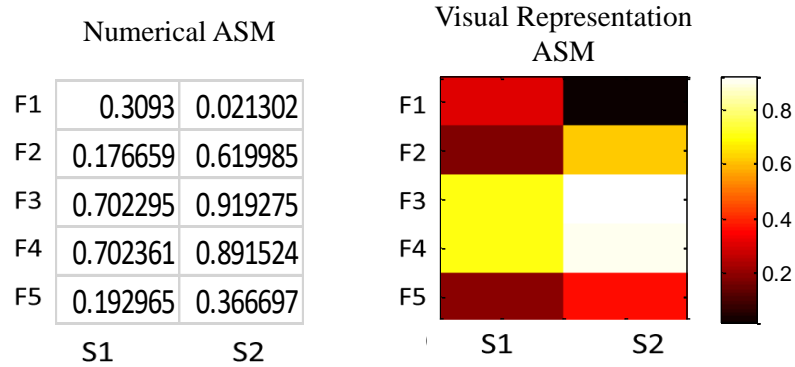
4- Create the stability matrix SM by calculating the standard deviation of multiple ASMs from different experiments.
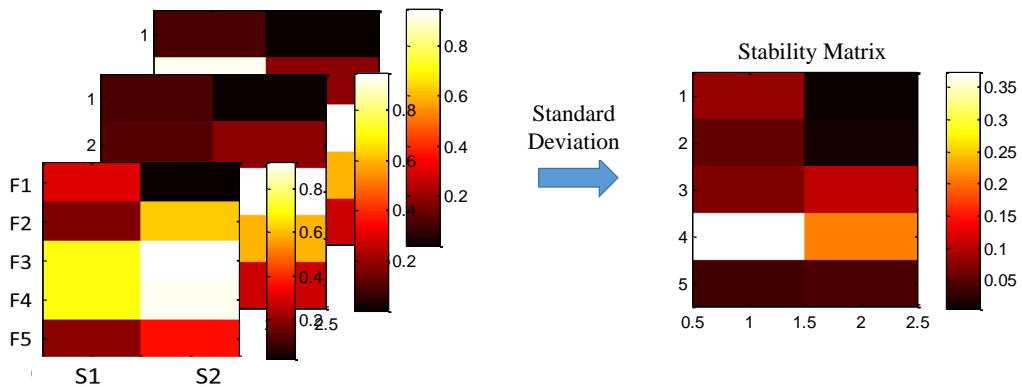
5- Calculate the resultant associated matrix RASM from the original data based on the ASMs.

$$SM = \sigma(\Delta M_1, \Delta M_2, \Delta M_3, \dots, \Delta M_n) \qquad (3\text{-}3)$$

Where:

SM: the Stability Matrix and σ: the standard deviation

6- Arrange the features vertically then rank them in ascending order

The features arranged vertically		The features Ranked (Z-A)	
F1S1	0.3093	F3S2	0.919275
F2S1	0.176659	F4S2	0.891524
F3S1	0.702295	F4S1	0.702361
F4S1	0.702361	F3S1	0.702295
F5S1	0.192965	F2S2	0.619985
F1S2	0.021302	F5S2	0.366697
F2S2	0.619985	F1S1	0.3093
F3S2	0.919275	F5S1	0.192965
F4S2	0.891524	F2S1	0.176659
F5S2	0.366697	F1S2	0.021302

7- Divide the ranked features to systems as in accordance to sensitivity

System 1		System 2	
F3S2	0.919275	F5S2	0.366697
F4S2	0.891524	F1S1	0.3093
F4S1	0.702361	F5S1	0.192965
F3S1	0.702295	F2S1	0.176659
F2S2	0.619985	F1S2	0.021302

8- Test the systems sensitivity using neural network algorithms

3.7. Data Processing and Analysis Techniques:

The data collected in this research work is divided into two categories, Signal and Images or in other word 1D and 2D signals. Both will be subjected to processing to extract the required information and features which are necessary for designing the proposed ASPS system.

3.7.1.   Pre-processing:

Images and signal are required to be pre-processed in order to remove unwanted noise to facilitate the processing and extracting the useful features. The unwanted noise exists in any image and/or signal causes confusion and leads to inaccurate results. Usually, any collected data (signals or images) have extra parts that might affect the processing operation. The Region of Interest (ROI) is the targeted area for testing and monitoring.

The ROI is a part of image/signal to be processed and analysed. As the images and/or signals are collected in many numbers for known area, it is possible to automate the process to delete the unwanted regions. Figure 3.12 shows an example for selecting the ROI and discarding the unwanted parts.
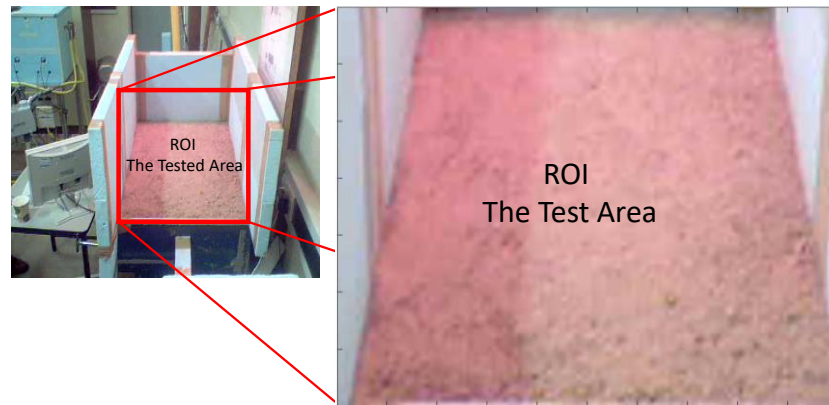
Figure 3.12: Region of interest in the visual image.

3.7.2. Signal Processing techniques:

In the image/signal analysis and processing field, the signals have to be transformed to facilitate its processing for easier extraction of the useful information from it. Signals are classified to continues or discrete signals and time domain or frequency domain. Fourier transform and wavelet transform are the main tools used in signal processing.

3.7.2.1. Time domain analysis

The signal is usually captured in the time domain. The time domain signal describes the event in a period of time, However, in general, the time domain signal do not emit enough information and whereas the vital information is hidden in the frequencies [107]. To extract features from a time domain signal, statistical analysis function such as the maximum, minimum, mean and standard deviation are used.

3.7.2.2. Frequency domain analysis

As the time domain do not show the hidden information in it, the signal transformed to frequency form presents the hidden information clearer than the time domain. Any real world signal (raw signal) can be transformed to multiple sine waves. In the frequency

domain signal resulted from the raw signal, the sine wave represented by a vertical line [108]. (Figure 3.13 and Figure 3.14)

3.7.2.3. Fourier Transform:

Fourier transform named also Fourier analysis is a transform of the single from time domain to frequency domain [33]. The Fourier transform reconstructs the signals and distribute it based on their frequency values rather than align them as a series of historical data based on time. The singularities in raw signals could not clear enough to be used as features but the FFT make them clearer in the frequency mode. Variation in the amplitude of the frequency of certain singularity from the searched signal could be a good indication of a change in the system parameters. The change could be a change from intact system to leaked system as the case in this research work. The equation $(3\text{-}4)$ and **(3-5)** are for Fourier Transform and the Inverse Fourier Transform [109].

$$F(w) = \int_{-\infty}^{\infty} F(x)e^{-iwx}dx \qquad \textbf{(3-4)}$$

$$f(x) = \frac{1}{2\pi}\int_{-\infty}^{\infty} F(w)e^{iwx}dw \qquad \textbf{(3-5)}$$

The Fourier transform function F(w) is the function of f(x) where:

$$i = \sqrt{-1} \qquad \text{(3-6)}$$

$$e^{i\theta} = \cos\theta + i\sin\theta \qquad \text{(3-7)}$$
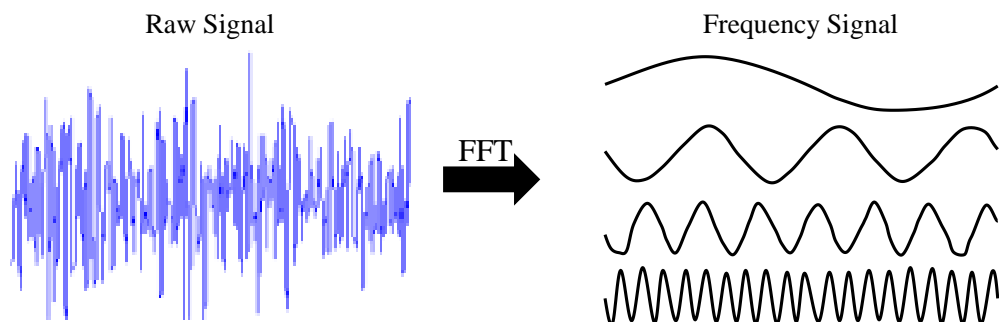
Figure 3.13: The raw signal transformed to multiple frequency signals
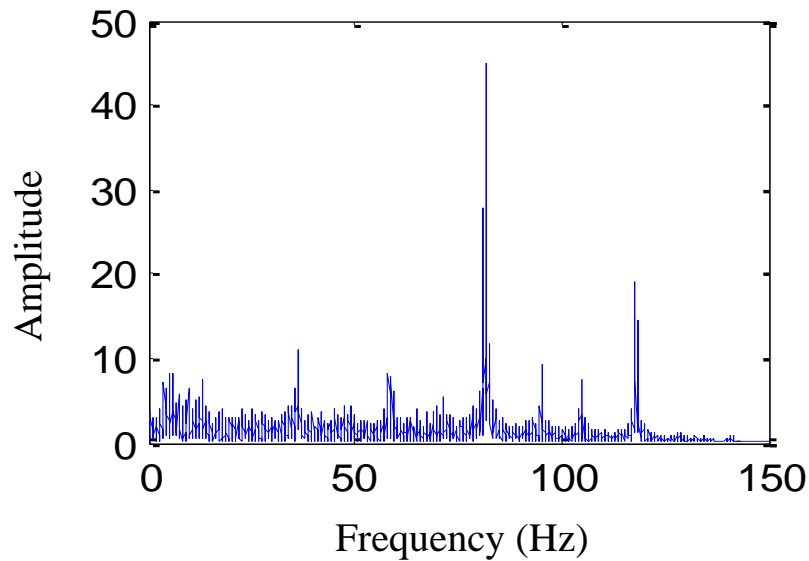
Figure 3.14: The frequency domain signal

3.7.2.4.   Wavelet Transform:

Wavelet transform (WT) is decomposition of the signal into multiple signals with different frequencies but keeps the time information as it also carries important features that cannot be ignored [33]. The wavelet transform is a time-frequency analysis method [4]. Compared to other time-frequency domain analysis, the wavelet transform is considered one of the best because it is able to carry out multi-scale analysis [110]. Figure 3.15 shows the decomposition tree of the wavelet transform. Each new decomposition of the signal can be decomposed in another level as same as the original signal. The process can be reversed to reconstruct the signal back again. The approximation decomposition is called the low pass and applies a scaling function coefficient (). While the detail decomposition is called the high pass and applies the wavelet function coefficient [111].
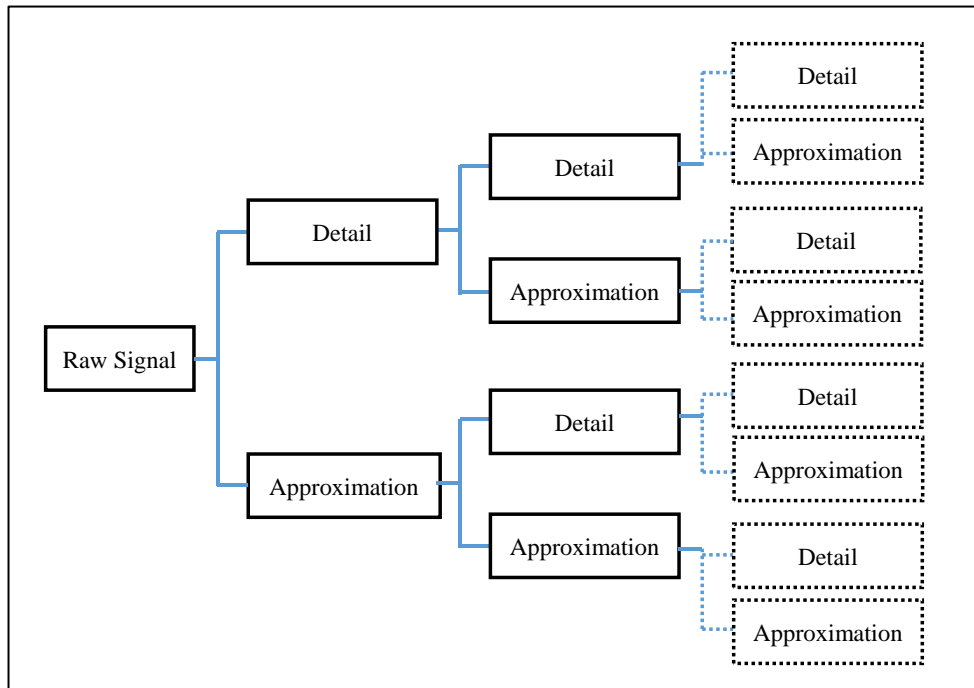
Figure 3.15: Wavelet Decomposition tree.

$$w(j, n) = \sum_{m=0}^{2n} w(j - 1, m) h(2n - m) \qquad \textbf{(3-8)}$$

$$w_h(j, n) = \sum_{m=0}^{2n} w(j - 1, m) g(2n - m) \qquad \textbf{(3-9)}$$

Where *W* is the scaling coefficient and *Wh* is the output

3.7.3.   Image processing

Image processing is the study of the representation and manipulation of pictorial information [112]. The image processing is the process of enhancing, transforming, changing the image to extract information (features) that cannot be seen in its original state. The thermal image is actually a digital image where the temperature sensed from an object is converted to a matrix to form the thermal image. Multiple image processing techniques have been used in this research work to enhance the visualisation of the image and to ease the operation of extracting the SCFs from it. The processing is carried out using Matlab software which is an efficient tool for image processing. The following is a brief of some of the used techniques.

3.7.3.1.   Thresholding

Is the process in which the image converted to black/white image (binary image) based on selected threshold value. In the threshold process, any specific shape exists within the image is extracted from the background using certain value [113]. The values below the selected threshold become 0 (black) and the rest become 1 (white). Counting the remaining pixels gives information about the remaining object such as its size. Thresholding one of the most techniques used in image processing [112]. The threshold changes the map of the image to grey scale.

$$S_{(x,y)} = 0, if\ g_{(x,y)} < T_{(x,y)} \tag{3-10}$$

$$S_{(x,y)} = 1,\ \ if\ g_{(x,y)} < T_{(x,y)} \tag{3-11}$$
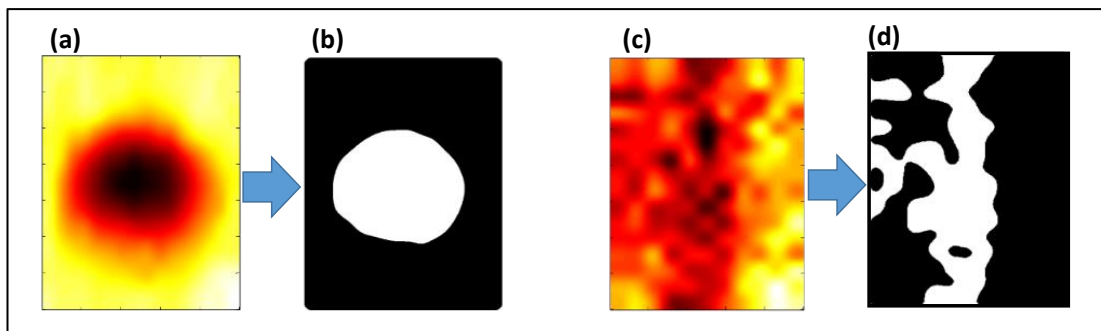
Figure 3.16: Example of thresholding. (a) Thermal images with leak & (c) thermal images with pipeline traces. (b) & (d) the binary images.

3.7.3.2.   Edge Detection

Edge detection is the method in which the boundary between different shapes inside an image is determined and highlighted. It is the process that locates the pixels in the boundaries and then enhances it to increase its contrast against the background. The ideal edge which can be located easily called step edge. While the usual edge is called the ramp and changing gradually across several pixels (see Figure 3.17). In this case, the edge is considered in the middle of the ramp [112]. Figure 3.18 shows an example of processed image using edge detection technique.

Figure 3.17: the step edge (a) and the ramp edge (b)

There are some known techniques to apply edge detection such as Sobel and Kirsch. Both of them are using a mask to apply the edge detection (Equations (3-12) and **(3-13)**).

$$S_x = \begin{matrix} -1 & 0 & 1 \\ -2 & 0 & 1 \\ -1 & 0 & 1 \end{matrix} \tag{3-12}$$

$$S_y = \begin{matrix} -1 & -2 & -1 \\ 0 & 0 & 0 \\ 1 & 2 & 1 \end{matrix} \tag{3-13}$$

And there are two advanced techniques classified as Mathematical Edge Detectors. The tow techniques are Canny and Infinite Symmetric Exponential.

Canny detection function.

$$M_{(x,y)} = \sqrt{I'_x(x,y)^2 + I'_y(x,y)^2} \tag{3-14}$$

Infinite Symmetric Exponential.

$$C_N^2 = \frac{4 \int_0^\infty f^2(x)dx . \int_0^\infty f'^2(x)dx}{f^4(0)} \tag{3-15}$$
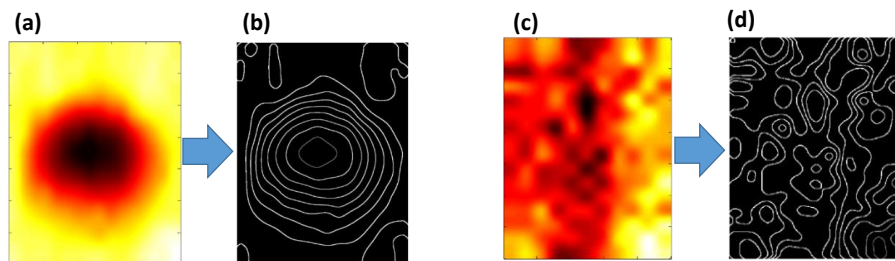
Figure 3.18: Edge detection. (a) Thermal images with leak & (c) thermal images with pipeline traces. (b) & (d) the images with edges.

3.7.3.3. Segmentation

The segmentation process is used to simplify the image to become easier for reading and extracting useful information from it. It segregates the image contents to ease their recognition and classification [114]. The segmentation is carried out simply by removing the decimal value of the image pixels by rounding the value to nearest integer value would increase the contrast of the image then apply another tool to select the required object within the image. For complex segmentation process, advanced filters for image processing such as median filter and histogram filter. The histogram enhances the contrast of the image so it contents will be extinguished effortlessly.
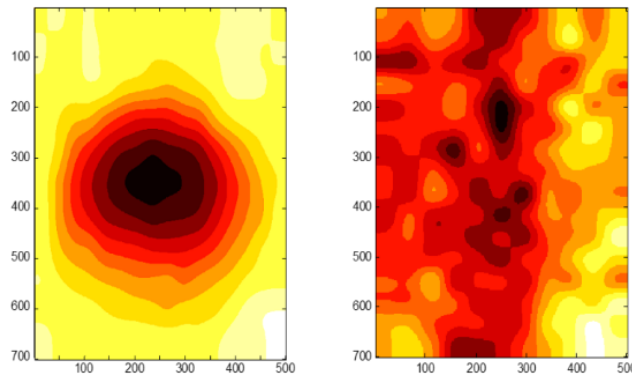
Figure 3.19: figure show two image after segmentation using integer value.

3.7.3.4. Filtering

There are multiple filtering techniques used in image processing such as histogram filter and median filter. The filters used in noise reduction, segmentation.

1. Median Filter:

The median filter is nonlinear operation used to reduce the noise (sometimes called salt and pepper) in the image. The median filter operates by replacing each pixel with the median value of its neighbour [115]. The output image of the median filter is calculated in equation **(3-16)**

$$g_{(x,y)} = med\{f(x-i, y-j), i, j \in W\} \qquad \textbf{(3-16)}$$

Where f(x,y) is the original image and g(x,y) is the output image. W is a two-dimensional mask.

2. **Histogram Filter:**

The histogram filter describes the frequency of a pixel inside the image within the selected region of interest [45]. The histogram enhances the contrast of the image.

$$P_{(g)} = \frac{N_{(g)}}{M} \qquad \textbf{(3-17)}$$

Where:

M is the number of pixels in the image and N(g) is the number of grey level.
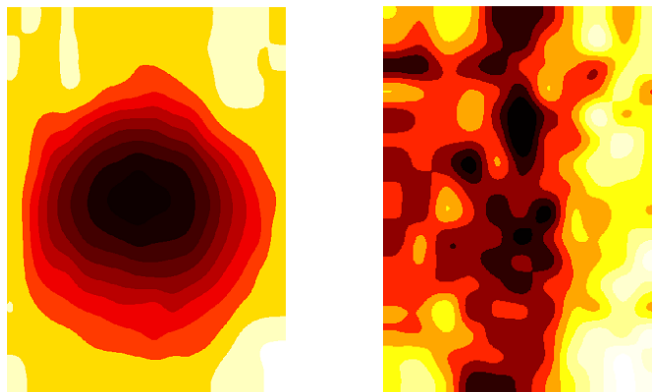
Figure 3.20: the figure shows the two image with histogram filter

3.7.4.   The schematic diagram of the image processing method

Figure 3.21 shows the general schematic diagram for the method used in this project work to acquire thermal images, processing it, and extract features from it to predict the no-leak/leak status using a neural network. The figure shows both high and low-resolution cameras used in this research work.
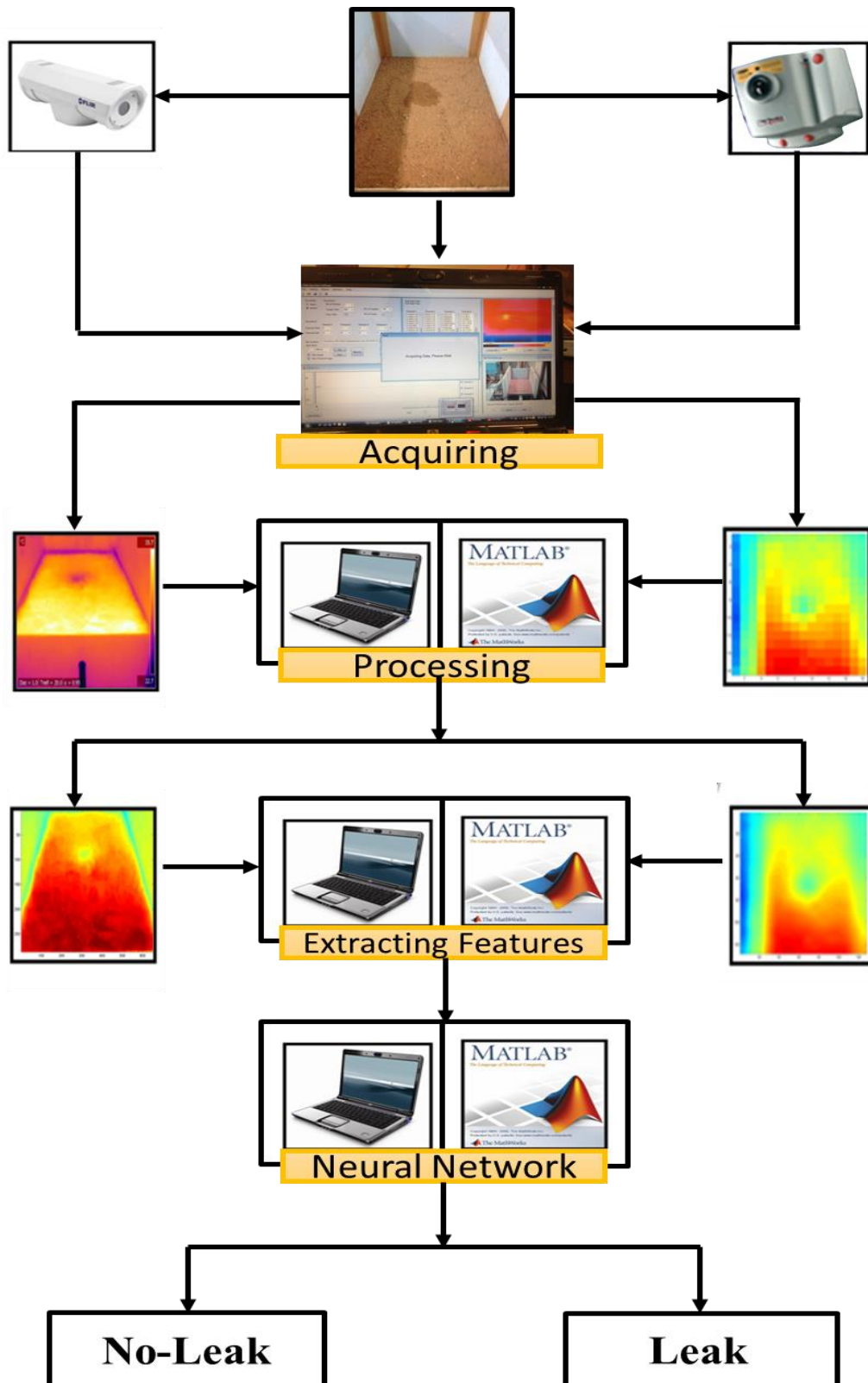
Figure 3.21: Schematic diagram for image processing and utilizing it in an automated leak detection system.

3.8. Neural Networks

Computer scientists have always inspired by human brain (biological neural network) and how it solves the problems [116]. The Artificial Neural networks (or Neural Networks as usually called) is an attempt to mimic human brain in processing information and solving problems by finding the correlation based on initial training target. It has been classified as a new development in programming paradigm which is based on how human brain process information [117]. The neural networks approach is the result of trails to produce artificial tool based on mathematical modules started more than half century ago [112]. Over the last three decades, the use of neural network have expanded to cover all fields and became applicable in many applications such as recognition, estimation, automation, prediction, classification and so on. [118]. The neural network designed to deal with tasks that have been classified as "easy-for-a-human, difficult-for-a-machine" [116]. They (the Neural Networks) can handle complex nonlinear data, missing information, a large number of parameters. And because of their learning nature, they can adjust themselves to changes and find the relations between various parameters [119]. One the attractive features of the neural networks it is based on training using existing data, not on conventional analytical models and statistical assumptions [120]. Also, it has the ability to learn [116]. The neural network is an intelligent tool that guesses the relationships between a complex and non-linear data (input data) and generates the output with high speed and high accuracy based on training [120]. Many researchers have found that the sophisticated data-driven tools such as neural network give much less rate error when compared to the conventional methods [121]. The use of neural networks saves the time of data processing, saves costs, and improves quality [86]. The learning in network is divided to several strategies [116]

1. Supervised learning

In this strategy the network guesses the answers then compares the answers with already known correct target and adjust its output accordingly [122]. The network then, readjusting the weights used in the neural network whenever there is a mismatch between the output and the target. Back propagation neural network is one of the supervised learning neural networks of the supervised learning strategy. In back propagation neural networks, the output is supervised and compared with the target. The process is carried

out by moving backwards and distribute the error on the weights that are connected to the output then adjusting the weights in the layer before and so on until the adjustment of the input weights. Once the input weights are adjusted the neural network moves forward again to get new output. The process then repeated several times till the error becomes zero and the target is reached.

2. Unsupervised learning

This strategy is used when the specific target is not available. In this case, the output will be an estimation based on the criteria of the input data. Learning Vector Quantisation (LVQ) is an example of this type of the neural networks.

3. Reinforcement learning

The reinforcement learning is built on observation where the decision will be taken depending on whether the observation is negative or positive.

3.8.1.   Neural networks structure:

Neural networks consist in general from input, hidden layer, output, weights and biases. The networks could be simple as one input layer, one hidden layer, and one output. The feedforward network usually used with only one single layer with sigmoid activation function [123]. As well as it could be very complex with multiple inputs, multiple hidden layers, and multiple outputs. Figure 3.22 show two examples of simple and complex network.
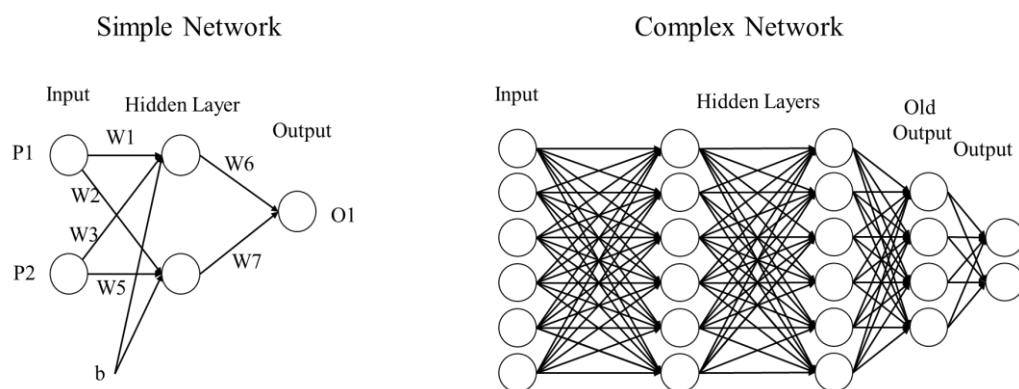
Figure 3.22: Example of neural networks structure.

3.8.2.   Neural network transfer functions

Neural network uses optimisation function called transfer function. Those functions can be used in the pre-processing stage or as incorporated part of the network [124]. The functions are often used in the multilayer neural networks. The functions are named log-sigmoid, tan-sigmoid, and purelin. See Figure 3.23.
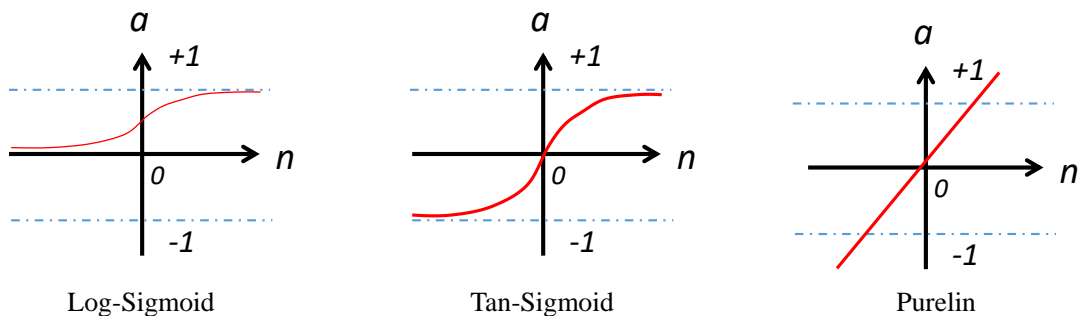
Figure 3.23: The transfer functions

3.8.3.   How to employ neural networks?

Using neural networks requires few steps to be accomplished to achieve the desired results. The neural network has to be learned correctly to produce correct results. Building a neural network required the data first to be prepared and organised properly such as the use of the normalisation. See Figure 3.24. The following steps summarise the procedure of using the neural network.

1. Collect the data using data acquisition devices, sensors, and cameras.

2. Prepare the data for use (E.g. Normalization).

3. Choose a proper neural network (Feedforward, LVQ … etc.).

4. Feed the neural network with the collected data and the required target for training.

5. Train the network based on the target.

6. Validate and confirm that the neural network has trained correctly. Adjust the weights as necessary.

7. Test the network by feeding the network with a completely new different data but of the same nature.
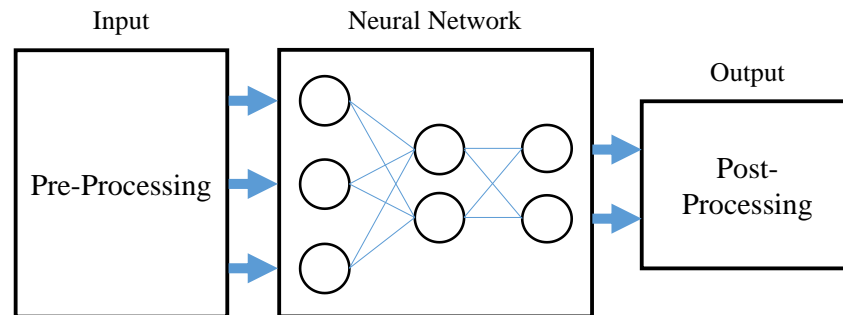
Figure 3.24: Network pre-processing and post-processing diagram.

3.8.4.   Example of neural networks application.

This example is to explain how the neural network are going to be used in water leak detection. The example shows how the network train itself and reduces the errors by adjusting the weights each time. The input data represent different states of the acquired data. The input data consist of 120 sample data. Each sample have two inputs to the neural data. The data categorised into four sections (Figure 3.25). The target is shown in Figure 3.26. From the data and the target it must be noted that only the target of the high/low data is equal 2 while the others are equal 1.
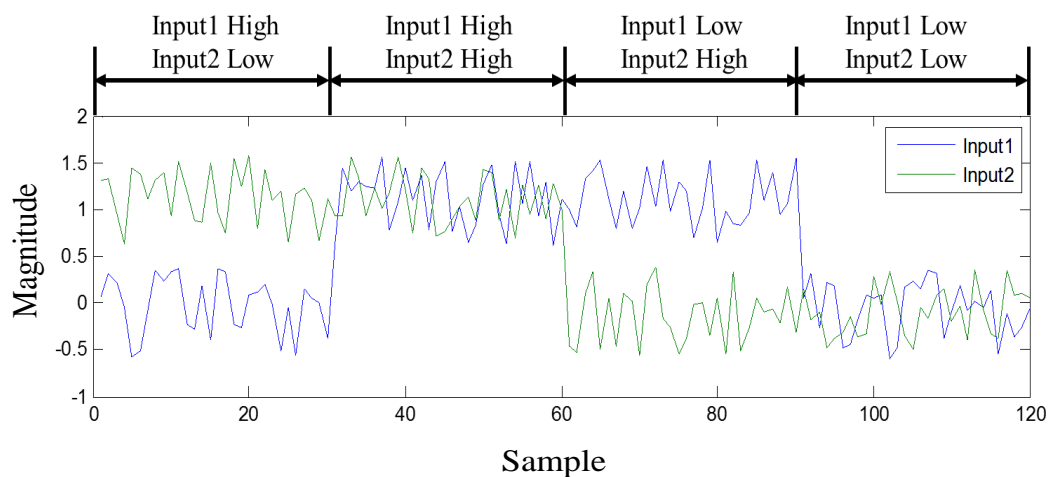
Figure 3.25: Example of Data
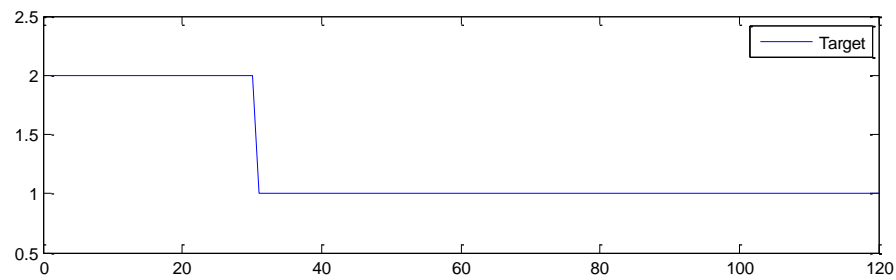
Figure 3.26: The required target

As there are two inputs, four input weights should be there in the network as each input have two weights. Figure 3.27 shows how the input weights are being corrected and adjusted by the neural network in each loop until they became consistent and no more adjustment is required because the desired output is reached.
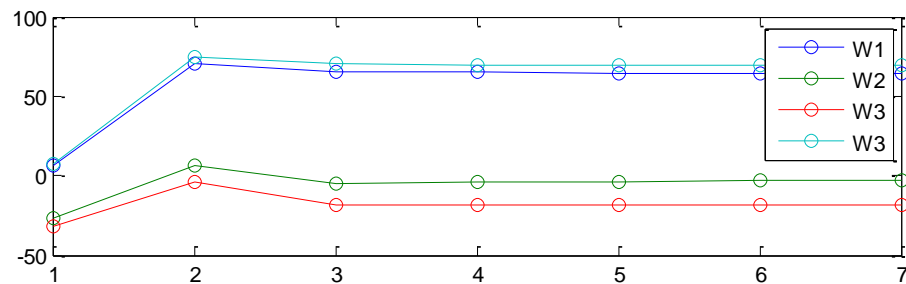
Figure 3.27: Weight correction graph

By correcting the weights in each time the error minimises as well. Figure 3.28 shows the sequence of how the error has reduced in each loop. The error changed from 25 errors in the first time to become 0 in the last loop. The method is carried out by adjusting the weight in each loop and compare the output with the target, whenever there is an error the weights is re-adjusted until the weights become consistent and the error minimised to the lowest percentage of error. To prevent endless loop for the neural network a threshold value of acceptable error percentage is set.
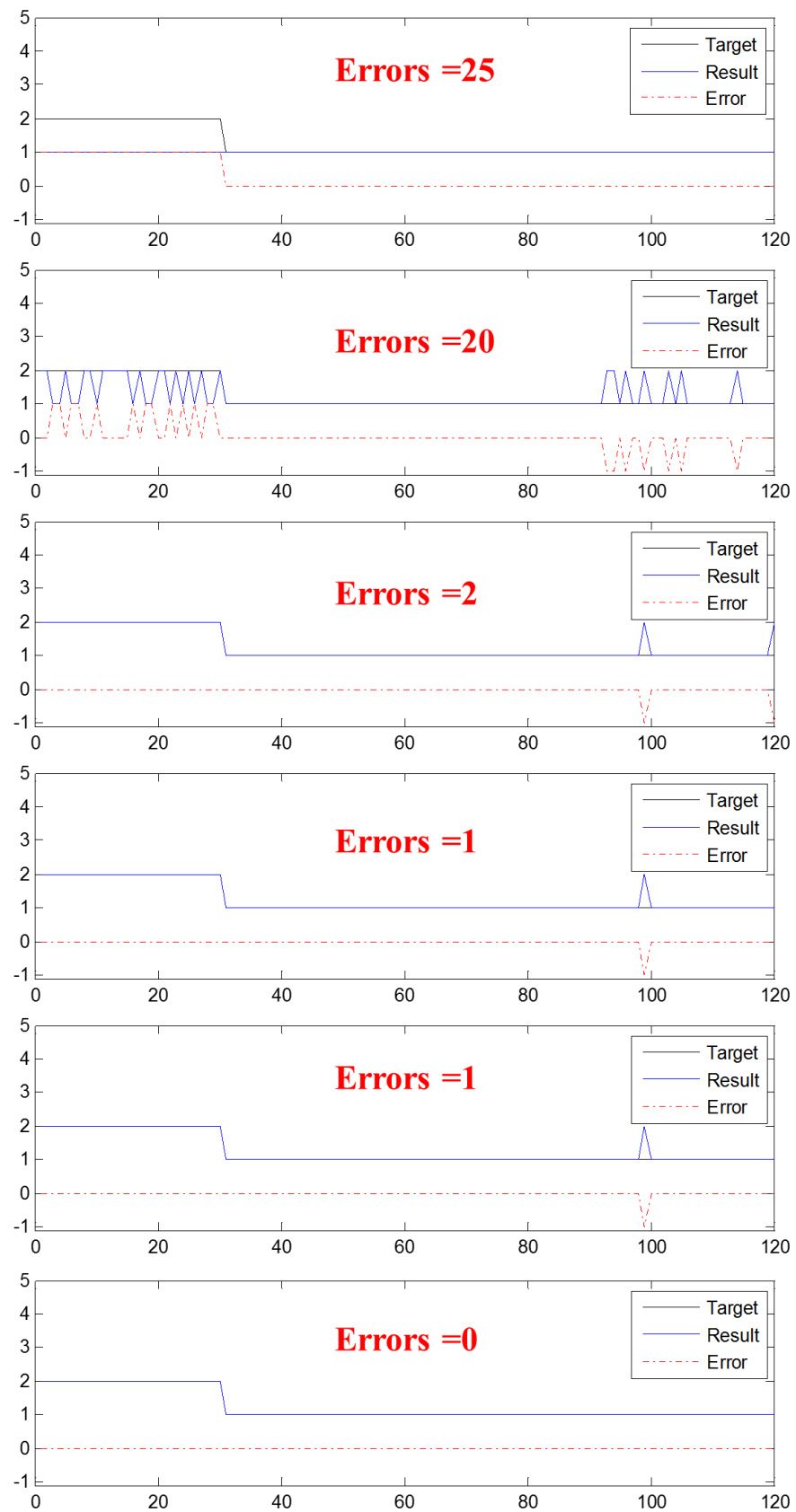
Figure 3.28: Error Reduction Sequence

3.9. Proposal for the use of the thermal cameras for pipeline inspection:

In order to facilitate the application of the proposed ASPS, The thermal cameras could be fixed in certain points for continuous monitoring especially for critical points of the pipeline where leaks are most expected. It also can be used as a mobile camera in routine inspection for the pipeline especially in large projects such GMRA or where it cannot be fitted in open areas. To ease the matter, It is suggested that the camera would be better used as a part of a sensor fusion system to confirm whether the leak exists or not. Therefore, the use of mobile cameras fitted in an unmanned moving device to establish a remote monitoring device would be an ideal idea. finding such devices is becoming mandatory in monitoring systems at open wide environmental regions where the use of devices with human intervention have several limitation [125].

The use of mobile cameras can be accomplished using several techniques. In this research work it is suggested that the camera could be fitted with either quadcopter drone or a helium balloon so the images can be taken from a higher and better point of sight. This might require being joined with GPS system in order to record the location of the image taken, see Figure 3.29 and Figure 3.30.

3.9.1.   The thermal camera with a helium balloon:

For larger projects with longer distances pipeline in open areas the camera can be fitted to a helium balloon. The balloon might be secured to a vehicle as shown in Figure 3.29.
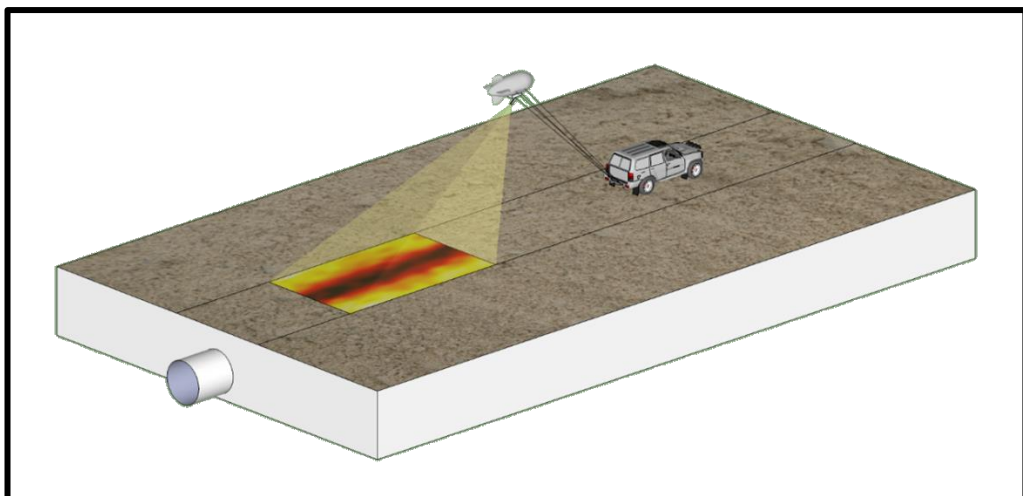
Figure 3.29: An infrared camera and a GPS system attached to a helium balloon.

3.9.2.   The thermal camera with quadcopter drone:

Another alternative is the use of the quadcopter drones to hold the camera and fly over the whole pipeline for a routine inspection or only over the suspected area of leak for inspection, Figure 3.30 is a 3D drawing for proposed drone.
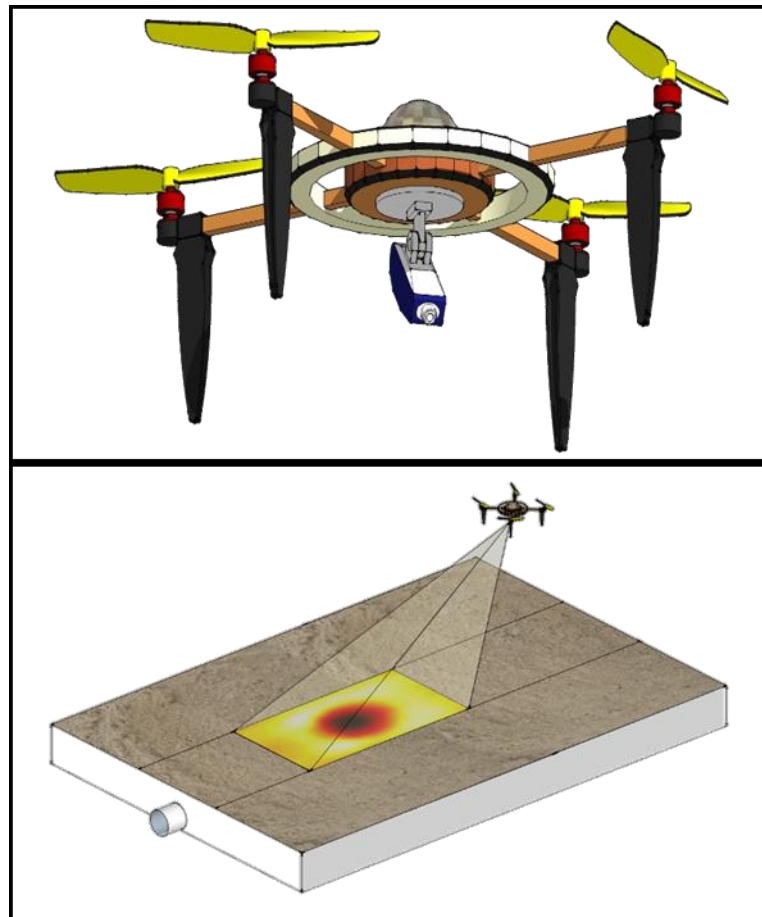
Figure 3.30: An artistic impression of the quadcopter drone with infrared camera and a GPS system.

3.10.   Expected Contribution to Knowledge:

The following areas are expected to enhance the current state-of-the-art in knowledge:

- Evaluating a sensory fusion model to enhance the reliability of the detection of water leakage in pipes.

- The evaluation of the ASPS approach for the selection of sensors and signal processing methods.

- Investigating different types of artificial intelligence methods to detect water leakage in pipes including neural networks and/or fuzzy logic.

- The novel use of combined infrared and visual image for the detection defects in pipes.

- Investigating the effect of pipe material on the sensitivity of the condition monitoring system.

- Investigating the scalability of the system.

3.11.   Summary

This chapter has presented the investigation methodology used in the research work. The work aims to enhance water leakage detection systems by addressing the drawbacks in the currently available systems in the water industry. An Automated Sensory Fusion Approach (ASPS) has been proposed and illustrated for the use in monitoring systems and water leakage detection and location. A test rig will be built with the necessary sensors and data acquisition system to capture the images and signals for analysis. Artificial intelligence systems will be used to search for the information related to pipe defects and/or water leakage.

Chapter 4.   Experimental Rig Setup:

4.1. System Requirement:

In order to implement the experimental work based on the suggested methodology, an experimental test rig of pipeline system with necessary sensors and cameras (thermal and visual) designed and installed in the laboratory, as well as a software able to collect data and images has been programmed. The test rig has been completely designed and constructed in the university laboratory. All instrumentations wired, connected, programmed and were tested in situ. The rig designed to resemble actual situation of buried pipeline and provided with infrared light for heating purpose to simulate the sun. Figure 4.1 illustrates the basic requirement to monitor the pipeline.

Figure 4.1: Basic view for the Computer software& hardware

4.2. Computer Software/Hardware:

To accomplish this project, special software is needed. The software must be able to read data from data acquiring device and capturing both infrared images and visual images for the inspected pipeline in order to determine the suspected leak points. To reach this purpose, two software have been developed. The first software has been created using Visual Basic.NET and second one developed by using LabVIEW. The software will

require hardware components such as Data Acquisition Device connected to several sensors, visual camera and Infrared camera.

4.2.1.   VB.NET Based Condition Monitoring Software:

Figure 4.2 shows the GUI of the VB Based Monitoring Software created by using the programming language Visual Basic.Net for this project. The Software is capable of capturing data (temperature or pressure readings), thermal images and visual images.

Figure 4.2 shows the in-house VB.net software in the background and is being used with the low-resolution camera (IRISYS). The Flir software in the foreground is used for the high-resolution camera (Flir A310). Both programs have successfully been tested with data acquisition devices and the cameras (Digital and Thermal cameras). The software is acquiring and saving a sequence of the captured data and images as required. Figure 4.3 shows the software during the capturing process with part of the rig.
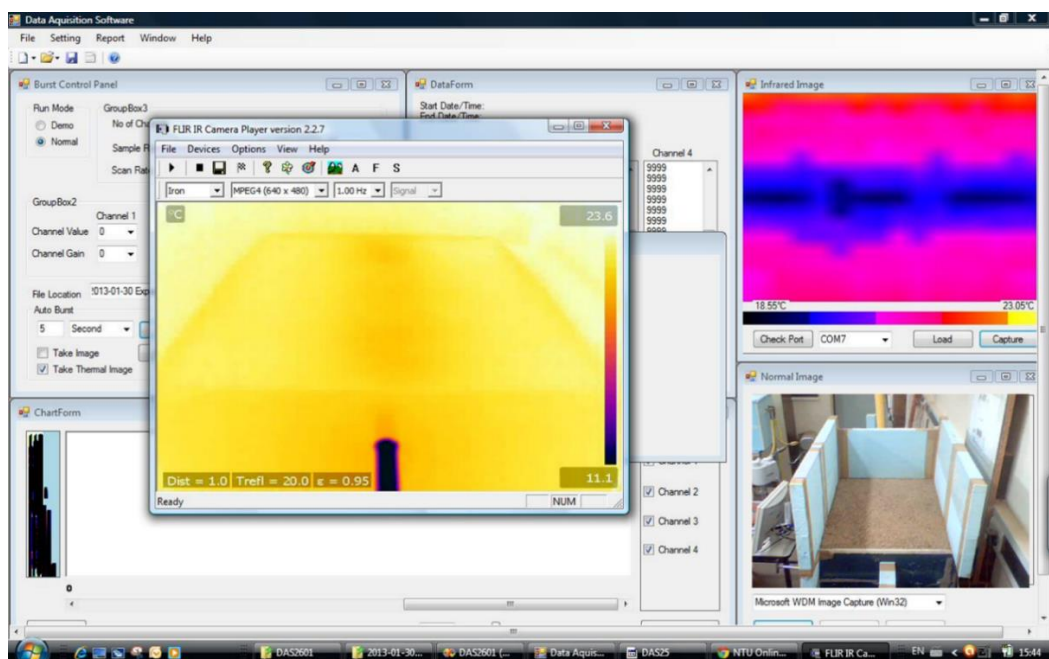
Figure 4.2: Screen capture of the software under operation, for leakage detection experiment. The GUI shows visual camera image, the low-resolution thermal camera and the high-resolution thermal camera.
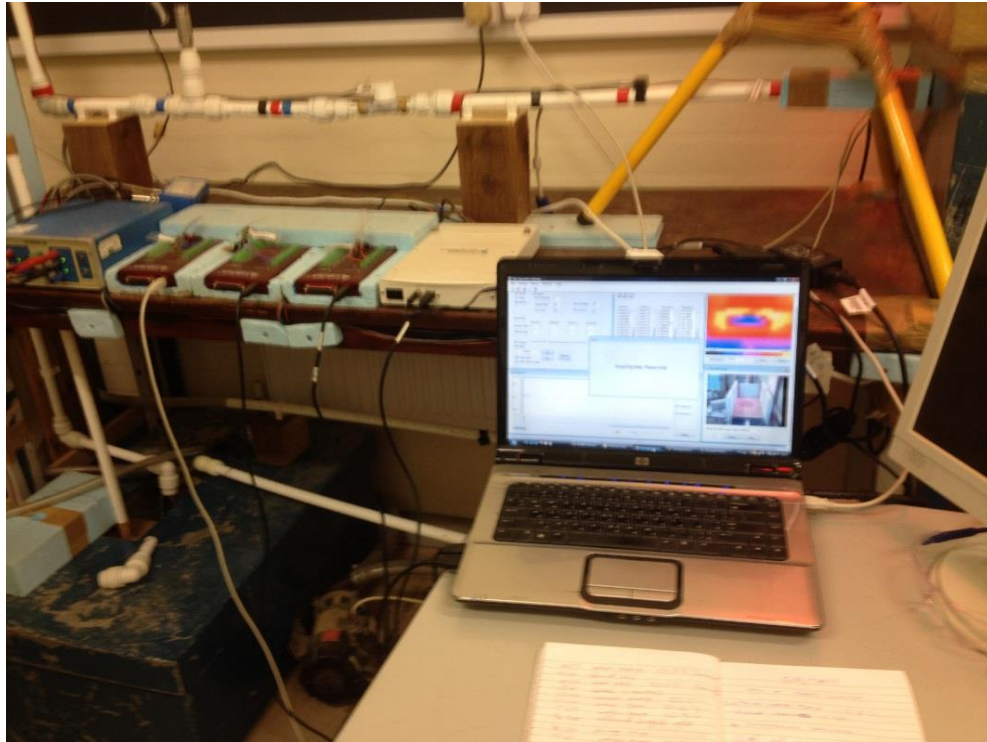
Figure 4.3: Part of the experimental rig with laptop during image and data acquiring process.

4.2.2.   LabVIEW software

LabVIEW (Laboratory Virtual Instrument Engineering Workbench) is a visual programing language designed for data acquisition by National Instrument. The source code of this language is based on structural block diagrams in which the programmers connects the block through connecting wires and nodes to build the program.

The LabVIEW used in this project to create two programs that can acquire data from the two flow sensors, two pressure sensors, and two AE sensors. Figure 4.4 and Figure 4.5 show the GUI for the two programs.

4.2.3.   Matlab

One of the powerful tools used in the analysis work and developing algorithms in this project is Matlab software. It is a high level programming language software with an interactive environment. It is classified as a matrix-oriented programming language. With Matlab, users can develop applications for image and signal processing, control systems, computational finance [126].
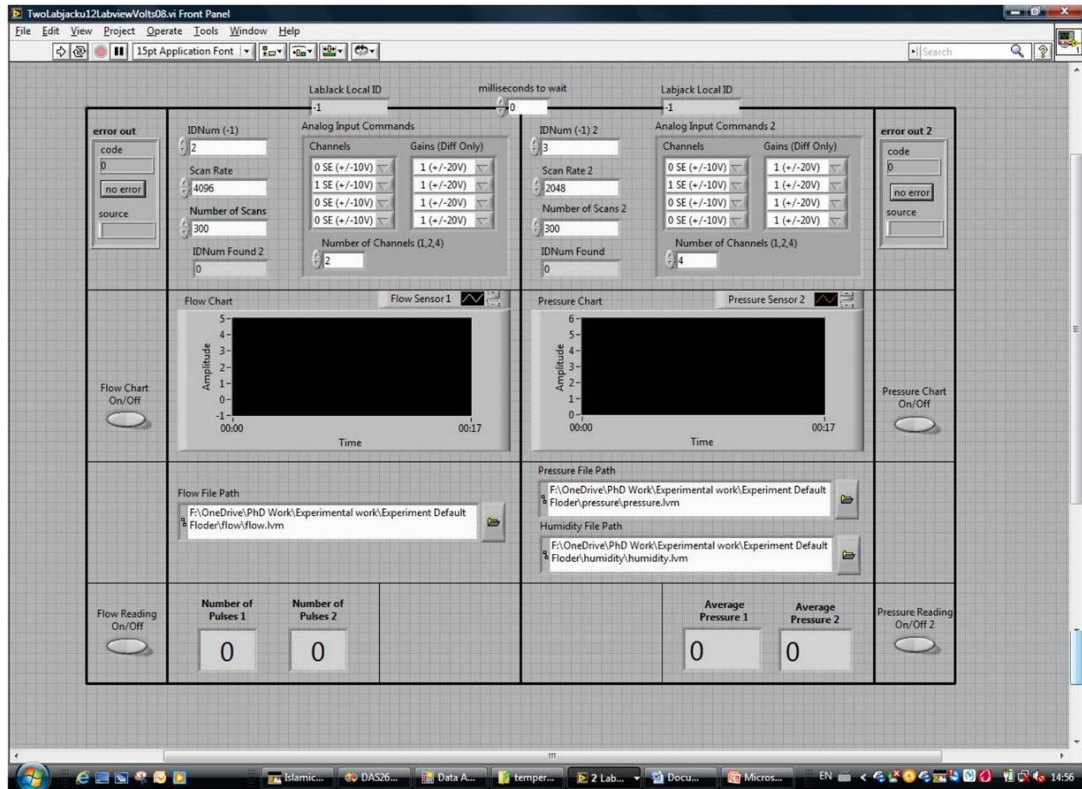
Figure 4.4: LabVIEW GUI for acquiring of flow and pressure readings
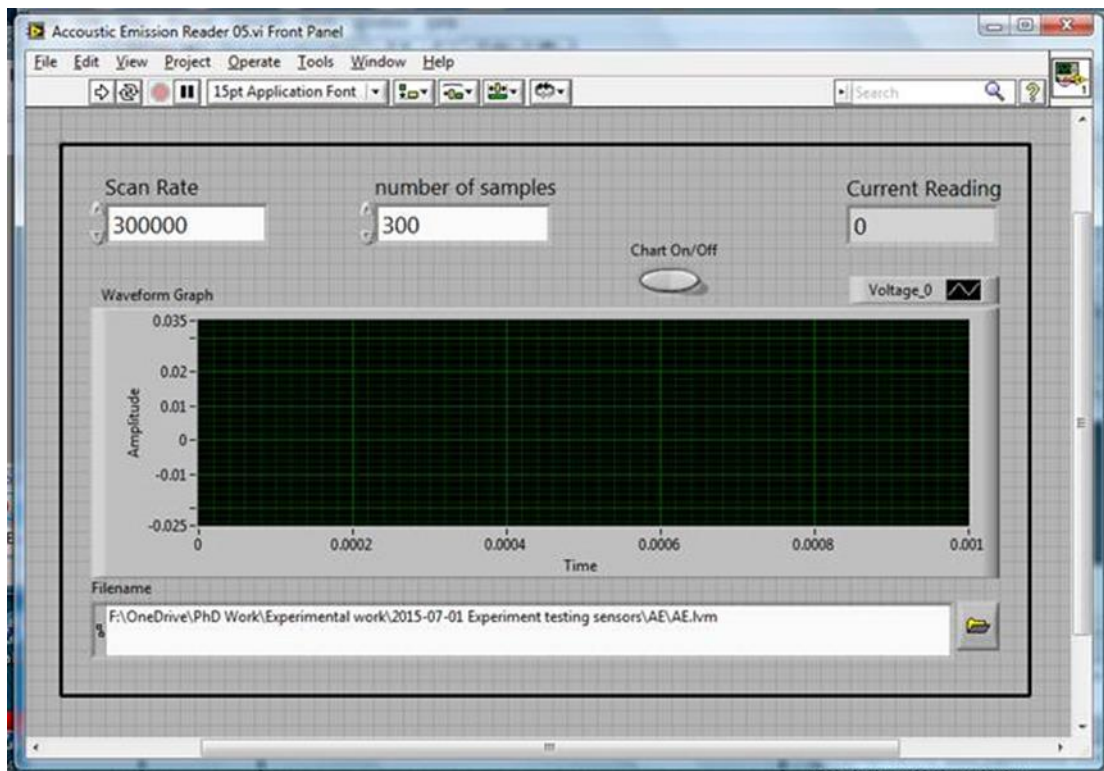
Figure 4.5: LabVIEW GUI for acquiring AE readings

4.3. The experimental test rig:

Figure 4.6 and Figure 4.7 show the final design of the rigs (2D and 3D) which implemented in the laboratory. The figure shows the complete test rig as it has been built in the laboratory. The rig consists of the pipeline, the test area, the high-resolution camera, the low-resolution camera, the infrared light, the water pump, the water source tank, the cooling machine, and the sensors (AE, pressure, flowmeter).
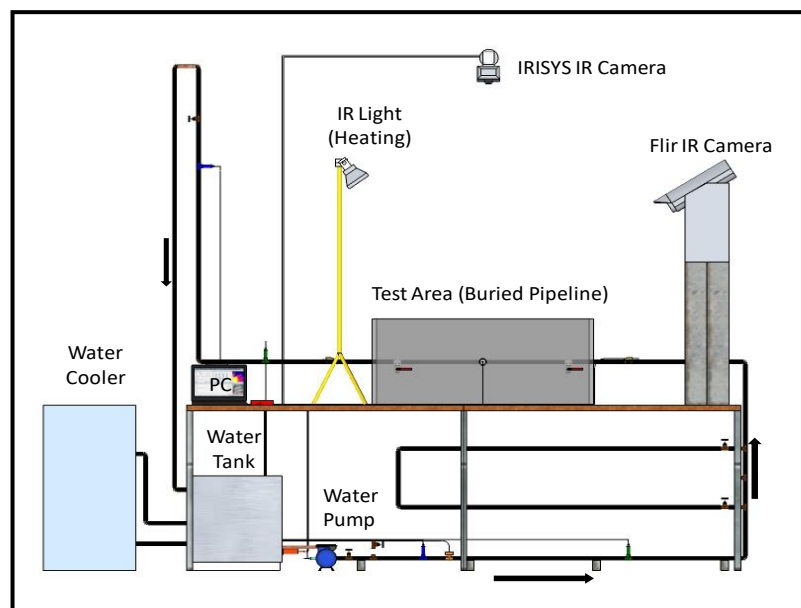
Figure 4.6: The final design of the experimental test rig.
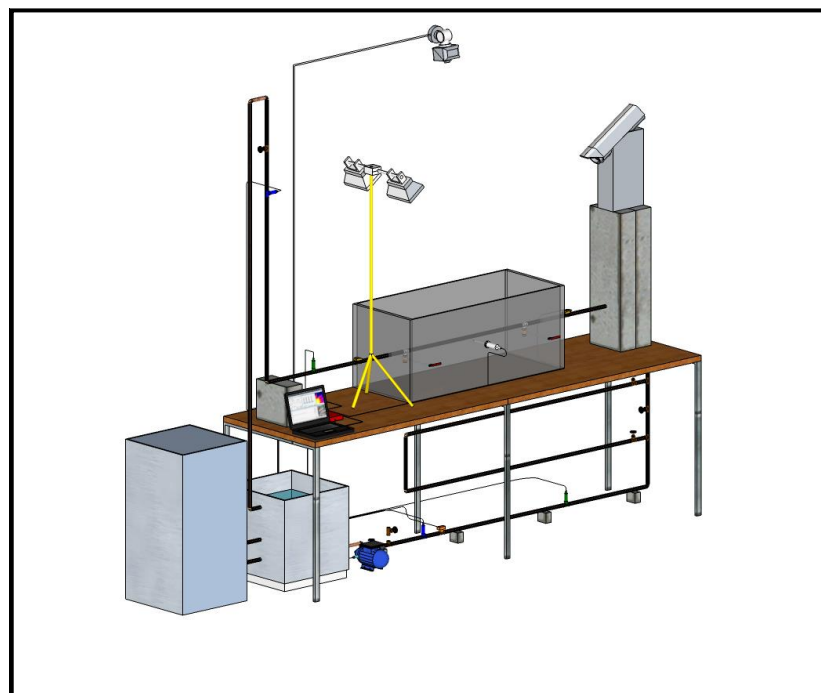
Figure 4.7: Final design of the Experimental Rig in 3D view.

4.3.1. Experiment Rig Setting Up Work:

The actual experimental rig is shown in Figure 4.8. All the pipe work and sensors installation installed in the lab.
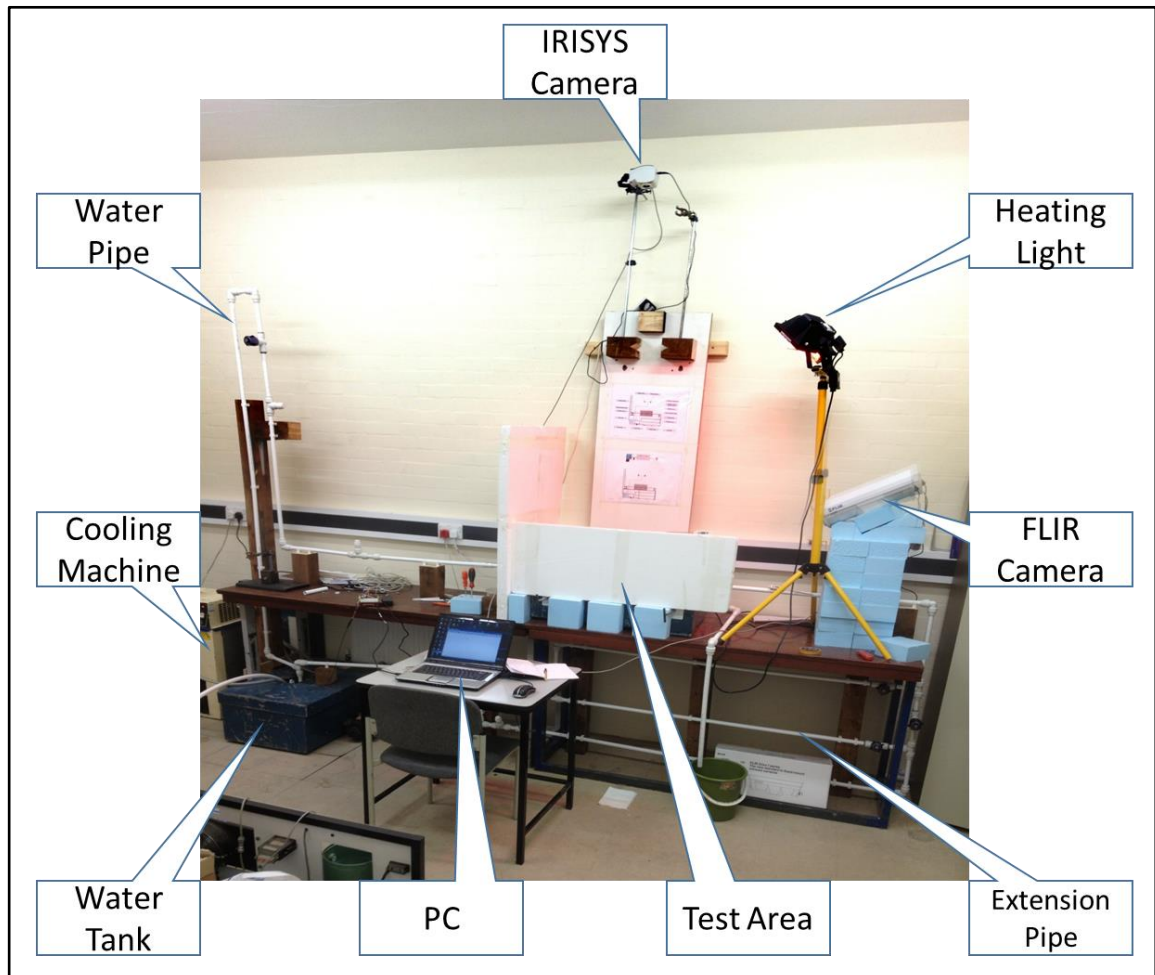
Figure 4.8: The complete actual test rig during operation

4.4. Sensors and Monitoring Devices:

4.4.1.   Thermal Camera (IRISYS 1011):

Figure 4.9: IRISYS Series 1011 Thermal Imager

The used IRISYS 1011 camera in this project is a low-resolution and low-cost infrared imager that can be easily used as a measuring device for temperature. Despite its low-resolution and low-cost it is still an excellent camera in thermal imaging techniques. It operates by either four standard AA size batteries or AC power. The thermal imager is connected to the computer through RS232 serial cable. Getting data of any image using this device requires sending a trigger command to the thermal imager to start and then sending back the image data. It programmed and worked with the in-house made software successfully. The IRISYS produces a 16x16 low-resolution image which can be transferred to a better resolution using interpolation method to enhance its visibility for human [46].
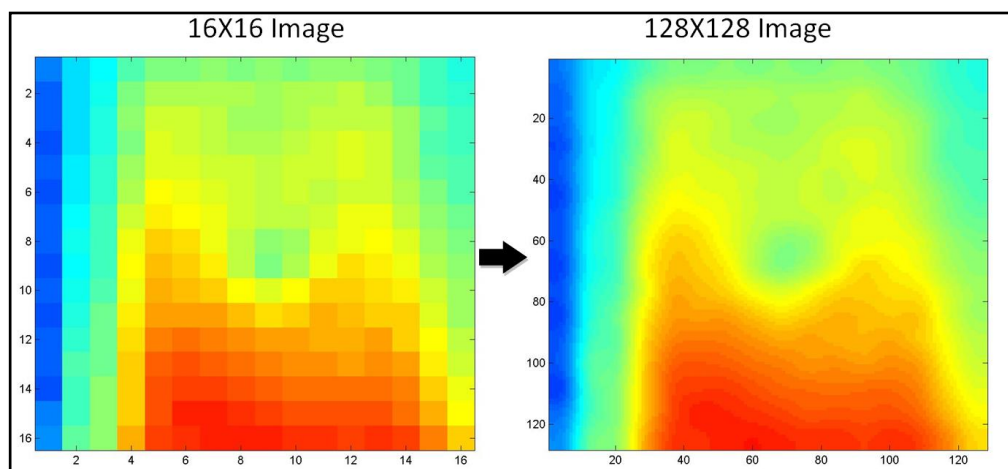
Figure 4.10: IRISYS Original Image and processed image.

The process of capturing data with this image starts with capturing the data in a form of one dimension array. The array then converted to matrix of temperatures processed using interpolation technique by a software such as Matlab to produce high-resolution images in different image techniques. Figure 4.10 shows the 16X16 original image created from IRISYS one dimension data and the 128X128 final processed image.

4.4.2.   Low-resolution Camera setting up:

In order to take the image of the exactly tested area, the corners and the centre of the tested area marked using small five hot water cups. The cups located in each corner so the camera adjusted accordingly.

Figure 4.11: Adjusting the low-resolution camera

4.4.3.   IRISYS Calibration:

The thermal camera tested to make sure that it is capturing and correctly measuring the temperature of the targeted area. The following image shows the result of a heated surface with a spot of water on it. Figure 4.12 shows that the point located on the water spot is cooler than the one located outside of water spot. The camera showed temperature of the surface close to actual temperatures measured for the soil as the emissivity of the dry soil and the saturated soil with water is high and ranges from 0.92 to 0.95.
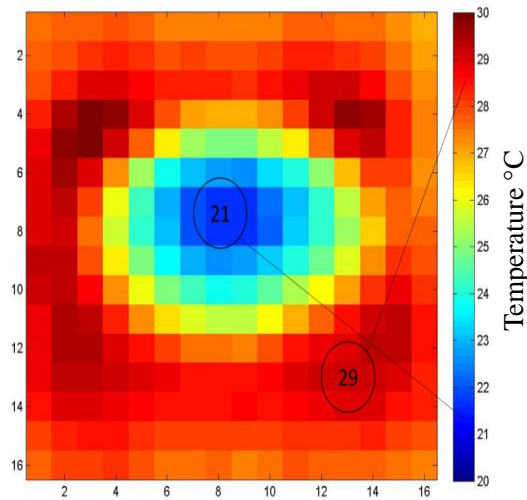
Figure 4.12: IRISYS image shows water spot.

4.4.4.   Flir Camera A310f

Figure 4.13: Flir IR Camera A310f.

Flir A310f is a relatively high cost, a high-resolution infrared camera of f-series camera with network connectivity. This camera takes videos and images and can be controlled online over a network. The resolution of the camera is 640X480 pixels that can produce images of greater details and superior detection. The camera is normally used for monitoring, process monitoring, quality control, fire detection in hazardous areas as well as a security camera.

Despite the camera producing high-resolution and high-quality images, the images require extra processing to extract the required features.
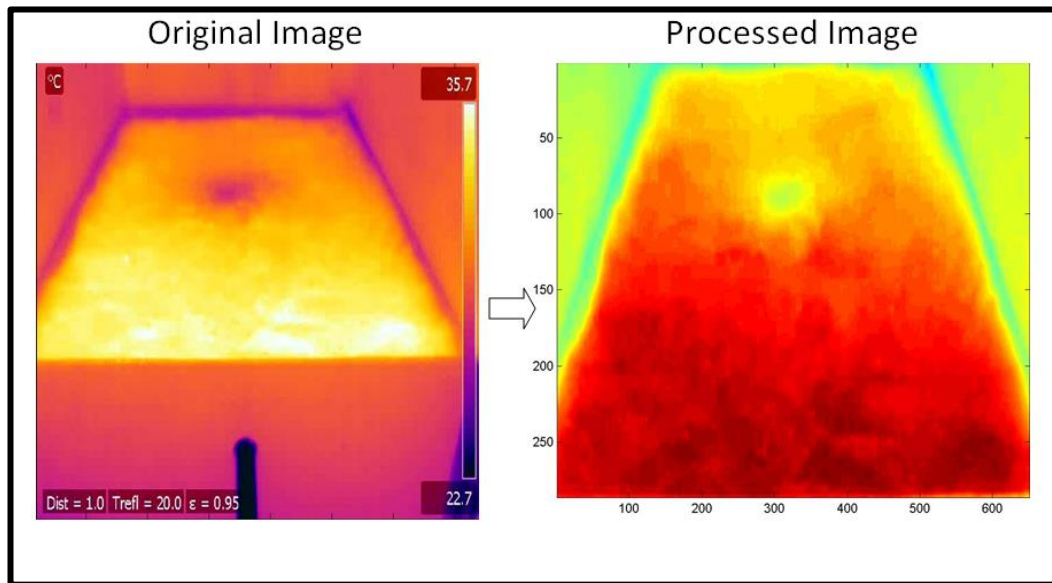
Figure 4.14: Flir Original Image and processed image.

4.4.5.   Flir camera calibration:

The Flir camera has been subjected to test to make sure that it is been set correctly and read correct temperature. The camera found to give temperature close to actual temperature. Figure 4.15 shows a cold spot which is the water on the soil surface. The camera showed temperature of the surface close to actual temperatures measured for the soil as the emissivity of the dry soil and the saturated soil with water is high and ranges from 0.92 to 0.95.
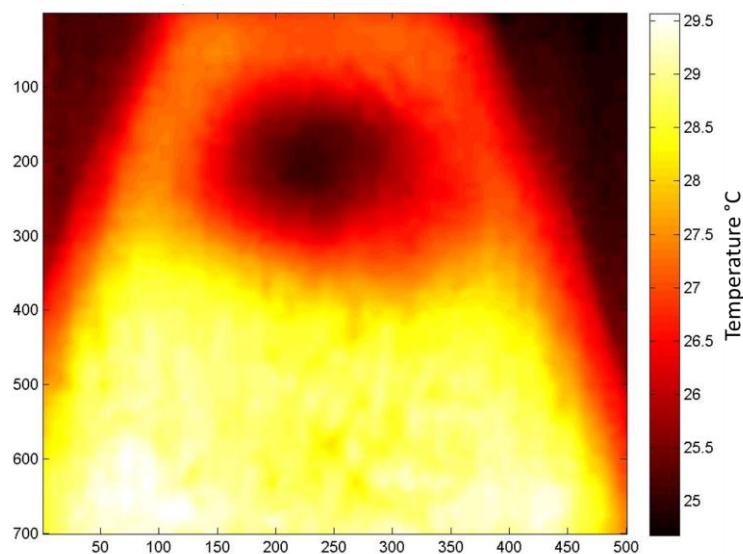
Figure 4.15: Flir image shows water spot

4.4.6.   Visual Camera (Microsoft Web Cam):

It is a 1.3 megapixel HD video capture and 5.0 megapixel interpolated image capture ability. The camera can be easily plugged into computers through USB connection. It has an adjusting ring around the lens to adjust the lens focusing Figure 4.16 and Figure 4.17
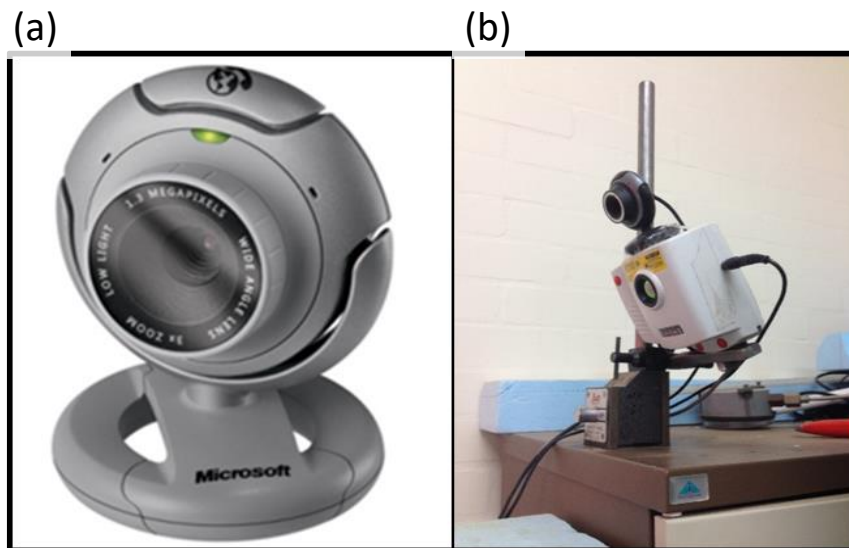
Figure 4.16: The Microsoft Web Cam (a) and the camera installed above the IRISYS imager (b).

Figure 4.17: The test area as seen by the visual camera.

4.5. Data Acquisition Devices

4.5.1.   LabJack U12

LabJack U12 (Figure 4.18) is a data acquisition device that can be used to connect several instruments to the computer. The LabJack U12 designed to operate with PCs running Microsoft Windows. The device does not need external power supply as it is simply connected to computers through USB connection which provides power and communication. The LabJack U12 has 8 terminals for analogue input signals. These signals utilised as eight single channels, four differential channels or combinations in between.

Figure 4.18: The LabJack U12.
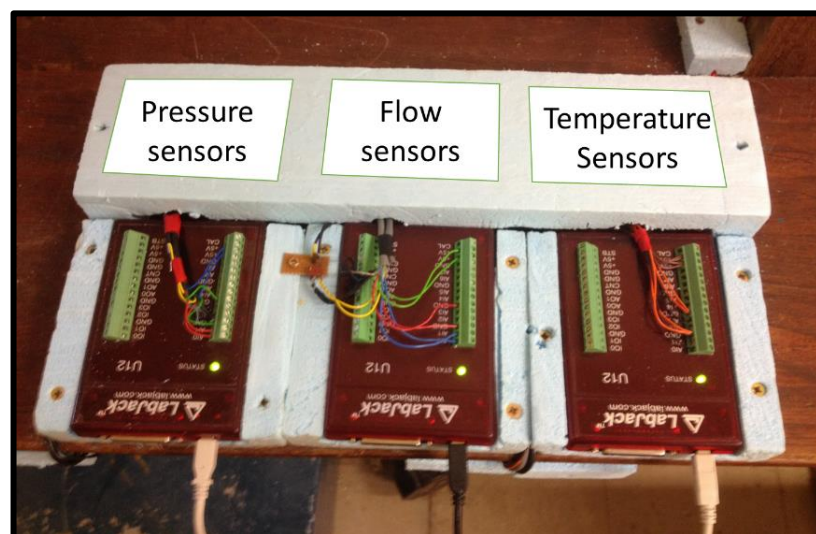
Figure 4.19: The data acquisition in situ.

4.5.2.   National Instruments DAQ USB

National Instruments data acquisition device is a high frequency and high accuracy data acquisition device with a high sampling rate up to 652k sample per second. This device has been dedicated to the AE sensor for its high-frequency data acquisition rate. The device provided with 32 analog inputs at 18 bits and up to 4 analog outputs.

(a)   **(b)**
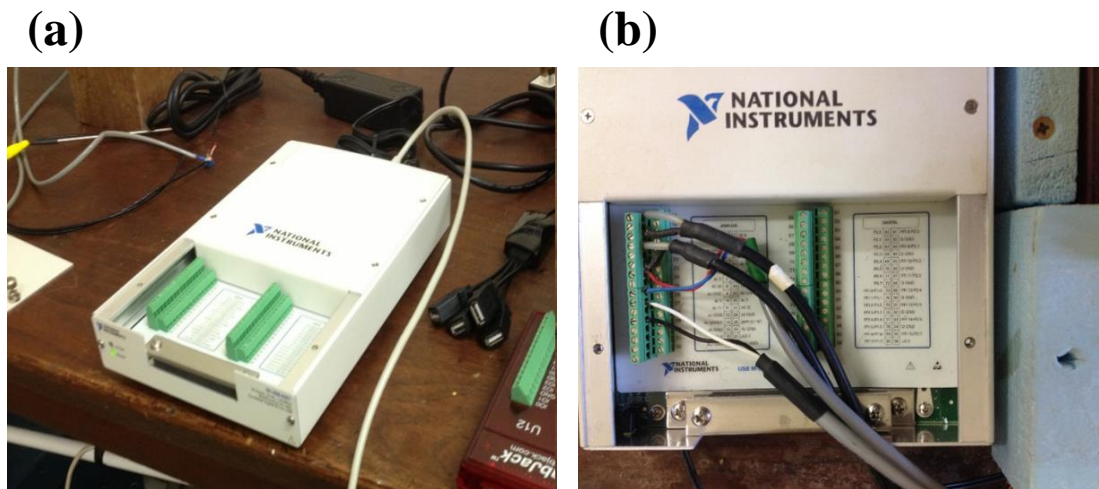
Figure 4.20: National instruments data acquisition device. Image (a) before connection. Image (b) after connection.

4.6. Sensors:

In order to capture the required signals a special set of sensors are installed on the test rig. All the sensors are connected to a computer system through the data acquisition devices to record the data by using the in-house software. The used sensors in this project are Pressure sensors, Acoustic emission sensors, Flowmeters, and temperature sensors.

4.6.1.   Pressure Sensor

It is a series voltage pressure transducer. It is an absolute, sealed pressure gauge sensor with maximum pressure operates in environment with -20 ℃ to 125 ℃ and produces analogue output of 0-5v. Its accuracy is 0.25%. The range of the sensor is 0 to 6 bar.

Figure 4.21: Pressure sensor

4.6.1.1.   Calibrating the pressure sensors

Two pressure sensors are used in this work. One is installed in the upstream side and the other in the downstream side. Before use, both sensors have been subjected to in-situ calibration at the same level in order to confirm that both pressure sensors produce an identical reading. (Figure 4.22).

Figure 4.22: Calibrating the pressure sensors

Figure 4.23 shows the result of the calibration results. As the output of the sensors is in volts, the readings converted into bars. The output of the sensor is 0-5V according to the specification provided by the data sheet and corresponds to 0-6bar. Therefore, the output can be easily coveted from volts to bars by multiplying the output value by 1.2 as a factor of conversion.

$$\text{Pressure}= 1.2 \ V \hspace{4cm} \textbf{(4-1)}$$

The upper subplot of the calibration shows discrepancy in reading between the two sensors when no pressure is applied (loose sensors). The two sensor is located on the same

level on the ground and subjected to no pressure at all. The difference in reading is calculated and used as a reference for corrections. The lower subplot shows the calibrated results. By calculating the mean value of each sensor and subtract it form the results of each sensor consequently the readings becomes identical at the same level and pressure.
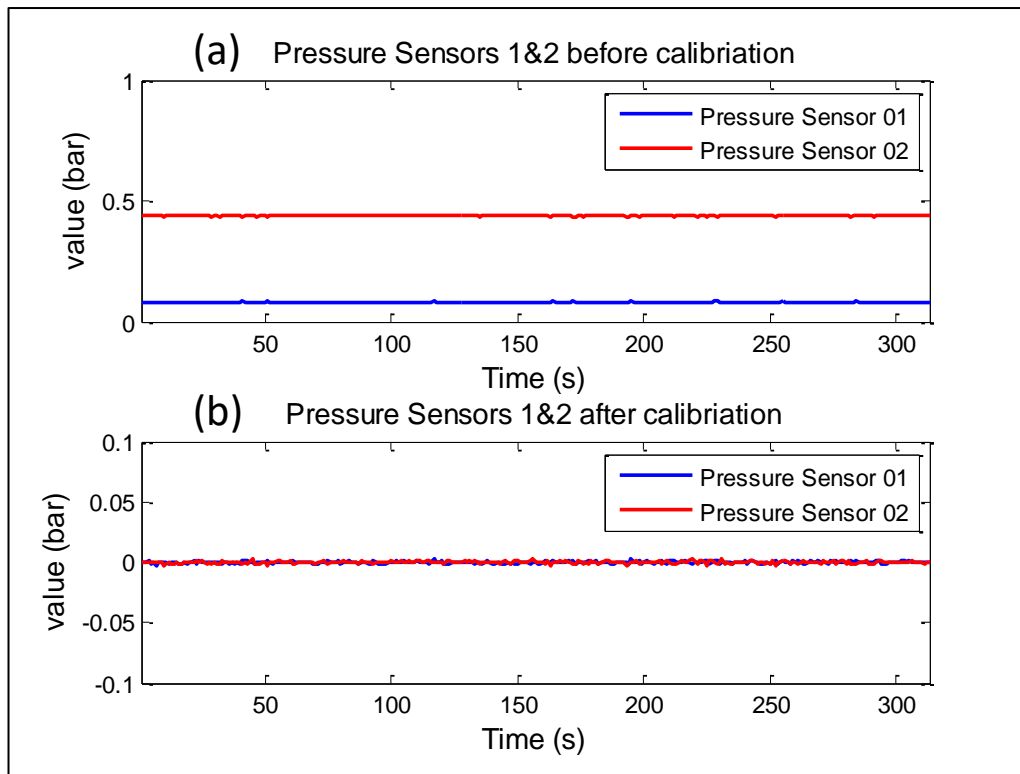
Figure 4.23: Calibration results for the pressure sensors. (a) Before calibration. (b) After calibration. In this case, both sensors tested with no pressure applied. The sensors are loose and at same level on ground.

Figure 4.24: The upstream pressure sensor in situ

The results of the two sensors (before and after calibration) once installed on the pressurised pipeline Shown in Figure 4.25 . The pipeline operated in several conditions

with the end valve open with different percentages from 100 to 0 and vice versa to get those results.
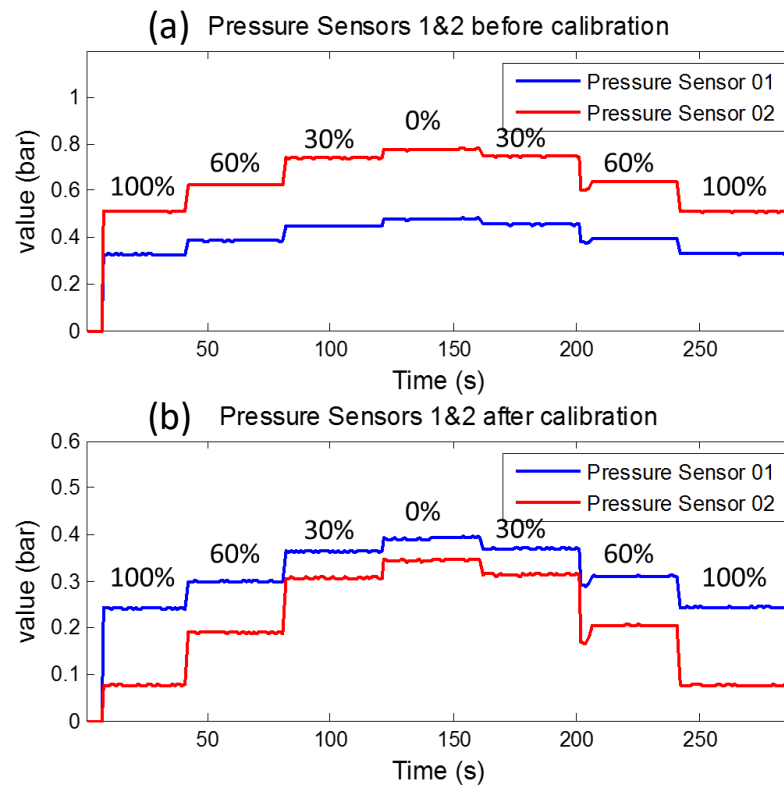
Figure 4.25: Calibration of the two sensors with multiple end valve open percentage. The pressure sensors before calibration (a). Pressure sensor 2 (downstream) incorrectly is higher than presser sensor 1 (upstream). The pressure sensors after the calibration (b).

4.6.1.2.   Verifying the sensitivity of the two pressure sensors to the leak

The sensitivity of the installed pressure sensors verified as a part of the calibration process in order to detect the leak once it occurs by the sensors Figure 4.26. The results show that the downstream sensor (sensor no. 2) is less sensitive to the leak than the downstream sensor (sensor no. 1) especially when the end valve is at 100% open or 60% open. This means that sensor 2 can detect the leak easily.
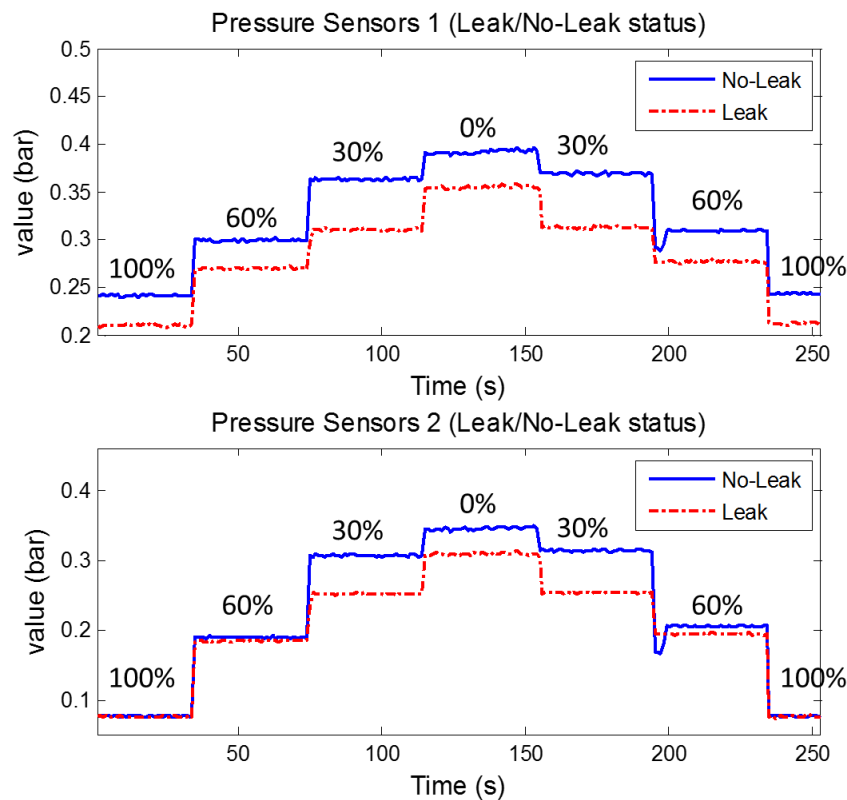
Figure 4.26: Sensitivity of the pressure sensor to the leak. The % is the amount of opening and closing the end valve to control the pressure in the pipeline.

4.6.2.   Acoustic Emission Sensor: Piezotron Acoustic Emission Sensor

The sensor has high sensitivity and wide frequency range robust, suitable for industrial use. It operates in -40°C to -60 °C temperature range. It operates with a Piezotron coupler. The coupler has a built-in RMS converter and a limit switch for processing the high-frequency acoustic emission signals received from the AE sensor (Figure 4.27). For technical details see Appendix H.

**Figure 4.27: Piezotron Acoustic Emission Sensor
(http://www.kistler.com/IT_en-it/13_Productfinder/App.8152B121/Acoustic-Emission-Sensor.html)**

Figure 3.27 shows the AE sensor installed on the rig. There are two sensors on the rig. One is installed on the upstream side which is located before the test area and the other one is located on the downstream side after the test area.

Figure 4.28: Acoustic Emission Sensors 1 & 2 in situ.

4.6.2.1.   AE sensor calibration:

The Piezotron Acoustic Emission Sensor is a new purchase from Kistler. This sensor is calibrated in the factory (See appendix H).

4.6.3.   Temperature Sensor:

The temperature sensor is installed on the rig for monitoring purposes to record the temperature of the water, the pipe, and the environment. Similar to all installed sensors the temperature sensor subject to calibration and programmed to work with the software. Figure 4.29 shows the temperature sensor installed on the pipeline. Figure (a) shows the sensor protected and (b) shows the sensor before protection.

(a)   (b)
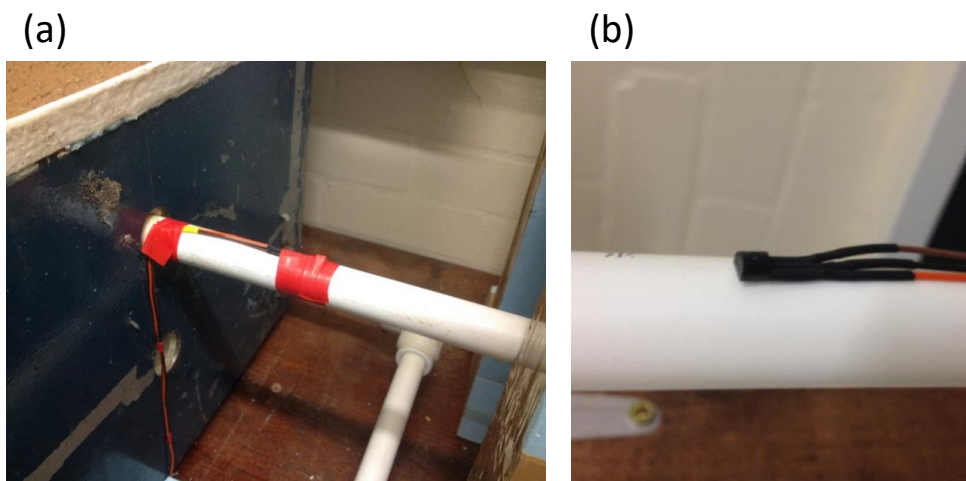
Figure 4.29: Temperature Sensor in situ on the test rig.

4.6.4.   The Flowmeter

A simple flow transducers (sensor/switch) without Indicator from RS Company designed to work with 4.5 - 16V dc and able to stand up to 20bar pressure used in this study. The flowmeter measures the flow by providing a pulse frequency proportional to flow rate. The pulse generated by LED and photodetector separated by a turbine. For technical details see Appendix H.

Figure 4.30: The upstream flowmeter in situ

Figure 4.31 shows the wiring of the flowmeter and the connection to the data acquisition device Labjack U12.
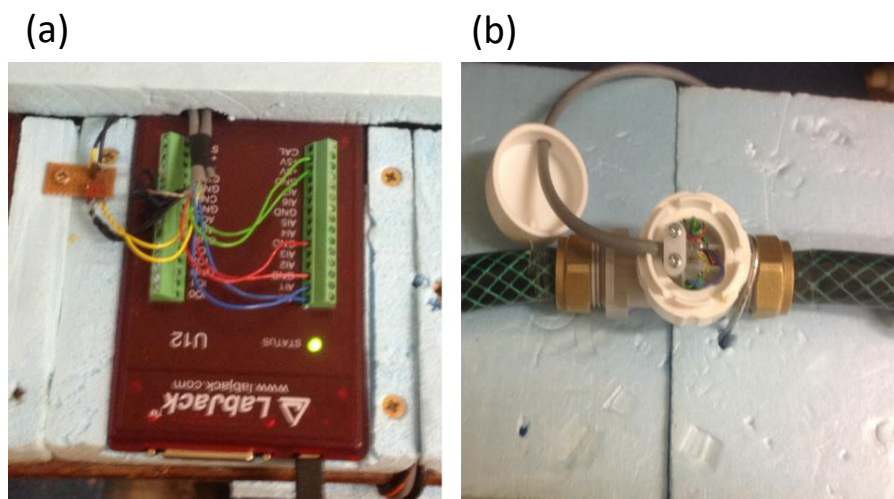
Figure 4.31: Wiring the flowmeter. Image (a) shows the wires of two flowmeters connected to the Labjack U12. Image (b) shows the wiring for one flowmeter.

4.6.4.1. Calibration of the flowmeter

The flowmeter is subjected to calibration before used in monitoring the flow. The flowmeter counting the flow by the number of rotations of its built-in turbine. One complete rotation of the turbine produces one complete pulse. In normal operation (End Valve open 100%), in average, each 18 readings acquired from the flowmeter produce one complete pulse (Figure 4.32). As shown in Figure 4.33, the flowmeter produces 16 to 17 pulse per second when the flow is intact and the end valve is 100% open. The pulses per second converted to a litre per second in accordance with the results of the actual flow measurements carried out manually in the laboratory (see Table 4-1). The measurement performed by filling a container several times for the same period of time and calculating the average of the amount of water filled the container. Accordingly, the average of water flow per second is 0.053 l/s which means that each pulse resembles 0.0033 l/s approximately. The calibration and the verification of the amount of water flowed per second through the pipeline system identified by calculating the amount of water level drop in the source tank.
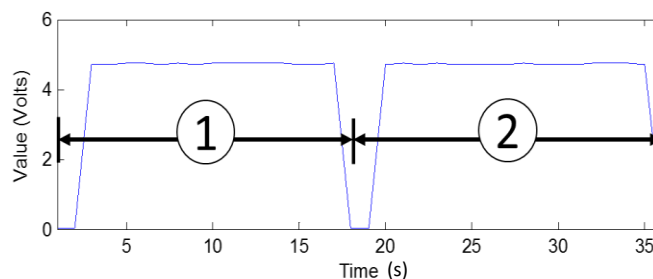
Figure 4.32: Two complete pulses produced by the flowmeter.
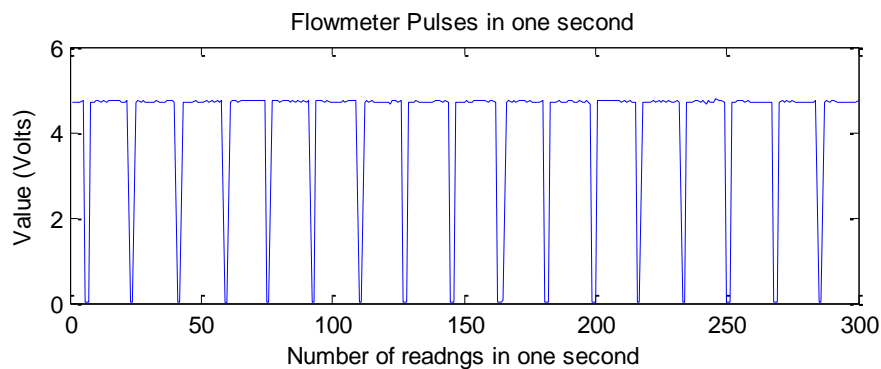
Figure 4.33: Original readings produced by the flowmeter per second in intact flow.

4.6.4.2.   Flow variation

When flow varies, the size of pulses varies as well because the number of the rotations of the turbine inside the flow change by the amount of flow. When the speed of the turbine increases the number of pulses increases and its size decreases while and vice versa.   In other words, larger size pulse lower flow and smaller size of pulses produce higher flow fig.
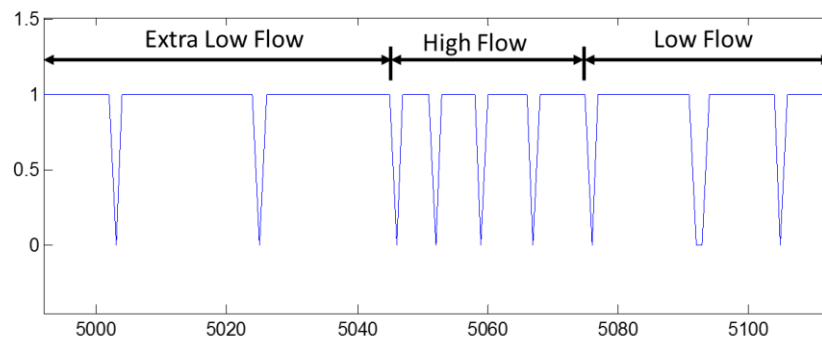
Figure 4.34: Variation of the flow

Table 4-1 shows the results of three trials of flow rate calculation where the amount of flow is compared with the number of pulses. The main tank water level used in judging the amount of water flowed in the assigned time.

Table 4-1: Experimental Rig Flow Rate Calculation

Trail	Elapsed Time (Minute)	Start Level (cm)	End Level (cm)	Level Drop (cm)	Length (cm)	width (cm)	Volume (cm3)	Volume (litre)	Flow Rate (l/s)
1	7	16.7	10.6	6.1	76	50.5	23411.8	23.412	0.056
2	7	16.65	10.75	5.9	76	50.5	22644.2	22.644	0.054
3	7	17.2	11.7	5.5	76	50.5	21109	21.109	0.050

Average flow (l/s)
0.0533
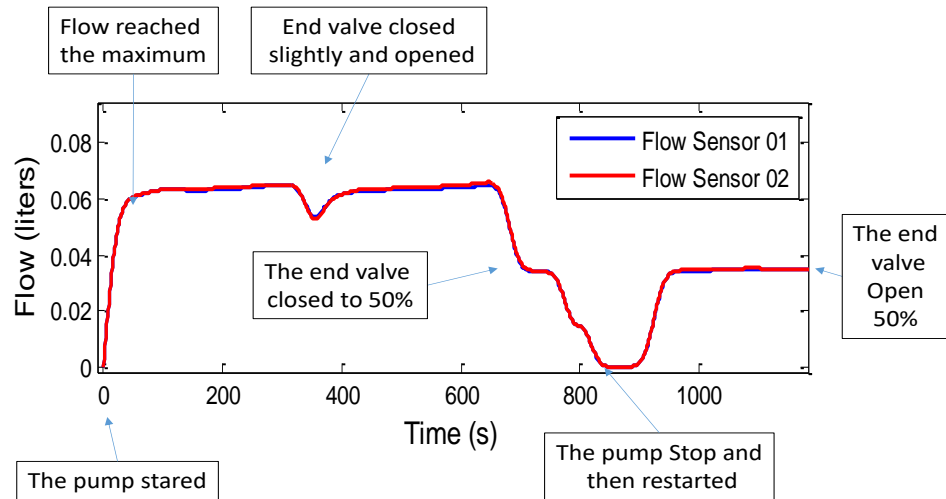
Figure 4.35: The response of the two flowmeters after calibration.

Figure 4.35 shows the profile of the flow rate per second for the two sensors together and how their profile change and varying with the change of the flow amount. The flow is controlled by closing and opening the end valve.

As shown in Figure 4.36 the flow rate via the two flowmeters before the leak is matching together and changed once the leak started. After the leak, the downstream flowmeter gave a higher flow rate as an extra amount of water escaped from the leak point. At the same time, the amount of water flowing through the downstream flowmeter has reduced.
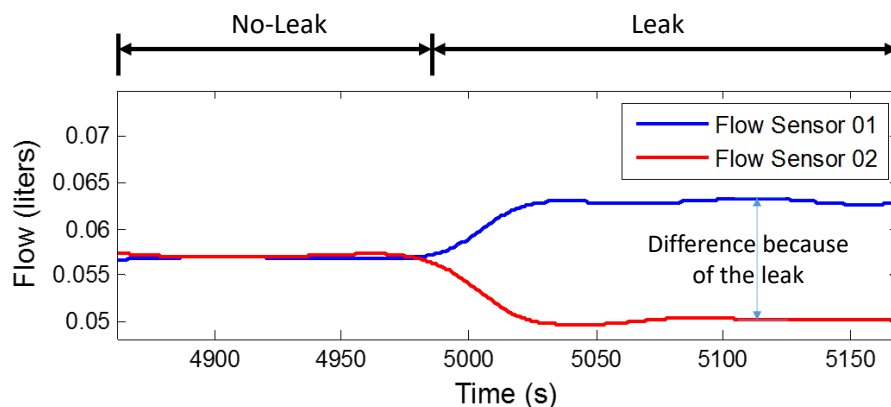
Figure 4.36: Flow rate change with leak for both upstream and downstream flow sensors

4.6.5.   Pipeline System Important components:

1. Water Pipe

The pipe is made of plastic material. The pipe with plastic material is selected because the plastic is known as non-conductive material as well the signal in plastic material are much weaker than the metallic material.

2. Water Tank

The main water tank is the main inlet and outlet point for water in the test rig. The water runs in a loop and returns to the same tank. The water level in the tank is monitored manually during the operation. Because the tank is the inlet and the outlet at the same time, the level should remain unchanged all the time as the water returns to the same tank. The amount of water lost because of the leak is calculated from the tank.

3. The Test Section (Test Area)

The test area is where the leaked pipe is located. It is a container (steel box) filled with soil. The test piece of the pipe is passing through the test section. The Figure 4.37 shows multiple photos of the test area in different situations.
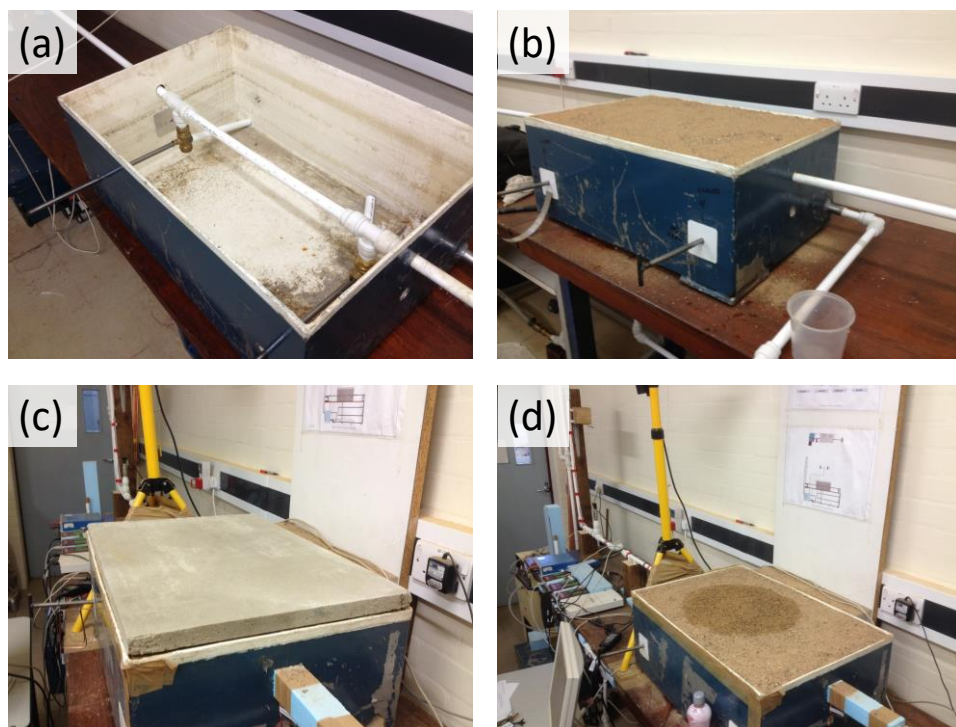
Figure 4.37: Test Area. (a) Empty and shows the test pipe. (b) The test box filled with soil. (c) The test area covered with concrete. (d) The Test area with leak spot.

4. **Valves**

 The valves are a ball valve type to easily control the size of the valve opening. There are several valves installed in the experimental rig to control the flow. The important valve is the end control valve because it is used to control the flow and the pressure of the pipeline.

5. **The Water Pump**

A centrifugal water pump with horizontal suction and vertical delivery used in the test rig. The pump is driven by an electrical motor 220/240 with auto reset thermal trip for overload protection.

Figure 4.38: the water pump/motor

4.6.6.   Infrared light

An infrared light used in order to create an environmental condition inside the laboratory similar to the real environmental condition in which the ground above the buried pipeline system heated up by the sun during the daytime and cooled down at the night time. The infrared light simulates the sun and heats up the test area when switched on. The period in which the infrared light is switched off simulates the night time where the soil in the test area cools down fig.

Figure 4.39: infrared light in use

4.6.7.   Cooling machine

A water cooler used to cool the water in the source tank to the required temperature in each scenario of the experiments (Figure 4.40).
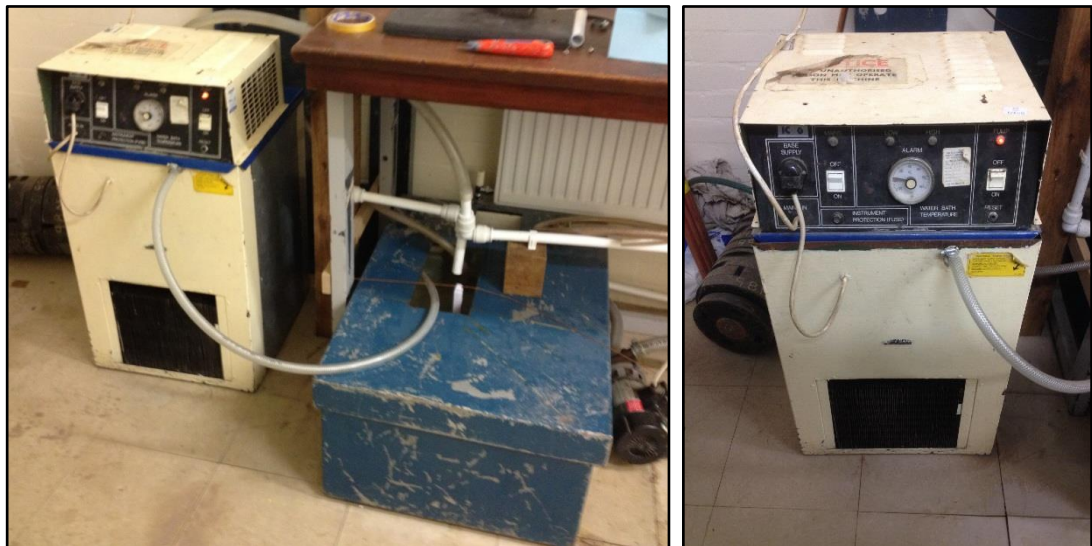
Figure 4.40: The water cooler connected to the source tank

4.7. Summary

The chapter provided details about the experimental rig and explained each item to be installed on the rig and illustrated their function. The use of its component. The chapter introduced the in-house software that used to save the data collected from different sensors and cameras. Details about the used sensors and how they are connected to the rig and how they have been wired, calibrated and linked to the software with the data acquisition devices. It has been demonstrated how the sensors are operated successfully.

The experimental rig designed to match with a real environment of a hot place as it has been equipped with infrared light which is used to simulate the sun. The rig also provided with a cooling machine to be used in cooling the source water .The chapter detailed all the work carried out to build the test rig inside the laboratory of the university.

Chapter 5. Experimental work for infrared technology

5.1. Introduction

This chapter outlines the experimental work carried out in the lab using the high and the low-resolution cameras. The high-resolution camera used only in the first few experiments which have been assigned to investigate the ability of both Low-resolution and high-resolution cameras in tracking the pathway of the buried pipeline and to detect the leak. These experiments used to compare the two cameras. Both cameras have been operated simultaneously to capture the same images in the same condition. The rest of experiments carried out using the low-resolution camera only. Cooling of the source water is used in some of the experiments to see the effect of the cold water in the detection process. Also, an infrared light is used to heat up the test area surface to simulate the sun when it is heating the ground. Figure 5.1 presents the main framework diagram of the experimental work for infrared cameras.
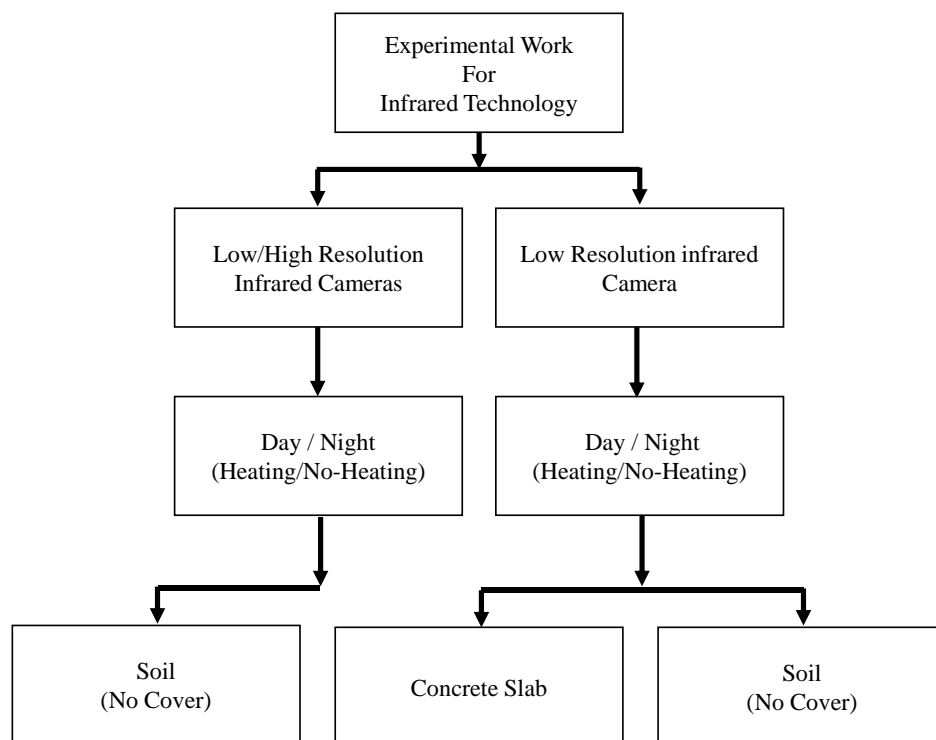
Figure 5.1: Main framework diagram of the infrared thermal cameras

Table 5-1 shows the details of the infrared cameras experiments. The experiments varied to simulate a different situation in a real environment. For example, the infrared light is used to heat the surface of the tested area to simulate the sun in reality.

Table 5-1: Details of the experiments.

Experiment No.	High Resoluiton Camera	Low Resolution Camera	No-Leak	Leak	No-Cooling (Water)	Cooling (Water)	No-Heating (Night)	Heating (Day)	Soil	Concrete Slab
1	✕	✕	✕		✕		✕		✕	
2	✕	✕	✕			✕ (Partial)	✕		✕	
3	✕	✕	✕			✕	✕		✕	
4	✕	✕	✕			✕		✕	✕	
5	✕	✕		✕	✕			✕	✕	
6	✕	✕		✕		✕		✕	✕	
7		✕		✕		✕		✕✕	✕	
8		✕		✕	✕			✕	✕	
9		✕		✕	✕			✕✕	✕	
10		✕		✕		✕		✕	✕	
11		✕		✕		✕		✕		✕
12		✕		✕	✕		✕			✕

5.2. Description of the processed images

Figure 5.2 shows three thermal images. Image (a) shows neither the pipeline nor the leak. Image (b) shows the pipeline as a thick vertical line. Image (c) shows the leak spot as a dark spot in the centre. Figure 5.3 and Figure 5.4 shows the pipeline pathway and the leak in 3D image respectively. Figure 5.5 shows the difference in temperature profile when the image contains leak spot or the image contains the pipeline pathway.
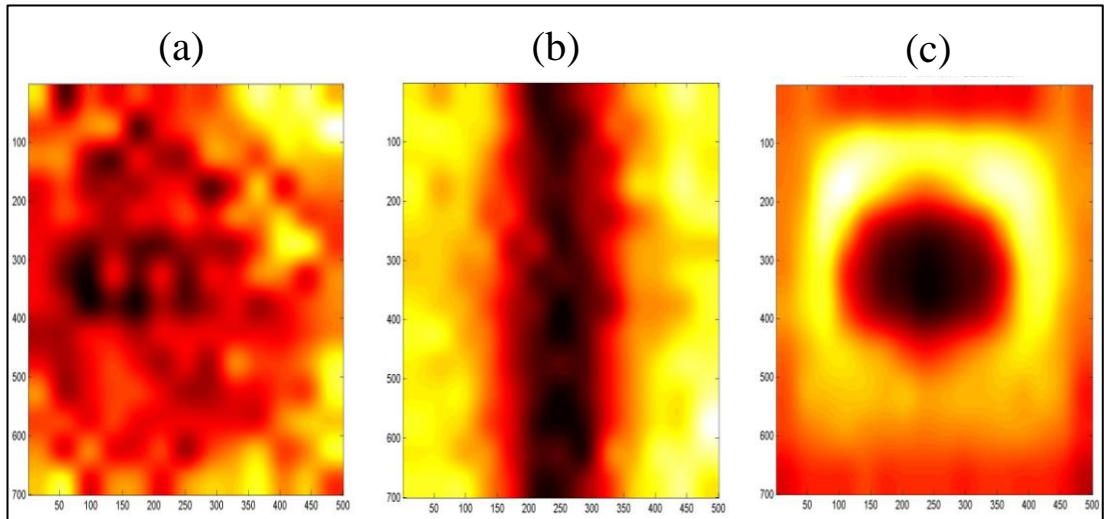
Figure 5.2: (a) image shows neither the leak nor the pipe, (b) image show the pipeline pathway, and (c) an image shows the leak spot.
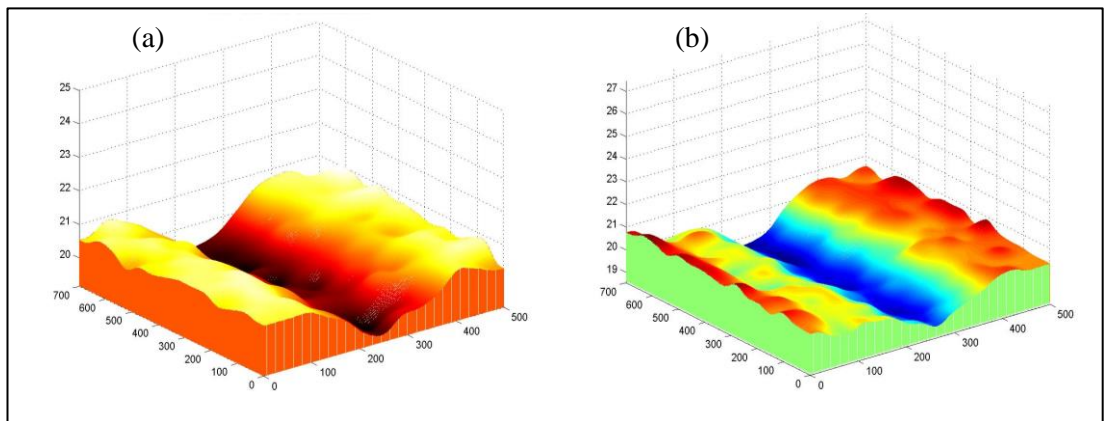
Figure 5.3: 3D representation of the pipeline pathway in two different colour maps. (a) An image in hot colour map and (b) is in jet colour map.
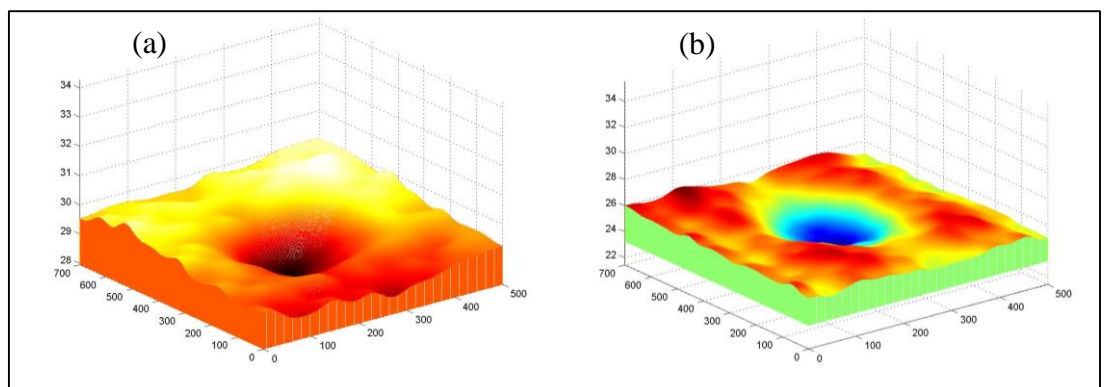
Figure 5.4: 3D representation of the leak in two different colour maps. (a) An image in hot colour map and (b) is in jet colour map.
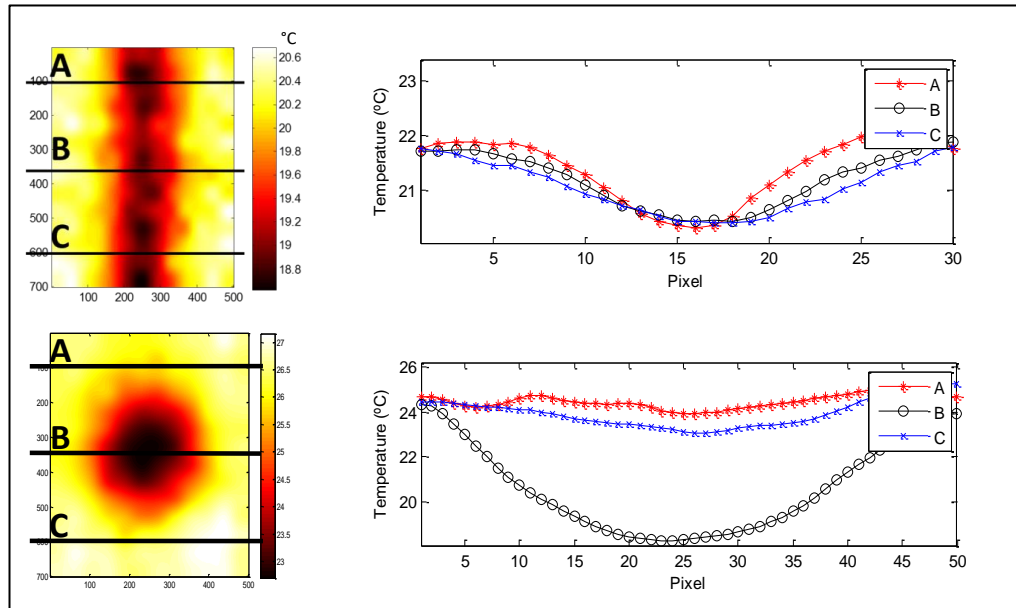
Figure 5.5: The figure shows the difference in temperature profile of the leak image and no-leak image.

5.3. Experiment no. 1 (No-leak, No cooling, and No heating)

The experiment run for three hours and revealed neither pipe pathway nor the leak. No cooling or No heating is used. Water temperature is 14.4 ℃ at the start and ended up with 15.6 ℃. The temperature of the experiment room is 18 ℃. Total of 81 images have been captured. Figure 5.6 present the results of the low-resolution camera and Figure 5.7 presents the results of the high-resolution camera.

Figure 5.6: Low-resolution camera images with max/min temperature graph.
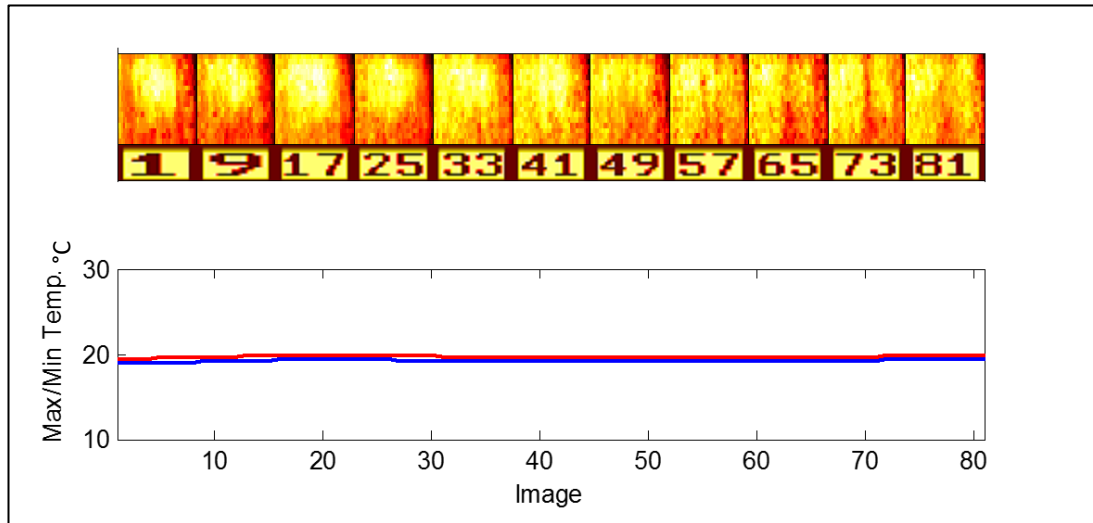
Figure 5.7: High-resolution camera images with max/min temperature graph.

The images of both cameras show no clear marks of the buried pipeline traces. However, in the last few images, the high-resolution camera show some blurred marks of the pipeline traces. As well as the low-resolution camera show some cold area in the middle of the last few images just above the pipeline. The temperature profile graph of the maximum and minimum temperatures in Figure 5.6 and Figure 5.7 for both cameras show no much difference between the minimum and the maximum temperatures. Figure 5.8 show an image of the low-resolution camera and the temperature profile of three lines across the image. Figure 5.9 show an image of the high-resolution camera and the temperature profile of three lines across the image.

Figure 5.8: Image of the low-resolution camera (a). Graph of the temperature profile of the lines A, B, and C across the image (b).

Figure 5.9: Image of the high-resolution camera (a). Graph of the temperature profile of the lines A, B, and C across the image (b).

5.4. Experiment no. 2 (No-Leak, Partial Cooling, and No-Heating)

This experiment has run for two and half hours. The water has been cooled to 10 °C at the beginning of the experiment and then left without cooling to become 15 °C at the end of the experiment. The temperature of the experiment room is 18.8 °C. Figure 5.10 and Figure 5.11 show images with max/min temperatures for both cameras.
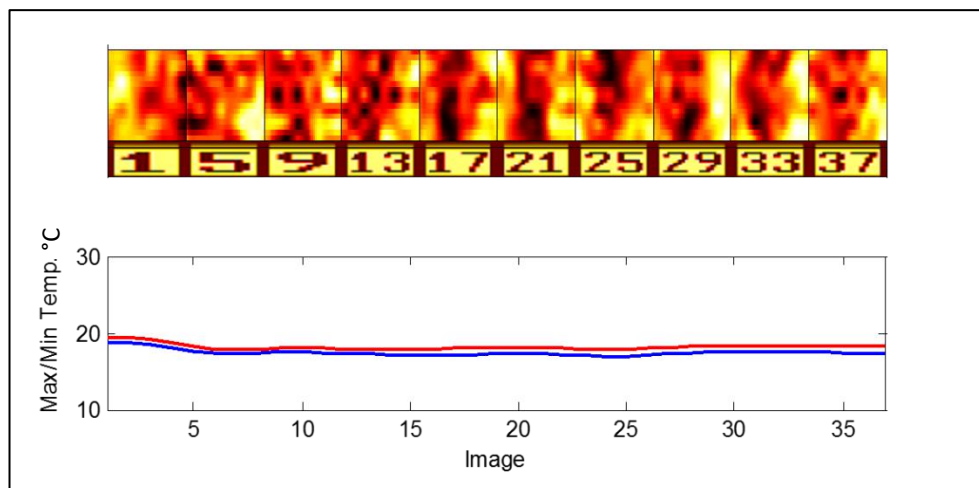
Figure 5.10: Low-resolution camera images with max/min temperature graph.

The two temperature profiles in Figure 5.10 and Figure 5.11 of both cameras show marks of the pipeline traces. However, the image from the high-resolution camera was clearer than the low-resolution camera as shown in Figure 5.12.
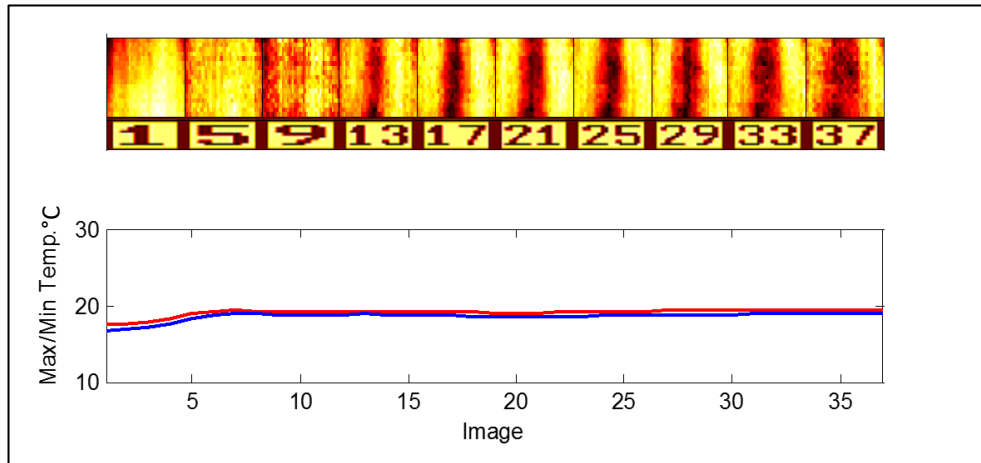
Figure 5.11: High-resolution camera images with max/min temperature graph.

Figure 5.12: Image of the low-resolution camera (a). Graph of the temperature profile of the lines A, B, and C across the image (b).
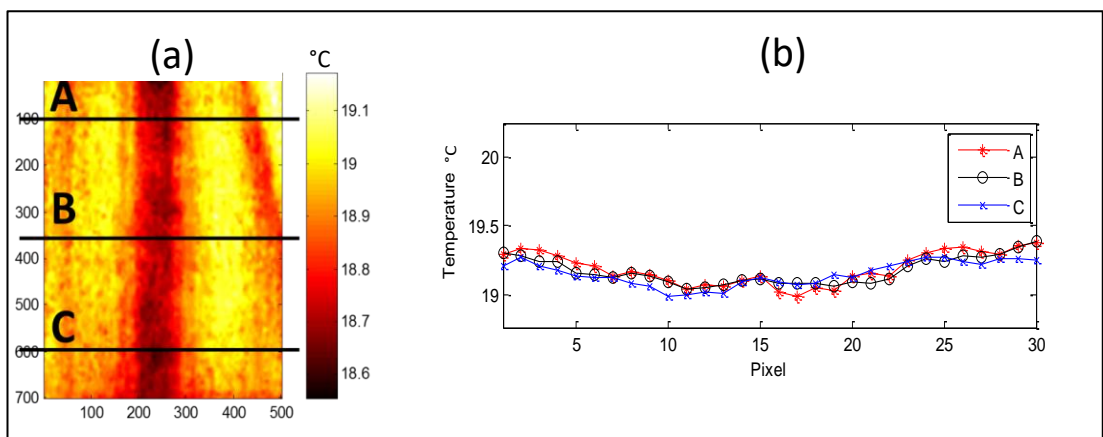
Figure 5.13: Image of the high-resolution camera (a). Graph of the temperature profile of the lines A, B, and C across the image (b).

This experiment demonstrates that after using a cooled water, both cameras have detected the pipeline pathway in a shorter time. However, the high-resolution camera is more precise than the low-resolution camera in finding the pathway. The series of images in Figure 5.10 and Figure 5.11 show that while the water was cooler, the visibility of the pathway was better in both cameras but when the water temperature increased, the pipeline pathway in the last few images started to fade out. The temperature profile in Figure 5.12 & Figure 5.13 shows lower temperature profile for the lines A, B, and C in the middle section which is located exactly above the pipeline.

5.5. Experiment no. 3 (No Leak, Full cooling, No Heating)

In this experiment, extra cooling has been added to the source water and run for a longer time than the previous ones. The experiment run for almost four hours. The temperature of the water cooled to 5 ºC. Using the cooling machine, the cooling process continued to the end of the experiment with an average temperature of 5 ºC. Figure 5.14 shows series of images with max/min temperature of the low-resolution camera. Figure 5.15 shows a series of images of the high-resolution camera with the min/max temperature. The min/max graphs show an increase in the difference between the max and min with the increase of the pipeline visibility.
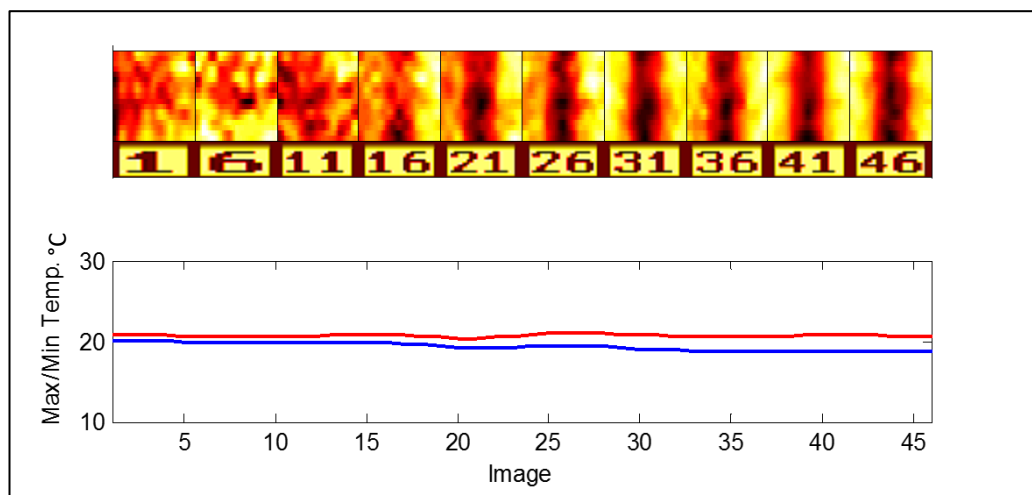
Figure 5.14: High-resolution camera images with max/min temperature graph.

This experiment has demonstrated that the continued cooling process of the source water has provided better results for both cameras. Figure 5.16 (a) and Figure 5.17 (a) show a clear pipeline pathway in the images. With cold water running in the pipeline, the cameras

can detect the pipeline pathway so easily. Figure 5.16 (b) and Figure 5.17 (b) show how the temperature profiles A, B, and C have a clear temperature drop in the middle.

Figure 5.15: High-resolution Camera images with Max/Min temperature graph.

Figure 5.16: Image of the low-resolution camera (a). Graph of the temperature profile of the lines A, B, and C across the image (b).
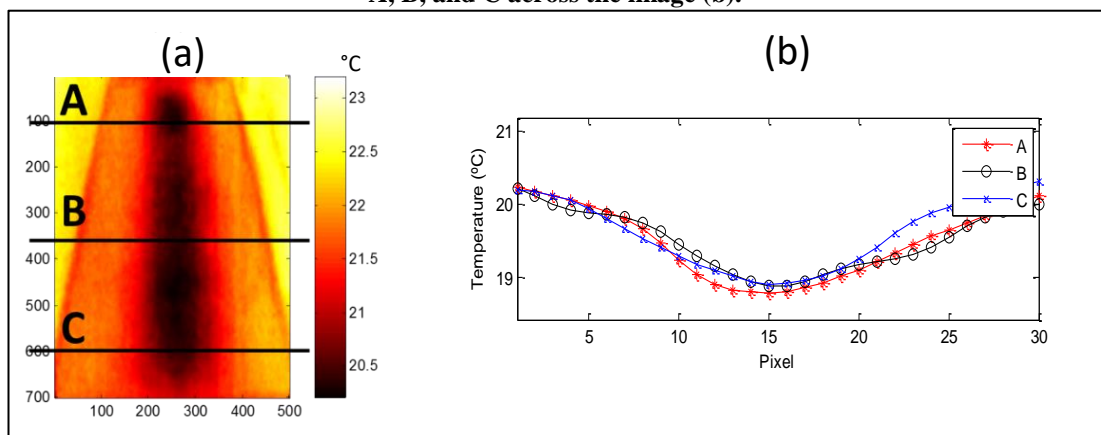
Figure 5.17: Image of the high-resolution camera (a). Graph of the temperature profile of the lines A, B, and C across the image (b).

5.6. Experiment no. 4 (No leak, Cooling, Heating)

The experiment run for eight hours. In this experiment, a heat source (Infrared light) is used for the first time to heat up the surface of the tested area to simulate the sun. While the surface is being heated up, the water is cooled as well. The temperature of the source water has been kept low as much as 4ºC along the time of the experiment. The average room temperature is 25ºC. The infrared light switched off one hour before the end of the experiment. Figure 5.18 and Figure 5.19 show series of images for both cameras with the max/min graph. The period of heating up the surface is shown in the figures. On switching off the infrared light, the min/max graph showed a decrease in temperature.
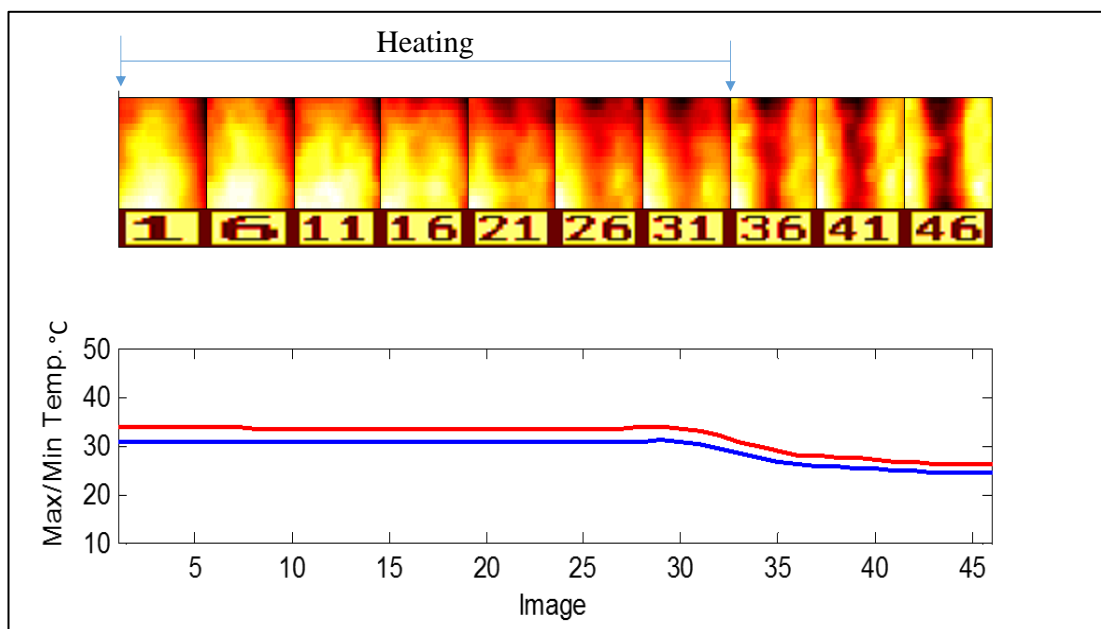
Figure 5.18: Low-resolution camera images with max/min temperature graph.

Figure 5.19: High-resolution camera images with max/min temperature graph.

Figure 5.20: Image of the low-resolution camera (a). Graph of the temperature profile of the lines A, B, and C across the image (b).

Figure 5.21: Image of the high-resolution camera (a). Graph of the temperature profile of the lines A, B, and C across the image (b).

Figure 5.20 (a) and Figure 5.21 (a) show that both cameras have clearly identified the pipe pathway. However, despite that the water is cool (4ºC), the detection of the pathway has delayed due to the heating up process. This experiment, show that the heating process of the surface is causing a delay in the detection of the pathway. Figure 5.20 (b) and Figure 5.21 (b) show a drop in the middle of the three temperature profiles.

5.7. Experiment no. 5 (Leak, No-cooling, Heating)

This is the first leak experiment. The leak hole is 1mm. Water temperature average is 15°c. The surface heated using the infrared light. The leak started at the beginning of the experiment.
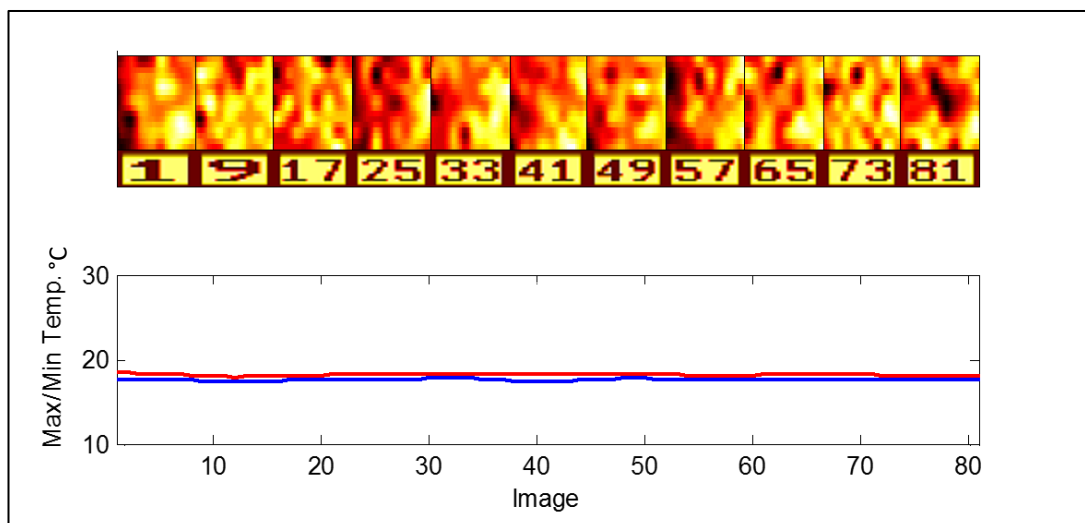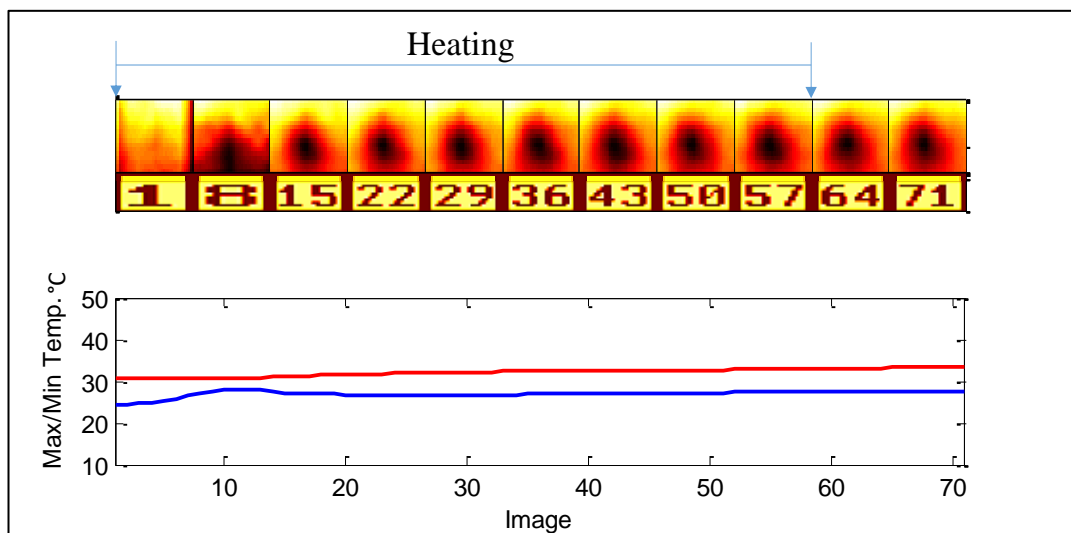

Figure 5.22: Low-resolution camera images with max/min temperature graph.
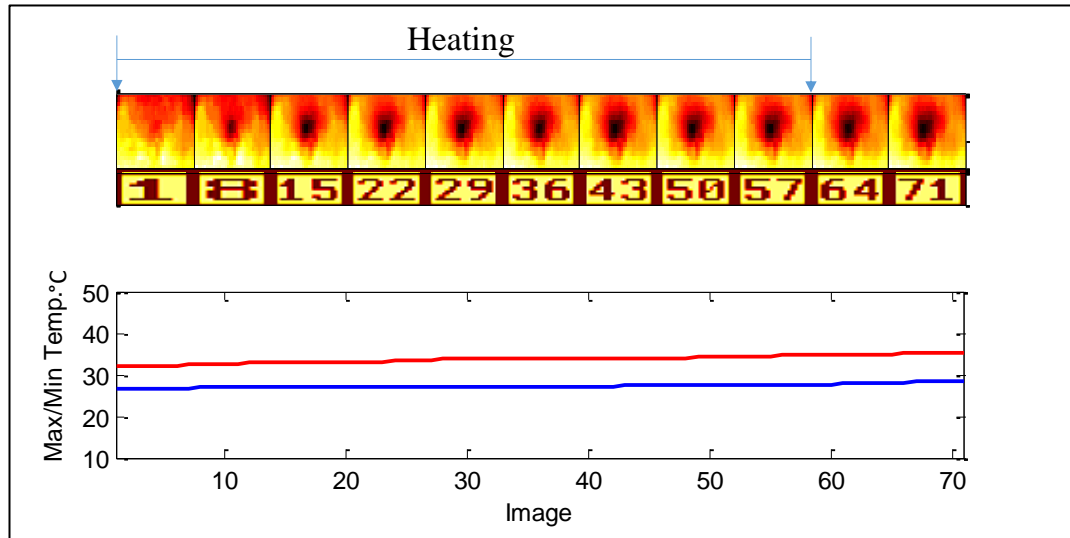
Figure 5.23: High-resolution camera images with max/min temperature graph.

Figure 5.23 and Figure 5.24 show that the images of both cameras showed the leak from the beginning. The leak started early once the heating started. This simulates an early morning in reality when the leak starts and the sun did not heat the ground yet. For this reason, the leak appeared quickly on the surface. Once the moisture of the leak reached the surface it continued to appear because it is cooling the surface each time the sun heat it up.
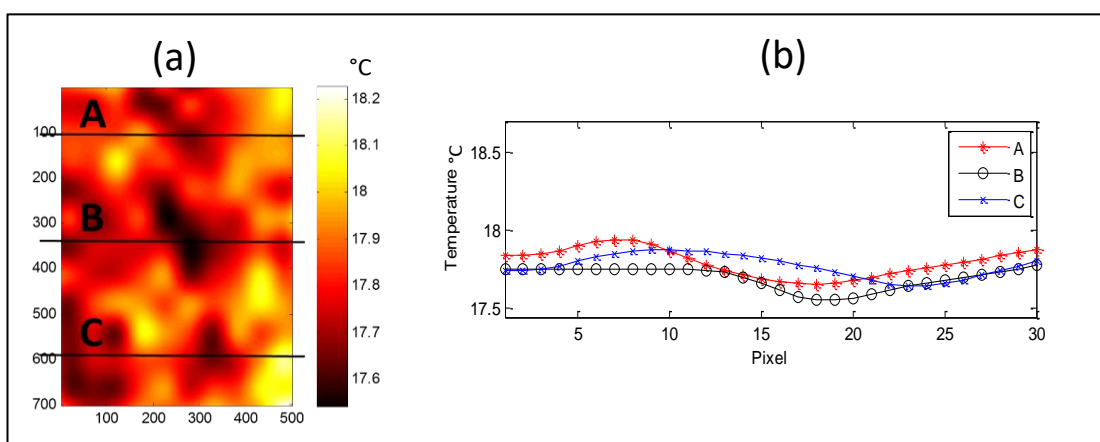

Figure 5.24: Image of the low-resolution camera (a). Graph of the temperature profile of the lines A, B, and C across the image (b).
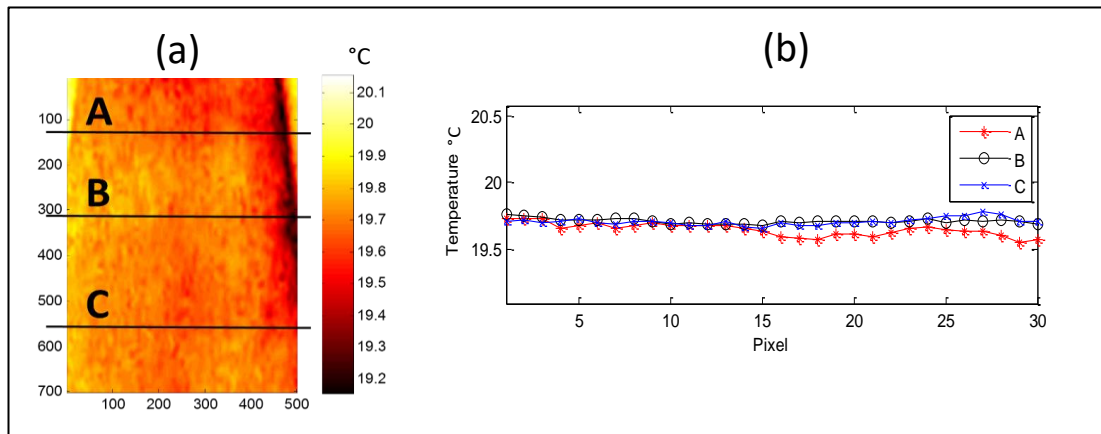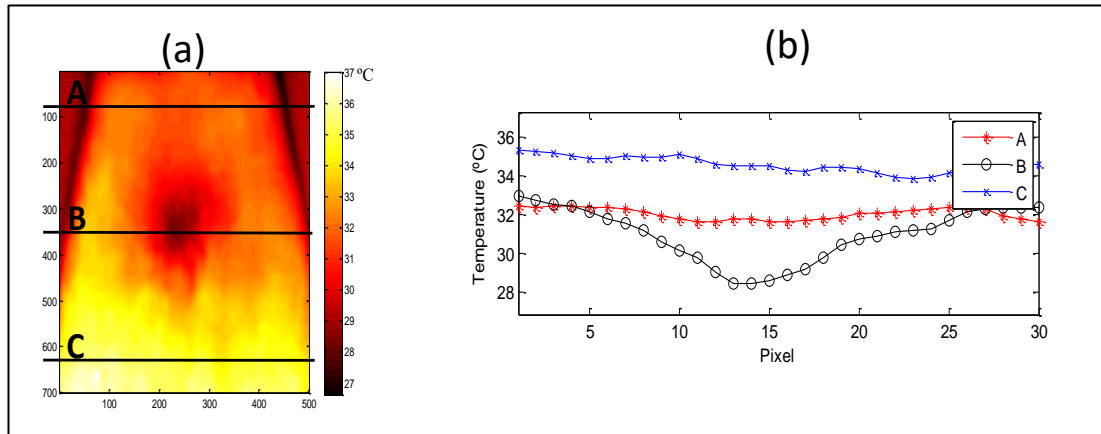
Figure 5.25: Image of the high-resolution camera (a). Graph of the temperature profile of the lines A, B, and C across the image (b).

Figure 5.24 (a) and Figure 5.25 (a) show that both low and high-resolution camera has detected the leak. Figure 5.24 (b) and Figure 5.25 (a) show that the profile of the line B which crossing over the leak in both images has lower temperature profile than the lines A and C.

5.8. Experiment no. 6 (Leak, Cooling, Heating)

The leak starts half way the heating process to simulate the leak starting at mid-day. The temperature of the water was 12 ºC. Figure 5.26 and Figure 5.27 show that the leak with both cameras did not appear properly for a while because of the heat from the infrared light. The leak appeared clearly in both cameras after the infrared light is switched off. This indicates the leak is detected at night.
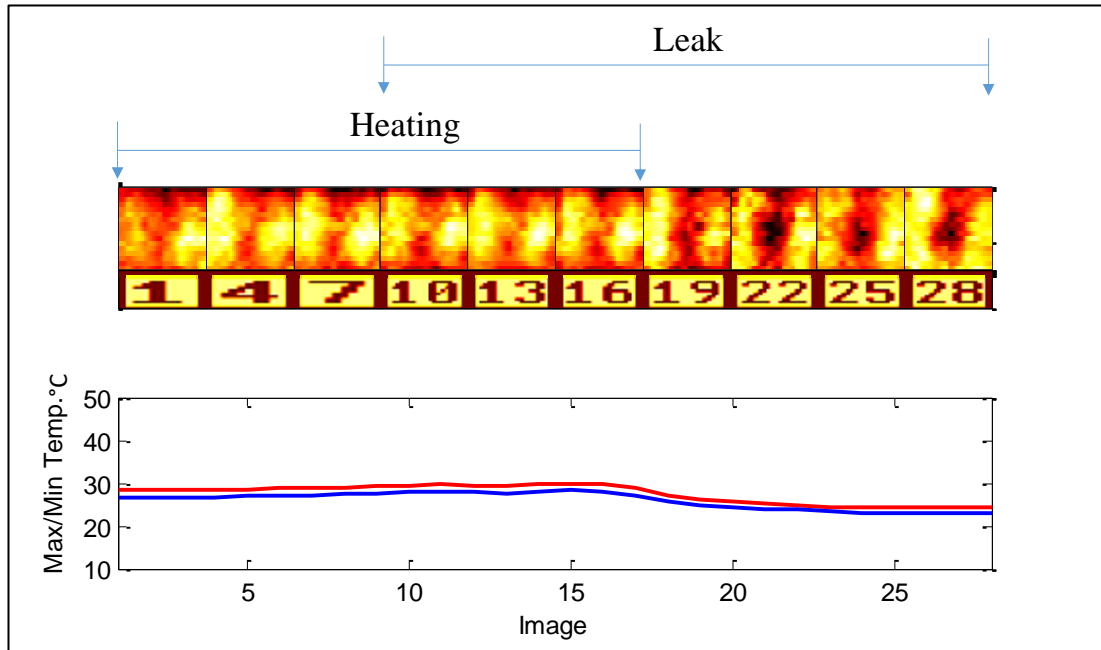
Figure 5.26: Low-resolution camera images with max/min temperature graph.
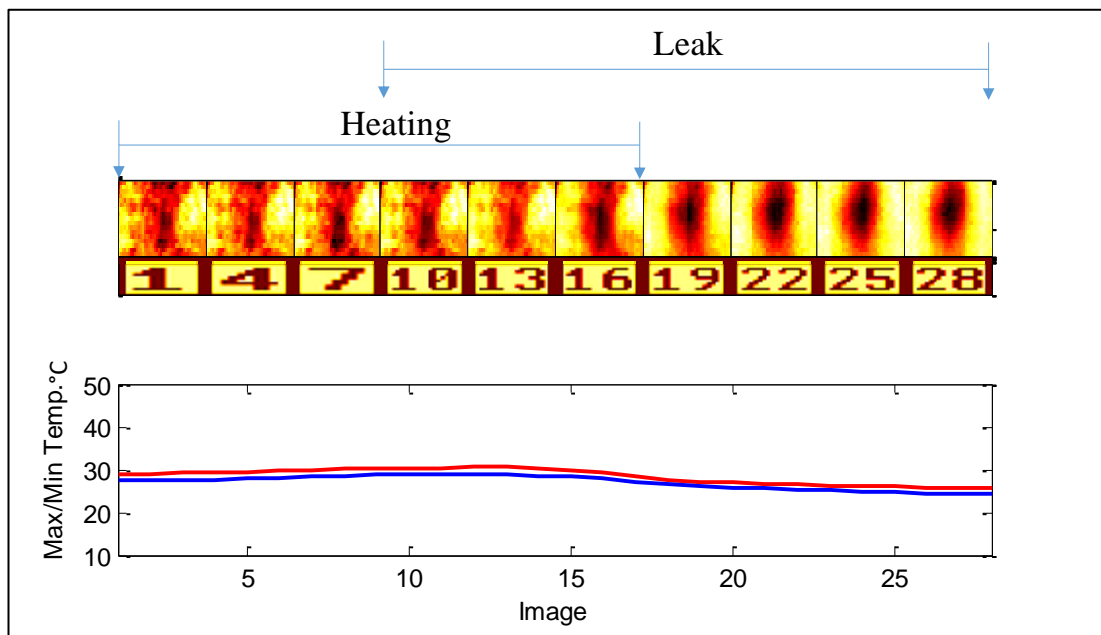
Figure 5.27: High-resolution camera images with max/min temperature graph.

Figure 5.28 (a) and Figure 5.29 (a) show that the leak in both images and Figure 5.28 (b) and Figure 5.29 (b) show that the profile of line (B) above the leak is lower than the profiles of A and C at the middle point.
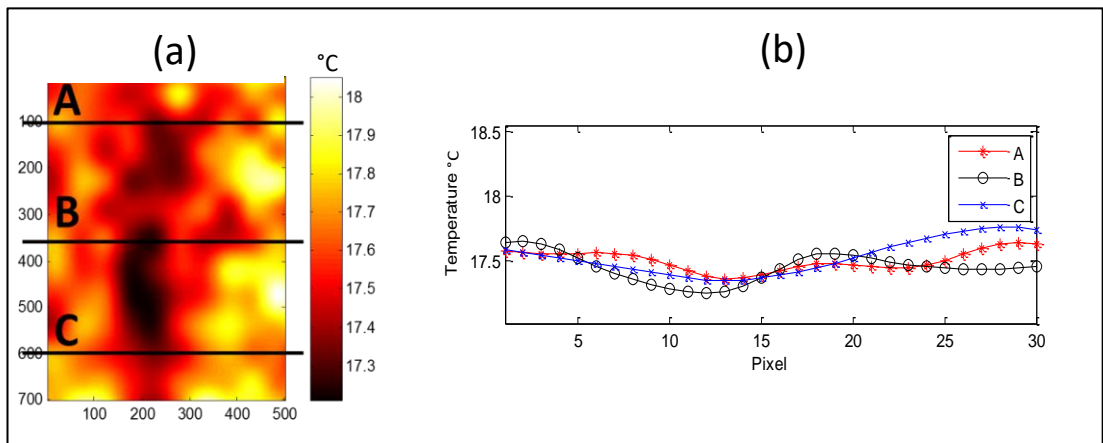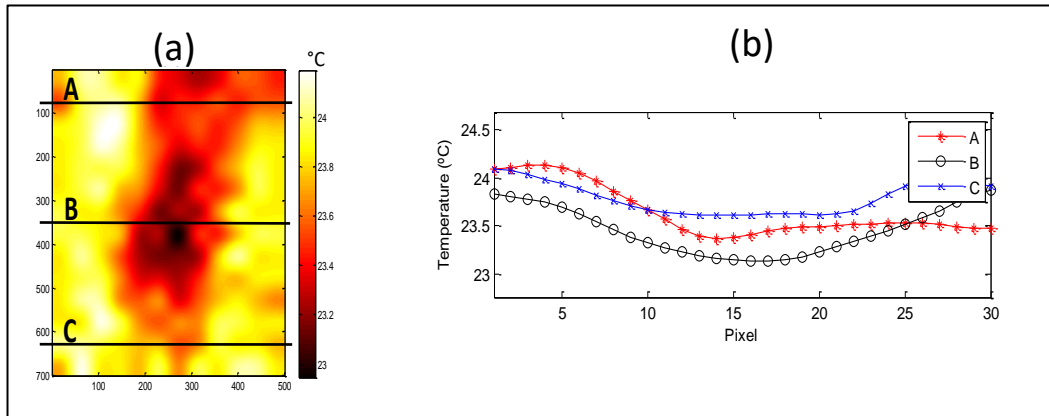
Figure 5.28: Image of the low-resolution camera (a). Graph of the temperature profile of the lines A, B, and C across the image (b).
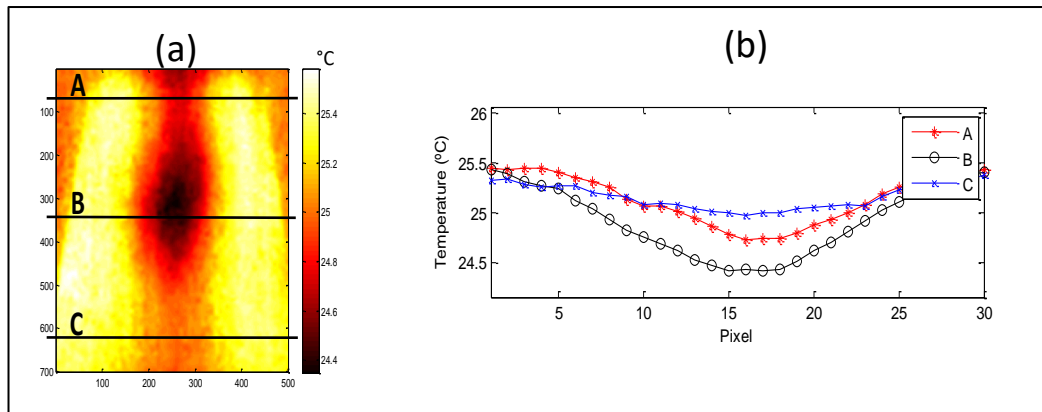
Figure 5.29: Image of the high-resolution camera (a). Graph of the temperature profile of the lines A, B, and C across the image (b).

Figure 5.30 shows a 3D representation of the leak for both cameras (a) for the high-resolution and (b) for the low-resolution camera.
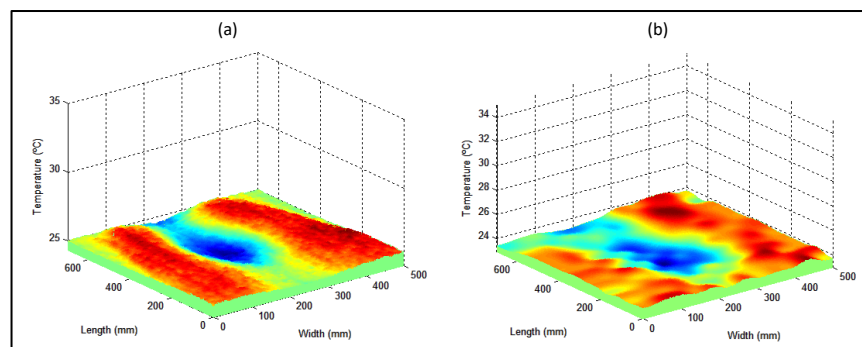
Figure 5.30: 3D image for the leak from both (a) Flir and (b) IRISYS

Both cameras detected the leak after the infrared light is off and they showed the leak and ended up with almost similar thermal images and similar temperature profiles.

5.9. Experiment no. 7 (Leak, Cooling, Two Cycles of heating)

In this experiment, only the IRISYS camera is used. The experiment simulates two complete days and one night (night-day-night-day-night). The infrared switched on for a period of time then switched off twice to simulate two days and nights. Figure 5.31 show the images from the low-resolution camera and the max/min graph. The leak in this experiment started the mid-time (mid-day) of the first cycle. The leak appeared just before the end of the first cycle of heating. The leak continued to appear even in the next cycle of heating.
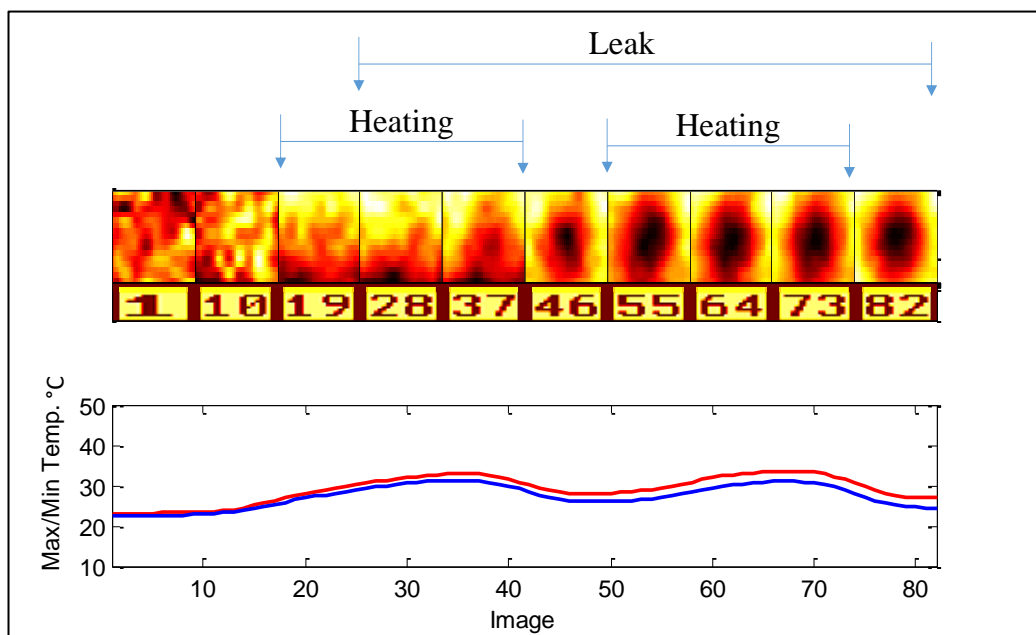
Figure 5.31: Low-resolution camera images with max/min temperature graph.
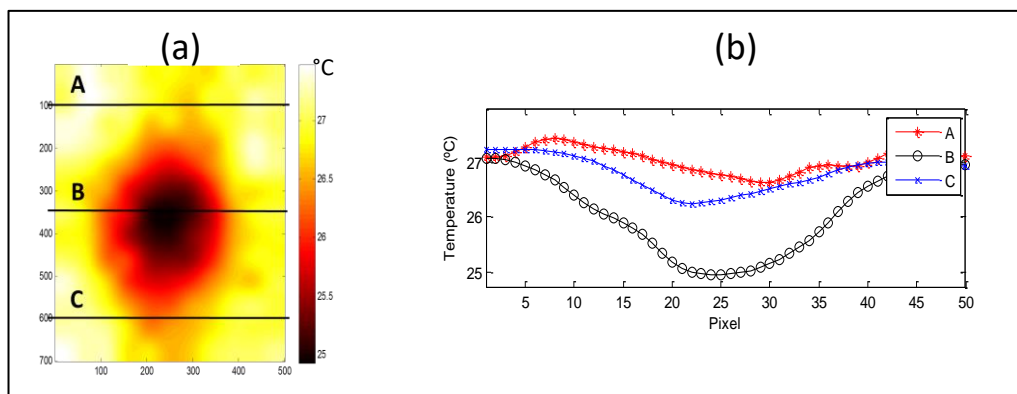
Figure 5.32: Image of the low-resolution camera (a). Graph of the temperature profile of the lines A, B, and C across the image (b).

Figure 5.32 (a) show the image with a clear leak spot and Figure 5.32 (b) show the temperature profile show that the line (B) across the leak point has a lower temperature in the middle than A and C. Figure 5.33 is a 3D representation of the leak.
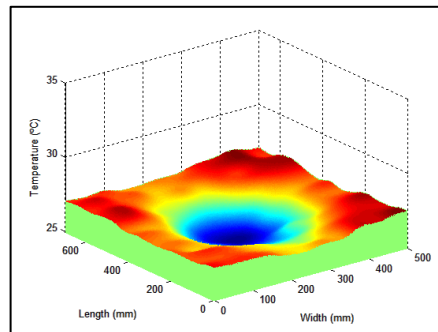
Figure 5.33: 3D image of the leak.

The camera is successful in detecting the leak. It did show the leak just before the infrared light is switched off but the leak was unclear. After the infrared switched off in the first cycle the leak became clearer. The leak continued to be clear in the thermal images even when the infrared is switched on again. This indicates that the cooling has enhanced the detection so the leak appeared before the heating stops

5.10.   Experiment no. 8 (Leak, No Cooling, Heating)

Figure 5.34 show that the leak started before switching on the infrared light. This experiment simulates a leak starts in the early morning before sunrise. The leak appeared before the infrared light is switched on but with a blurry shape. The leak continued to show even when the infrared light is switched on.
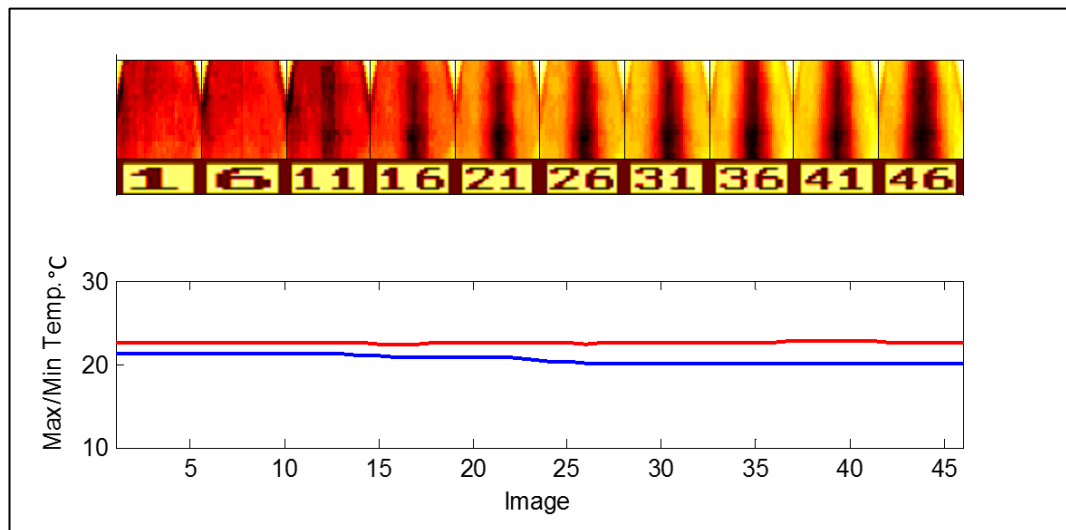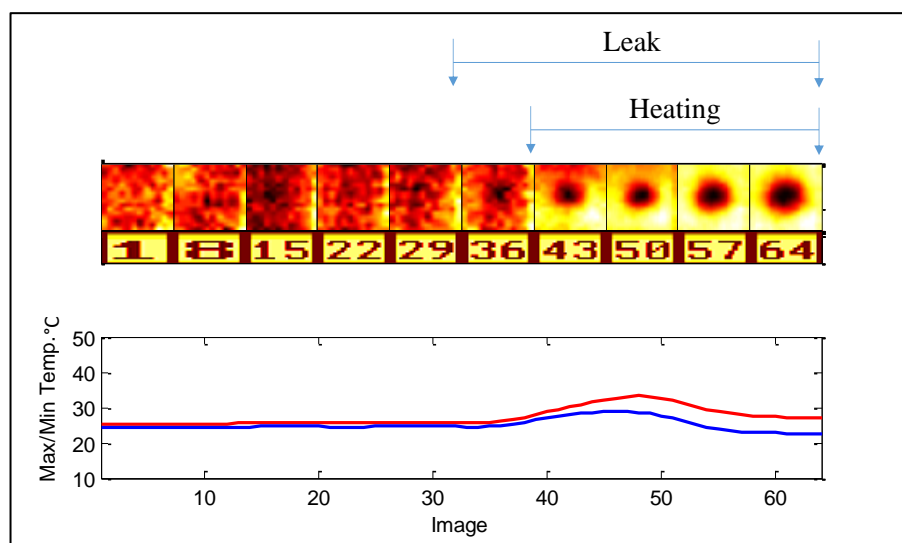

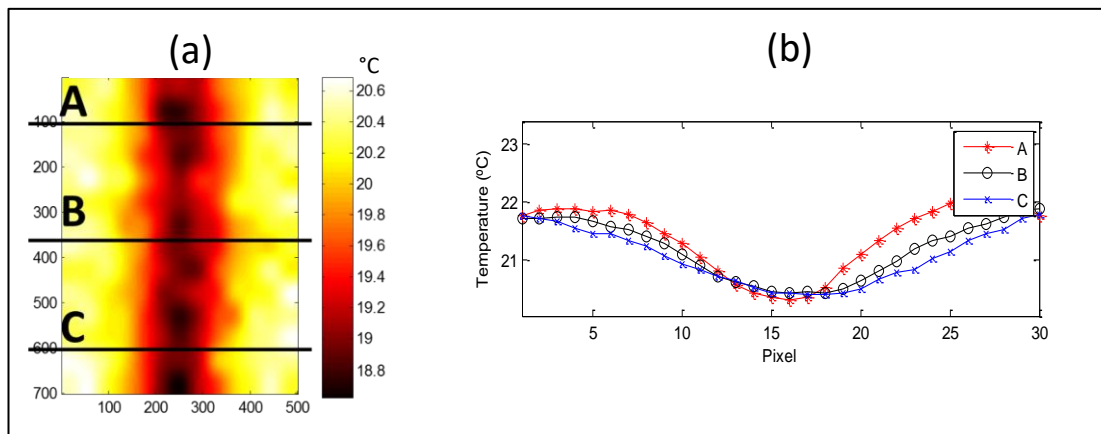**Figure 5.34: Low-resolution camera images with max/min temperature graph.**
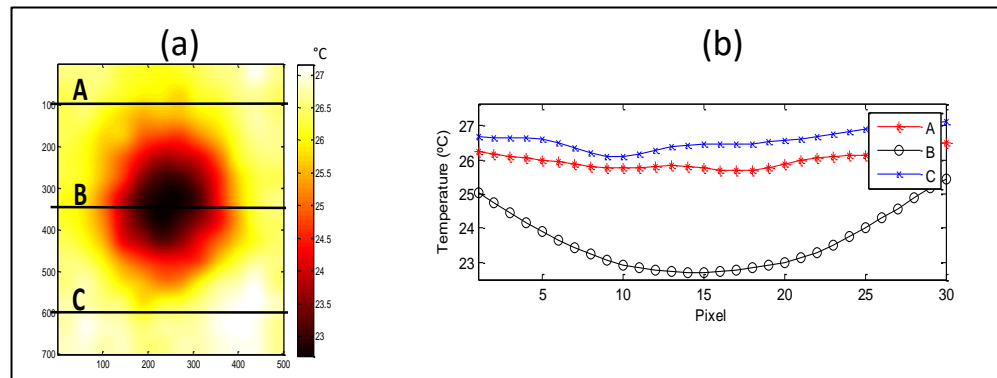
Figure 5.35: Image of the low-resolution camera (a). Graph of the temperature profile of the lines A, B, and C across the image (b).

Figure 5.35 (a) shows that the thermal camera clearly detected the leak. The temperature profile graph Figure 5.35 (b) shows a clear drop in the temperature profile of line B above the leak point. Figure 5.36 shows 3D representation image of the leak spot.
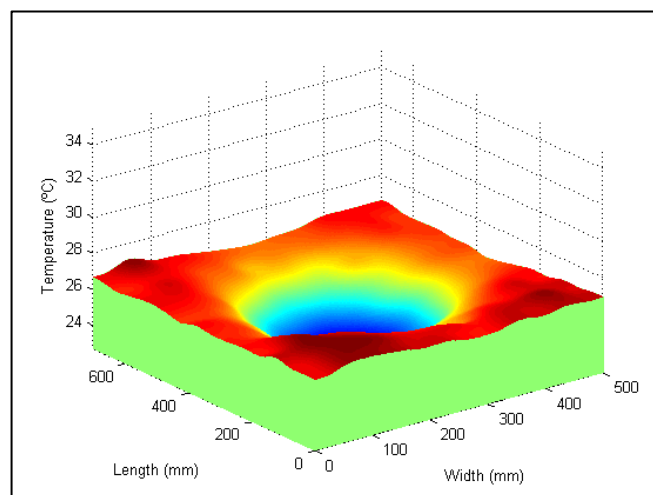
Figure 5.36: 3D image of the leak.

5.11. Experiment no. 9 (Leak, No Cooling, Two Cycles of heating)

Figure 5.37 shows the experiment images. The experiment simulates a leak starts on the night after long hot day and then continued for another hot day. The case simulates a summer season when the days are longer than nights. The leak did not appear until it is early morning and continued to show even the infrared light is switched on again.
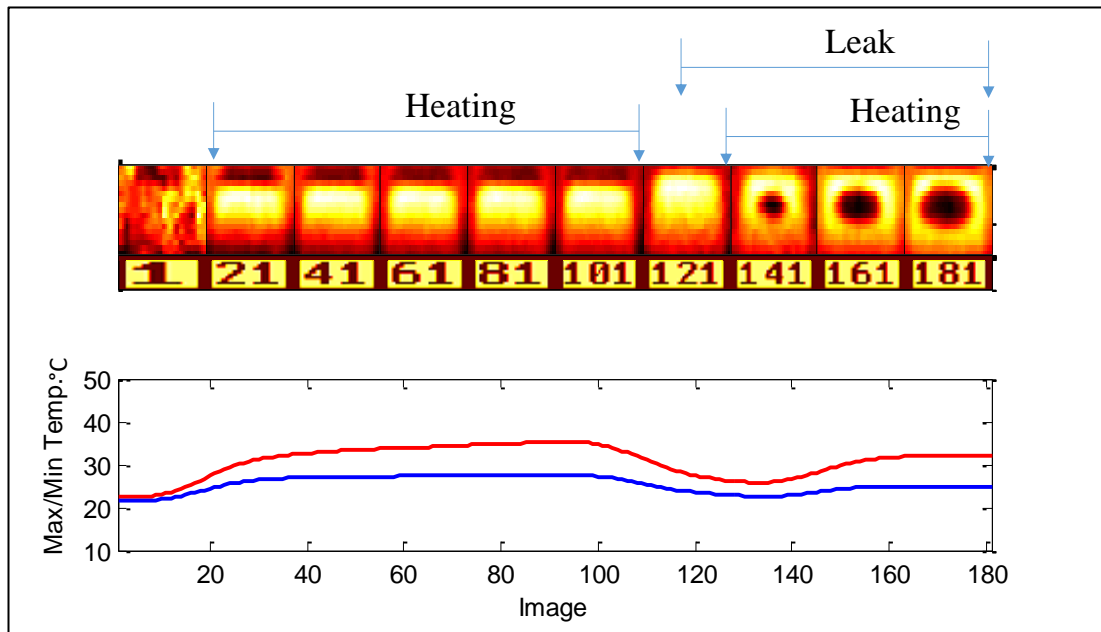
Figure 5.37: Low-resolution Camera images with Max/Min temperature graph.
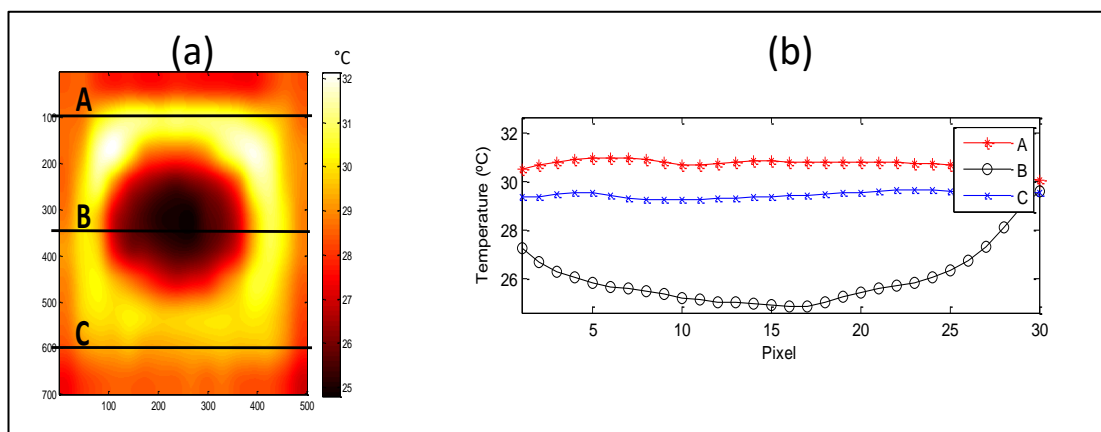
Figure 5.38: Image of the low-resolution camera (a). Graph of the temperature profile of the lines A, B, and C across the image (b).

Figure 5.38 (a) shows the leak image. Figure 5.38 (b) show the temperature profile of line B above the leak is lower than the temperature profiles of A and C.

5.12. Experiment no. 10 (Leak, Cooling, Heating)

Figure 5.39 show that the leak started in the first half of the day. Cold water with temperature 11°C is used in this experiment. The cooling machine continued to cool the water to the end of the experiment.
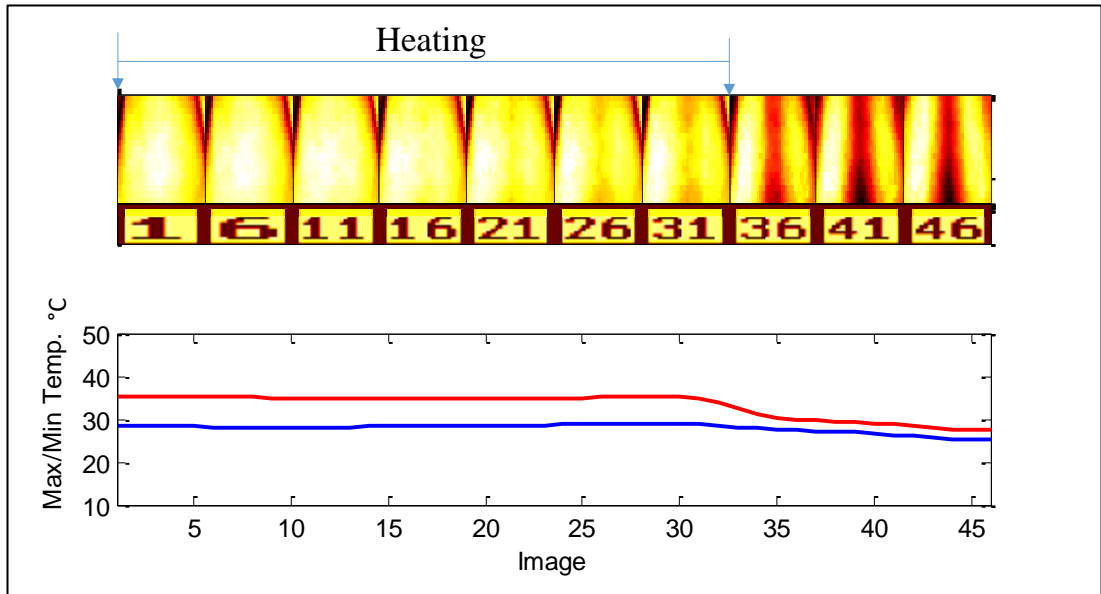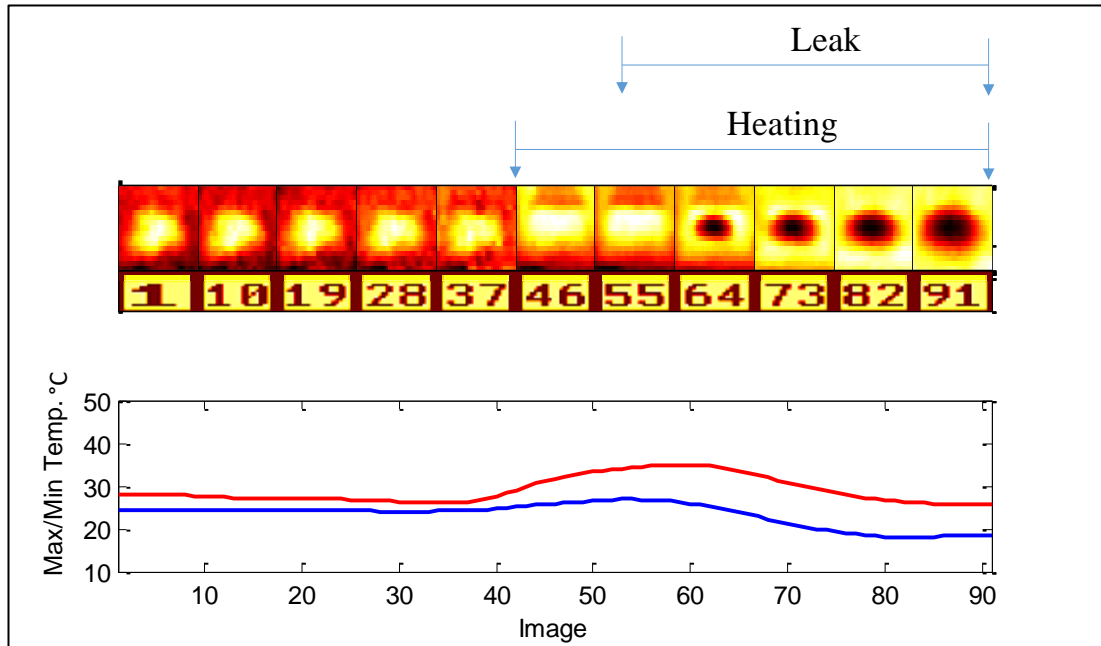
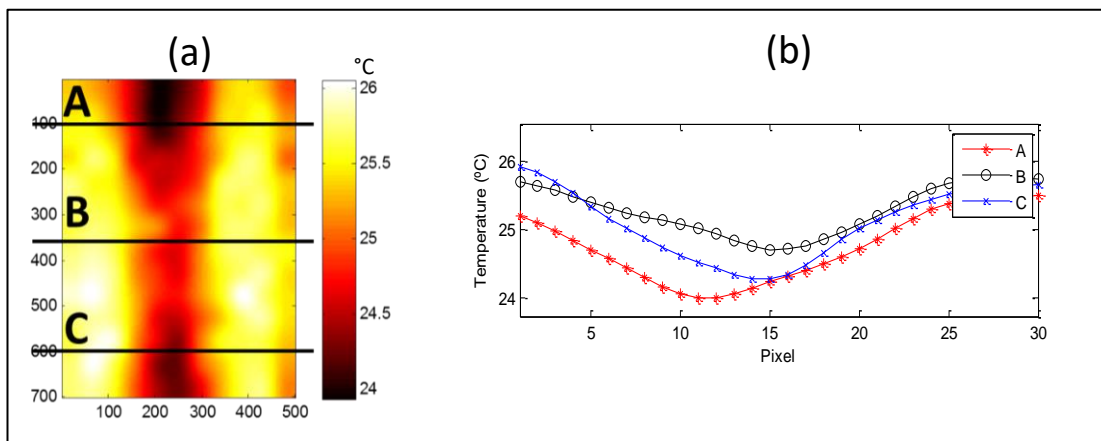**Figure 5.39: Low-resolution camera images with max/min temperature graph.**
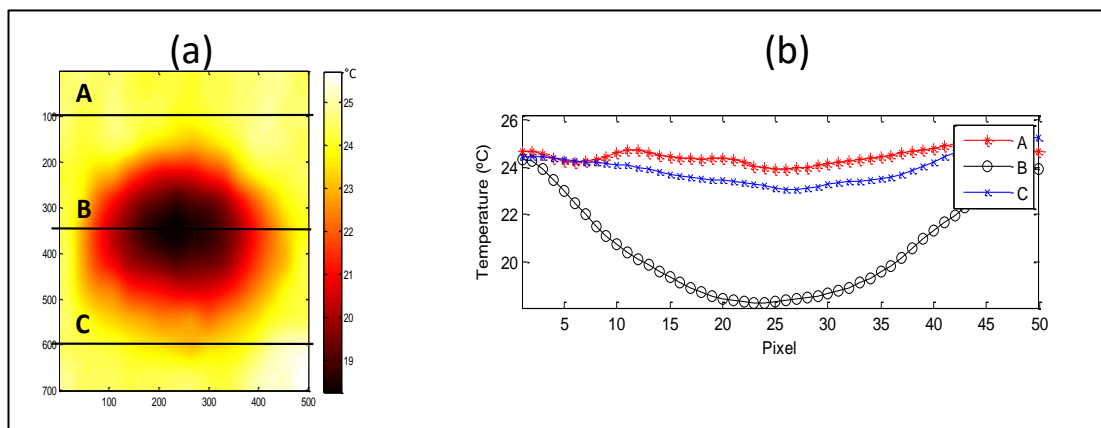
Figure 5.40: Image of the low-resolution camera (a). Graph of the temperature profile of the lines A, B, and C across the image (b).

Figure 5.40 (a) show that thermal camera detected the leak. Figure 5.40 (b) show that the temperature profile of line B above the leak point is lower than the temperature profile of A and C.

5.13. Experiment no. 11 (Leak, Cooling, Heating, Concrete Slab)

This experiment is one of the experiments in which a concrete slab is used to cover the test area to simulate a pipeline buried under concrete walkway or road. The infrared is

used to heat the surface of the concrete slab. Two days cycle is tested in this experiment. Figure 5.41 shows that the leak started with the start of the second cycle of heating (second day). The source water is cooled as well. Water temperature ranged from 10 °c to 14 °c.
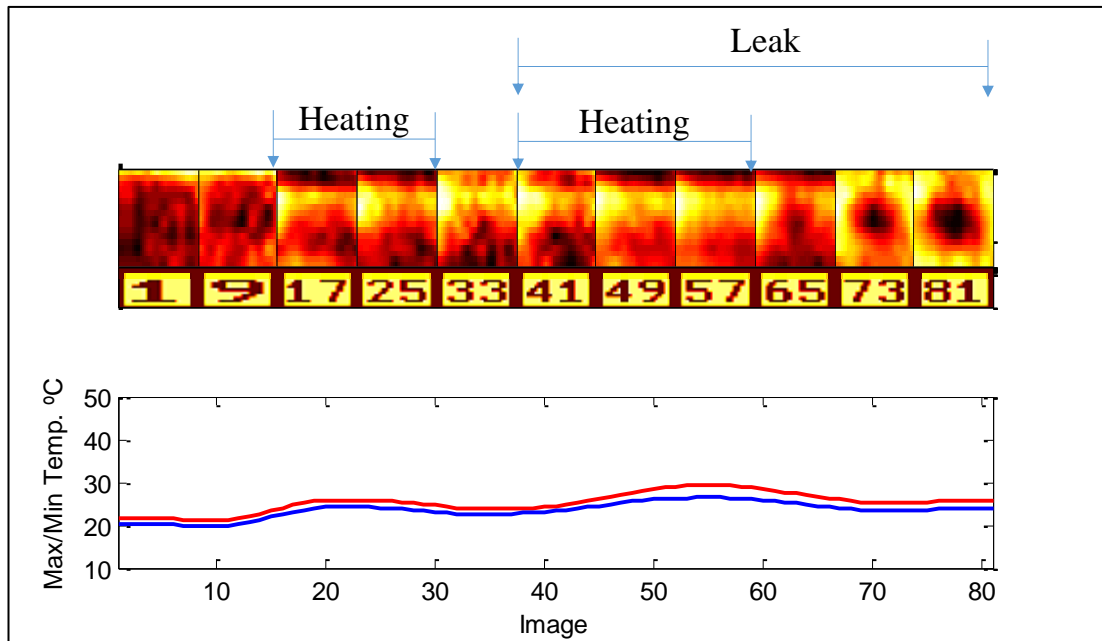
Figure 5.41: Low-resolution camera images with max/min temperature graph for an experiment with concrete slab.

Figure 5.42 (a) show that the low-resolution camera detected the leak even the test area is covered with a concrete slab. Figure 5.42 (a) show the temperature profile above the leak point is lower than the temperature profiles of the other two lines A and C.
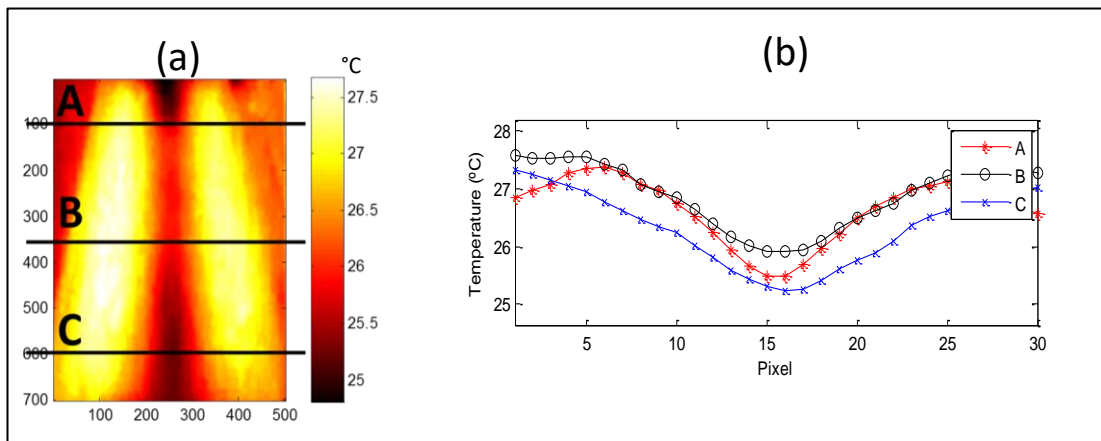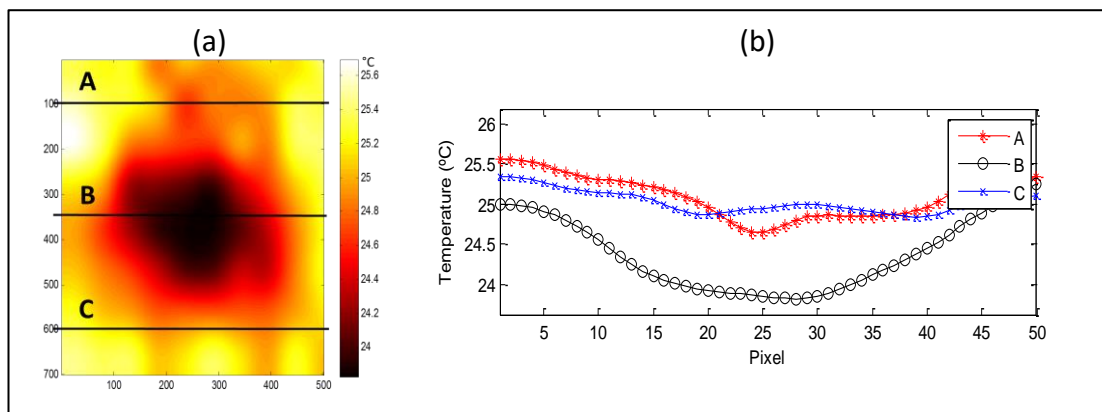

Figure 5.42: Image of the low-resolution camera (a). Graph of the temperature profile of the lines A, B, and C across the image (b).
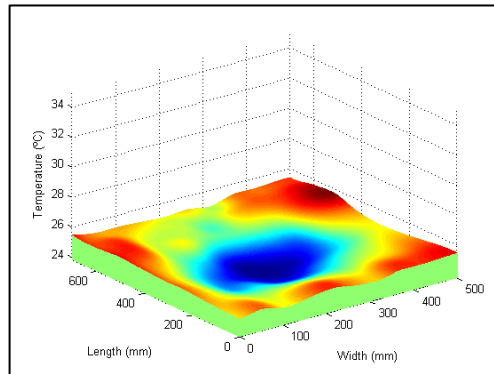
Figure 5.43: 3D image of the leak

5.14. Experiment no. 12 (Leak, No Cooling, No Heating, Concrete Slab)

Figure 5.44 shows the images for the concrete slab experiment. No cooling and no heating are used in this experiment. This experiment simulates leak occurred at night time under a walkway. The images in Figure 5.44 have showed the leak with some delay due to the absence of the cooling.
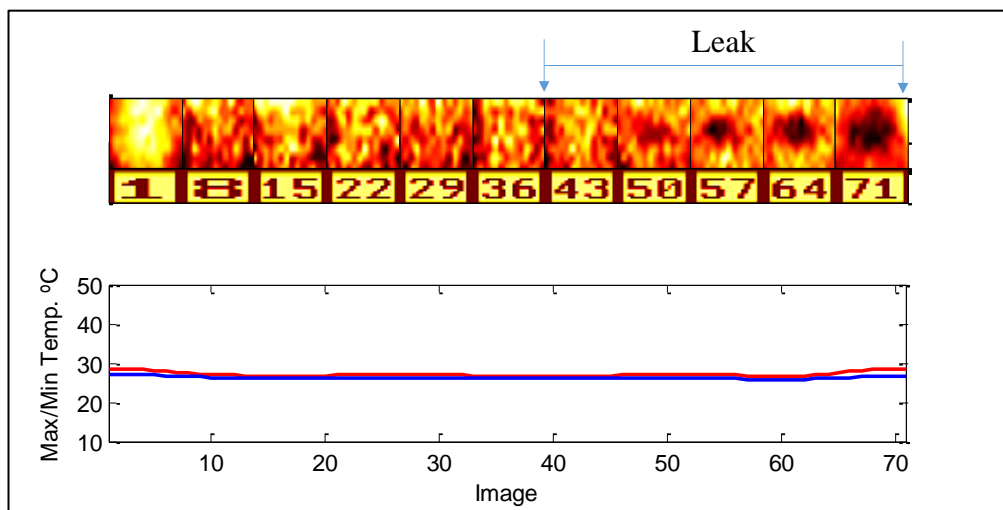
Figure 5.44: Low-resolution camera images with max/min temperature graph for an experiment with concrete slab.
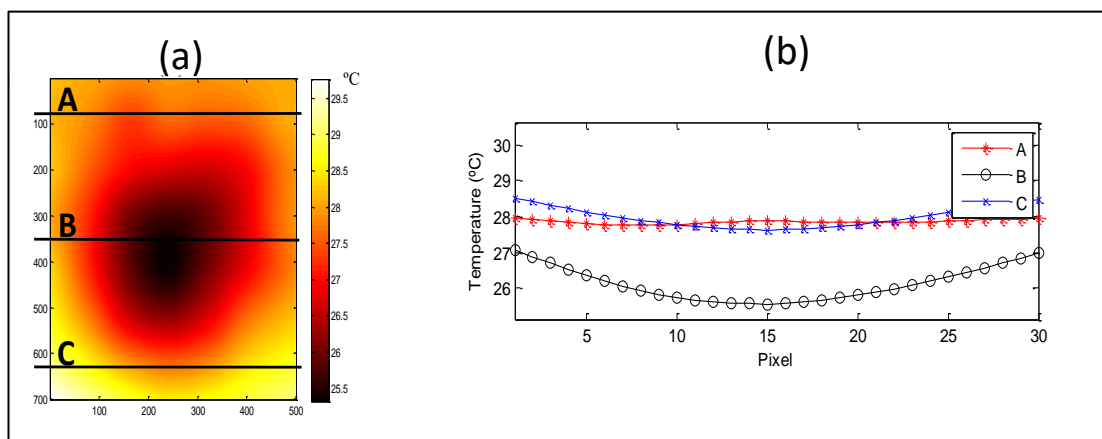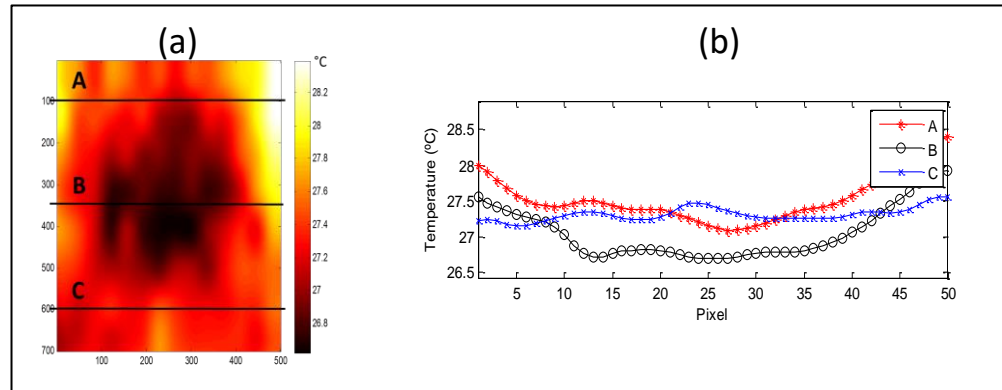
Figure 5.45: Image of the low-resolution camera (a). Graph of the temperature profile of the lines A, B, and C across the image (b).

5.15.   Comparison between the high and low-resolution cameras: (Flir & IRISYS).

5.15.1. Non-leak condition

In the No-leak condition, the processed images from both cameras have showed the pipeline pathway successfully as a different colour along the image from the middle. Figure 5.46 shows a group of images for both Flir and IRISYS of the same experiment for comparison.
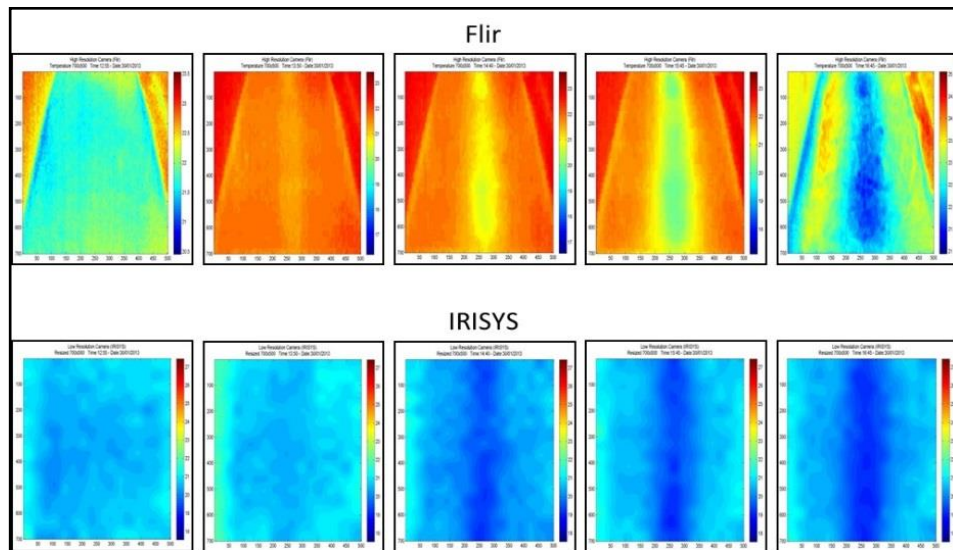
Figure 5.46: IRISY vs Flir in non-leak condition

5.15.2.   Leak Condition
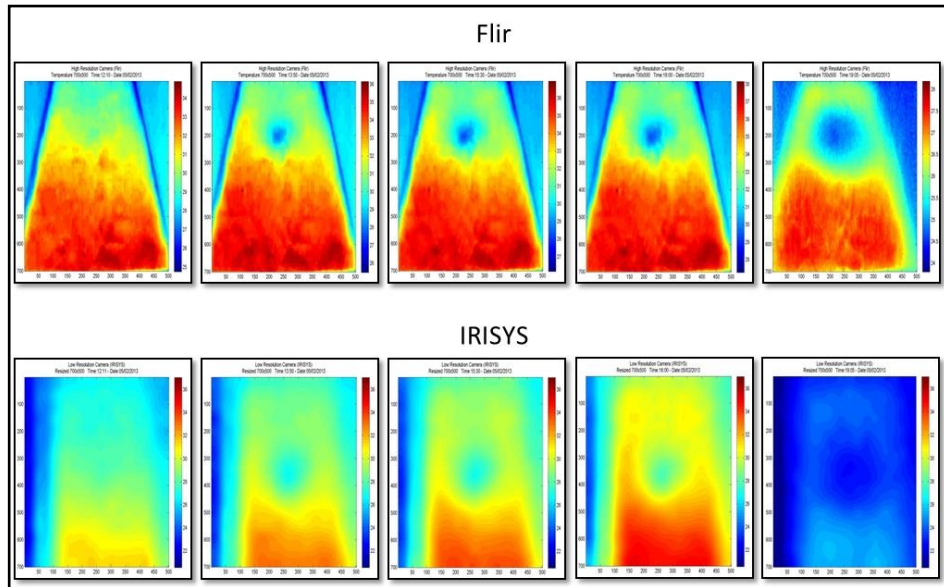
Figure 5.47: IRISYS vs Flir in leak condition

Figure 5.47 is a group of images for Flir and IRISYS in the condition of the leak. Both cameras have showed round shape inside the image which is the leak point. Again the images are from the same experiment.

5.16.   Comparison between Leak and no-leak condition.

In order to be able to compare leak and no-leak conditions using a line graph, at least three temperature profile lines have to be plotted for a three locations across the pipeline. The following examples are for IRISYS imager.

5.16.1.   No-Leak Condition:

In the no-leak condition, the graph shows that any lines drawn across the image are of the same or nearly the same temperature values in the middle point (Figure 5.48). That's because the pipeline is affecting the temperature of the surface above it. The figure shows that the profiles of the three lines are identical to each other.
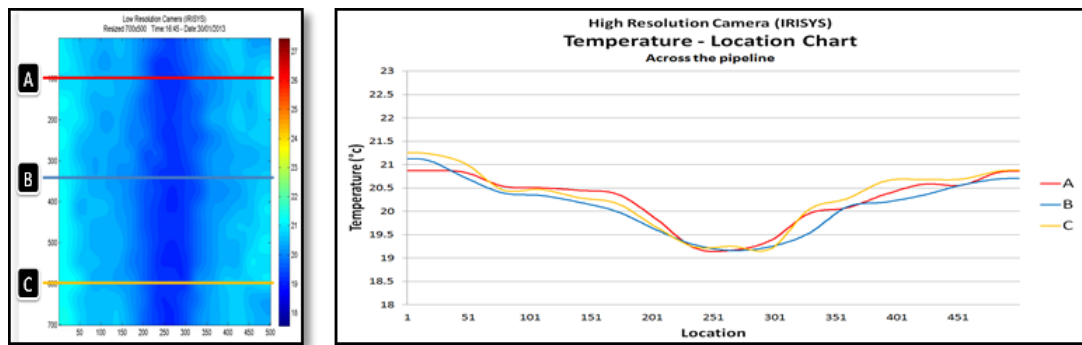
Figure 5.48: IRISYS Image for no-leak condition

5.16.2. Leak Condition:

Figure 5.49 shows that the only the profile of the line passing through the leak point has a different profile with a temperature in the middle point and it would be easily detected from other lines.
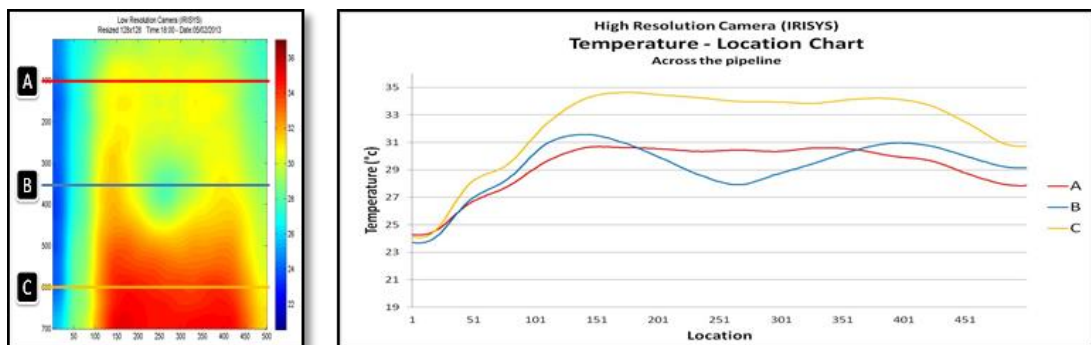
Figure 5.49: IRISYS Image for leak condition

5.16.3. Differentiation between leak and no-leak condition using 3D Mesh Image.

The thermal image shows the leak as a spot on the suspected leak point while it shows the path of the pipeline in case there is no leak. The 3D mesh image as in Figure 5.50 shows the leak as a 'sinkhole' in the middle of the suspected area while it shows the path of the pipeline as a trench along the pipeline length.
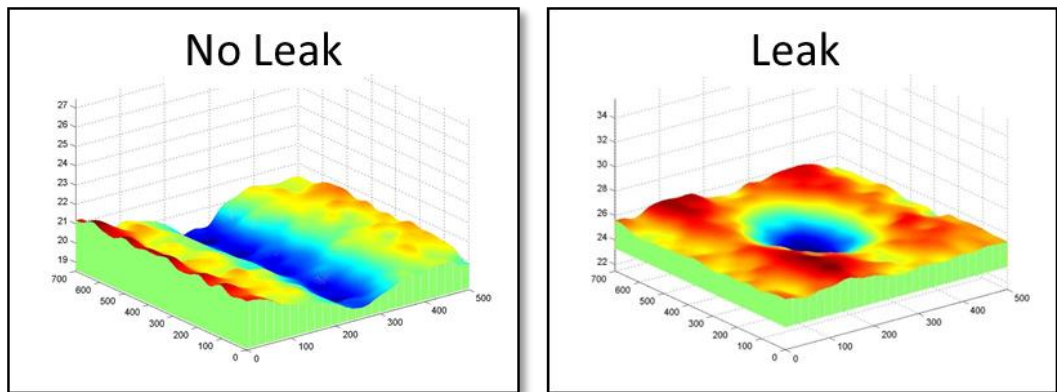
Figure 5.50: 3D image for leak and no leak conditions.

5.17.   Using threshold technique to distinguish the leak and the pipe path.

Thresholding technique is one of the effective image process techniques. The thresholding technique converts grayscale images to a binary image in which the image consists of a foreground and a background only. The thresholding is used to isolate objects and to easily extract them from the image.

Figure 5.51 shows a sequence of processed images using thresholding technique, the pipeline is clearly shown as a vertical wide white line on the image.
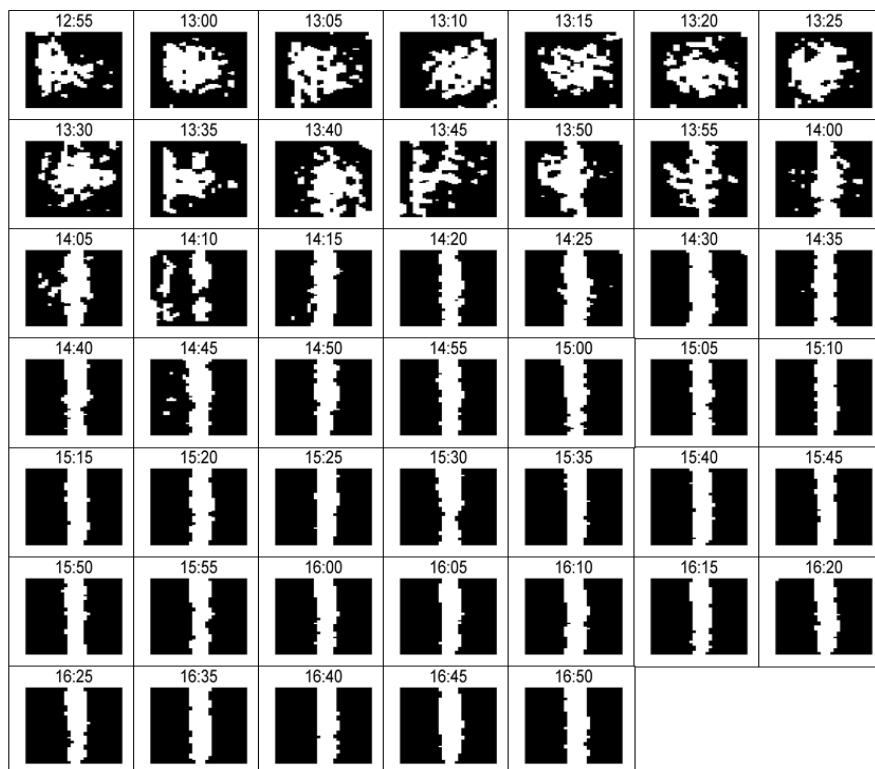
Figure 5.51: Example of leak detection pipeline pathway using threshold technique
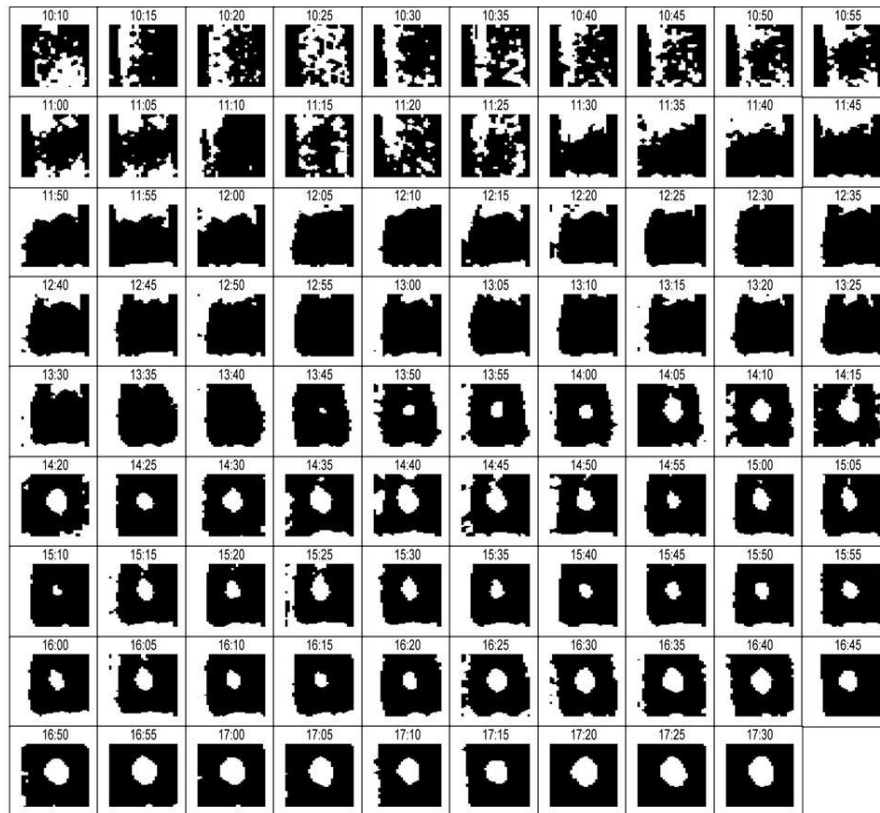
Figure 5.52: Example of leak detection sequence using threshold technique

Figure 5.52 demonstrates the leak detection process using threshold technique. The figure shows that the size of the white round shapes which is the leak spot becomes smaller in the middle group. This is because the heating process has restarted but because the leak has already appeared before the heating process, it did not disappear totally and once the heating stopped the leak spot started to grow up again.
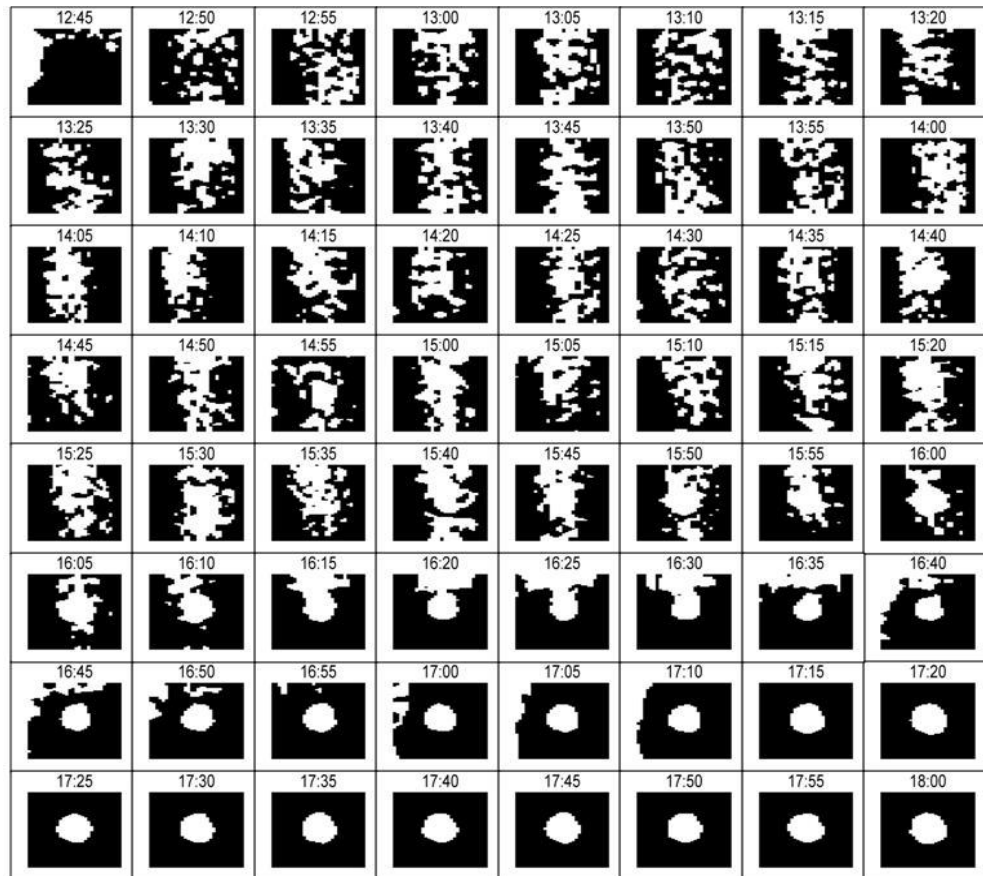
Figure 5.53: leak detection sequence using threshold technique.

Figure 5.53 shows an example when no cooling nor heating is used. The camera did detect the leak clearly but with longer time than when cooling is used.

5.18.   Merging the Visual Image and Thermal Image

As it has been observed from the images of the low-resolution thermal camera, the thermal images do not clearly demonstrate the surroundings because it is produced with low-resolution. The low-resolution thermal camera produces a vague image of 16x16 matrix created from the original vector data generated by the camera. Despite this matrix of 16x16 can be interpolated and resized to a higher resolution of any number (in our case it has been converted to 700x500 to match the tested area size), it is still requiring extra processing to be understood and to describe its contents. As well as the visual image from the webcam does not show the leakage unless the leakage appears on the surface.

To overcome those two problems, to enhance the visibility of the thermal image and to locate the leakage on the visual image, a combination of both the thermal and the visual images was done to produce one readable image. The newly generated image should definitely show the spot of the leakage on the visual image clearly. With this step, the leakage would be located on reality perfectly and the thermal image would be interpreted easily. The merging process requires some image pre-processing and processing operations to get both thermal and visual images merged. The following paragraphs illustrate how the process have been carried out.

Firstly, read both the original visual images and the thermal images (Figure 5.54). The thermal imager has to be adjusted for the target area to take exactly the region of interest ROI.
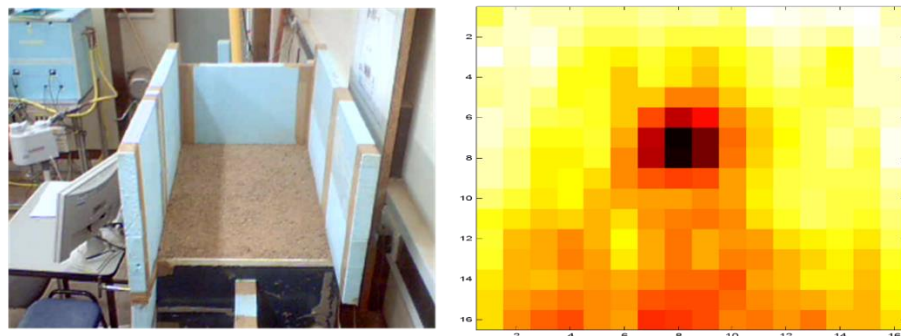
Figure 5.54: Original visual and thermal images

Secondly, crop and resize the images as necessary to match each other and to match with the targeted area (Figure 5.55). After cropping, both images should have the same size (same size matrix with the same number of pixels). In this case, it would be 700 rows by 500 columns to match the actual size of the test area. The actual size of the test area is 700 mm by 500 mm.
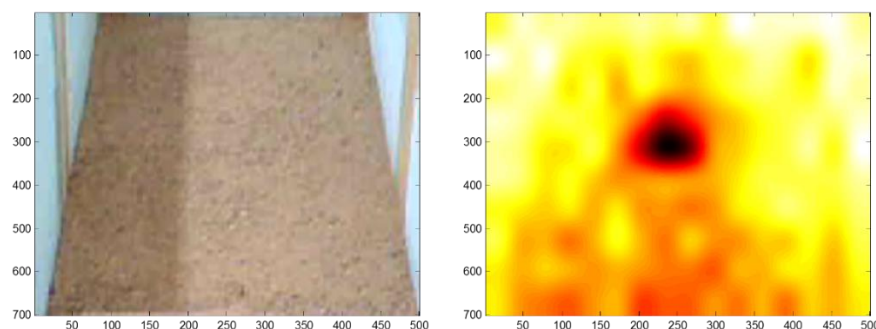
Figure 5.55: Cropped and pre-processed images

Thirdly, separate the true colours which are Red, Green, Blue (RGB) components of the visual image to create three indexed matrices of the image. The thermal image is an index matrix (one component) therefore, it will be used three times as it is. When the index matrices are ready, add each matrix from the visual image to the thermal image (Figure 5.56). The true colour matrices of the visual image have to be converted to double precision in order to be added to the thermal index matrix. Also, they have to be processed with some filter (e.g. Median filter) to reduce the noise. All the indices have to be normalised before adding so they will have the save weight.
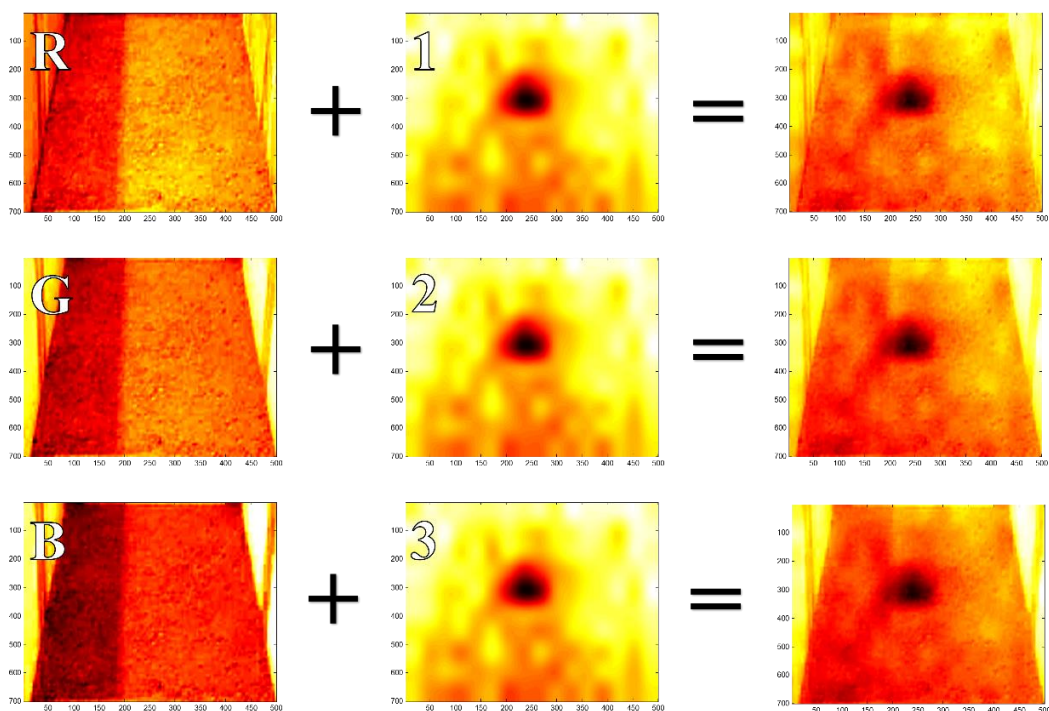
Figure 5.56: Process of combining the thermal and visual images

Finally, the resulted three index images have to be converted to an unsigned integer in order to create the final RGB (Red, Green, and Blue) image in which both thermal and visual are combined together. Figure 5.57 shows the final image with the leakage spot on it. The image is now showing the leak spot on the exact location where the actual leak is. In this technique, the whole thermal image transferred to the visual image. The visual image shows the heat distribution on the whole surface where the dark areas are the coldest. Instead, as in Figure 5.58, the thermal image could be converted to B/W image with the leak spot in the middle by using threshold technique and then merge it with the visual image to show the leakage spot only on the visual image.
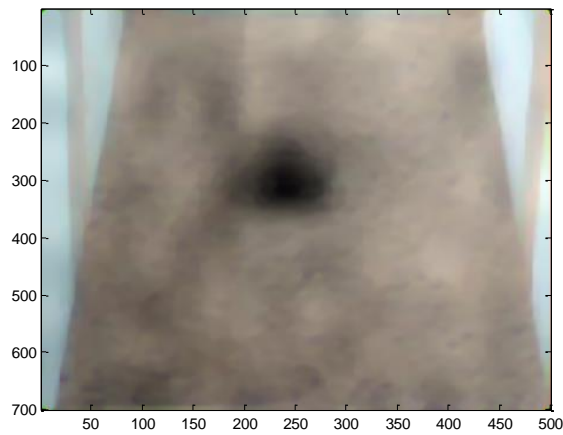
Figure 5.57: Final image of the combined thermal/visual image
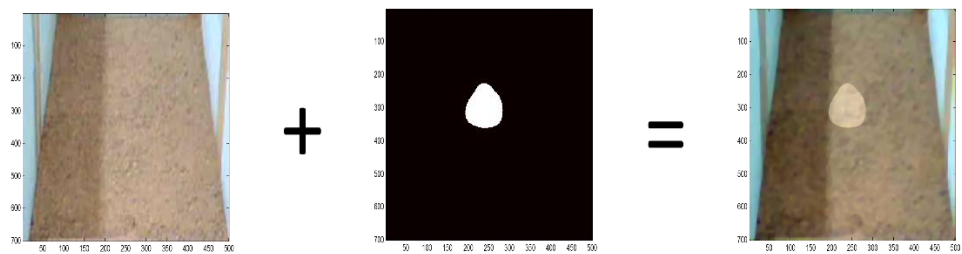
Figure 5.58: Merging the B/W of the thermal image to the visual image
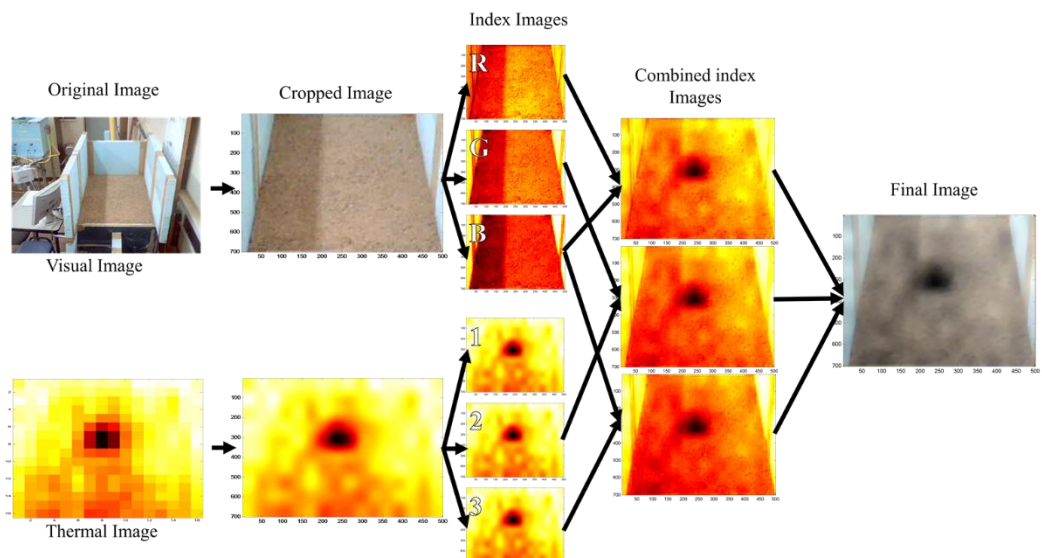
Figure 5.59: Example of merging both images from laboratory results

Figure 5.59 and Figure 5.60 show a detailed graphical explanation of the merging method for both images (the thermal and the visual) resulted from the laboratory experiments as well as from the field work.
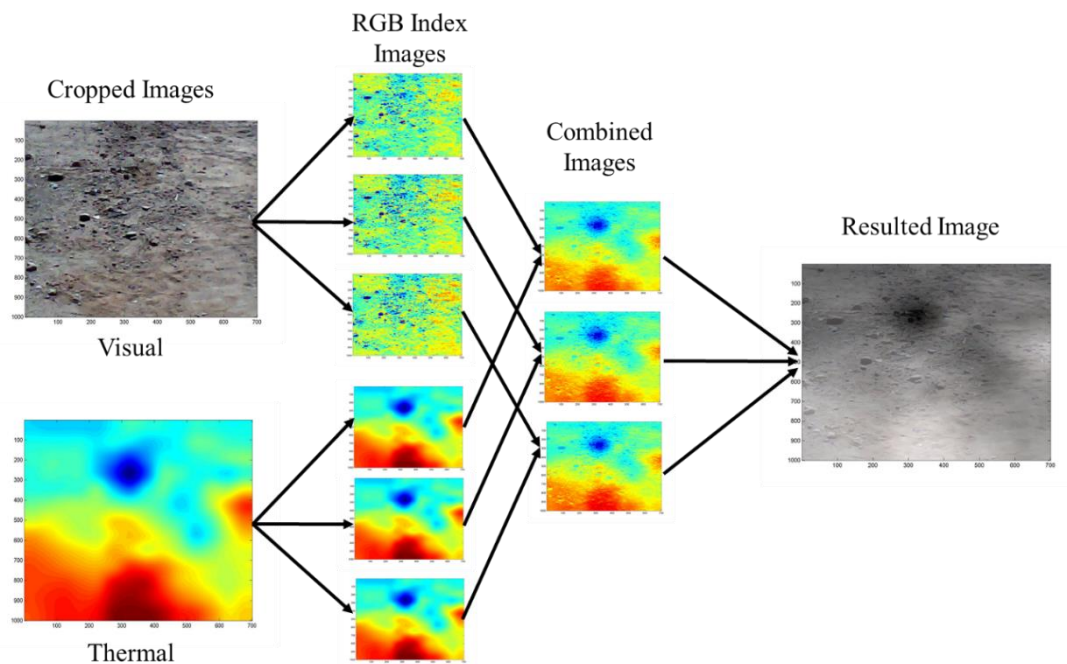
Figure 5.60: Example of merging the thermal/visual images from field work

5.19.   Effect of colour on the thermal image

In order to investigate how the colour of the object is affecting the thermal image, a printed paper of six known colours have been subjected to thermal image capturing. The paper tested in both cold and hot conditions. The result revealed that once the object exposed to heat, the dark colours becomes the hottest parts as it does absorb more heat than the others. While in the cold condition the majority of the colours have a temperature close to the temperature of the whole body.
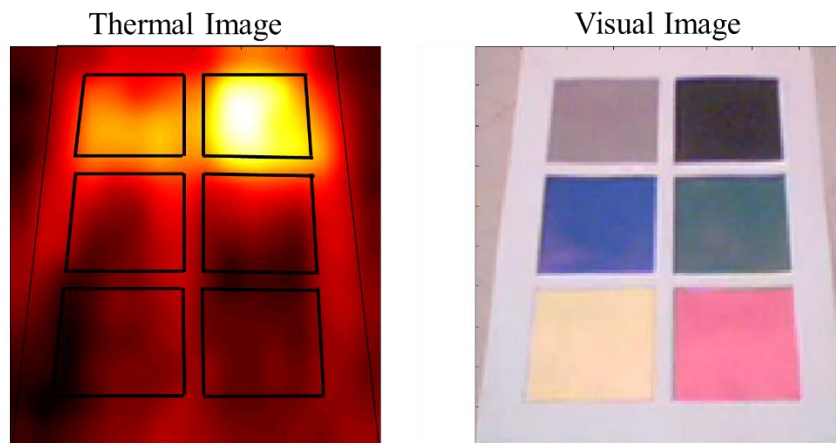
Figure 5.61: Effect of colour on thermal image. Thermal image on the left and visual image on the right.

Figure 5.62, illustrates the temperature profile of each colour on the test piece. From the graph, it can be seen that the black colour has the higher temperature while the yellow colour has the lower temperature.
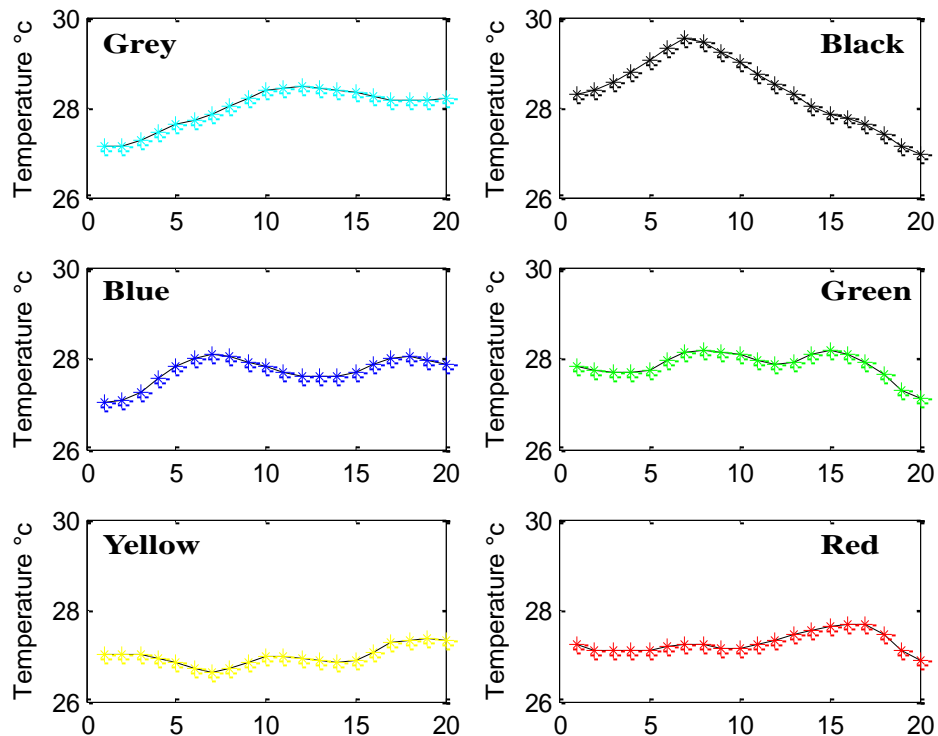
Figure 5.62: Temperature profile of each colour

5.20. Effect of different material on the thermal camera

The effect of different materials on the thermal image has been investigated. The container has been made to hold six types of soil. The test sample subjected to external heat source and the thermal images has been taken. The Figure 5.63 shows that some of the material have absorbed more heat than the others. The darker soil material have more temperature profile as shown in Figure 5.64. The other material have very close temperature profile.
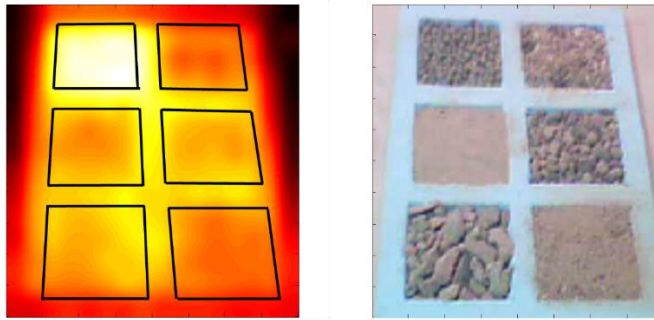
Figure 5.63: Effect of material on thermal image. Thermal image at left and visual image at right
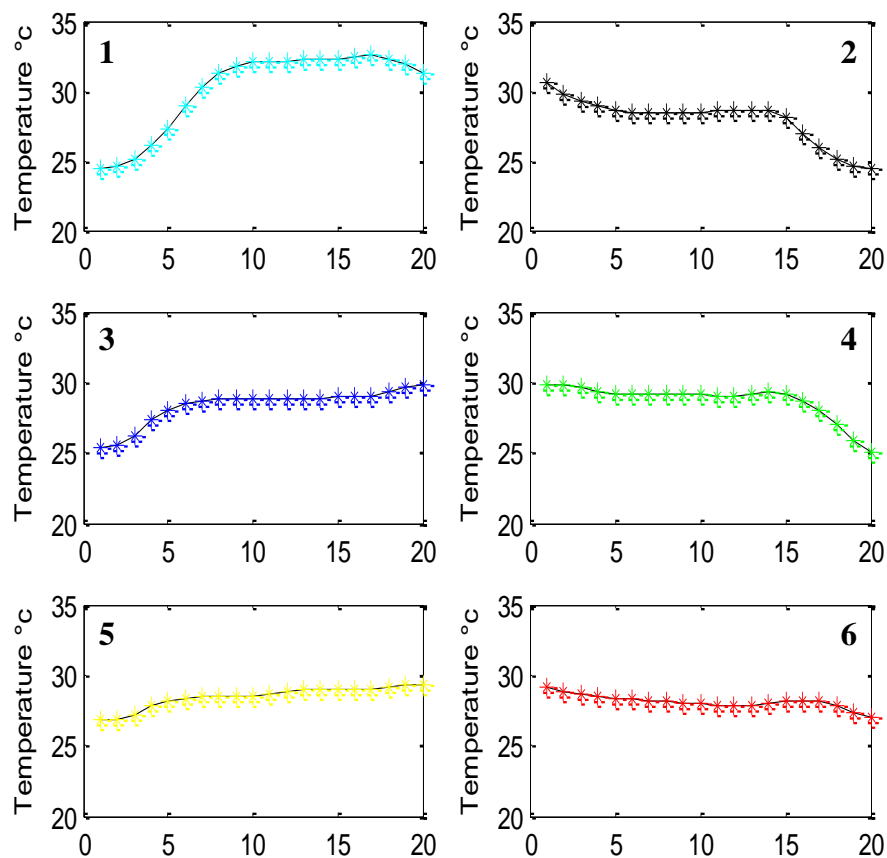
Figure 5.64: Temperature profile of each material.

5.21.   Summary:

The findings relating to the detection of the pipeline pathway and/or the leak using both the high-resolution and the low-resolution (IRISYS and Flir) cameras are summarised as follows:

5.21.1. No Leak

1. When the temperature of the water and the surface are close to each other, both cameras did not show any signs of the pipeline detection. Only blurry marks seen in the last few images which means that water must be running for longer times to detect the pipeline.

2. With some cooling, both cameras were able to detect the pipeline, however the high-resolution showed images of a better profile than the low-resolution.

3. With extra cooling, both cameras detected the pipeline with no difficulty. The profile clearly showed the pipe in both cameras.

4. Heating the surface has affected the detection despite the water is extra cold. This means that during the sunshine the thermal cameras ability decrease.

5. The low-resolution camera was able to detect the pipelines similar to the high-resolution camera if the correct image processing is selected.

5.21.2. Leak detection

1. If the leak started before or with the start of the heating period (sunrise) before it heats the surface, the thermal cameras are able to detect the leak because the surface did not heat up yet.

2. For the first stages of the leak, the best time to detect the leak is when the surface is not hot yet (night or early morning).

3. Once the moisture of the leak reaches the sub-surface or the surface, the leak will appear on the thermal image even the surface is hot.

4. Use of cold water improves when the surface in not hot yet. If it is hot already, the effect of cold water in detection will reduce.

5. The heat on the surface delays the leak detection as the surface absorbs more heat more heat with time and prevent the moisture to cool the surface.

6. Once the water from the leak reaches the surface, the leak obviously become detectable by the thermal cameras.

7.   The low-resolution camera is able to detect the leak similar to the high-resolution camera.

8.   The low-resolution camera image can be improved if combined with visual cameras.

9.   Selection of the correct image processing technique improves the detectability.

10. The correct selection of the region of interest is important to detect the leak as the incorrect selection leads to false results.

11. Objects inside the image with a lower temperature than the leak point, negatively affect the detection of the leak in the thermal image.

12. Colours and materials of the tested object have to be considered in the detection process.

13. Visibility of the low-resolution camera can be enhanced by merging the visual image with the thermal image of the low-resolution camera.

Generally, thermal technology is successful in detecting the leakage and both cameras are able to detect the leakage. The low-resolution is able to detect the leakage similar to the high-resolution. Cooling the source water improves the visibility of the leakage in the thermal image. Overheating of the surface reduces the ability of both cameras in detecting the leakage. The best time to detect the leak is at night. Selection the proper image processing technique and the exact region of interest enhances the detection process.

In addition, enhancing the visibility of the low-resolution camera is investigated and carried out by merging the visual image and the thermal image. As well as the effect of the colours and the material under test is investigated and found they are affecting the thermal image as the dark colour and some material are absorbing much heat than others.

Chapter 6. Field Work Experiment (Libya)

6.1. Introduction

This chapter is discussing the field work test which has been carried out in Libya in a real environment to test the technology of water leak detection in a buried pipe using low-resolution thermal imager. The field work aims to collect a real environmental data acquired by the thermal imager affected by real factors such the wind, the shade, and the sun. The field work has been carried out in an open area with a natural atmosphere condition in Benghazi city in Libya in October 2103.

6.2. The Field Work

The experimental work is started at the mid of a sunny day and continued with a non-stop flow for 48 hours. The water source was from a normal tap connecting to a water pipeline system.

The test area was in an open area directly exposed to sun rays most of the day with some trees shade before the sun set. The nature of the ground of the selected test area is a mixed backfill material of rocks and sand. A trench of about 270.0 mm deep excavated to install a water tube of 24.0 mm diameter. The selected tube is made of plastic material which known with its low thermal conductivity. The leak hole was one millimetre diameter to create a slow leak. The cameras used in this experiment are the thermal imager IRISYS and the digital web cam. The cameras are located in a wooden compartment to protect them from direct sun rays and any other environmental factors.
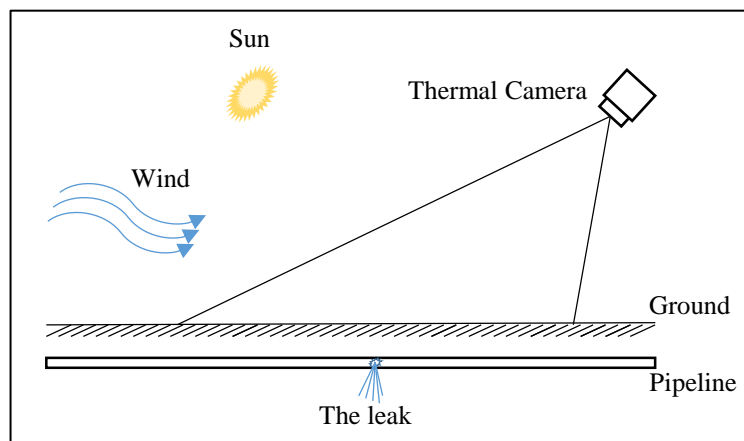
Figure 6.1: Schematic diagram for the field work.

In the first 24 hours of the experiment, no leak was allowed in order to test the ability of the thermal camera to detect the buried pipeline (the water tube) of that size and material in that environmental condition. Also to see the ability of the camera to detect a pipeline buried in a depth with a backfill cover equals to ten times its diameter. The next 24 hours (the second day) the water allowed to leak through the pre-prepared leak point to run for 24 hours. That was to check the ability of the cameras to detect the leak during the day and night times. As well as to allocate the best time the camera can detect the leak. Figure 6.2 shows the general view of the experiment area showing the cameras' compartment and the test area. The photo in the figure is taken at the end of the experiment as the leak is evident on the surface of the test area.
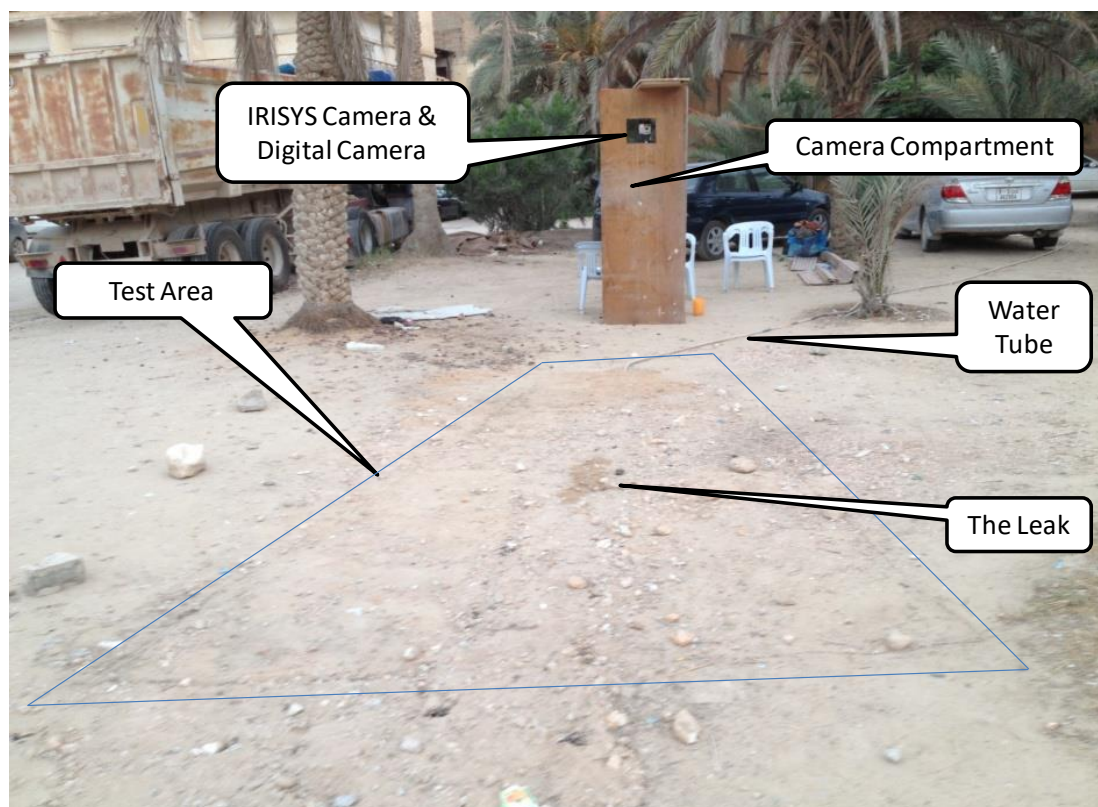
Figure 6.2: General view for the test area and the cameras' compartment.

6.2.1. Thermal and Visual camera setup

Figure 6.3 shows the cameras and their setup. The digital camera fitted on the top of the thermal camera and then fitted on a tripod. The cameras are located in a container as shown in Figure 6.4 to protect them from exposure to direct sun rays and other environmental influences.

(a)   (b)
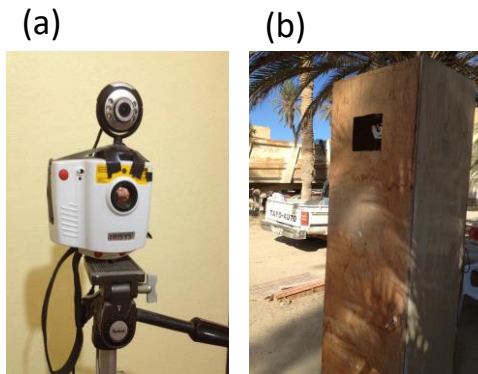
Figure 6.3: The cameras (a) and their setup box (b).

Figure 6.4: The cameras and the computer inside the compartment.

6.2.2. The Trench

The trench has been excavated in the test area in front of the camera compartment as shown in Figure 6.5. The length of the trench is five meters long and its width is 270.0 mm. Figure 6.6 shows the depth of the trench measured at two different locations before and after positioning the tube inside it. With this depth, the cover material above the tube is ten times the tube diameter.

(a)   **(b)**
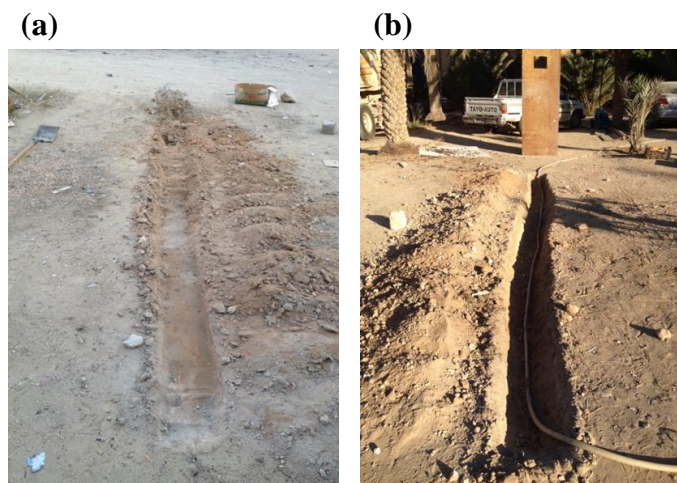
Figure 6.5: Image (a) shows the start of the excavation and image (b) shows the complete trench with the tube.

(a)   **(b)**
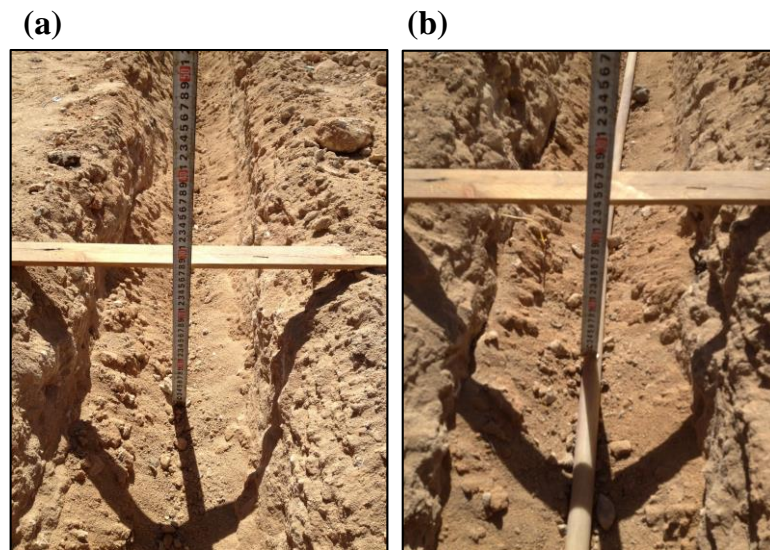
Figure 6.6: The depth of the trench with and without the tube at different locations.

6.2.3.   The pipe

The used pipe is a reinforced flexible hose usually used in water irrigation systems. The hose is a normal tube that is made of plastic material. The tube outside diameter is 24.0 mm (Figure 6.7). The reason for selecting this type of tubes is that their material is known with its low thermal conductivity.

Figure 6.7: the size of the tube

6.2.4.   The leakage Point

To have a leak during the test period, a steel wire with tapered end prepared to create the leak hole. The leak hole made by inserting the tapered wire through the tube wall and left it stuck in the tube to prevent any leak till the time of leak should start. The leak hole made at a midpoint of the trench as shown in the next photos. It was located three meters from the nearest end of the trench towards the cameras compartment. See Figure 6.8.
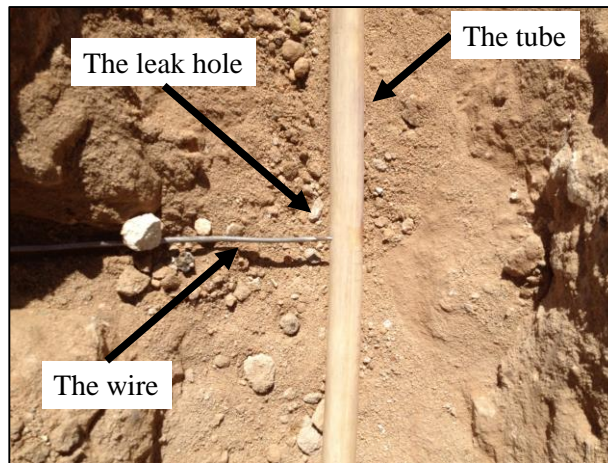
Figure 6.8: Figure shows the steel wire inserted in the tube for the leak event.

6.2.5.   Test Area Dimensions

The test area that can be detected by the thermal camera is identified and marked on land and then measured. As the camera is placed at the inlet side of the test area and because it is set on low height (2 meters), the test area that appears in both thermal and visual camera is narrow at the inlet side and wide at the outlet side. The dimensions of the test area are shown in Figure 6.9
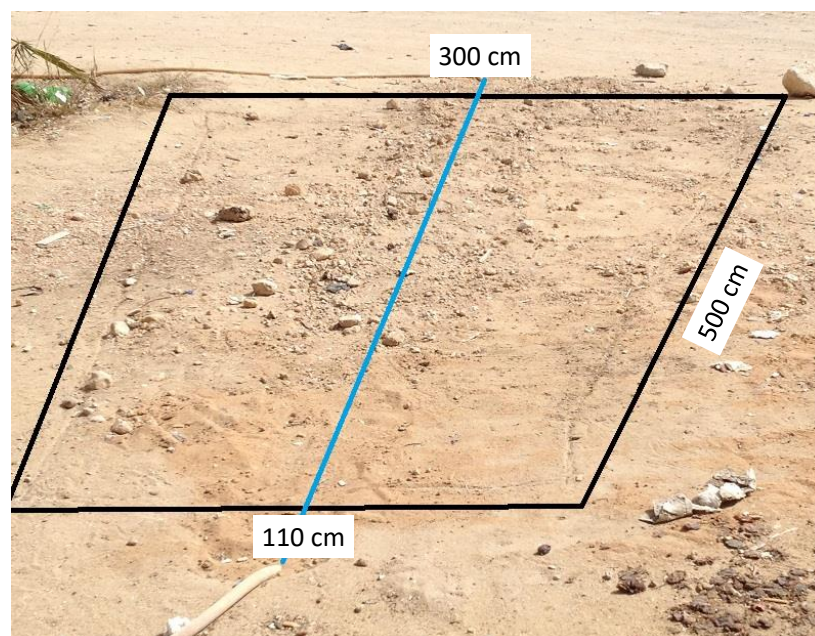
Figure 6.9: Outlined image shows the test area boundary (back line) and the pathway of the pipe (blue line).

6.2.6.   Water Flow:

Water flow has been measured manually each 15 to 20 minutes interval using one litre size container. The process carried out by filling the one litre size container and monitoring it using a stopwatch timer. The flow found to be ranged from about 0.06l/s (Litre/Second) to nearly 0.2l/s. The flow left as it is coming from the mains with its own pressure which was low. No extra pressure has been applied to the water flow. The following chart Figure 6.10 shows the records of water flow taken throughout the whole experiment period. As illustrated in the figure, the flow rate reaches its peak at night time.
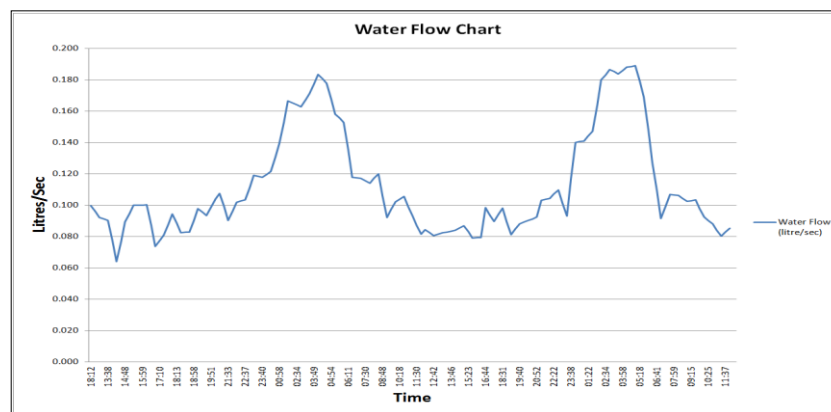
Figure 6.10: Measured water flow chart

6.2.7.   Weather

Generally the weather at the time of the experiment was calm, sunny and fine. See Figure 6.11. It was hot in the day hours and pleasant at night hours. The sky was clear and cloudless.

Figure 6.11: Typical Libyan desert weather.

6.2.8.   Water and Atmosphere temperatures

Water temperature and atmosphere temperature have been monitored approximately every 15 minutes to 20 minutes for 48 hours started mid-day at about 12:17 stopped at 12:30. As shown in Figure 6.12 the water temperature which ranged between 29 and 31 degrees centigrade changed slightly with the change of the atmosphere temperature. The weather was generally hot and the temperature of the atmosphere was lower at night than day time and ranged from 23 to 37 degrees centigrade.
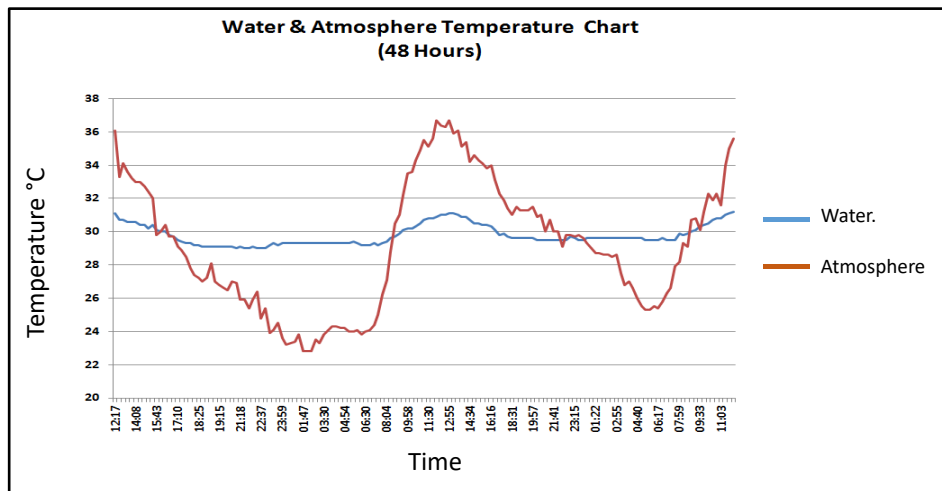
Figure 6.12: Water and Atmosphere recorded temperature Chart

The following tables Table 6-1 show the records of the weather in details during the 48 hours of the experiment. The table show the average temperature, rain, wind and humidity, for each day with interval of three hours. The records form "world weather online" website.

Table 6-1: Records for the weather information during the three days of the experiment.

Day	Time	Weather	Temp	Feels	Rain	Cloud	Wind	Gust	Humidity	Pressure
Sun 29 Sep	02:00		24 °c	26 °c	0.0 mm	0%	8 mph ENE	13 mph	57%	1015 mb
	05:00		23 °c	25 °c	0.0 mm	0%	6 mph E	12 mph	57%	1014 mb
	08:00		26 °c	27 °c	0.0 mm	0%	6 mph ESE	7 mph	53%	1015 mb
	11:00		31 °c	32 °c	0.0 mm	0%	2 mph SE	2 mph	42%	1015 mb
	14:00		32 °c	31 °c	0.0 mm	0%	7 mph NW	8 mph	33%	1014 mb
	17:00		31 °c	31 °c	0.0 mm	0%	12 mph NNW	14 mph	35%	1013 mb
	20:00		27 °c	27 °c	0.0 mm	0%	10 mph NNE	14 mph	46%	1013 mb
	23:00		26 °c	27 °c	0.0 mm	0%	7 mph ENE	13 mph	44%	1013 mb

Day	Time	Weather	Temp	Feels	Rain	Cloud	Wind	Gust	Humidity	Pressure
Mon 30 Sep	02:00		26 °c	26 °c	0.0 mm	0%	9 mph ESE	17 mph	45%	1012 mb
	05:00		24 °c	26 °c	0.0 mm	0%	12 mph SE	23 mph	57%	1011 mb
	08:00		26 °c	27 °c	0.0 mm	0%	14 mph SE	18 mph	56%	1012 mb
	11:00		32 °c	31 °c	0.0 mm	0%	13 mph S	15 mph	35%	1012 mb
	14:00		34 °c	34 °c	0.0 mm	0%	14 mph SW	16 mph	30%	1010 mb
	17:00		33 °c	33 °c	0.0 mm	0%	12 mph SW	14 mph	30%	1008 mb
	20:00		30 °c	29 °c	0.0 mm	2%	7 mph SSW	14 mph	33%	1009 mb
	23:00		29 °c	28 °c	0.0 mm	2%	7 mph SSW	15 mph	33%	1009 mb

Day	Time	Weather	Temp	Feels	Rain	Cloud	Wind	Gust	Humidity	Pressure
Tue 01 Oct	02:00		26 °c	26 °c	0.0 mm	10%	7 mph SW	15 mph	35%	1008 mb
	05:00		25 °c	26 °c	0.0 mm	10%	6 mph NW	14 mph	58%	1008 mb
	08:00		27 °c	29 °c	0.0 mm	3%	9 mph NNW	10 mph	70%	1008 mb
	11:00		29 °c	31 °c	0.0 mm	14%	13 mph NNW	15 mph	56%	1009 mb
	14:00		31 °c	33 °c	0.0 mm	3%	19 mph NW	21 mph	52%	1008 mb
	17:00		31 °c	35 °c	0.0 mm	4%	19 mph NW	22 mph	62%	1008 mb
	20:00		28 °c	31 °c	0.0 mm	54%	17 mph NW	19 mph	72%	1010 mb
	23:00		27 °c	29 °c	0.0 mm	54%	15 mph NW	17 mph	74%	1010 mb

Source: http://www.worldweatheronline.com/v2/weather.aspx?q=Benghazi,%20Libya&day=21

The average of the high and low temperatures in Benghazi throughout the year are shown in Figure 6.13. This chart gives an idea of how hot or cold Benghazi is. The chart readings were close to the readings taken during the experiment.
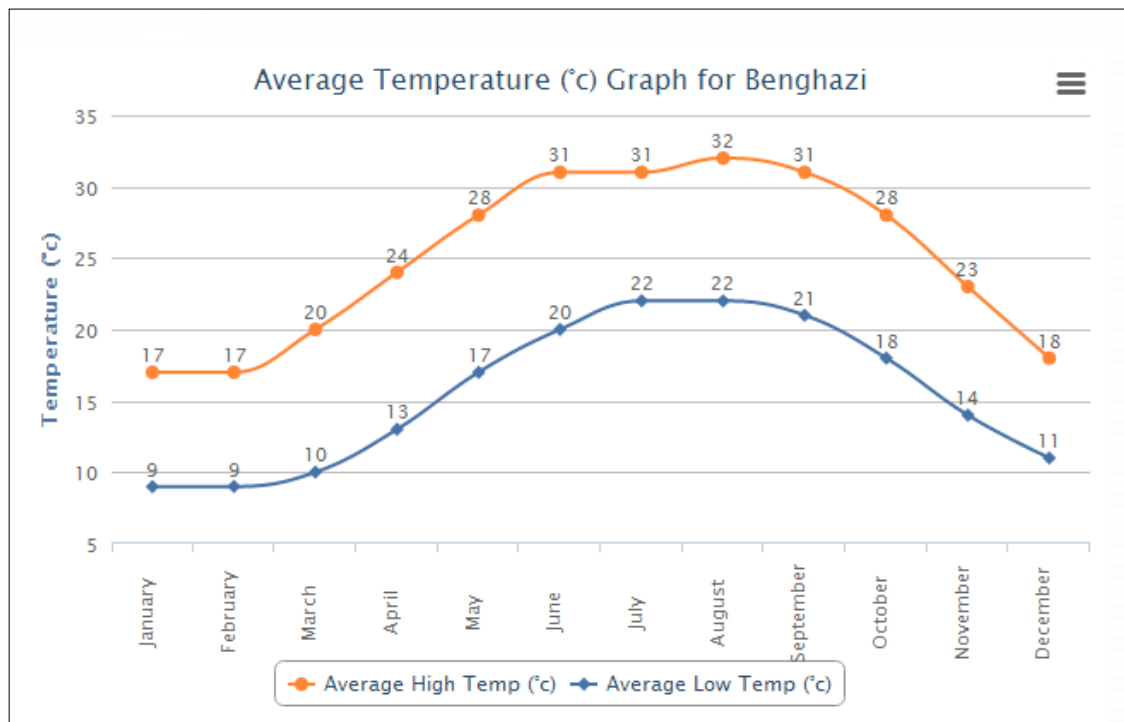
Figure 6.13: Average High/Low Temperature for Benghazi, Libya.
Source: http://www.worldweatheronline.com/Benghazi-weather-averages/Banghazi/LY.aspx.
28/10/2013
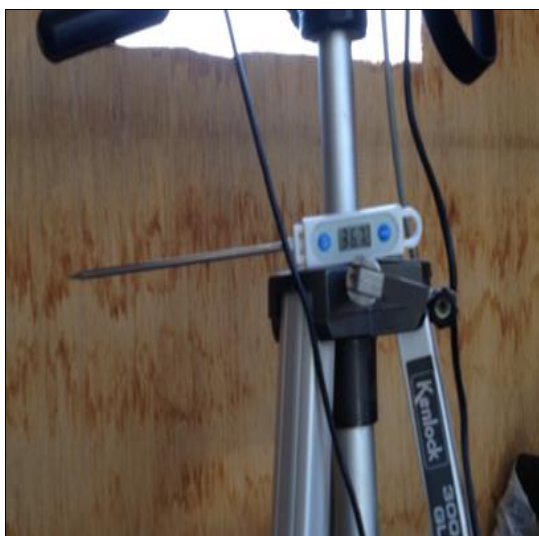
(a) **(b)**
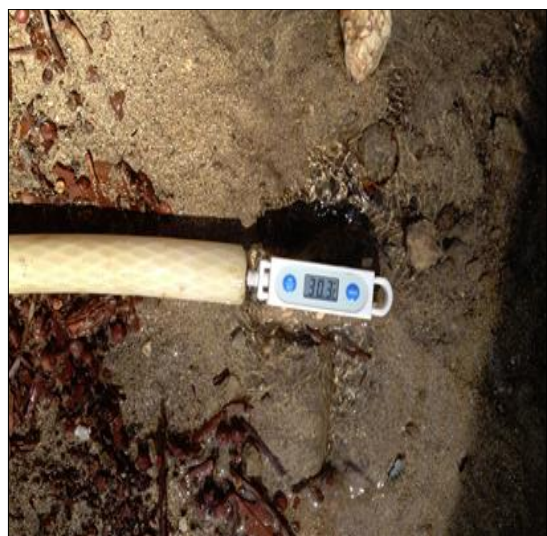
Figure 6.14: Monitoring of the atmosphere (a) and water temperatures (b).

The water and the atmosphere actual temperatures have been monitored manually in 15 to 20 minutes time intervals. The thermometer for water temperature located at the last end of the tube while the thermometer of the atmosphere located inside the compartment where the thermal camera and visual camera were located in a shade area; See Figure 6.14.

6.2.9.   Actual Leak:

Figure 6.15 shows the actual image of the leak after it became clearly visible on the surface. The Figure 6.16 shows the leak part of the tube after it was exposed.

(a)   (b)
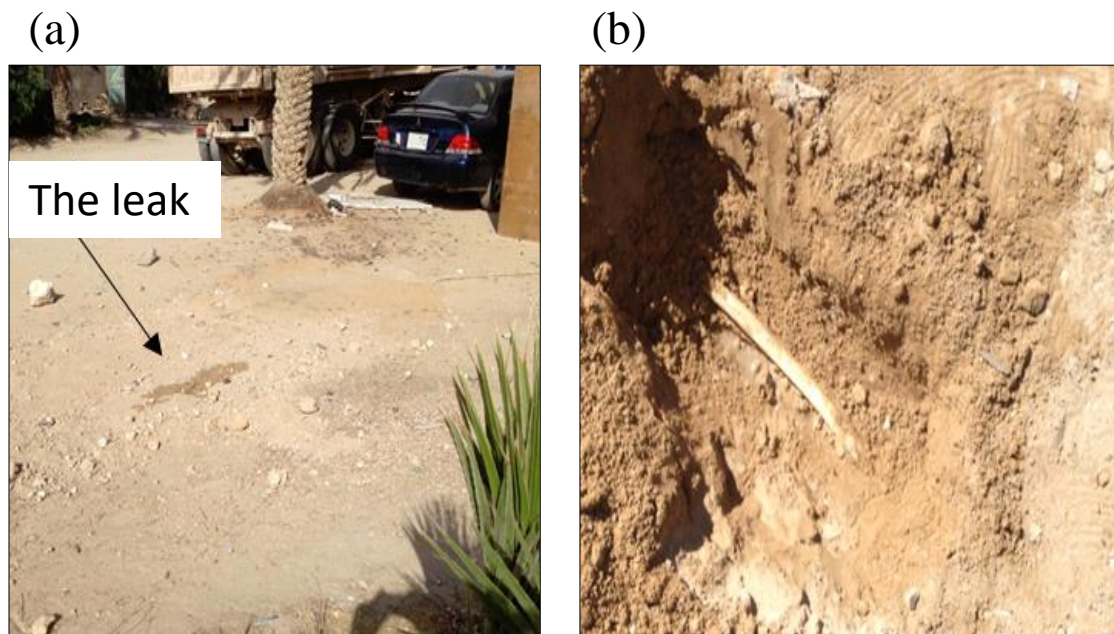
Figure 6.15: Leak images, (a) image shows the leak on the surface and (b) shows the leaked tube.

Figure 6.16 shows a very thin stream of the leak. The leak flow rate was low and has no noticeable effect on water flow in the pipe. This low rate of leak is expected because the leak hole was as small as 1mm and the pipe is not pressurised. Figure 6.17 shows the leak hole after cleaning the pipe.
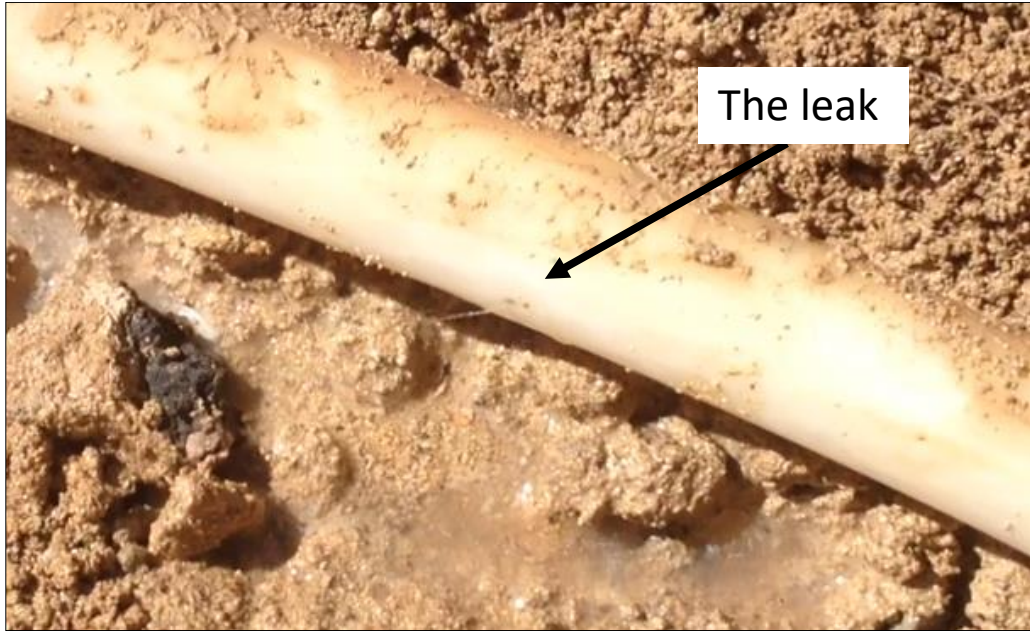
Figure 6.16: The image shows the leak stream

Figure 6.17: The leak hole after cleaning

6.3. Discussion and Analysis:

6.3.1.   Processed IRISYS Images Vs Digital Camera Images:

In this section, the processed thermal imager from the thermal camera (IRISYS) is presented in detail and compared with the visual camera images taken at the same time. Some of the visual images are taken at night time and revealed nothing (black image) because the test area was dark (no lighting). At the beginning of the experiment, a thermal image and visual image have been taken to the test area before the backfill and the water flow has already started. Figure 6.18 (a) shows the trench with the pipe before backfilling and (b) shows the thermal image. The thermal image clearly showed cold area along the pipeline.
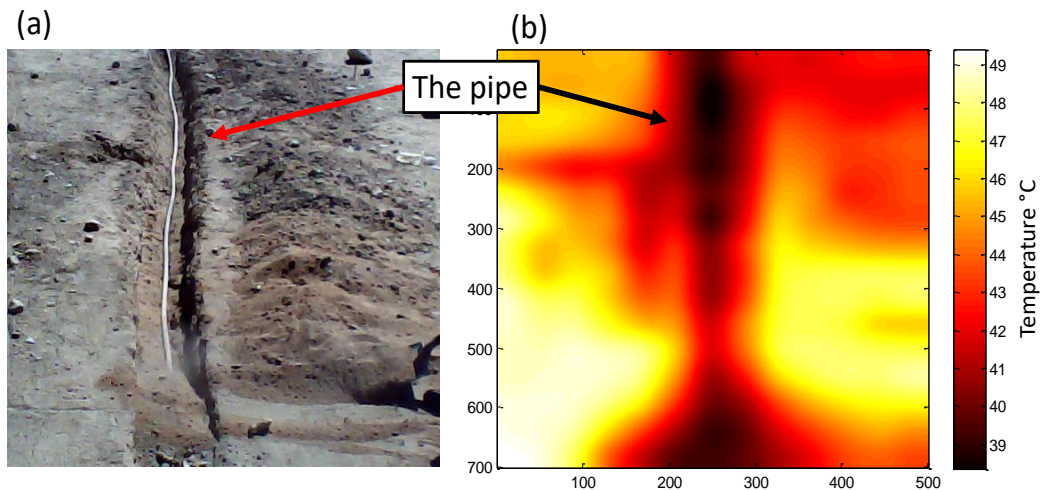
Figure 6.18: Visual images (a) and thermal image (b) for the trench and the pipe at 12:30.

After backfilling the thermal image did not show any thing because of the sun. The temperature of the ground exceeded 50 °C. The temperature distributed unequally on the ground. Some parts showed a higher temperature than others. See Figure 6.19. Late afternoon, some trees shade moved over the test area and affected its temperature widely (Figure 6.20). In the late afternoon, the temperature of the ground decreased from over 50 ℃ to nearly 40 ℃.

(a)   (b)
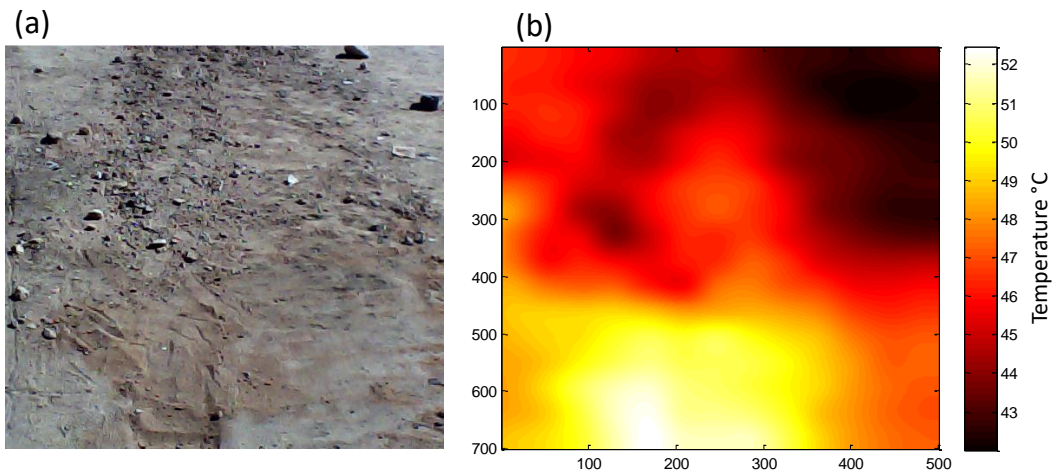
Figure 6.19: the visual image (a) and the thermal image (b) after backfilling at 14:10.

(a)   (b)
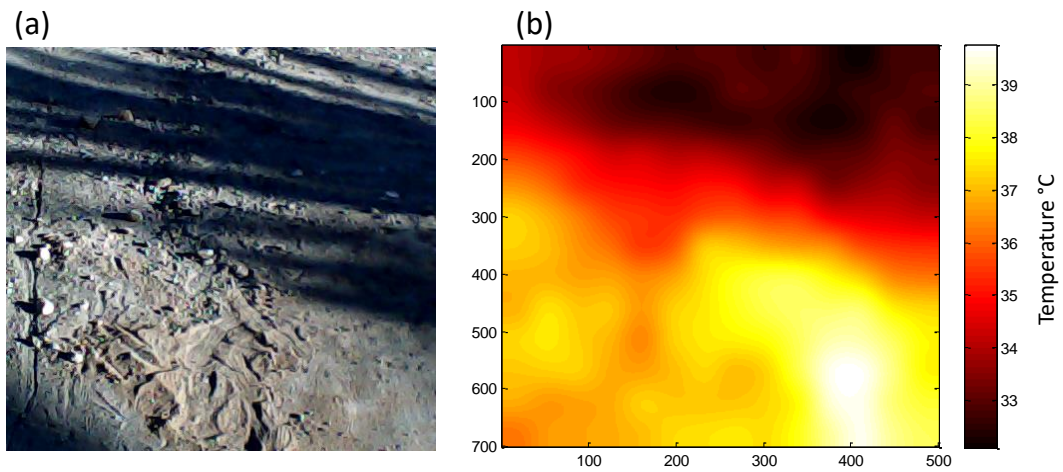
Figure 6.20: Trees shade over the test area at 16:45.

The effect of the trees shade continued during the sunset period (Figure 6.21).

(a)   (b)
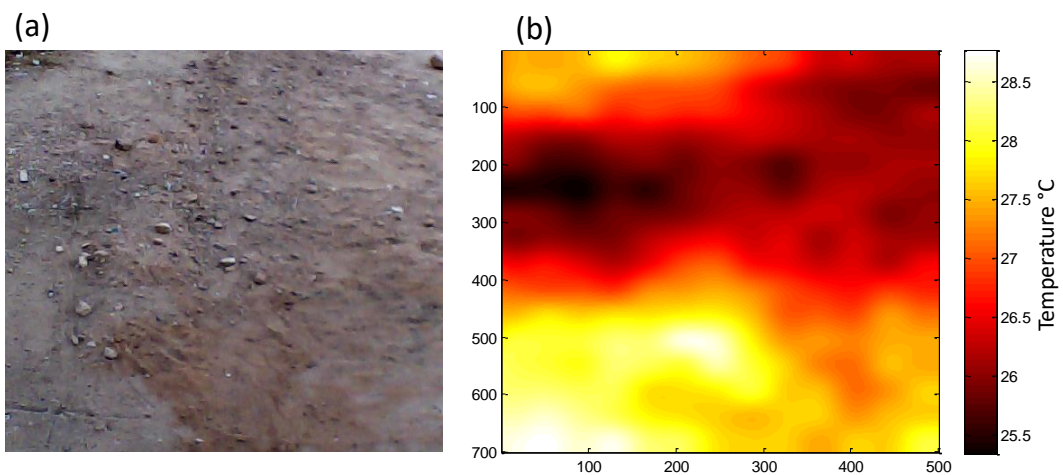
Figure 6.21: The effect of the shade continued at 18:35.

Figure 6.22 (a – e) shows a series of five visual and five thermal images for the period just before the sunset till the period just after the sunset. The visual image failed to show any images (c-d) because the area of the test has no light. The thermal images still showing the effect of the shade even after the sun set.
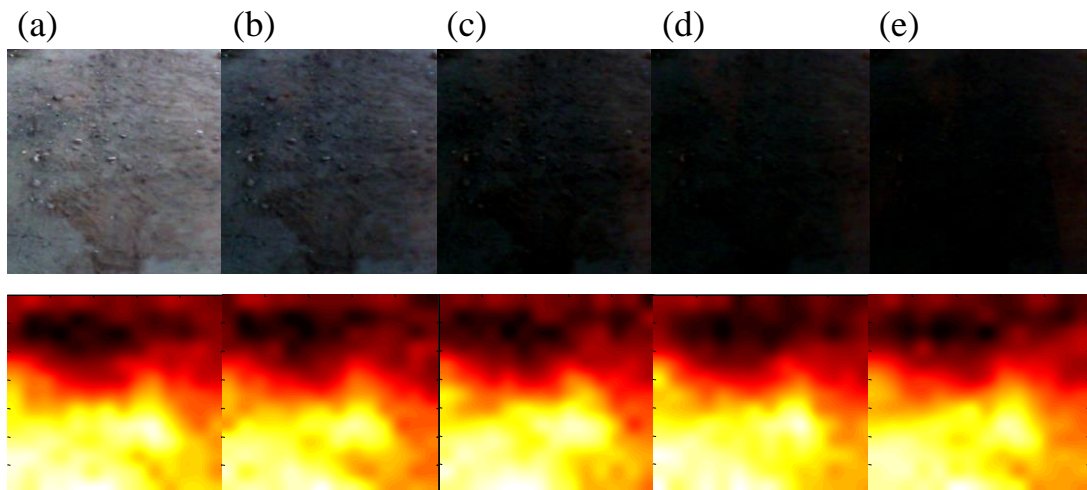
Figure 6.22: Images before and after the sun set. Time from 18:41 to 18:51.

At 21:05 the surface of the ground cooled and the thermal image showed the traces of the pipeline.
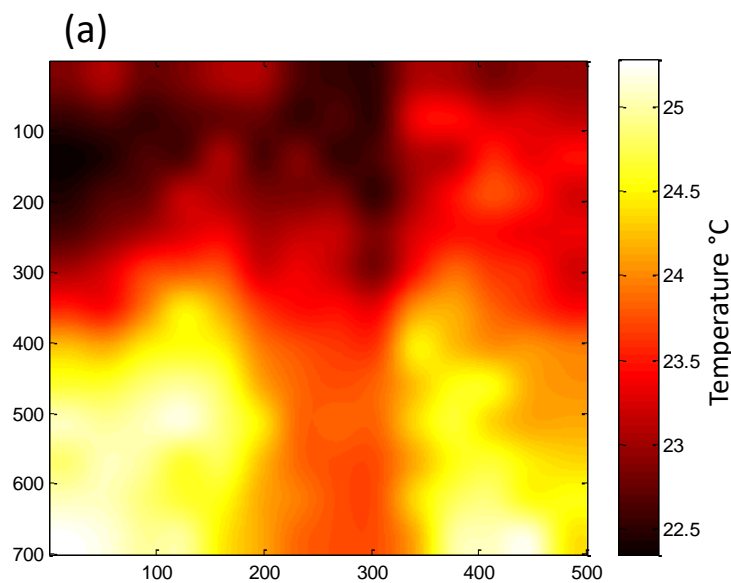
Figure 6.23: Traces of the pipeline at 21:05.

During the night after hour 21:00, the thermal images continued to show the pipeline traces until the next day morning at 07:50. Figure 6.24 (a-c) shows the thermal images

during the night. The pipeline traces are clear in the thermal images. The best visualisation of the pipeline traces was at 04:40 am.
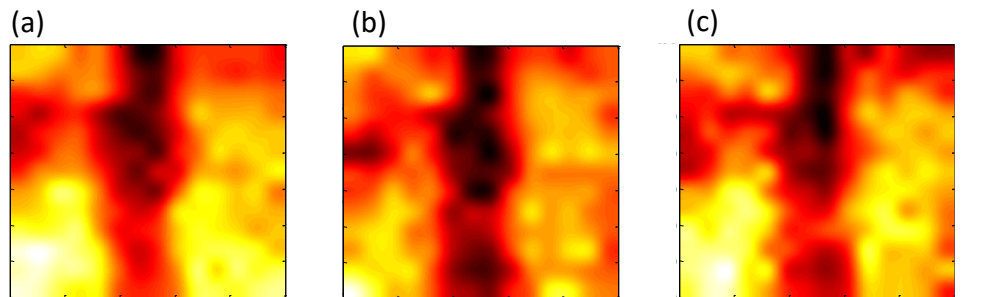
Figure 6.24: the thermal image shows the pipeline traces at night. Image time at 03:00 am (a), at 04:40 am (b), and at 06:40 am (c).

Figure 6.25 shows a series of five visual images and five thermal images for the transition period from night to day (06:06 am to 06:40 am). The thermal image continued to show the traces of the pipeline.
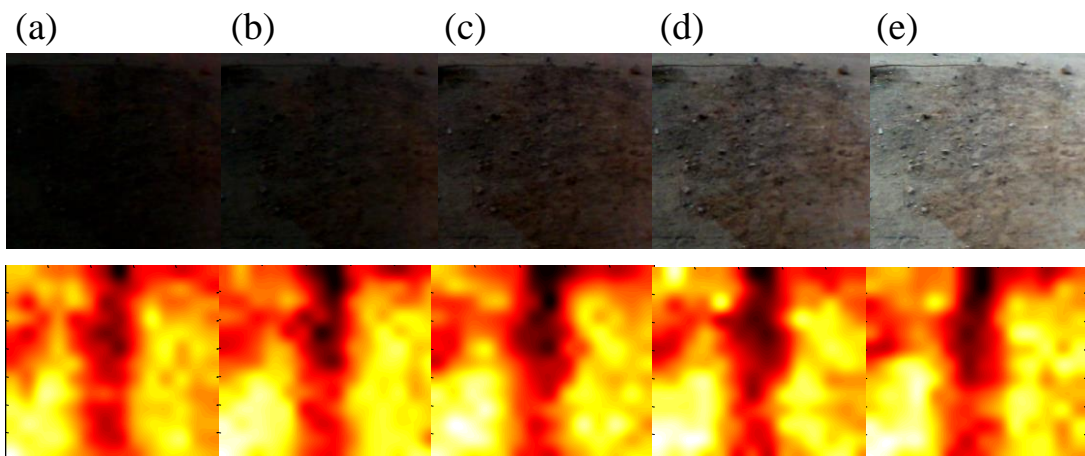
Figure 6.25: Visual images and thermal images for the transition period night to day from 06:06 to 06:14.

At 08:00 am, the pipeline traces disappeared completely as the sun was rising up. Figure 6.26 shows the thermal image at 08:00 am. The image shows some cold area at the upper left side because of a small tree shade nearby the test area.

(a)   (b)
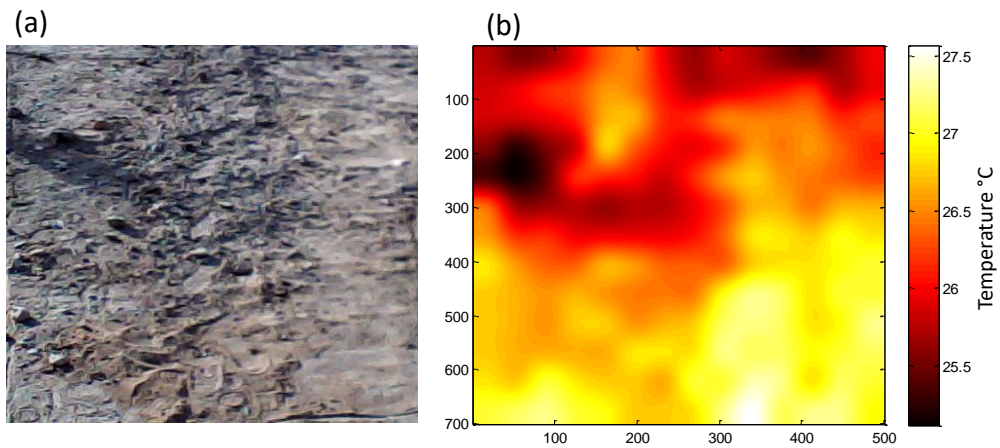
Figure 6.26: The thermal image at 08:00 am shows nothing due the sunrise

The thermal image continued to show nothing important until late afternoon. Apparently, the high level of heat on the ground because of the sun affected the ability of the thermal camera. The temperature of the ground reached its peak at 13:00 and ranged from 47 ℃ – 54 ℃.

(a)   (b)
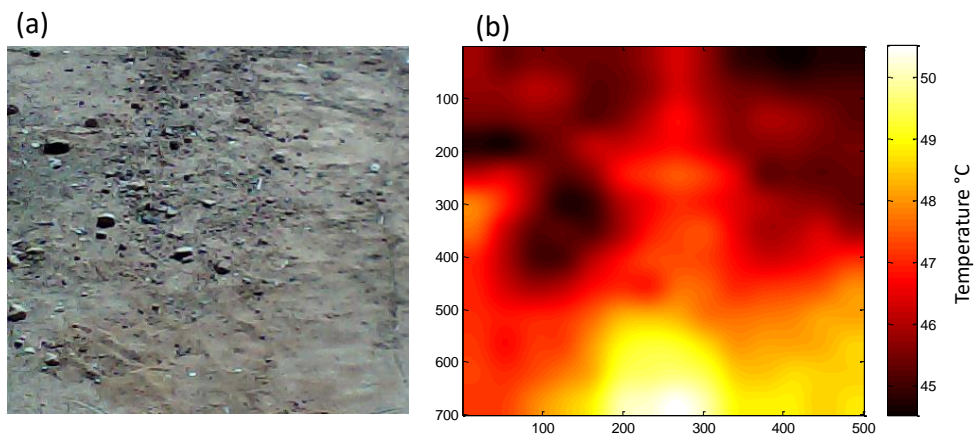
Figure 6.27: Visual and thermal images taken at 12:00 pm when the leak started.

(a)   (b)
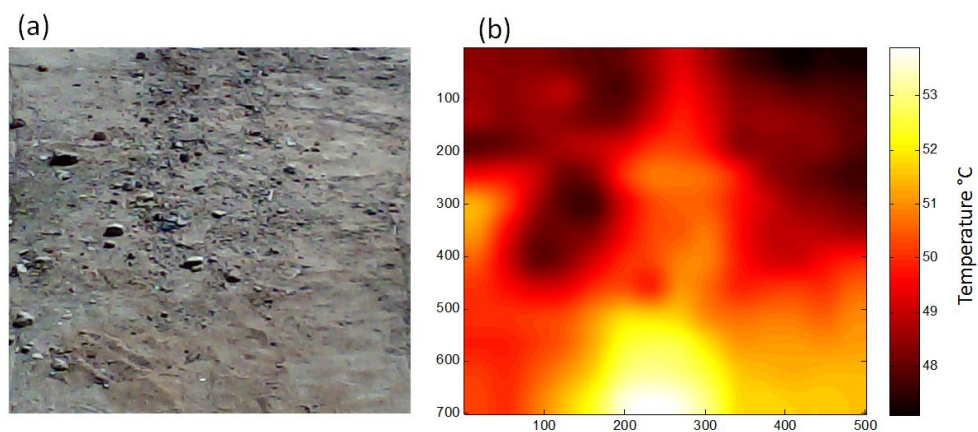
Figure 6.28: images taken at 13:00 when the temperature of the ground reached its peak.

6.4. The leak period

The leak started at 12:00 afternoon of the second day by removing the steel wire attached to the pipe. The leak is small because the hole of the leak is only 1.0 mm and the pressure in the pipeline is low. The First traces of the leak have been seen at 15:40 as shown in Figure 6.29. The area above the pipeline has been warmer than the surroundings which could be because that area is excavated recently and therefore it absorbs more heat than the surrounding. Even though, the leak flow rate is low and the surface heat is high, the leak appeared for a little time and then disappeared.
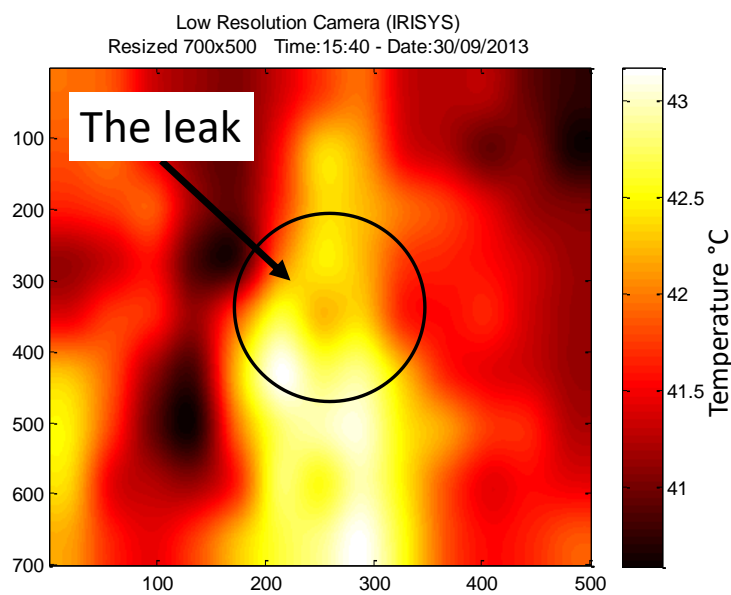
Figure 6.29: First traces of the leak
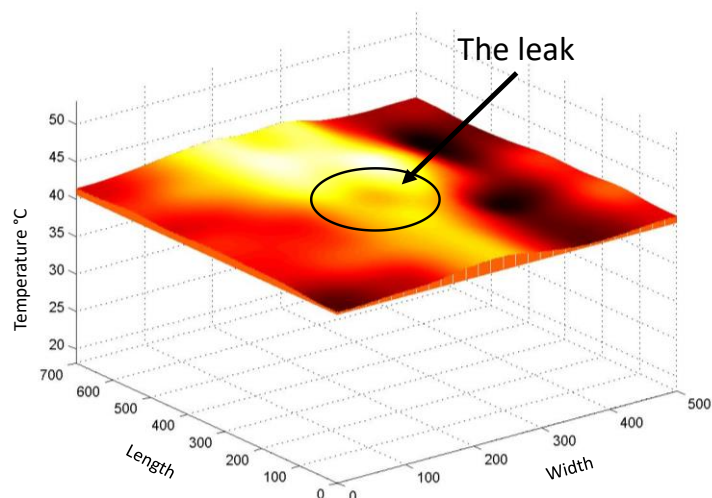
Figure 6.30: The leak traces in 3D mesh.

In Figure 6.31, the leak disappeared and then appeared several times on the thermal images because of the temperature changing as shades of some tress passes over the test area. The shade affected the detection of the leak because the shade cools the ground down. At the same time when the shade passed over the test area the leak appeared in some images then disappeared again. See Figure 6.31 and Figure 6.32.
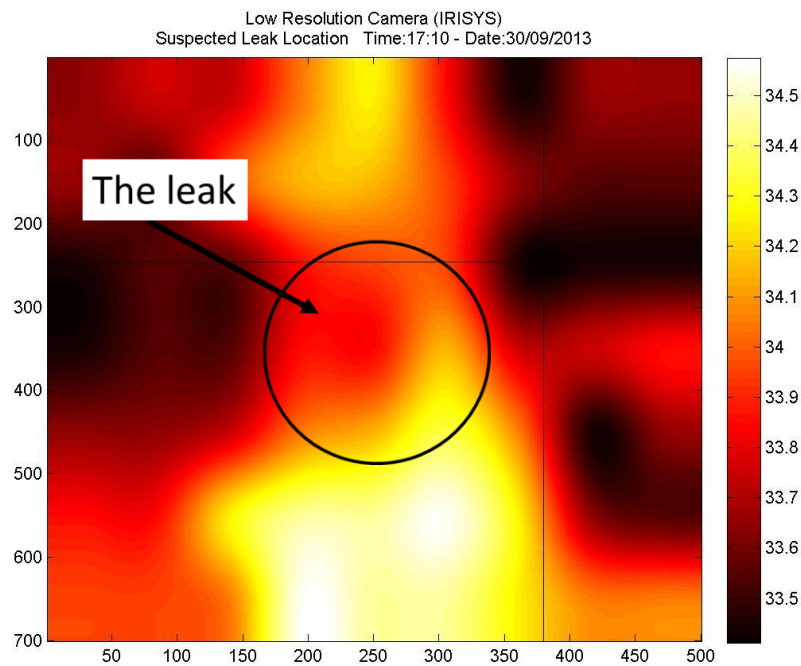
Figure 6.31: Traces of the leak fades out
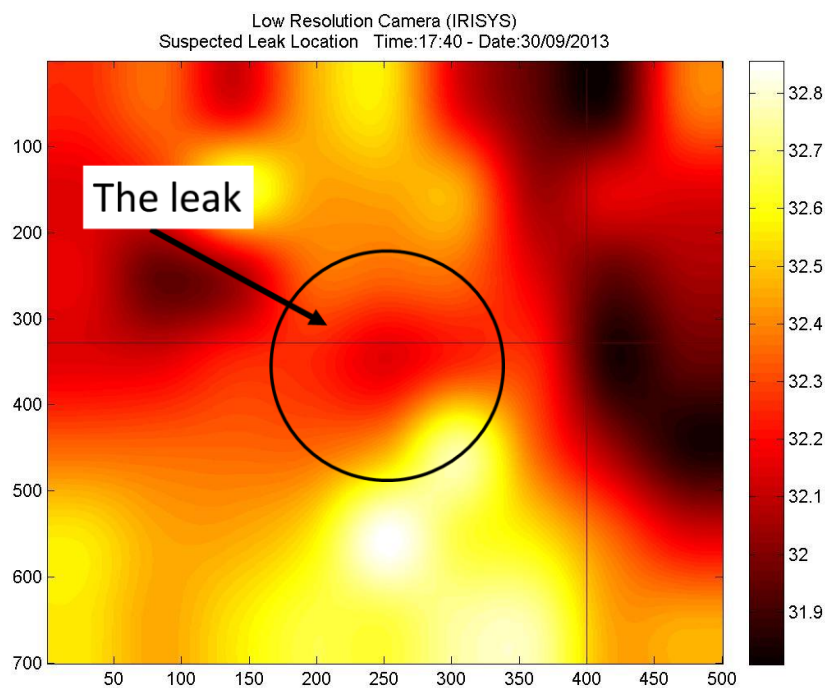
Figure 6.32: The leak appears while the shade of trees covers the test area.

During the transition period from day to night which started at 18:40 to 18:48 as shown in Figure 6.33 (a-e) the leak did not show. The visual camera again became useless during the night.
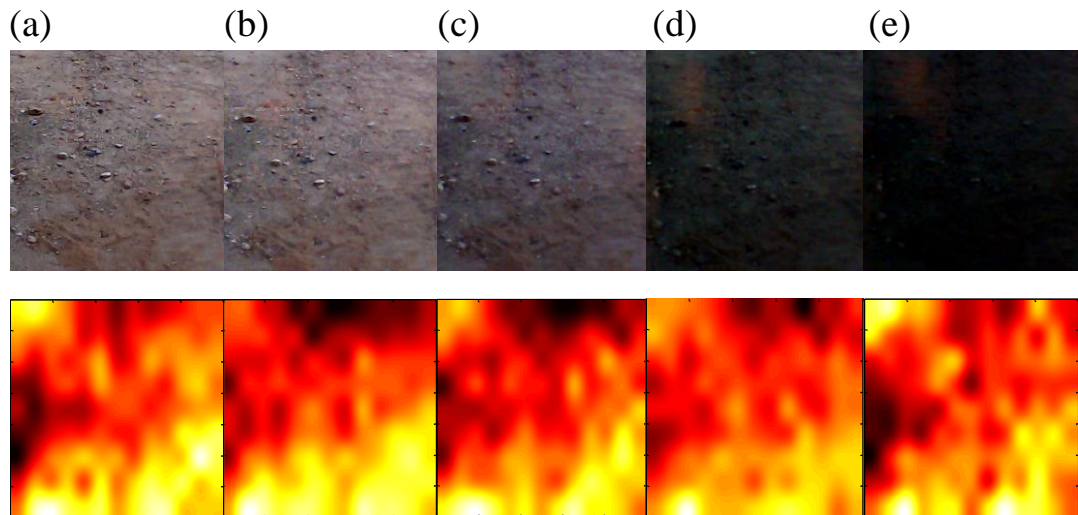
Figure 6.33: the visual image and thermal images during the transition period at sun set.

After sunset the leak becomes more evident however after while disappeared again (Figure 6.34) and this might be due to the cooling down of the ground.
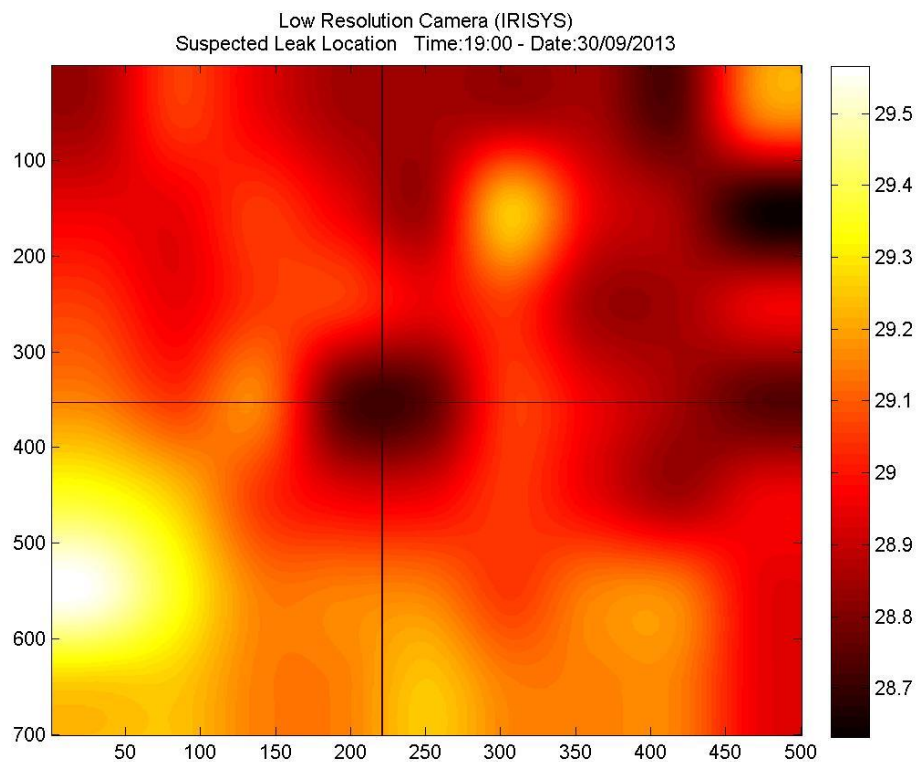
Figure 6.34: The first time the leak becomes so evident in the thermal images.

At 20:10, the leak appeared again not as a round spot this time but as a long oval shape extends along the pipeline. It seems that the leak is affecting the area nearby as well (Figure 6.35).
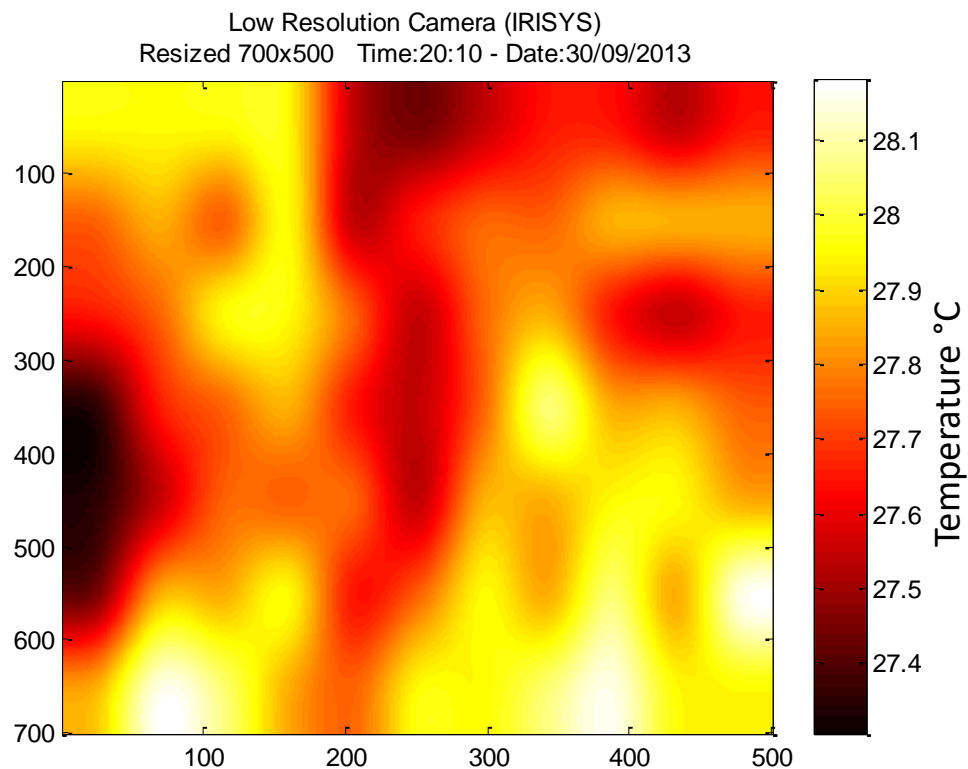
Figure 6.35: The leak appearing as longer ellipse along the pipeline.

The leak again disappeared and appeared until 21:00 image no. 1 in Figure 6.36 until disappeared at 21:30 images no. 4 & 5 to appear clearly at 21:50 in images 6 to 8 then faded out in images 9 & 10. At 22:40 the leak appeared clear again in image no. 11 after which it became consistent and continuously appeared in the thermal image until it is 04:50 early morning in image no. 21 to fade out again and appears at 05:40 but not clear enough. In image no. 24 at 08:15 to appeared clearly and stayed consistent even after the sun rise as the water from the leak reached the surface.
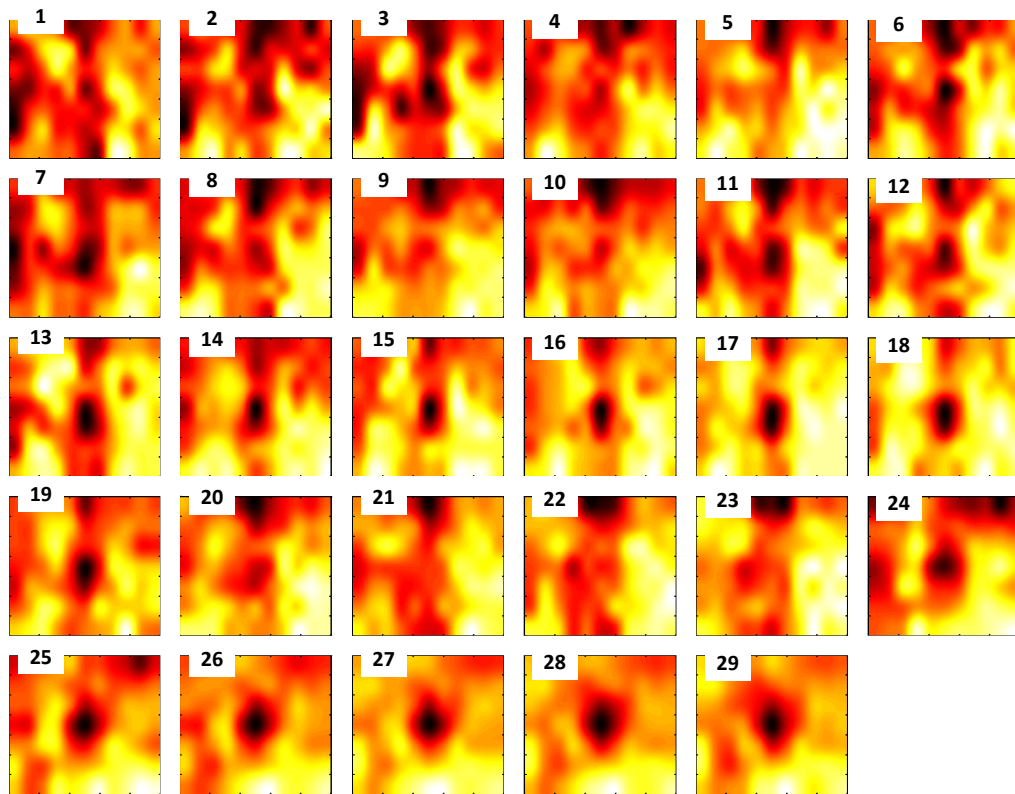
Figure 6.36: A series of thermal images summarise the leak status during the night.

6.4.1.   Temperature Chart (Water, Air and Soil)

Figure 6.37 shows the temperatures chart incorporated with some thermal images for certain milestone points. The thermal images for critical points presented as the peak, neutral and bottom points in the chart close to each other. The chart illustrates that, at the peak and bottom points, the pipe pathway or the leak was detected easily but at the neutral points it was difficult and that can be due the fact that the temperatures of the water, atmosphere and soil are very at the neutral points.
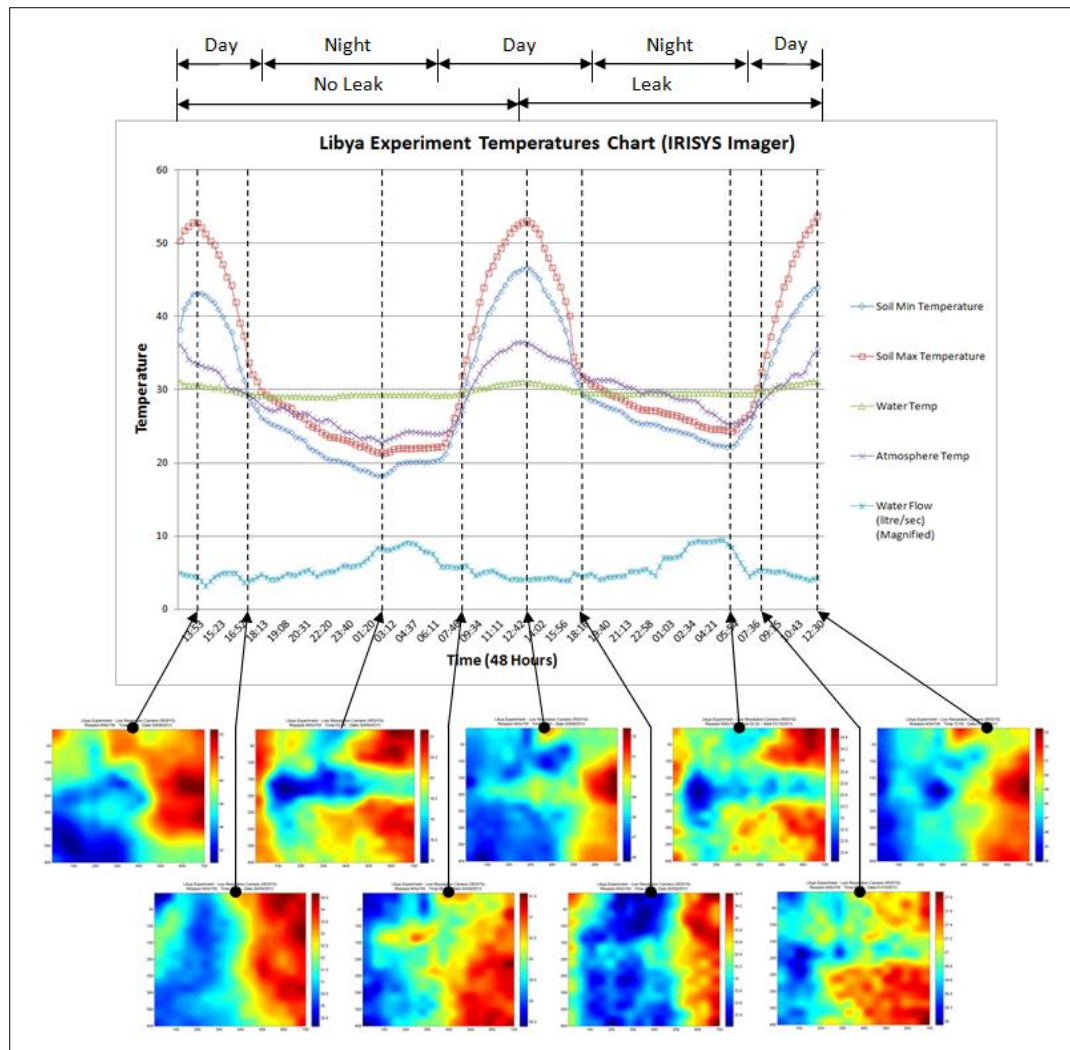
Figure 6.37: Soil, Air, Water temperatures chart incorporated with the associated IRISYS images.

It is worth mentioning that, the actual leak was neither visible by eye nor captured by the visual camera as it began at the night time and there was no artificial source of light in the vicinity of the experiment area.

6.4.2.   Analysis of the experiment image using thresholding:

6.4.2.1.   First 24 Hours (No Leak)
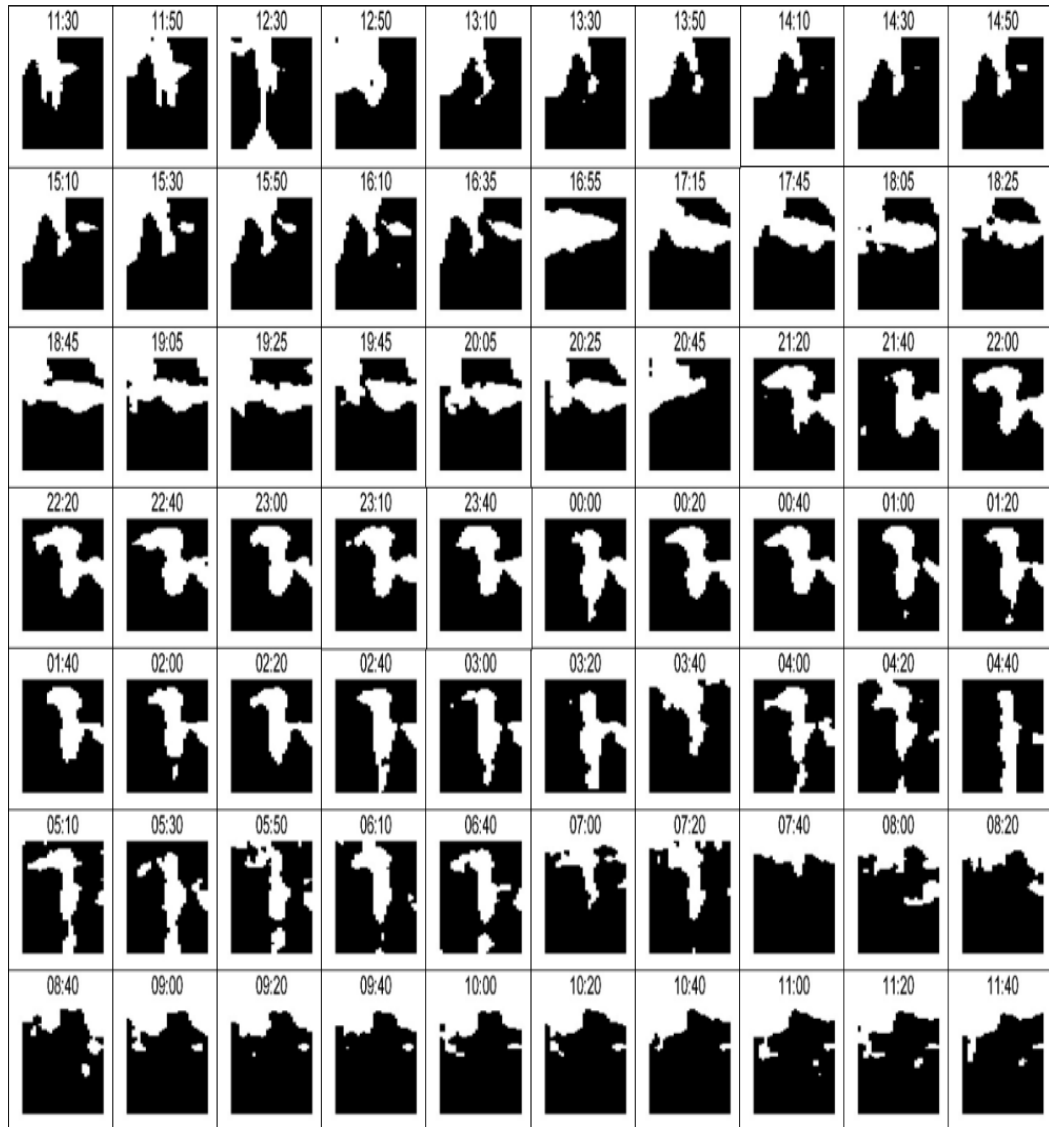
Figure 6.38: series of process image for the first day (No Leak)

The first group of the images on Figure 6.38 showed that the camera were able to detect the pipeline with some difficulties. However, the camera could not detect the pipeline when some trees shade passed over the test area. Moreover, when sunrise up, the heat of the sun affected the pipeline detection. The best time to detect the pipeline as revealed by this image is during night time

6.4.2.2.   Second 24 Hours (Leak)
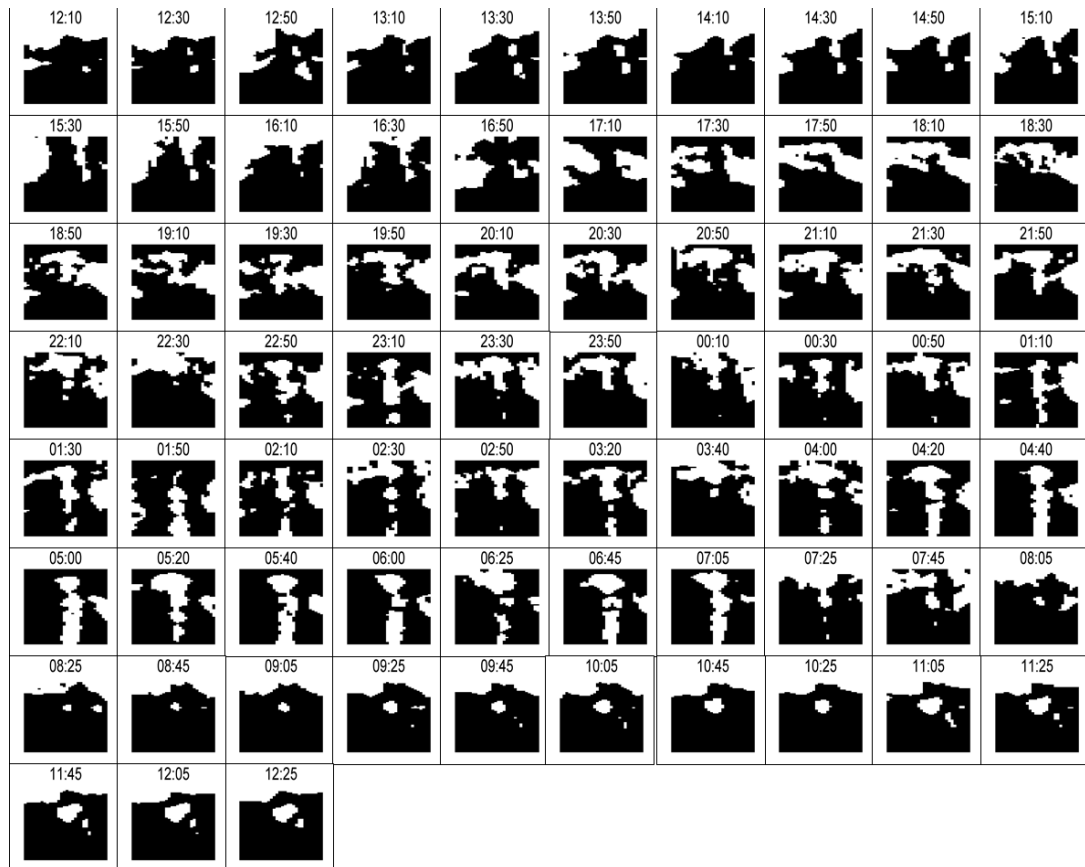
Figure 6.39: A series of process image for the first day (Leak)

Figure 6.39 shows the second group of images when there is a leak in the system, the camera is able to detect the leakage in the day time with some difficulties as well. However during the shade that passing over the test area, the images showed some signs of leakage. In the next day morning when the sun rise up the camera were able to detect the leak without difficulties.

6.5. Summary

The chapter illustrates in detail the methodology of applying the thermal technology in a field work in a real warm environment which is Libya. The first section of the chapter presents the camera, the software, the pipe used, the trench and the test area dimensions, and the tools used to perform the field work. A brief about the weather status has been provided as well. The second section of the chapter has provided a detailed discussion and analysis of the leak detection process during the field work. It has been illustrated that the leak started to appear before the sun set but because the movement of the

temperature due to natural factors such the wind and the shade of trees, the leak was not consistent. It did appear and disappear several times until it became consistent and evident at the night time. The next day, the leak became visible and continued to appear on the thermal images even when the sun is there.

In a summary, the thermal technology can detect the leak in a real warm environment. This requires selecting the best image processing technique and the time of detection which as revealed in this field work is at night.

Chapter 7. Thermal Image processing

7.1. Extracting Features from the thermal images for leakage detection.

In order to automate the process of leakage detection using the thermal image, Image's features were identified to differentiate between the images with and without leak spots. Shape recognition is carried out by using two methods; 1) comparing the image with a previously stored image of the same state and 2) defining a number of metrics in the image to identify the required shape [113]. In this research work, many features is selected and tested to identify the images with leak spots based on the method number two by defining the number of metrics or the features in the image. Five features were found to be the best features for the leak identification from the image. Other features affected by day and night failed in identifying the image condition. That is because the heat during day time affects the result of the feature. The five selected features gives a good result regardless of the day and night conditions. The following are the principles of selecting the five features.

1. The leak image has a round or circular shape in the middle.

2. The centre point in the image has the lowest temperature value.

3. The image is symmetrical when rotated 90 degrees.

4. The standard deviation in the leak image is larger than the image with no leak.

5. The mean absolute deviation in the leak image is larger than the image with no leak.

The following section explains in detail how those five features have been extracted using image processing techniques with Matlab code.

7.1.1.   Round Shape Recognition

To recognise the round shape in the image as a leak spot, the image has to be processed several times. The round shape has to match the four parameters as follows:

1. The round shape should be in (or close to) the centre of the image.

2. The round shape should have the lowest temperature value (Or the highest in case the liquid in the pipeline is hotter) compared to the surrounding.

3. The round shape should be round or near-round shape as the moisture from the leak usually spreads equally around the leak point forming a circle alike when detected by thermal imagers.

4. It should be a round shape with uniform boundary and with almost equal axes.

7.1.2.   Recognising the round shape process.

7.1.2.1.   First method of determining the round shape:

The first method used to determine the round shape achieved by converting the original image to a binary image (black/white) based on a certain threshold value, labelling the resulted shapes inside the image using the labelling technique in Matlab and then discarding any shapes which is not round and not in or close to the centre of the image. Figure 7.1 shows the round shape recognition process.
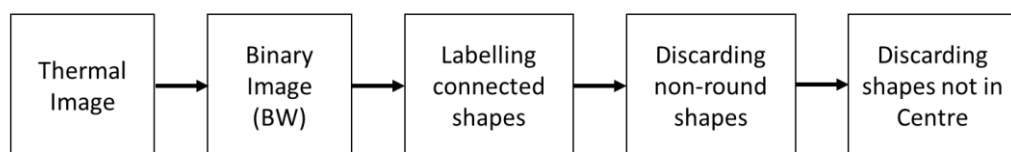
Figure 7.1: Image processing diagram for round shape recognition

The labelling process defines each individually connected items with a unique serial numbering order to determine it easily for further work. For more clarification, in Figure 7.2 there are three connected shapes in the binary matrix at the left. The labelling technique gave numbers 1 to 3 to the connected shapes as it can be clearly seen in the matrix at the right. In defining the connected objects the labelling technique starts from left to right and top to bottom.
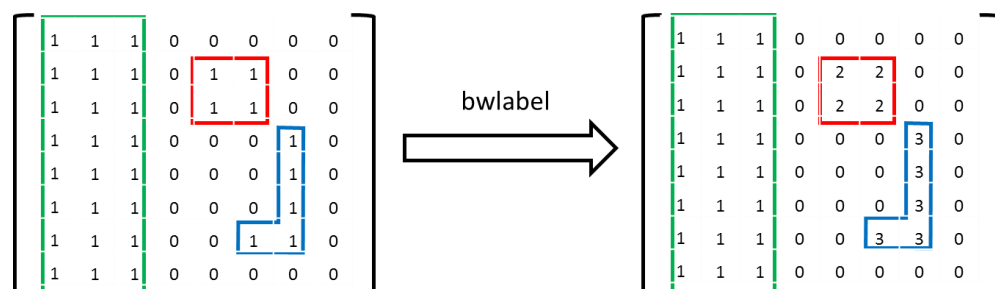
Figure 7.2: Labelling Technique

After labelling process, the algorithm loops throughout the entire image to find the labelled shapes and delete any shapes which do not match the conditions of the round object established earlier.

Round shape detection carried out using Matlab command for region properties named 'regionprops'. The command measures a set of properties for any individual labelled shape inside the binary image. The command provides information about the important parameters of any shape such as the area, the bounding box dimensions, centroid, intensity, and axes lengths. The bounding box is used to determine if the shape is round or not because it is the smallest rectangle that surrounding the targeted region or the shape in the image.

Usually, the leak does not produce a perfect round shape above it however, the shape is often near round. In some cases, the thermal camera detects an oval shape with a big difference in its axes. This oval shape is usually not a leak spot and could be a result of detecting the pipeline itself as the pipeline affecting the temperature of the surface as well. To differentiate between oval shapes in both conditions of the leak and no-leak, a limit of the difference between the bounding box axes has been established.

Figure 7.3 illustrates some binary images with round and non-round shapes identified using bounding boxes. The first image at the left shows an oval object and the second image shows a near-round shape for a leak spot while the last one is almost round object and definitely identified as a leak spot.
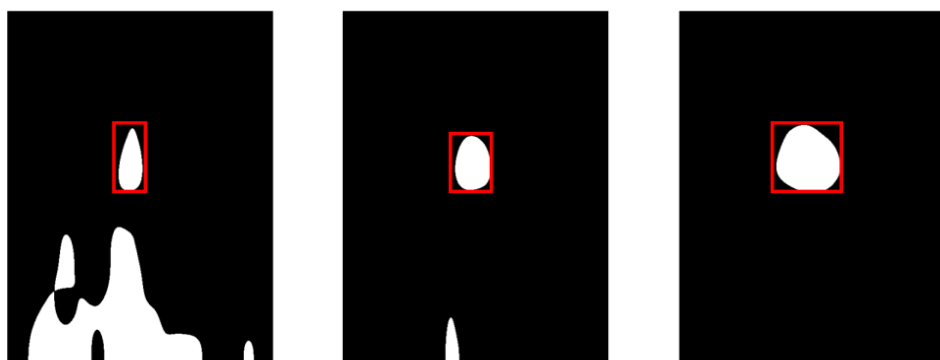
Figure 7.3: The use of the bounding box to determine the dimensions of the round shape

7.1.2.2.   Second Method for finding the round shape:

This method carried out by enhancing the image contrast using histogram filter. To enhance the contrast, the image is first scaled from 0 to 1 value then converted to integer to remove the decimals and then the histogram filter applied. After the use of the histogram filter, a threshold with certain value applied to remove all other objects in the image and to keep the round object only. In other words, the image converted to B/W image to easily remove the unwanted shapes from it. Later, the number of pixels counted to get the value of the round shape.
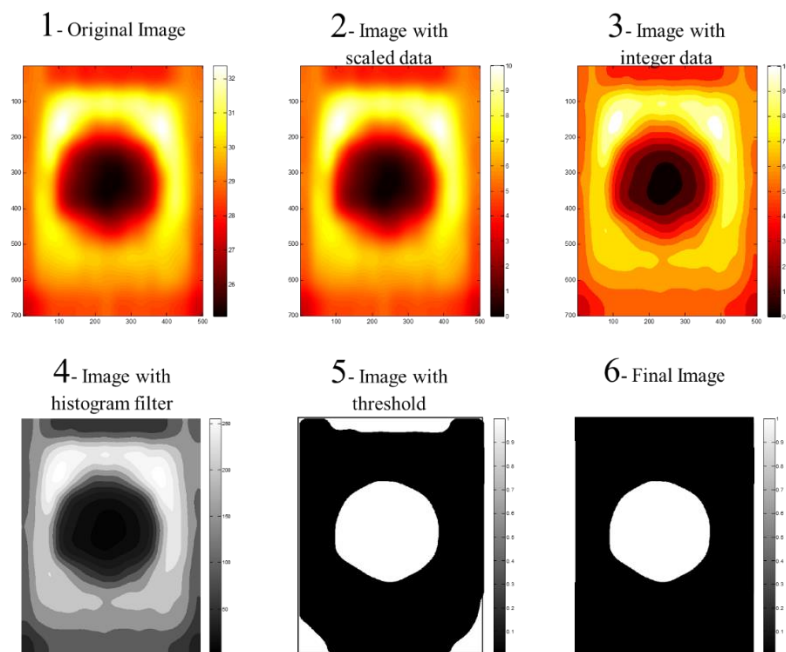
Figure 7.4: The filtering technique used to determine the round shape.

The following are some examples of how the images have been identified as a leak or non-leak image using the round shape recognition method.

The first example (Figure 7.5) shows an ideal round spot with the least temperature in the centre of the image. It was easy for the code to identify this image as a leak image in the first loop as there was one spot left in the centre when the image converted to B/W image.
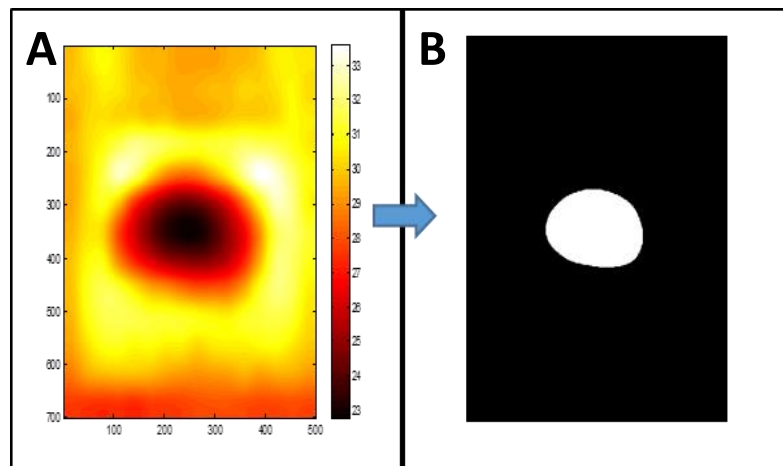
Figure 7.5: Original thermal image (A) converted to B/W image (B) in one processing step

The second example (Figure 7.6) is again an ideal example for the round spot with low temperature value in the centre, however, there are some other parts at the bottom of the image have the same temperature as the round spot. In this case the image subjected to extra processing in order to remove that extra part to produce the final image with a white spot in its centre only.
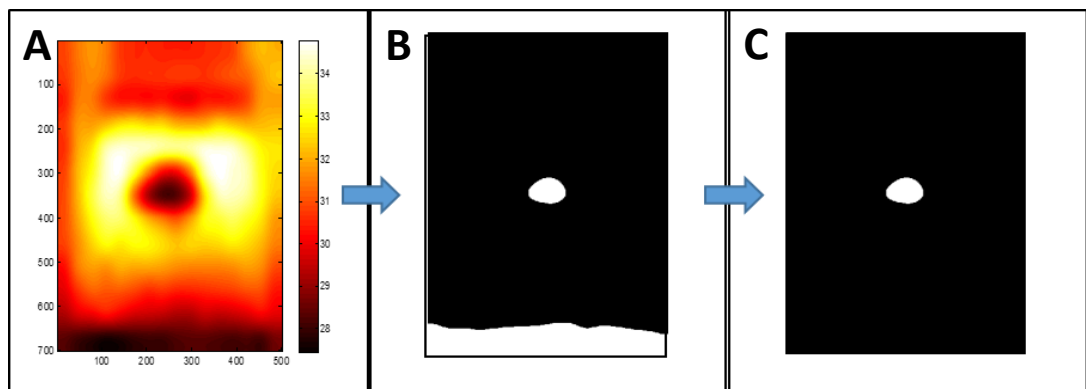
Figure 7.6: The original image (A). B/W image with extra part (B). Final B/W image with the leak spot only (C)

The third example (Figure 7.7) is the image without any signs of a leak. In this case, the image subjected to several processing loops to clean the image and to bring final clean black image without any white spot in the centre. The result of such images means there is no leak.
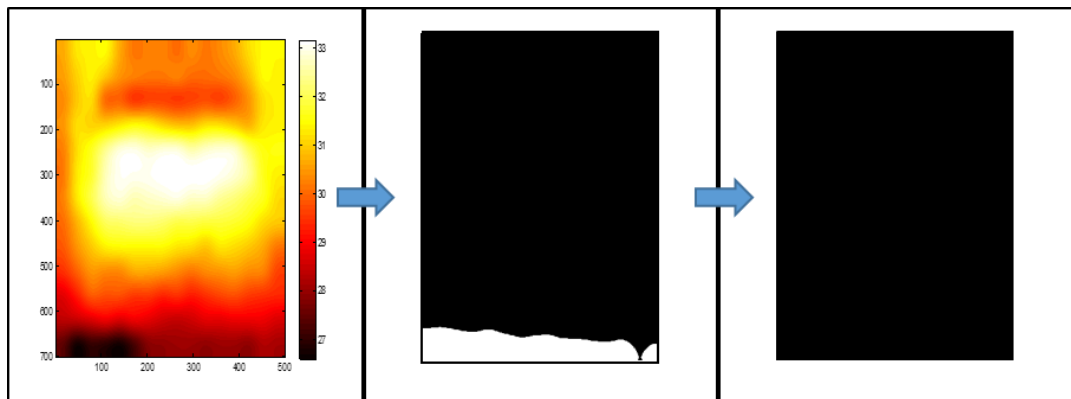
Figure 7.7: No-leak image required several processing steps to show nothing

It is worth mentioning that, after the detection of the round object it is important to confirm whether the round shape having a uniform perimeter or random shape. In some cases the shape in the centre is matching most of the parameters set for the round shape however, its perimeter is not uniform which means it is not generated by a leak. This is carried out by measuring multiple distances (vertically, horizontally, and diagonally) between two opposite sides of the shape perimeters. If the distances vary above certain level the shape excluded and considered no-leak spot.

7.1.2.3.   The feature sensitivity:

Figure 7.8 shows a sample of thermal images processed using the round shape recognition. The figure shows the thermal image stacked in the first row and the B/W images in the second row. To test the sensitivity of the image relating to finding the leak, the number of pixels remained in the image after the processing is counted. Larger number of pixels indicates larger amount of leak. The number of pixels in each B/W image have been used to produce the graph in the figure. The graph clearly shows a profile line with high slope. The higher slope, the higher sensitivity. From the figure it can be said that this feature is sensitive for detection however, the feature failed in the first few image and did not show the leak.
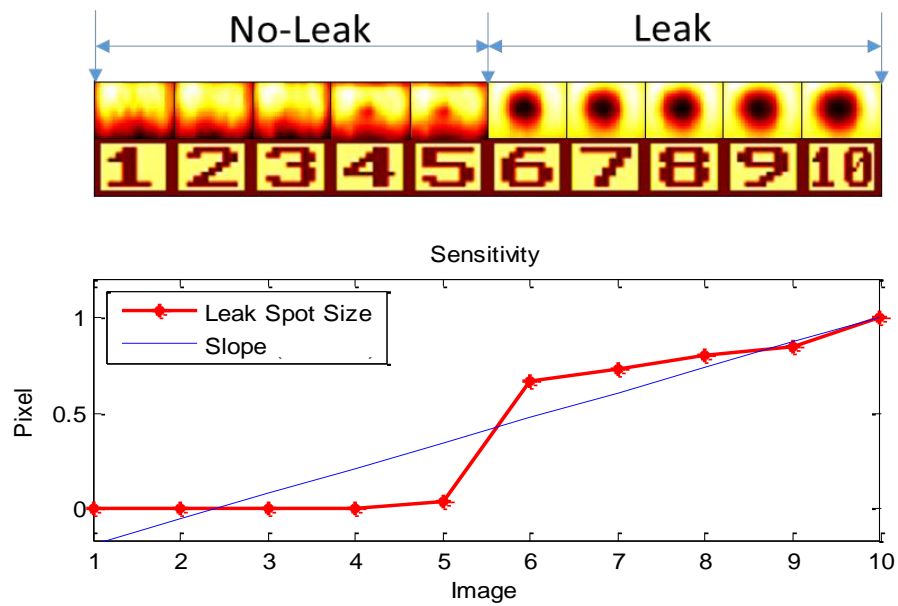
Figure 7.8: Round Shape Sensitivity

7.1.2.4.   Example of Round recognition results:

Figure 7.9 and Figure 7.10 show a series of images taken from a complete experiment processed using the shape recognition method. The images illustrate the progress of the leak detection against time using round object recognition method. The first row in the figures shows the thermal images and the second row shows the black/white images and the third shows the number of each image. The figure have two graphs attached to them. The first graph in the figure is for the calculated number of pixels of each black/white image while the second graph is for the actual measured leak from the experiment. Form the two figures it can be noticed that the shape recognition feature have successfully detected the leak spot in each image. The resulted graph of the number of pixels give a clear profile of the leak matching with the actual measured leak.
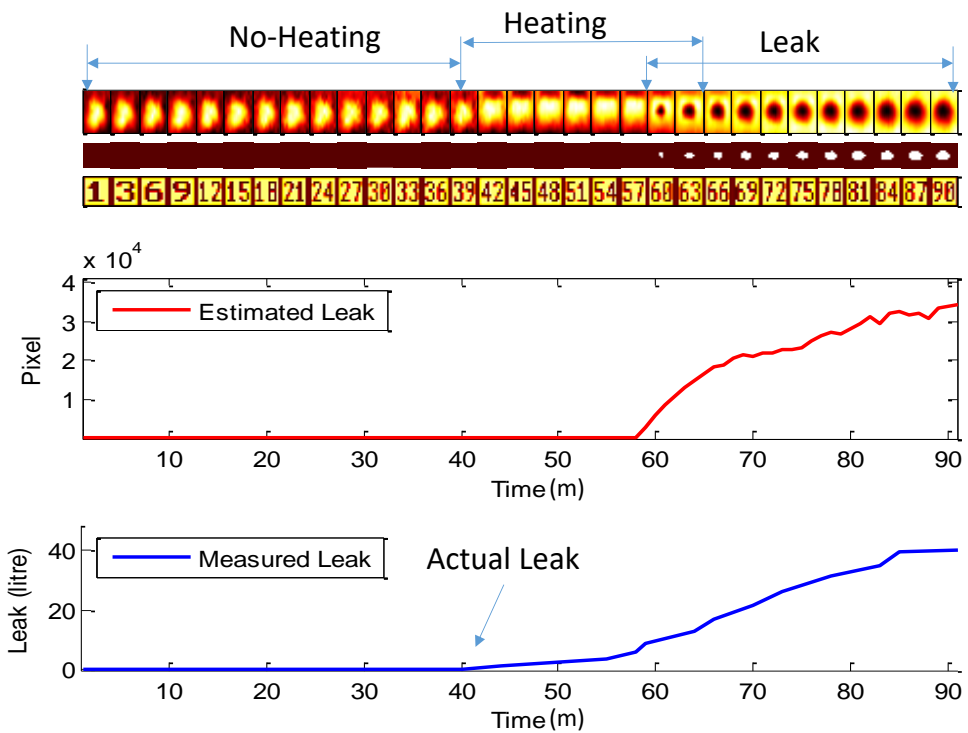
Figure 7.9: A set of image from one complete experiment subject to round objected recognition
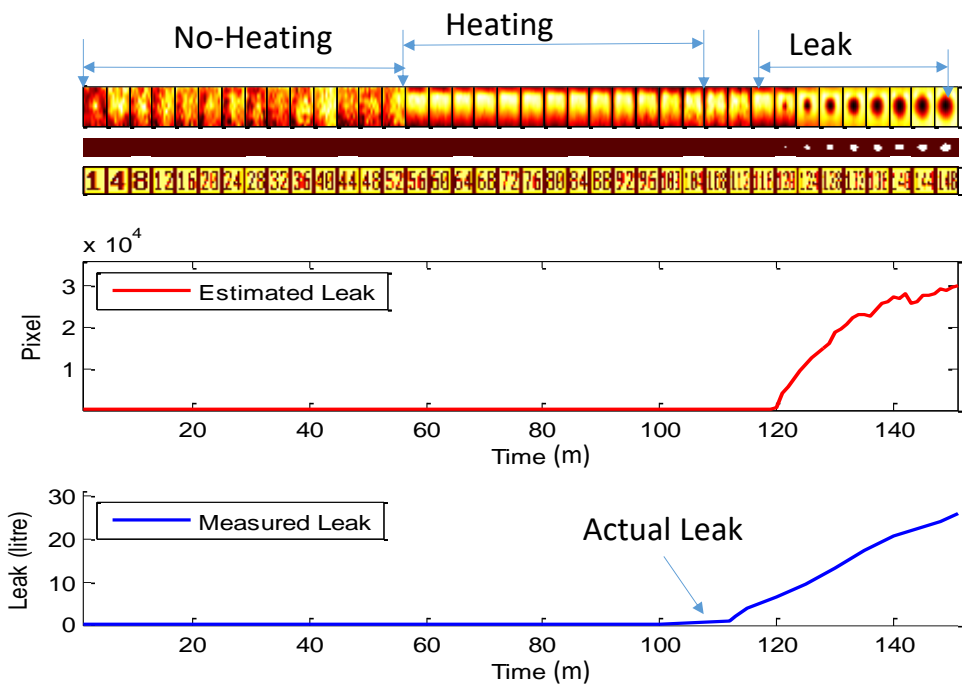
Figure 7.10: A set of image from one complete experiment subject to round objected recognition

7.1.3. Lowest temperature in the centre of the image and higher depth value (d-value)

The d-value is the lowest measured value in the centre of the image. The image with leakage spot has a lower temperature at its centre. The profile of a line passing through the leak point in the image produces a curve with a larger value between the maximum point and the minimum point of that profile at the middle. Figure 7.11 illustrates an ideal profile of a leak image with d-value.
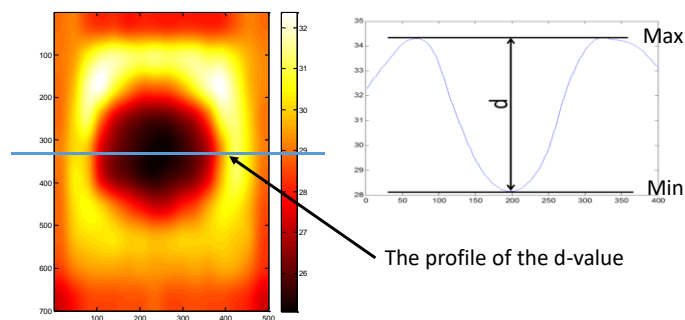
Figure 7.11: A profile for line passing through leak point

Figure 7.12 shows three image examples for getting the d-value from the image. The three images are A) image with no-leak, B) image with small leak spot, and C) image with large leak spot. The figure shows that the image with the large leak spot (C) has higher d-value than the image with a smaller leak spot (B). The no leak image (A) has a negative value as the maximum point at the both ends of the profile has a lower value than the middle.
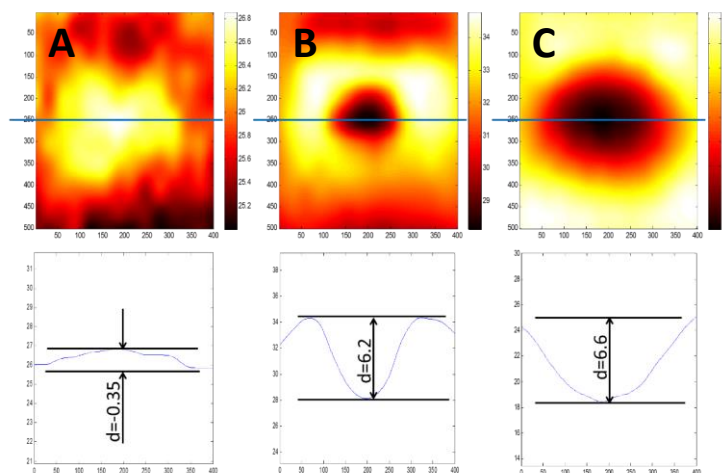
Figure 7.12: Several image shows how d-value differs

7.1.4.   Sensitivity of d-value feature:

As the d-value give an indication of how big the leak could be, the d-value is sensitive in detecting the leak. D-value is a good feature to depend on for deciding whether the image shows the leak or not. Figure 7.13 illustrates ten selected series of thermal images showing the progress of the growth of the leak spot in one experiment. The result of the d-value as a feature has produced a graph showing the difference between the images with a leak and the image with no-leak. The slope of the resulted graph from the d-values is high which means that the d-value feature is dependable in detecting the leak image with spots.
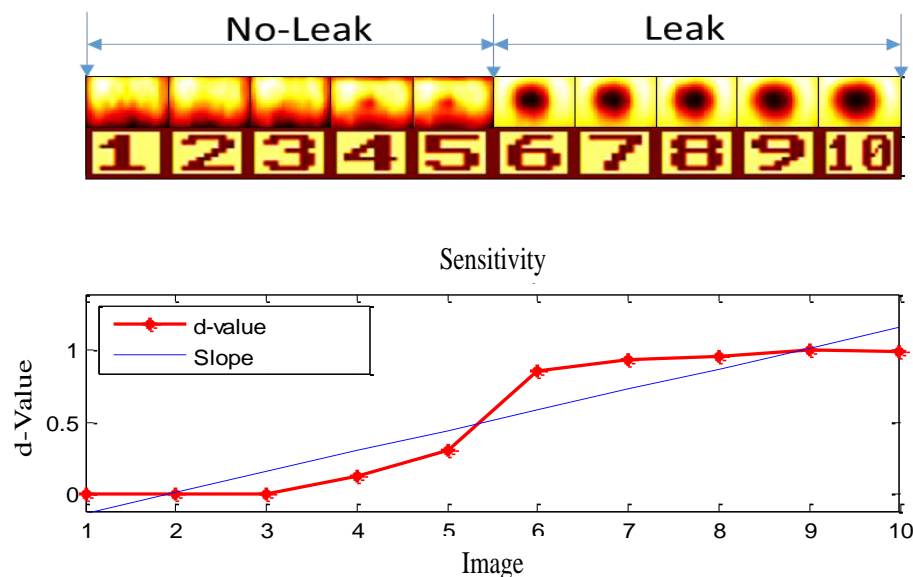
Figure 7.13: Sensitivity of the d-value.

Figure 7.14 and Figure 7.15 show the result of the d-value of two complete experiment images. The two experiments are for two different periods. The first one is for night-day-night while the second one is for night-day-night-day. The figures are attached with two graphs each. The first graph which is plotted in red is for the profile across the whole images. The measured d-value in each image has affected the graph in the leak period. The graph in the leak period has a sharp zig-zag shape due the notable change in d-value. The graph in blue is the value of the d-value itself in each image. The profile of the d-value shows the sharp change in the value for the leak period compared with the no-leak period.
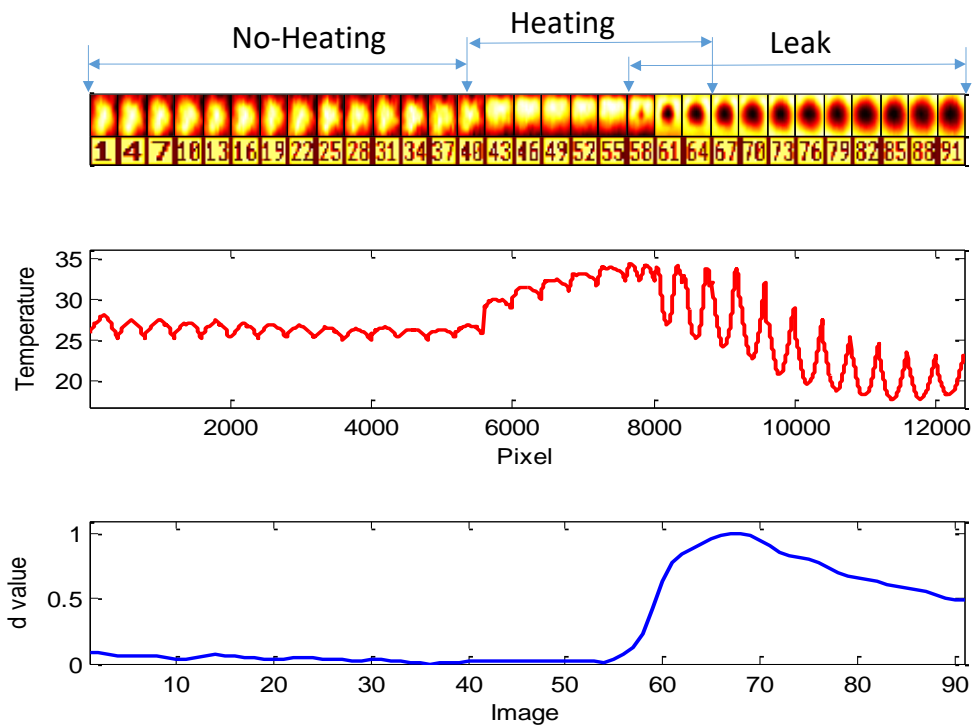
Figure 7.14: Calculated d-value for a series of images from one experiment
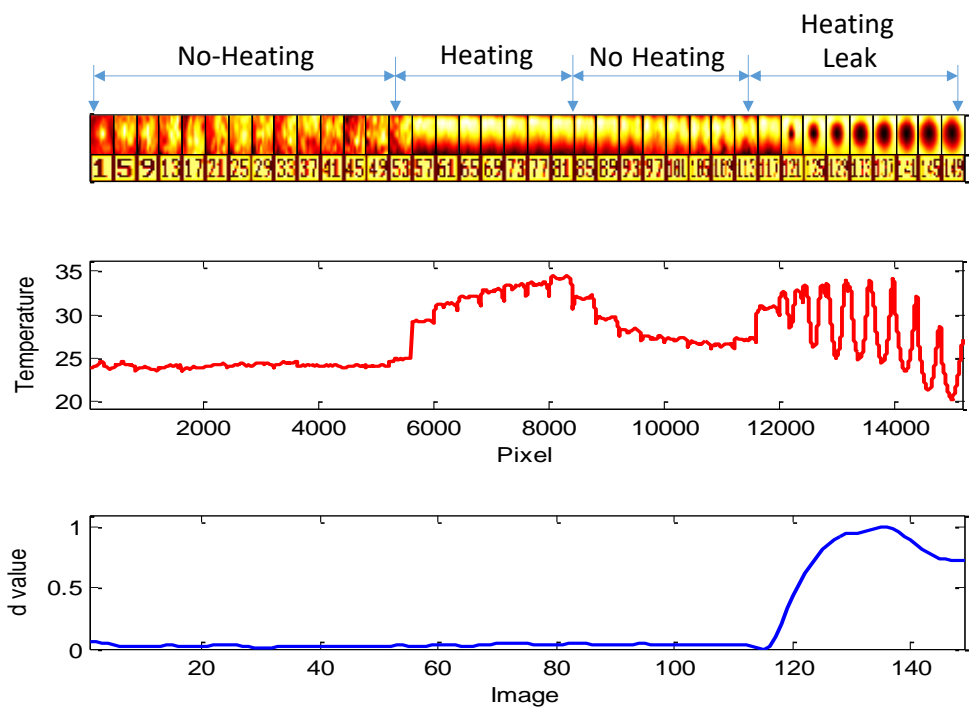
Figure 7.15: Calculated d-value for a series of images from one experiment

7.1.5.   Symmetricity

As the leak creates round object in the centre of the image, therefore its shape should not differ much once it is rotated 90º. This feature suggests that the camera is set in a position where the spot of the leak appears in the centre of the image. Otherwise, the image has to be processed to relocate the spot in the middle of the image e.g. by cropping the ROI.

To extract this feature from images, the images is resized to a 3X3 image in order to define the least temperature area in the image. The resulted matrix produces an image of nine segments. Each segment represents the average of temperature of a group of pixels. One of the segments will highlight the area of the lowest average temperature in the image. Certainly, in the leak image, the segment with the lowest temperature is in the centre of the image while in the no-leak image it is on either sides or corners of the image. In the leak image, the shape of the 3x3 matrix does not change when rotated 90º, however, in the no-leak image, the shape of the image changes and differs because the location of the segment with the least temperature have changed. After changing the size of the image, it has to be changed to B/W image using a threshold based on the lowest temperature. The result is a B/W image with one black spot. The location of this spot will be in the middle when processing leak image and will be in another side when processing no-leak image.

Figure 7.17 shows the processing sequence of the no-leak image in both states of the original and the rotated orientation. The figure number A, the original image, resized to the image B of the 3x3 matrix and then converted to B/W which is the image C. this process applied to the two image situations (original and rotated). The result (D) shows two different images because the least temperature was not in the middle. Figure 7.17 shows the processing sequence of a leak image. The image processed exactly the same way explained earlier. The result gave the same image for both conditions of the image.
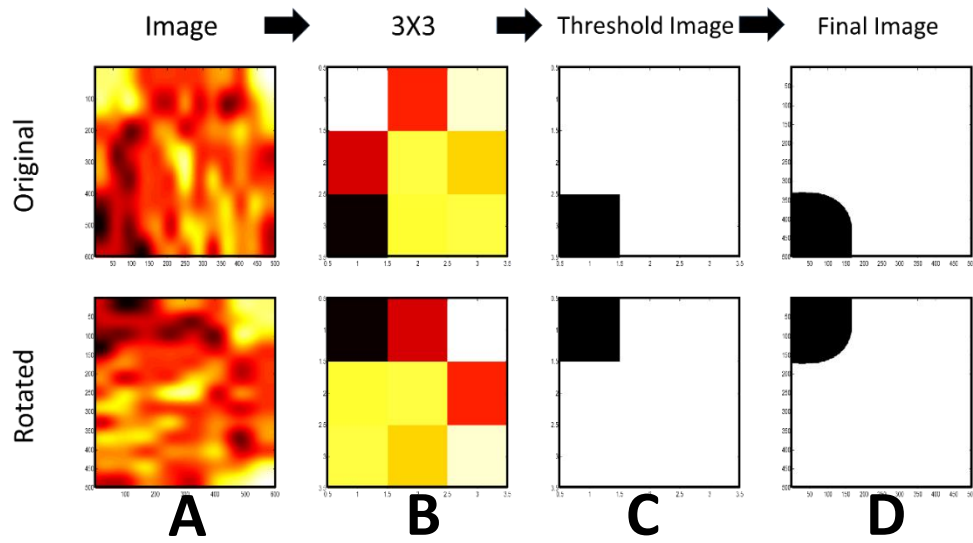
Figure 7.16: Comparing original image with rotated image (no-leak image)
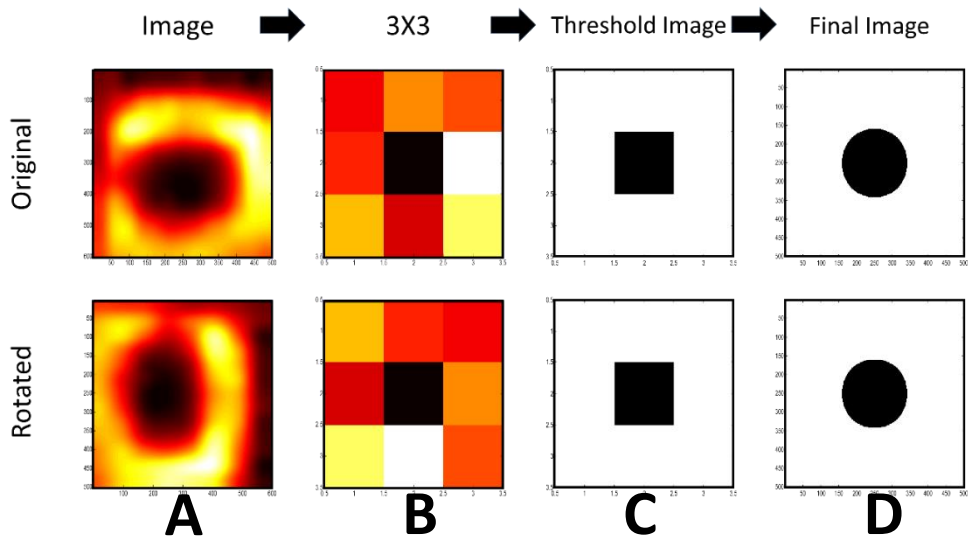
Figure 7.17: Comparing original image with rotated image (leak image)

From the two figures above it can be clearly seen that both original and rotated image has produced different final image when there is no leak while they have produced the same image when there was a leak.

Sensitivity of the symmetricity:

Apparently, the symmetricity is able to detect the images with the leak spot. However, in some cases, the feature failed because the image has a lower temperature at the middle despite it is not a leak image. Figure 7.18 shows a result of ten selected images. The feature produces a result of either 0 or 1 for the no-leak and the leak states. The slope of the profile line in the graph shows that the feature has a high degree of sensitivity.
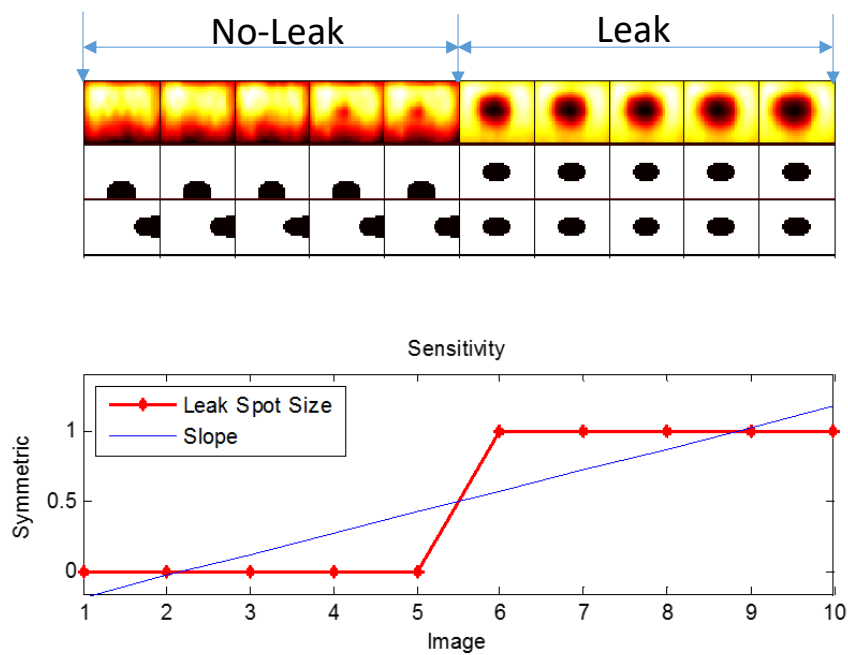
Figure 7.18: Sensitivity of the Symmetricity

7.1.5.1.   Example of the symmetricity application:

Figure 9.19 and Figure 8.20 are for two experiments. The first row of images shows the result of the processed original image while the third row is for the rotated image. The resulting graph, in red, shows that the feature differentiated between the images with and without leak spots properly. The third graph, in blue, is the measured leak for comparison purpose. Unlike the previous two features, the symmetricity cannot give an estimation of how big is the leak spot as it gives 0 or 1 result only.
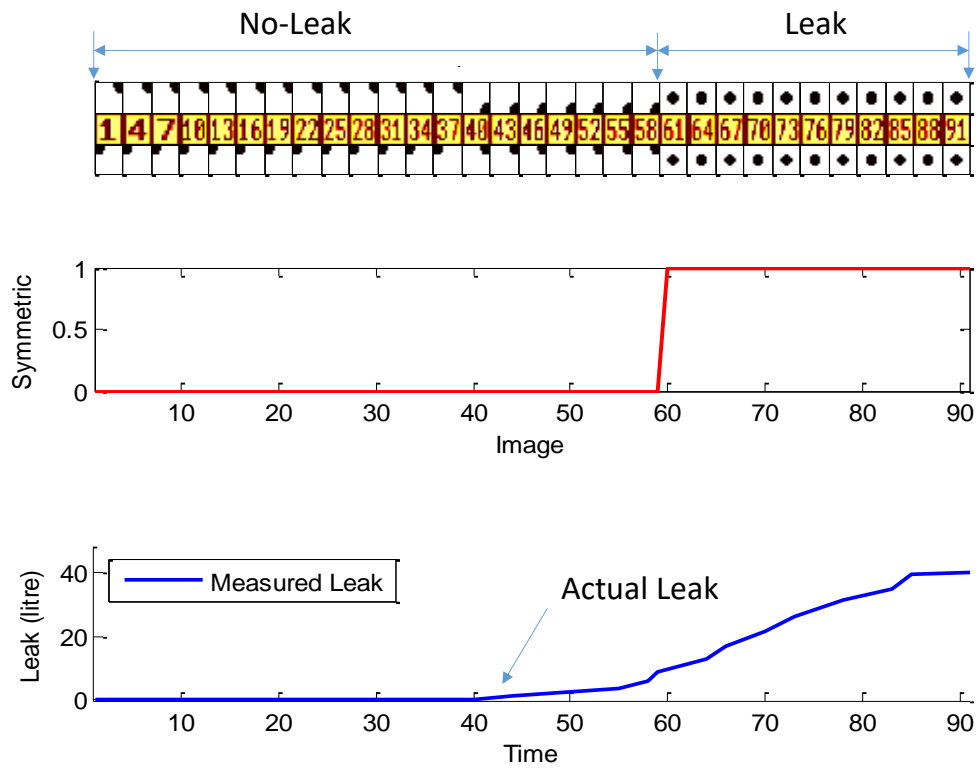
Figure 7.19: Results of the symmetricity of one complete experiment
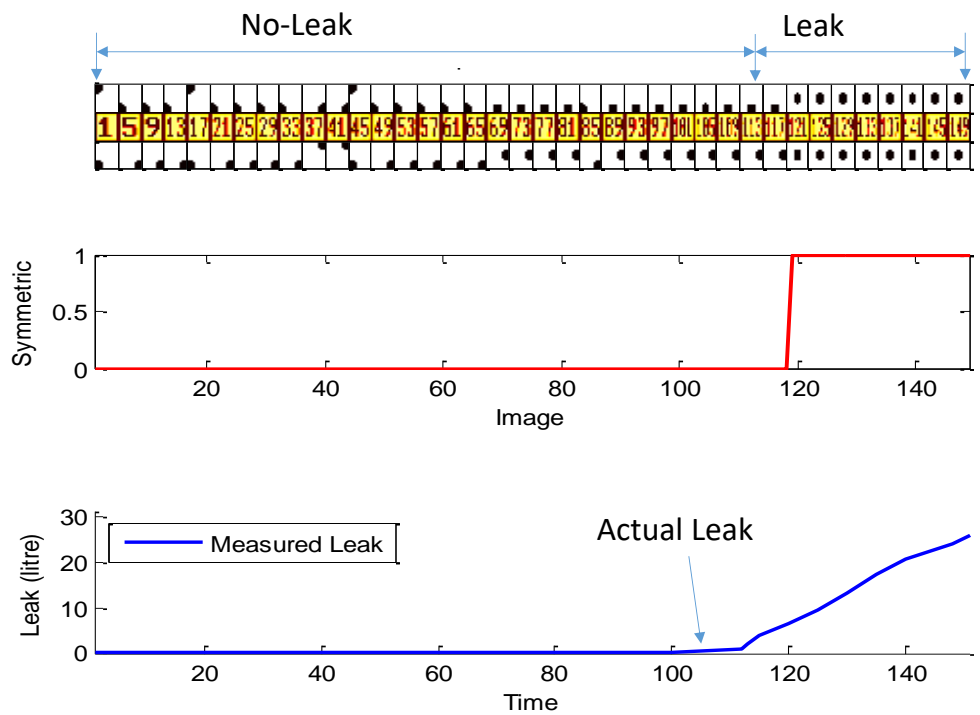
Figure 7.20: Results of the symmetricity of one complete experiment

7.1.6.   Standard Deviation.

Standard deviation is the measure of the deviation of a set of value from the mean. If the value of the standard deviation is close to zero it will be close to the mean. A higher value of standard deviation means the value is spreading out far from the mean. The standard deviation of the thermal images in this study has revealed that the images of the leak have a higher value than the image with no leak.

7.1.6.1.   Feature Sensitivity:

Figure 7.21 shows how the images with leak spot have a higher value than the image with no leak. However, some of the images have shown signs of leak spot and their value of standard deviation remained in the range of the no-leak images. The figure shows the slope on the graph is high which indicates that this feature is dependable.
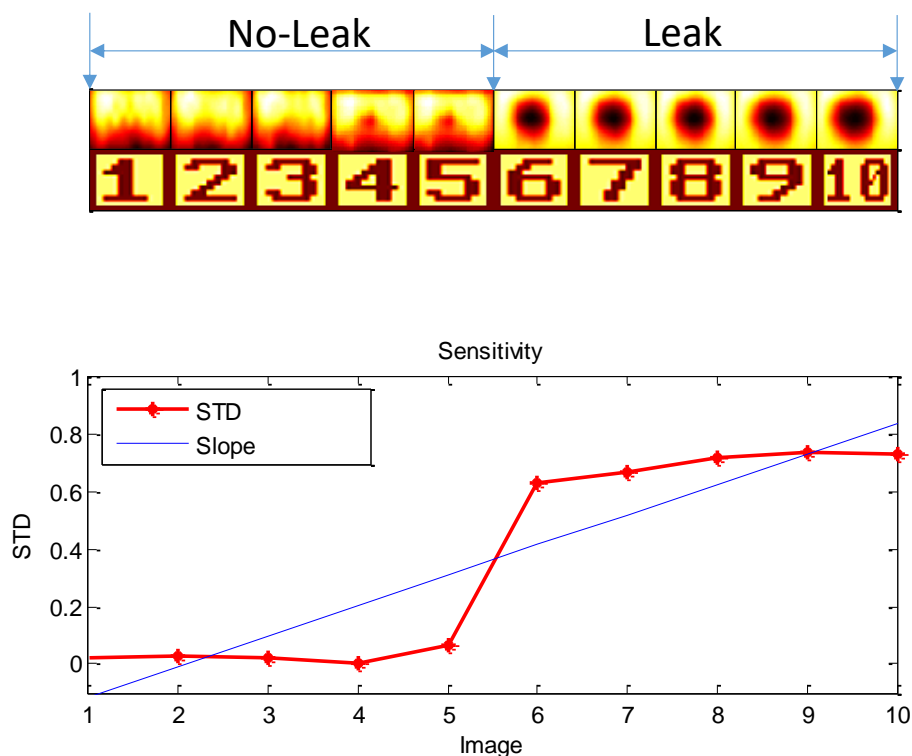
Figure 7.21: Standard Deviation Sensitivity

7.1.6.2.   Example of the standard deviation application:

The examples in the Figure 7.22 and Figure 7.23 are the result of the processed images from two different experiments with different parameters such as ambient temperature,

water temperature. The first experiment represents one and half day starting with a night and ending with a night as well. And the second one represents two and half days (night-day-night-day-night). The figures show that a higher standard deviation value for the leak images while the lower value for the no-leak images. the maximum and minimum temperature are also shown in the top of the figures.
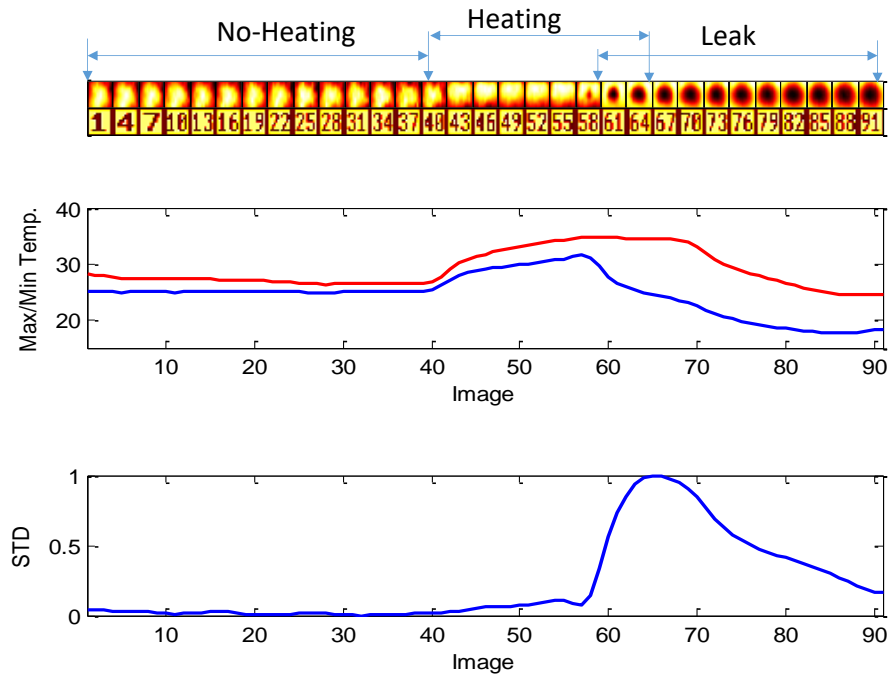
Figure 7.22: Standard deviation for the first experiment
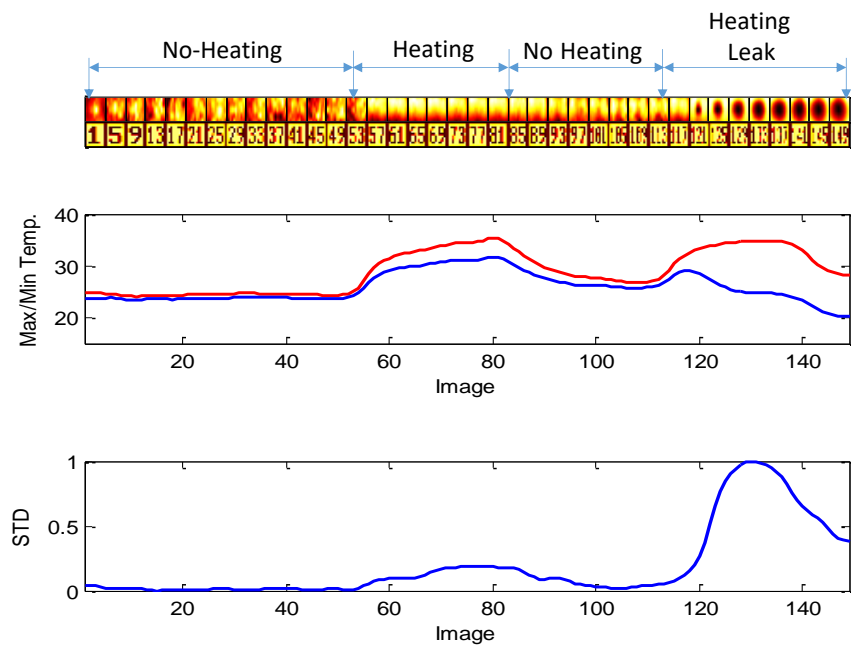
Figure 7.23: Standard deviation for the second experiment.

7.1.7.   Mean Absolute Deviation (MAD)

The Mean Absolute Deviation (MAD) of a set of values is the average distance between any individual value and the mean of that set of values. The calculation for the MAD of the images has revealed that the MAD of the leak images has a higher MAD value than the other images.

7.1.7.1.   MAD feature sensitivity

The outcome of the mean absolute deviation is shown in Figure 7.24. The figure shows that the MAD of the image with a leak is higher than the images with no-leak.
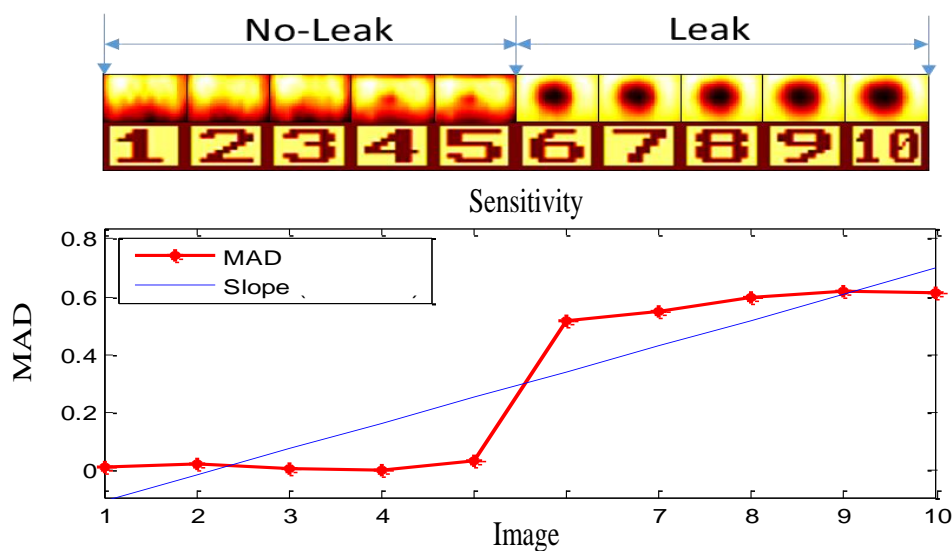
Figure 7.24: The figure shows how the MAD is change with the change in the state.

7.1.7.2.   Example of the Mean Absolute Deviation application:

The MAD has been applied in two different experiments. The results are shown in Figure 7.25 and Figure 7.26. As explained above the two experiments represent two different situations. The MAD has a higher value for the leak images especially at the beginning. The MAD identifies the images with a leak once the thermal image starts to show the leakage.
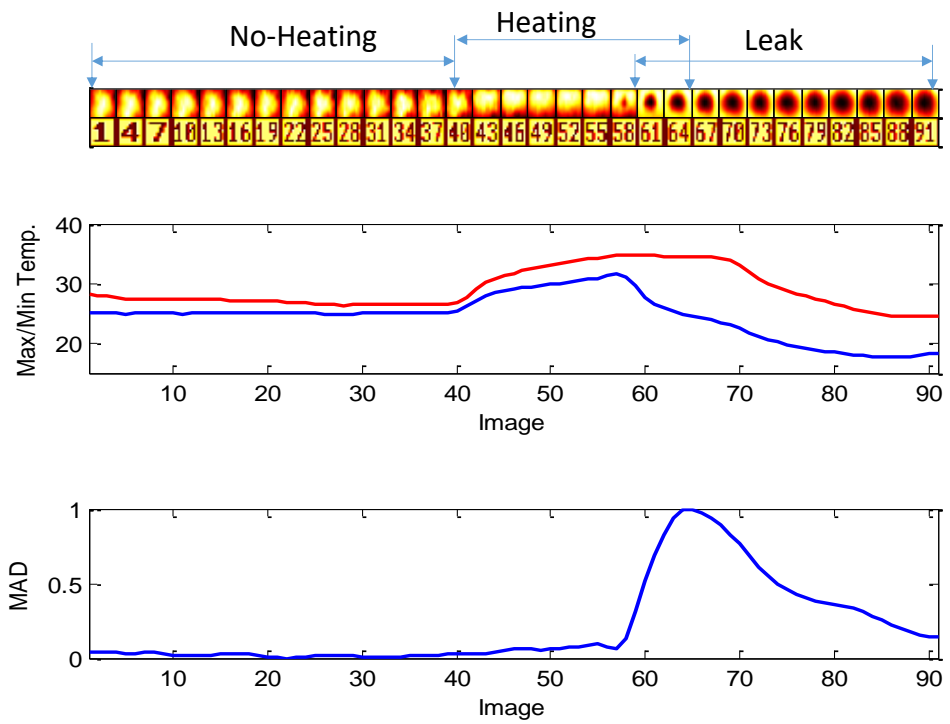
Figure 7.25: Mean absolute deviation for the first experiment.
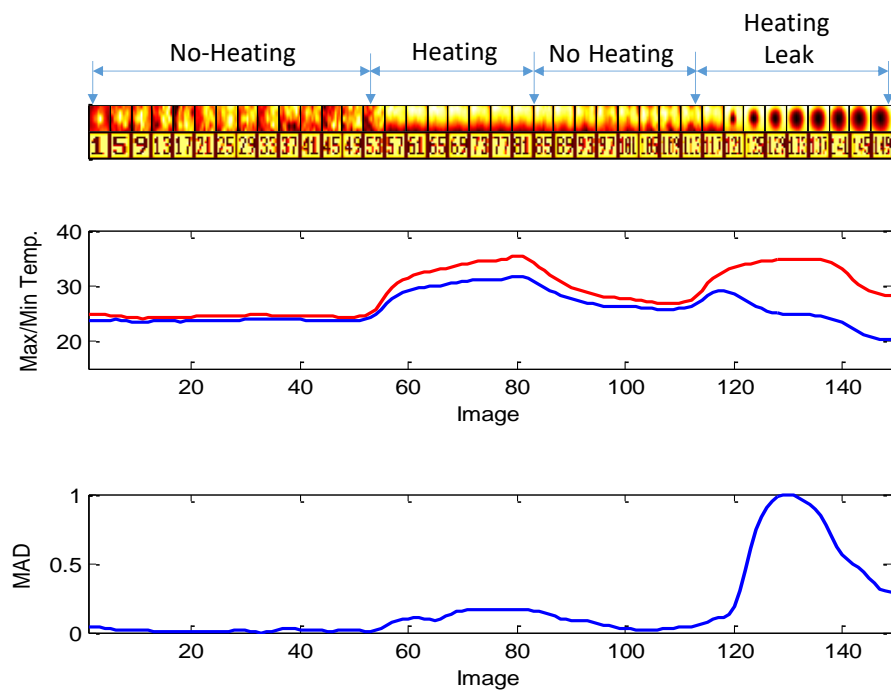
Figure 7.26: Mean absolute deviation for the second experiment.

7.2. Result of the five features

Figure 7.27 shows the five features in one plot with a subplot contains the average of the features. The figure shows that the features are working together and giving a good average presentation which clearly determines the area of the leak.
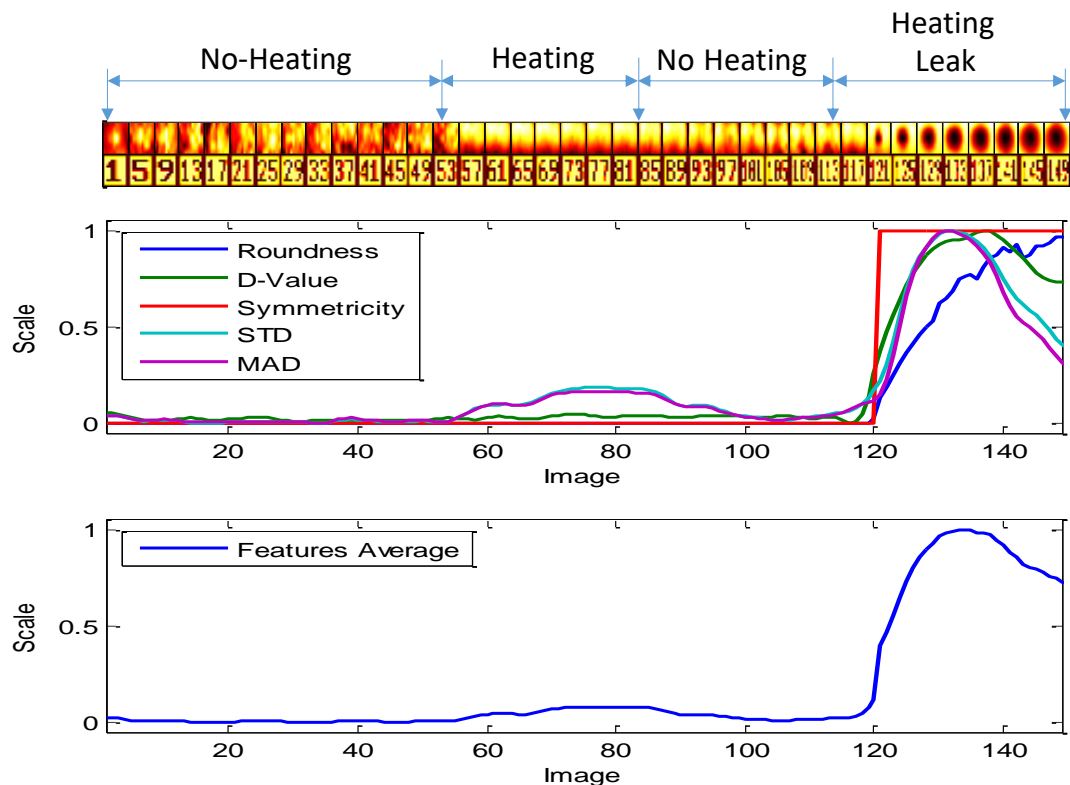
Figure 7.27: The five features in one plot with a subplot shows the average.

7.3. Application of the ASPS approach on the thermal camera.

7.3.1.   Extracting the SCFs

The ASPS approach examining the sensitivity of both the sensors and the image processing techniques. It helps in finding the best combination of sensors and signal/image processing for designing a condition monitoring system [33]. The five features have been subjected to further processing in order to extract the required SCFs and to select the best image processing technique. A number of advanced processing techniques has been applied on all five features. The processing techniques are:

7.3.1.1.   Statistical Analysis using 13 selected statistical functions.

Statistical functions have been applied on the raw signal (the five features) in order to extract the sensitive features (SCFs). The thirteen statistical functions are Mean, Max, Min, STD, MAD, Kurtosis, Skewness, RMS, Covariance, Range, Variance, IQR, and Crest Factor

7.3.1.2.   Fast Fourier Transform (FFT).

The five features have been converted to FFT signal. From the FFT signal, three values have been extracted in both conditions of the leak and no-leak. The values are the frequency value at both minimum and maximum amplitude and the maximum value of the FFT signal amplitude.

7.3.1.3.   Discrete Wavelet Transform (DWT).

The DWT produced two level representations of the original signal (the five features). Then the resulted new signal subject to statistical analysis using the thirteen statistical function.

7.3.2.   The Associated Matrix of the ASPS approach

The result of the processing method explained above is calculated using the simple mathematical approach of calculating the percentage of the difference between the two different situations (Paragraph 3.6.3). The percentage represents the sensitivity of the sensors and the image processing method. The results are arranged in the associated matrix in Figure 7.28.
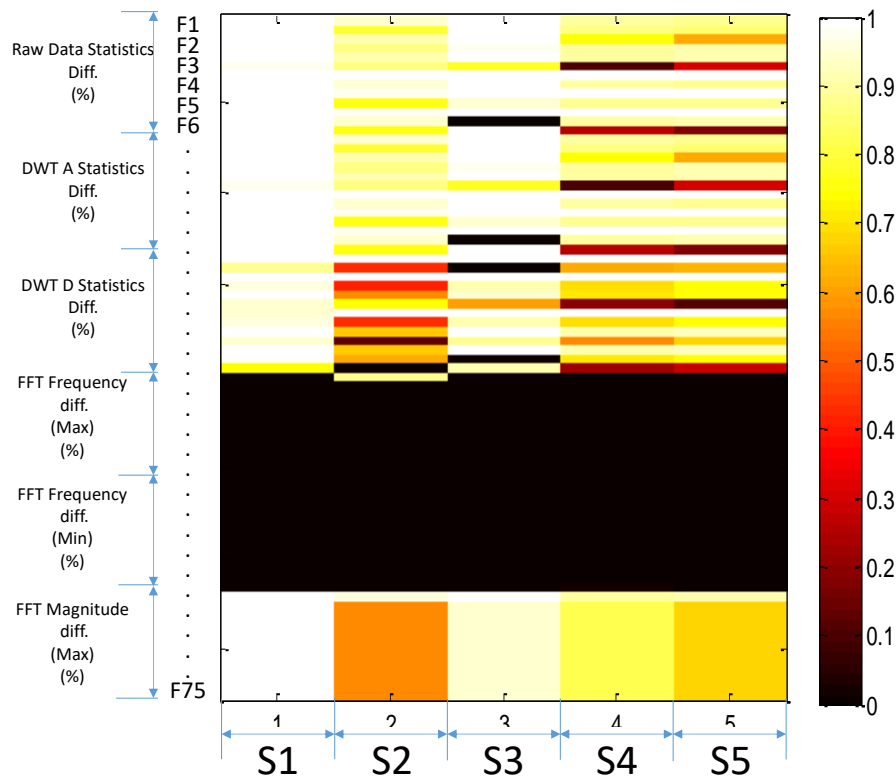
Figure 7.28: the ASM of ASPS approach for the Thermal Camera

The y-axis in the ASM represent the features and numbered as F1, F2 to F75. While the sensors are arranged in the x-axis from S1 to S5. Any feature appears in the ASM as bright light is the feature with the highest sensitivity. Features of the black colour are the features of the lowest sensitivity. All the features in the ASM are ranked from the maximum value to the minimum value in order to select the sensitive features SCFs.

7.3.3.   Application of Neural Network for thermal image.

7.3.3.1.   Training Data Set

A data from one complete experiment (continued series data) have been used as training data for the neural network. The total numbers of the used images are 151 images. The data is for two periods of heating and no heating (2 days and 2 nights). In other word, the data contains images with heat, images with no heat, images with a leak, and images with no leak. The actual leak started at the end of the second cold period (early morning of the second day) when the image count reached to number 114. The leak in thermal images

starts to be visible at image number 120. The result of the five SCFs is shown in Figure 7.29 with detailed information about the leak. This result has been used as the training data for the neural network.
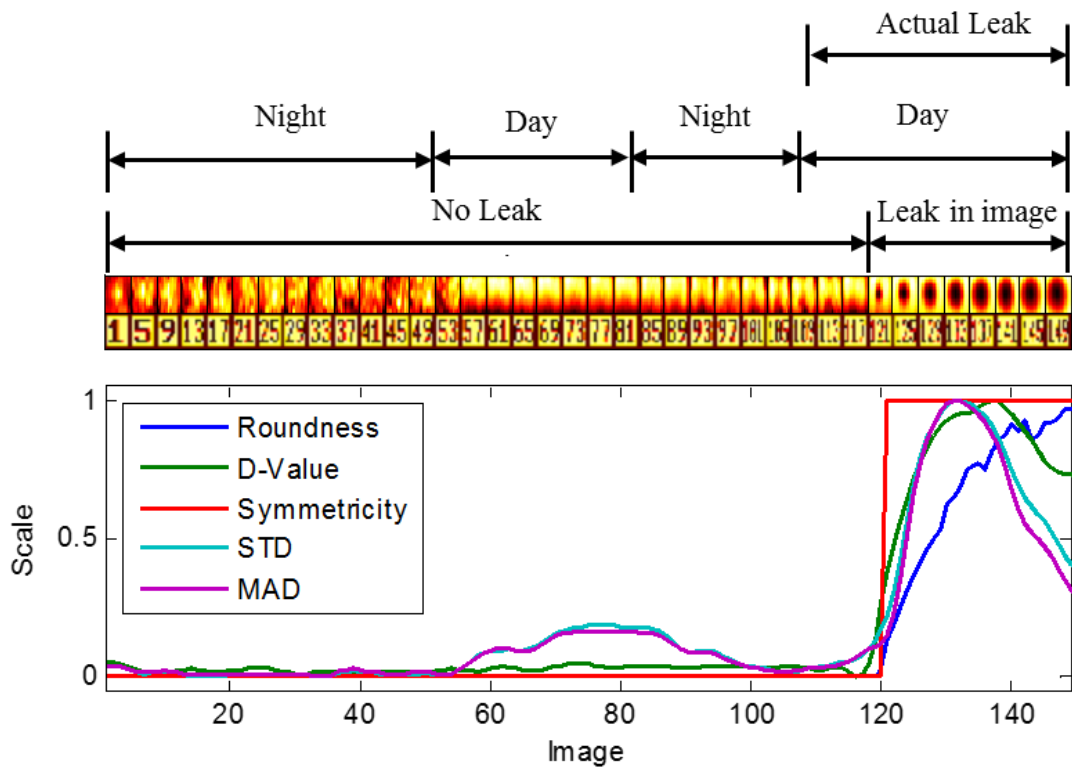
Figure 7.29: Result of five selected features for thermal images used as input data to the neural network.

The result of the trained neural network is shown in Figure 7.30. The result of the training was perfect and matched the target exactly. The neural network was successful in learning which image has a leak and which has no leak. The figure shows the target in the upper subplot and the training result in the lower subplot.
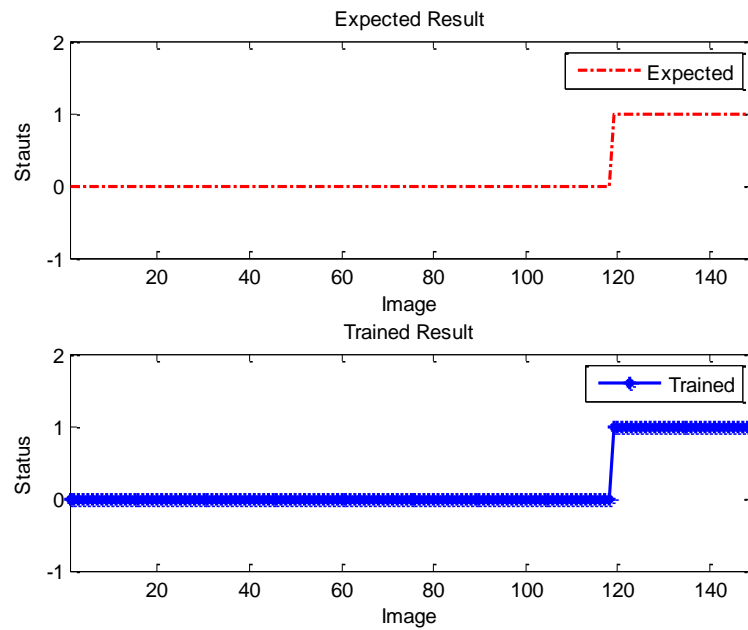
Figure 7.30 Training data result and Targeted data

To test the neural network and to make sure that it has learnt to differentiate between the leak and no-leak images based on the five features, a new set of different data from a different experiment have been tested. Figure 7.31 shows the prepared data graphs to be tested with the neural network. No target has been provided this time.
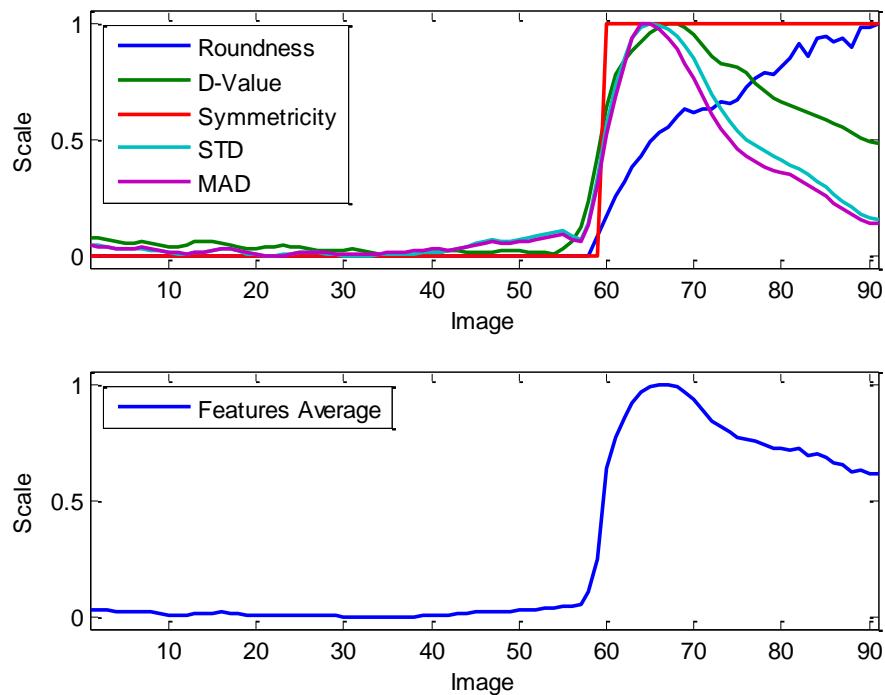
Figure 7.31: Testing data

The result of the neural network gave similar profile and successfully identified each image with a high degree of accuracy.
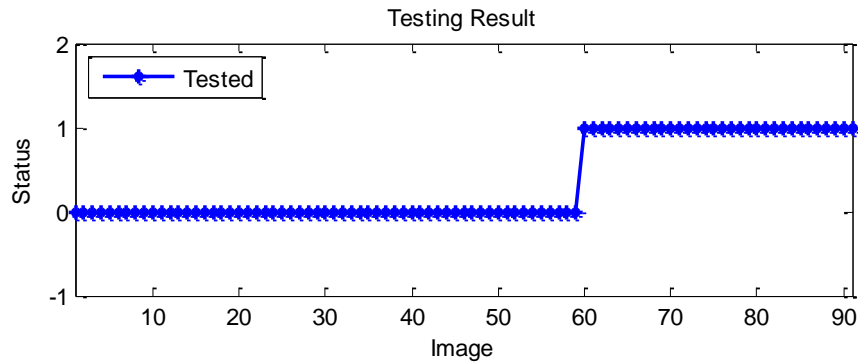
Figure 7.32: Result of the test data

7.4. Summary

Image processing is an important step to extract useful information from the image in order to be used in an automated system. This chapter explained in detail step by step the utilised systematic procedure to extract the useful features from the thermal image. The useful features, in this case, are the features that tell if the image does show the leak or not. After an extensive investigation work, five features have been identified. The features are round object recognition, d-value, symmetricity, standard deviation, and mean absolute value. The features have successfully classified the image and it is now possible to recognise the image either it is a leak image or not. To automate the process the systematic ASPS approach has been applied to the five selected features, thirteen statistical features, and two advanced image/signal processing techniques have been applied on the data of the five features. The ASPS produces associated matrix classifies the features based on their sensitivity. The ASPS shows the sensitive sensor based on the feature sensitivity and best image processing used. In a final stage, a neural network has been applied and successfully learned to classify the images. The result of this chapter is part of the aimed fusion system using the ASPS approach that is applied in Chapter 9.

Chapter 8. Signal Processing

8.1. Introduction

This chapter presents the implementation of the signal processing for the 1D data section of this research work in order to accomplish the proposed ASPS approach for water pipeline monitoring and leak detection. The chapter explains in detail how the signal processing method has been implemented for all the three pairs of the used sensors on the test rig. The sensors are two AE sensors, two pressures sensors, and two flow sensors.

8.2. Experimental work

A number of experiments have been carried out in order to test and investigate the sensors installed on the pipeline system such as pressure sensors, AE sensors, and flowmeters. The sensors are installed in pairs on the rig. Three sensors (one of each type) are installed on the upstream side (before the leak area) and the other three are installed on the downstream side (after the leak area). See Figure 8.1.
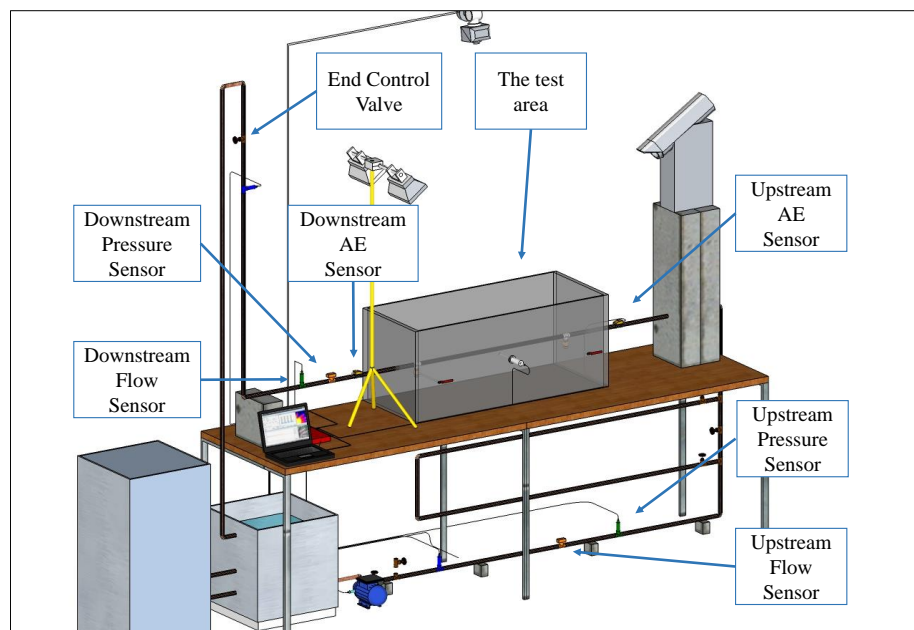
Figure 8.1: Locations of the three pairs of the sensors and the control valve on the test rig.

The experimental work for this purpose is divided into three categories based on the percentage of the end valve opening. The categories are low pressure, medium pressure, and high pressure. The raw signals acquired for all sensors have been subjected to

processing to extract the sensitive features. The pressure of the pipeline has been controlled by closing and opening the end valve to certain percentage to create the three different cases. Figure 8.2 shows the percentage of the end valve open which produces the condition of low, medium and high pressure in the pipeline.
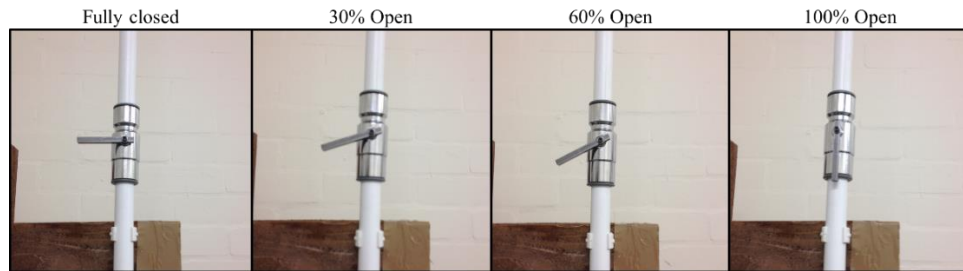
Figure 8.2: End valve with different open positions.

8.3. Selection of the right signal for investigation.

As the time of the leak event is identified in the experimental work, two samples of the signal to be investigated have been chosen with certain lengths before and after the leak point. The reason for this selection is that each signal contains the full information of the pipe condition before or after the leak. Figure 8.3 shows an example of signal selection using windows for both no-leak and leak conditions. The windows of the signal which is used for investigation are the windows located before and after the leak.
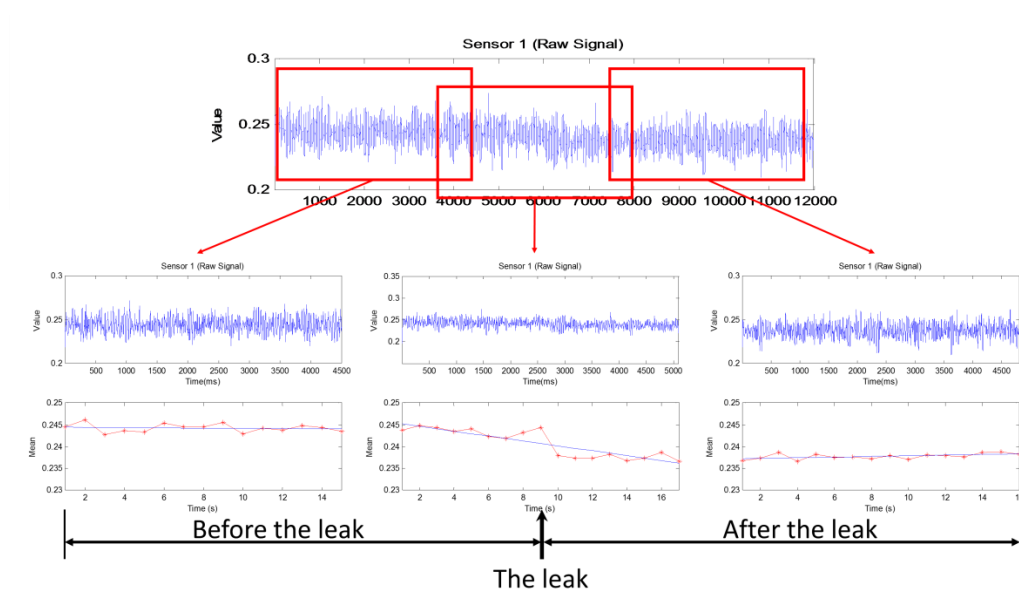
Figure 8.3: Signal classification for investigation purpose

AE, Pressure, and flow sensors are sensitive to any changes in the system parameters for multiple reasons such as starting or stopping the water pump, closing or opening valves, as well as when leaks occur. However, except the change because of the leak, all other changes that are happening in the system for the other reasons are either well known or planned or would be identified easily.

8.4. Extracting features from sensors:

To extract features from the signal, it has to be first processed using known signal transformation techniques such as DWT, FFT where they can depict hidden information (features) that cannot be seen in the raw signal. Statistical functions such as Mean, Max, Min, STD, MAD, Kurtosis, Skewness, RMS, Covariance, Range, Variance, IQR, and Crest Factor would be used to help in extracting the sensitive features. For the FFT, because it is a frequency based signal, the slight deviation in the frequency between the no-leak and leak situation is used to estimate the condition.

8.4.1. Fast Fourier Transform (FFT) Analysis:

An analysis of the sensitive sensors' signals (Pressure sensor and AE sensors) have been carried out using the Fast Fourier Transform (FFT). This analysis is to extract the hidden features from the signals based on their frequency values. As it is known, the FFT is a technique that transforms the signal from time domain to the frequency domain. The FFT displays the frequency content of the signal rather than arranging it as a series of historical data reliant on time.

The FFT produces a graph for the frequency spectrum of the acquired signals with a number of bins equal to the number of the total samples. The right side of the graph is a mirror image of the left side. Therefore only the left side of the graph which is half of the number of bins is utilised in the processing. To represent the frequency graph in Hertz, the remaining number of bins easily converted to Hertz. The half number of the frequency in bins is always equal to the number of frequency in hertz. While, the frequency in Hertz is always fixed and equal to the half of the sampling rate. Therefore, the number of the remaining bins is equal to the half of the sampling rate no number of bins is. Figure 8.4 shows an example of a sample of data of 18000 sample acquired with a sampling rate of 300 sample per second.
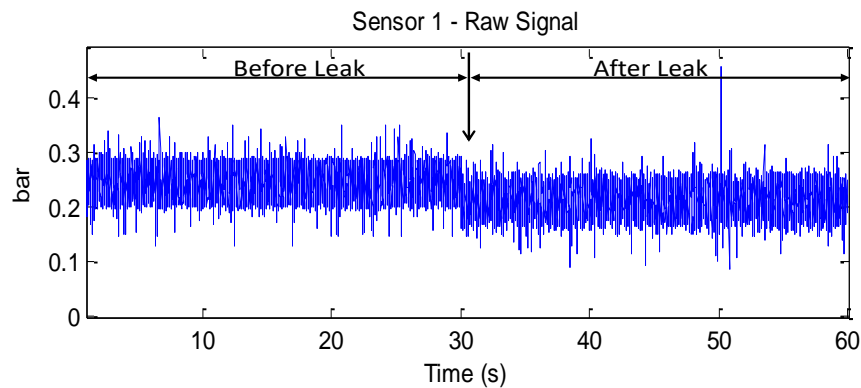
Figure 8.4: Sample of raw signal acquired in 60 seconds.

Figure 8.5 shows the result of the processing using the FFT technique for the first half of the signal which is the before leak section. The length of the sample is 9000 samples. The left side graph is the left half of the signal which is 45000 bins. The right graph is the same graph at the left but in hertz after converting the pins to hertz. The maximum hertz value is 150 because the sampling rate is 300 sample per second.
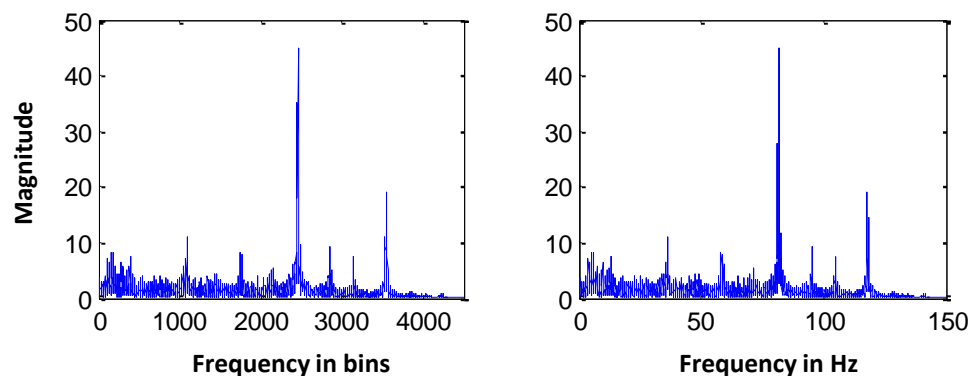
Figure 8.5: The same graph in bins and in hertz

8.4.2.   Pressure sensor:

Figure 8.6 shows the acquired raw signal and the resulted signals for both upstream and downstream pressure sensors. Visually as an initial assessment for the upstream sensor (sensor 1) from the figure (the raw data signal), it can be noted that the leak has affected the signal and reduced the pressure. The figure shows that the part before the leak is higher than the part after the leak. The upstream sensor showed clear pressure drop after the leak has just occurred. While the downstream pressure sensor (sensor 2) apparently showed no significant changes in this case. This is could be because of the leak is so small and

the pipeline is not under extra pressure. The occurrence of small leak led to no visible change to the head available in the system and consequently no visible change on the downstream pressure sensor which is located after the leak point. Figure 8.6 shows from top to bottom the raw signal, dwt (high pass), dwt (low pass), FFT signal processing. Those different forms of the signal have been subjected to investigation for the best feature using the thirteen statistical functions mentioned earlier.
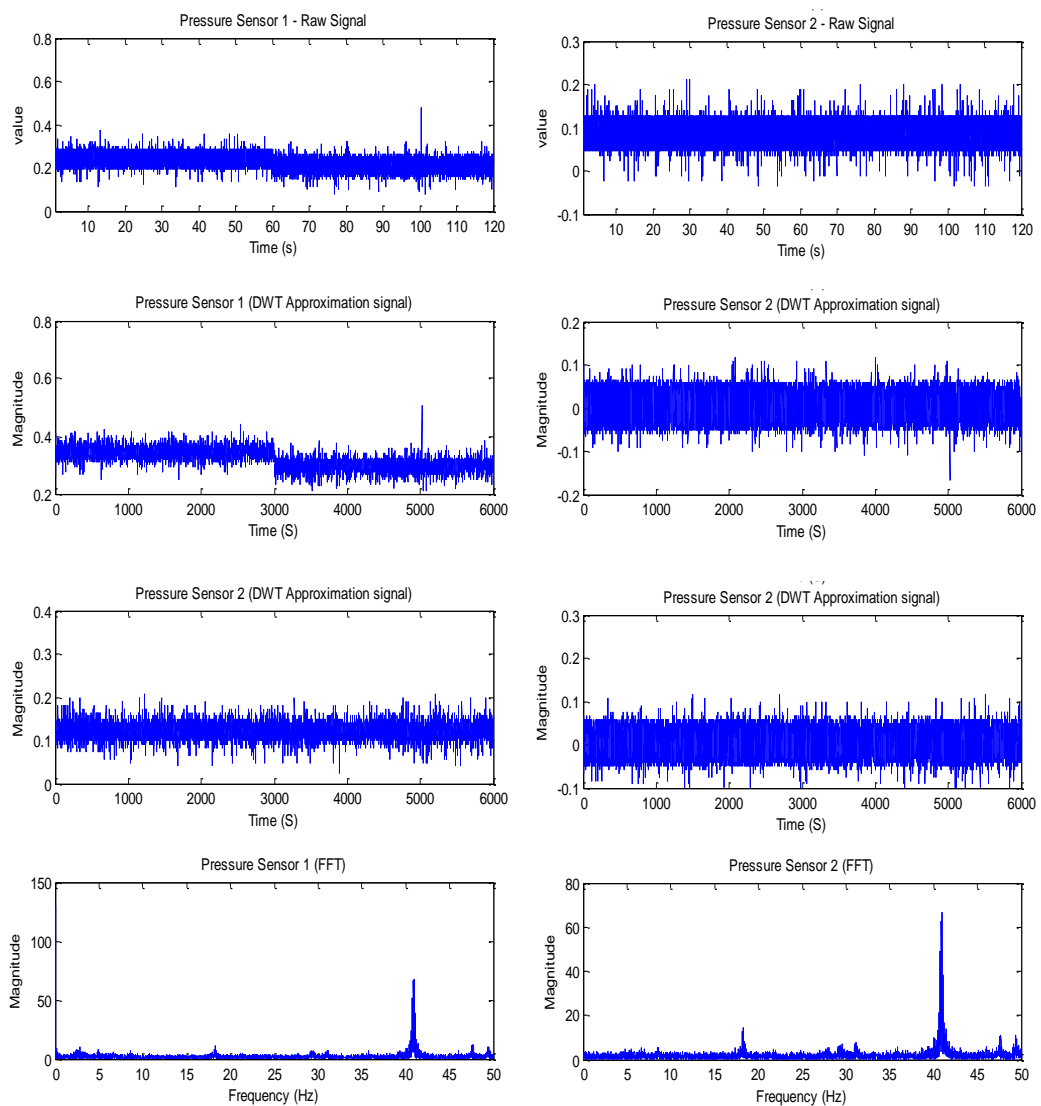
Figure 8.6: Raw and transformed signals for both sensors.

Figure 8.7 and Figure 8.8 are examples of the raw signals at different percentage of end control valve open. The valve has affected the signals because it has increased the pressure in the pipeline.
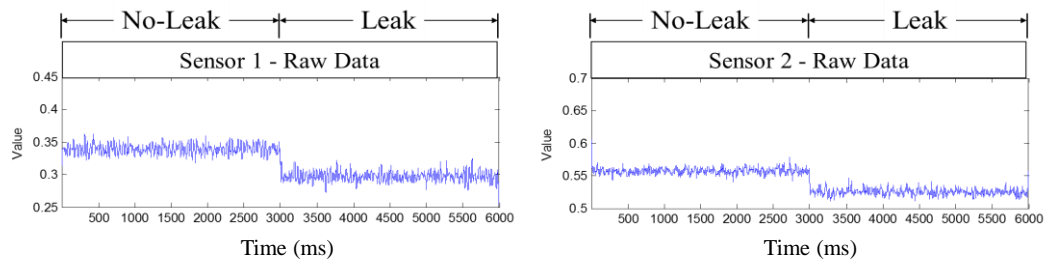
Figure 8.7: The raw signal when the end valve is closed partially (60% open).
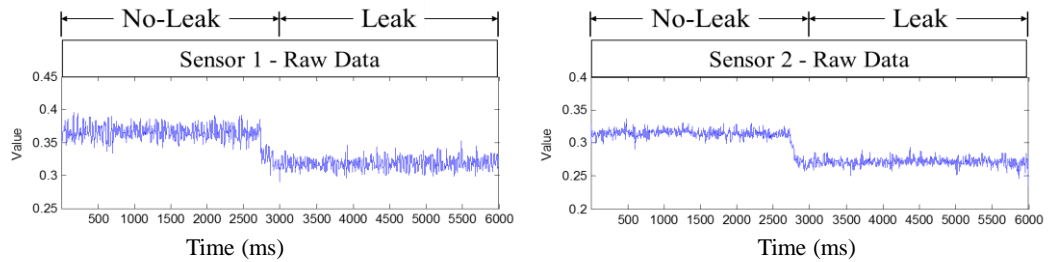
Figure 8.8: The raw signal when the end valve is closed partially (30% open).

Figure 8.9 and Figure 8.10 show two examples of the same feature which is the Mean value, in this case, has been applied to each sensor. Figure 8.9 shows the result of the Mean value for the upstream sensor (sensor 1). The figure shows that the slope of the mean value of the sensor 1 is high. Figure 8.10 shows the same feature for the downstream sensor (sensor 2). The figures show that the feature for the sensor 2 has a lower slope value.
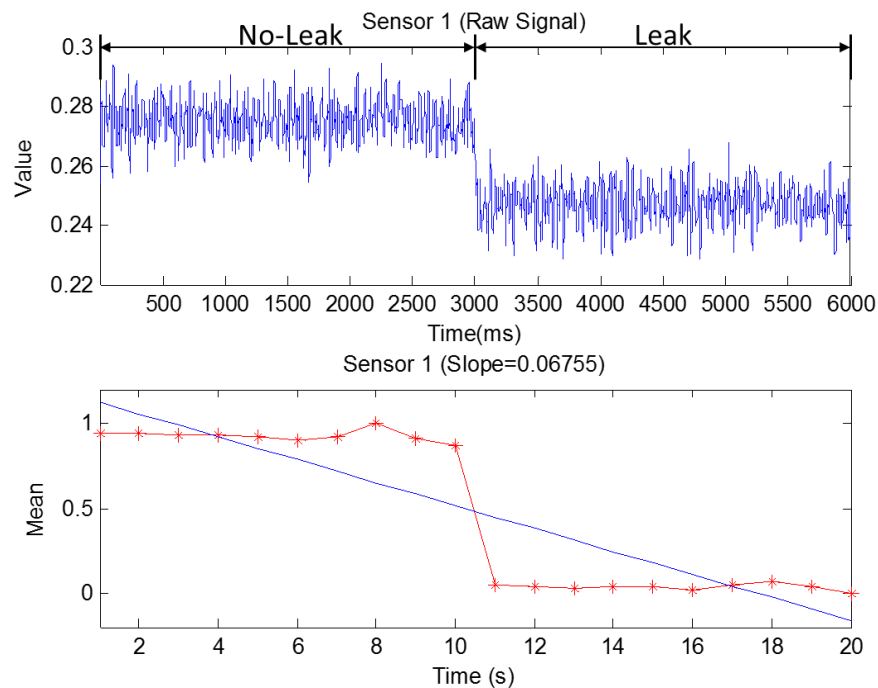
Figure 8.9: example of high sensitivity feature (sensor 1)
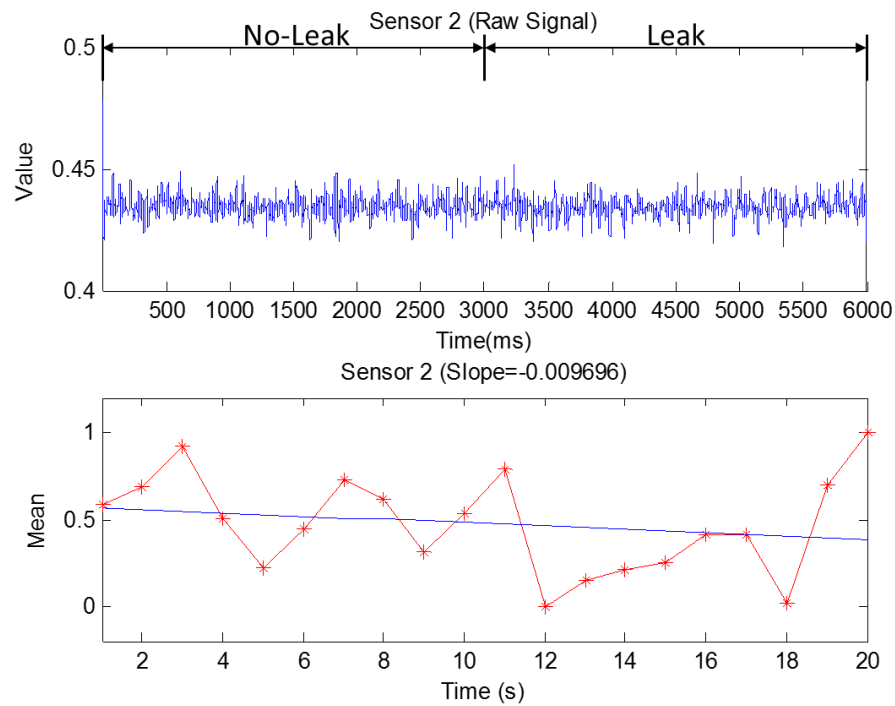
Figure 8.10: example of low sensitivity feature (sensor 2)

8.4.3. The FFT for the Pressure Sensors

Figure 8.11 shows the raw signal which is acquired with a sampling rate of 300 samples per second in three minutes. This signal contains a leak incident in the middle of the acquiring time. The two singles are for the upstream sensor no. 1 and the downstream sensor no. 2.
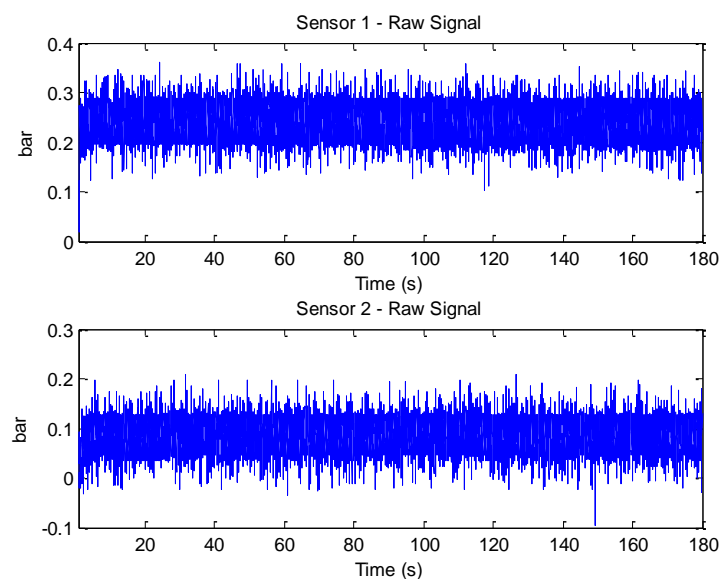
Figure 8.11: Pressure Sensors (1 & 2) Raw Signal

The raw signals have been divided into two sections. One section represents the healthy condition of the pipeline when there is no leak and the other section is for the leak period. The signals of the each two sections (No-Leak and Leak) for both sensors are shown in Figure 8.12. Initial visual assessment of the Fast Fourier Transform (FFT) signals illustrates that the two signals are identical in shape and have the same number of large peaks each. This means that both sensors are influencing in of the same manner with water flow characteristics and leaks. In the figure, the highest peak is the second from the left.
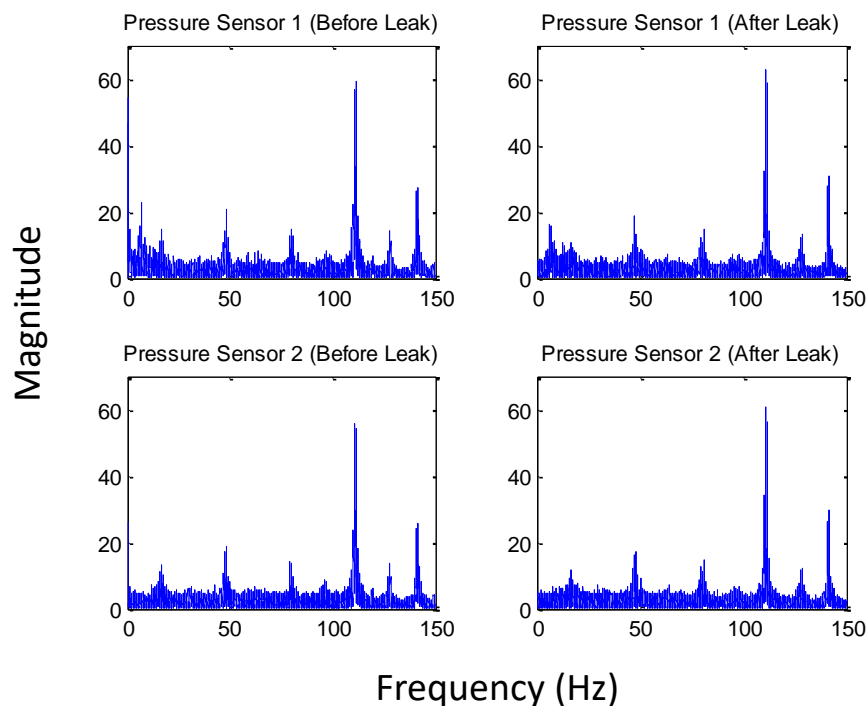
Figure 8.12: The FFT result of the two pressure sensors (Before and after the leak)

However for better discrimination between the two situations of the leak and no-leak the two sections of the Fast Fourier Transform (FFT) signal for each sensor have been split into twelve small partitions. Figure 8.13 contains the full two sections of the signal together in the same plot. The figure demonstrates the twelve selected partitions to be analysed for each signal.

8.4.4.   Extracting the SCFs using the displacement of the frequency for the pressure sensor.
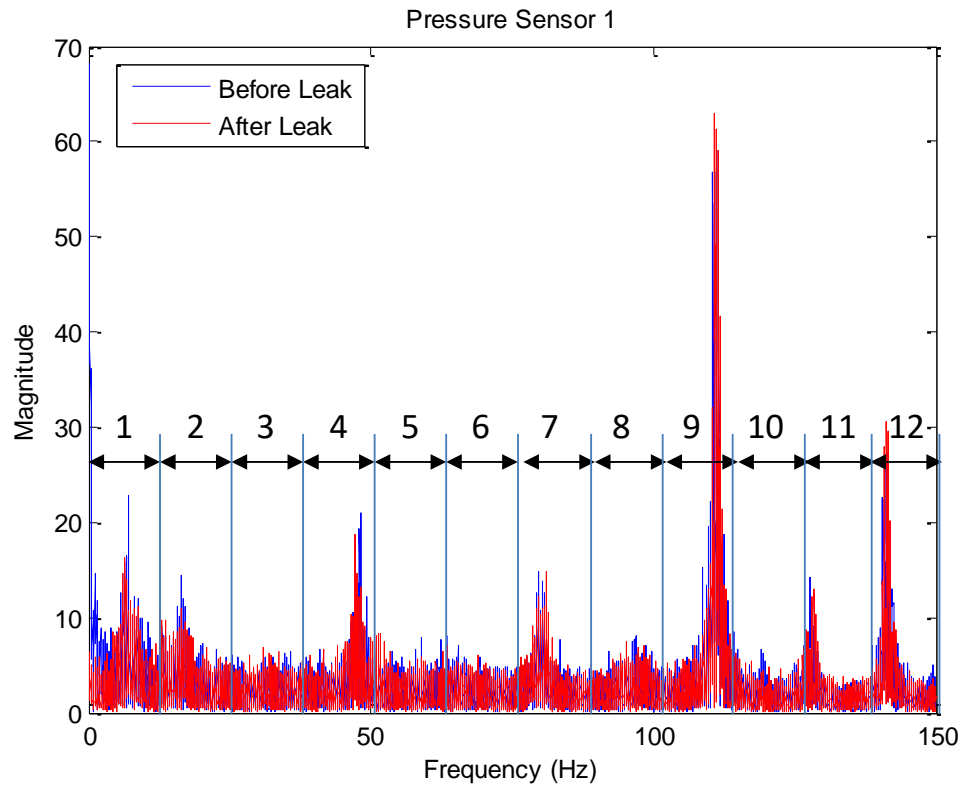
Figure 8.13: The two FFT signals in the two conditions of the leak and no-leak in one plot

For more clarifications and comparison, Figure 8.14 shows the partition number nine from Figure 8.13 in separated subplots. The initial visual assessment reveals that the two portions have exactly the same profile with a little difference in magnitude and displacement.
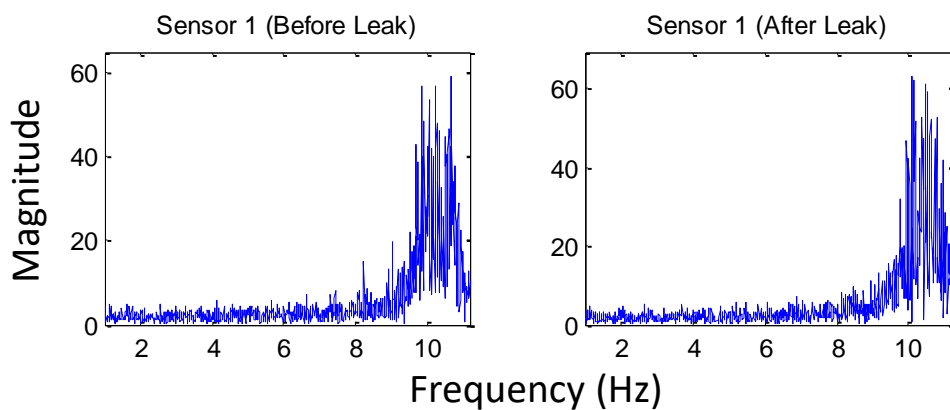
Figure 8.14: Partition no. 9 from previous figure.

If the two signals are reconstructed together in the same plot as in Figure 8.15 the differences in the magnitude and the displacements will be more evident. These differences could be the indication of the system state.

To extract the SCFs from the FFT signal partitions, first, the maximum and the minimum peaks in the signal are located with their position in x-axis which is the frequency in Hz. For example in Figure 8.15 the maximum peak of the no-leak (Before leak) condition is 10.68 Hz and for the leak (the After Leak) condition the maximum peak is at 10.09 Hz while for the minimums are 5.07 and 5.54 Hz consequently as shown in Figure 8.16.
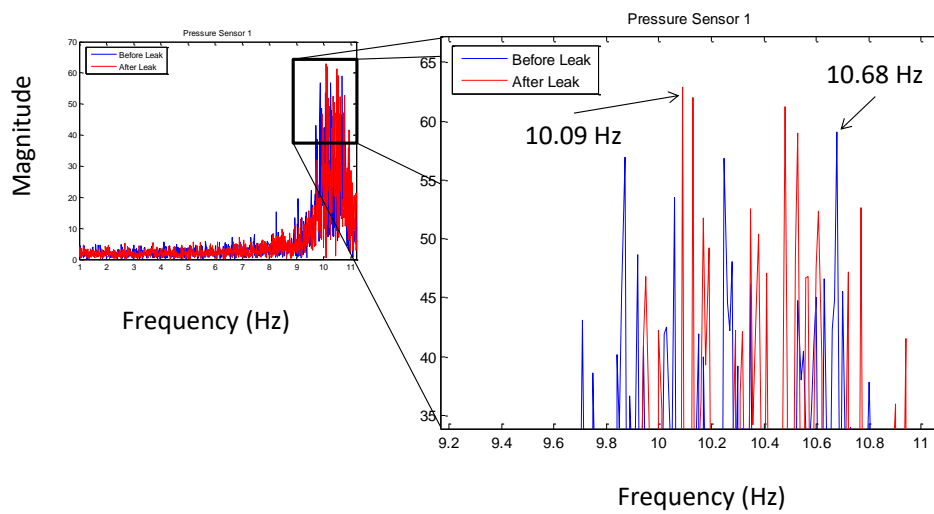
Figure 8.15: The partition no. 9 (frequency of the maximum values)
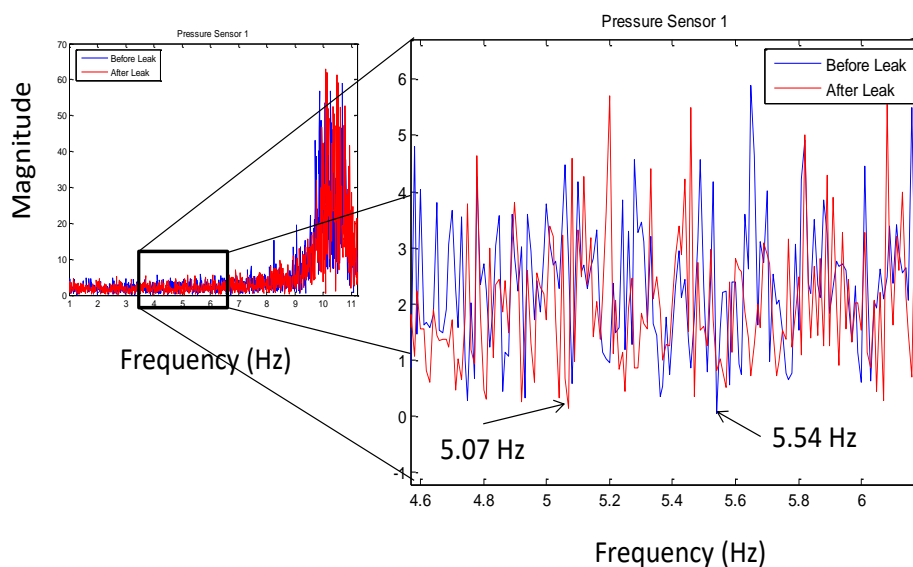
Figure 8.16: The partition no. 9 (frequency of the minimum values)

On finding the maximum and minimum peaks of each partition in each condition, the percentage of the difference (Δ) between the two maxima is calculated. As well as, the percentage of the difference between the two minima is also calculated. Figure 8.17 shows the results of calculating the frequency values for the FFT signal partitions of the two sensors. Figure 8.18 shows the result of the calculation. It shows the percentage of the delta for all maxima and minima of all partitions.
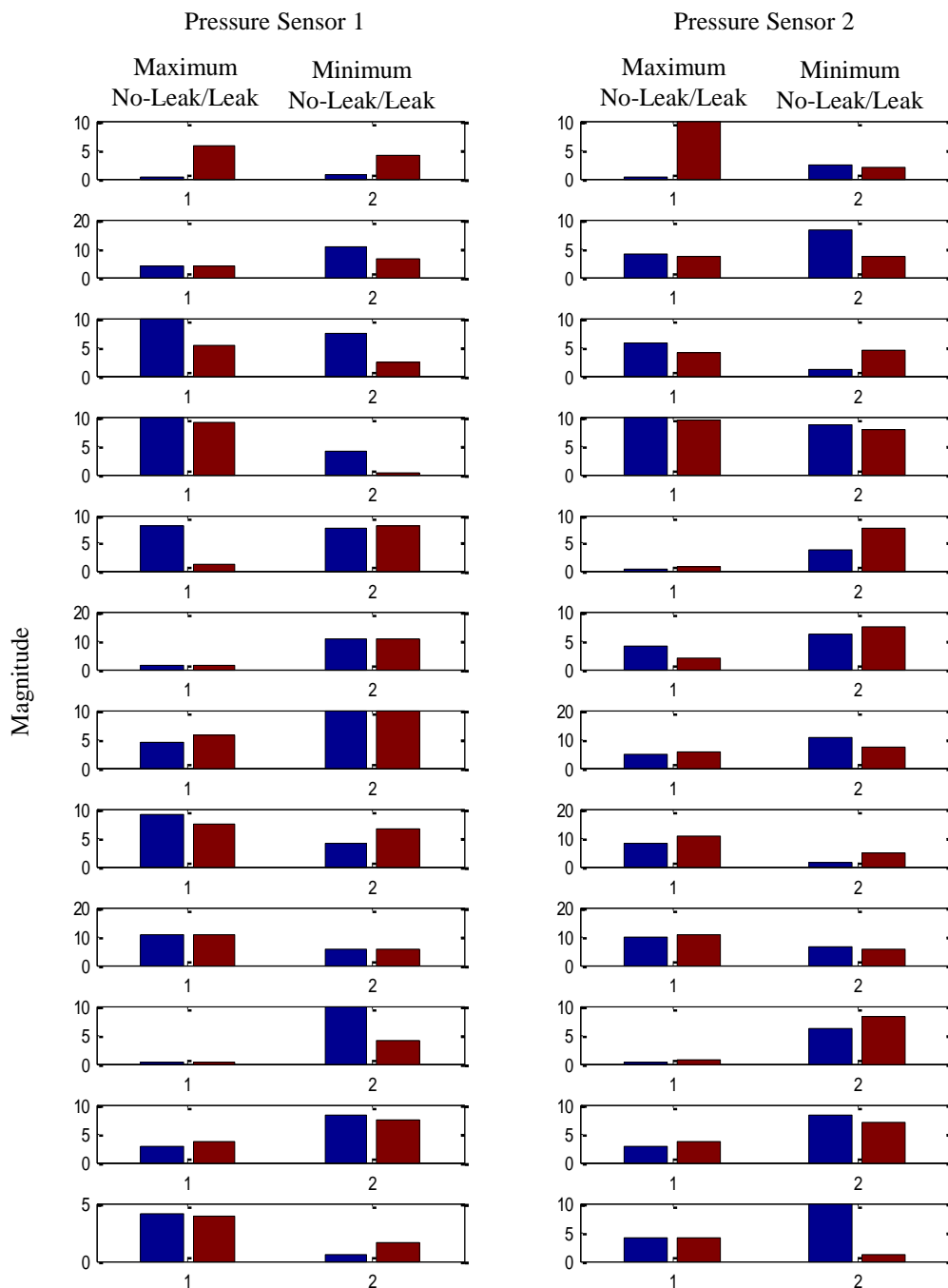
Figure 8.17: the result of the twelve partitions of the FFT signal
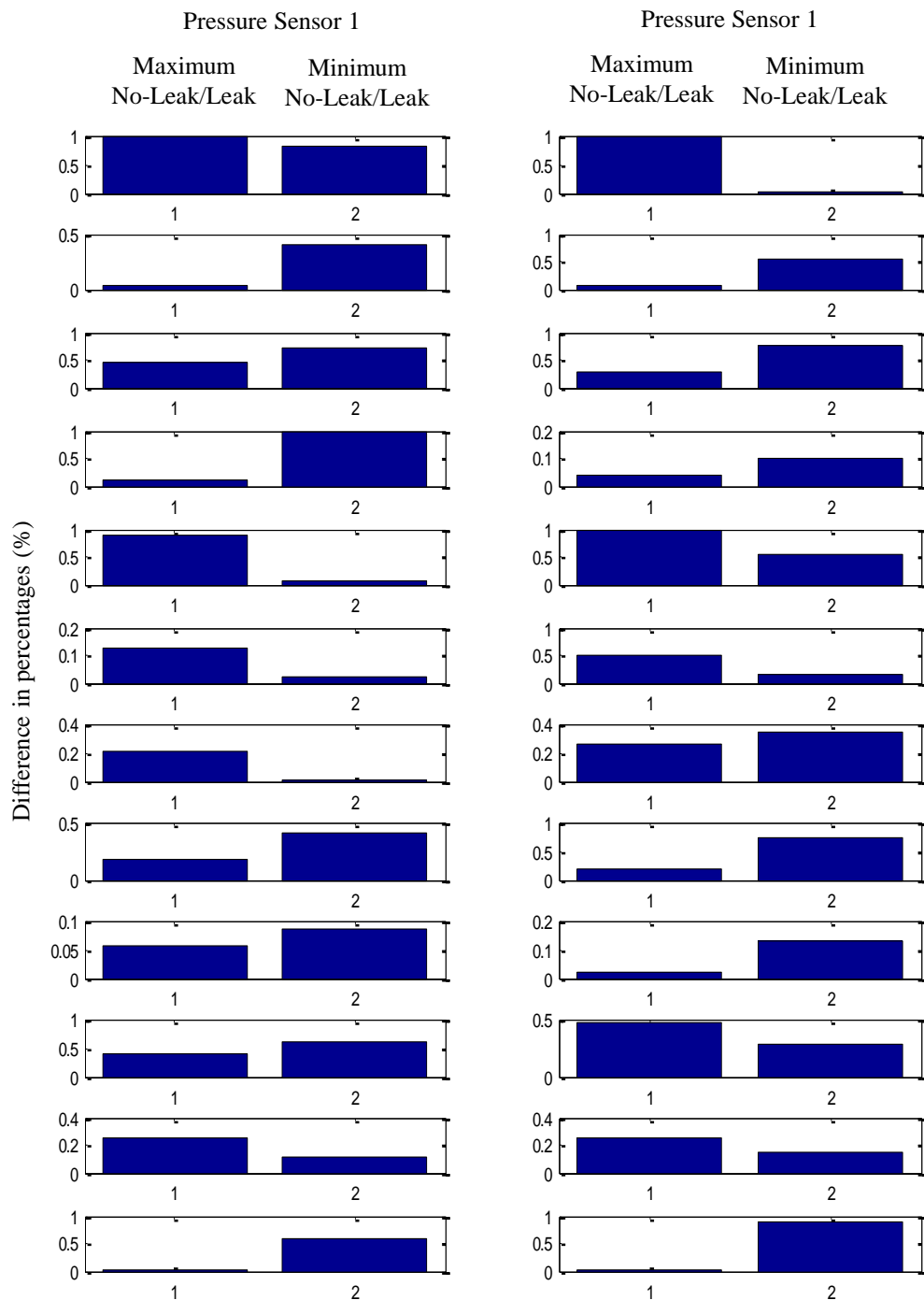
Figure 8.18: The percentage of difference for Maxima and Minima

8.4.5. Discrete Wavelet Transform (DWT) for the pressure sensor.

The discrete wavelet analysis has been applied to the raw signal to produce two components of the signal as shown in Figure 8.19. The two components are the

approximation component and the detail component. Both components have been subject to analysis using thirteen statistical functions.
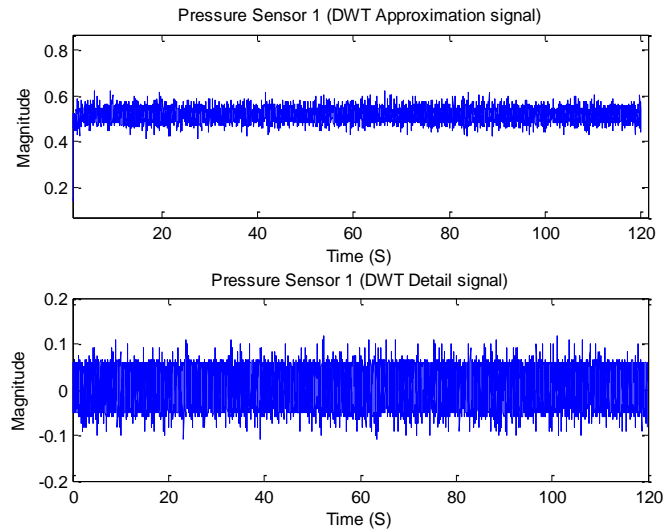
Figure 8.19: Wavelet transform signal for the pressure signal.

8.4.6.   AE Sensor

Figure 8.20 shows the raw signal of the two AE sensors which was acquired with a sampling rate of 600 samples per second in two minutes. This signal contains a leak event in the middle of the acquiring time. The two singles are for the downstream AE sensor no. 1 and upstream AE sensor no. 2
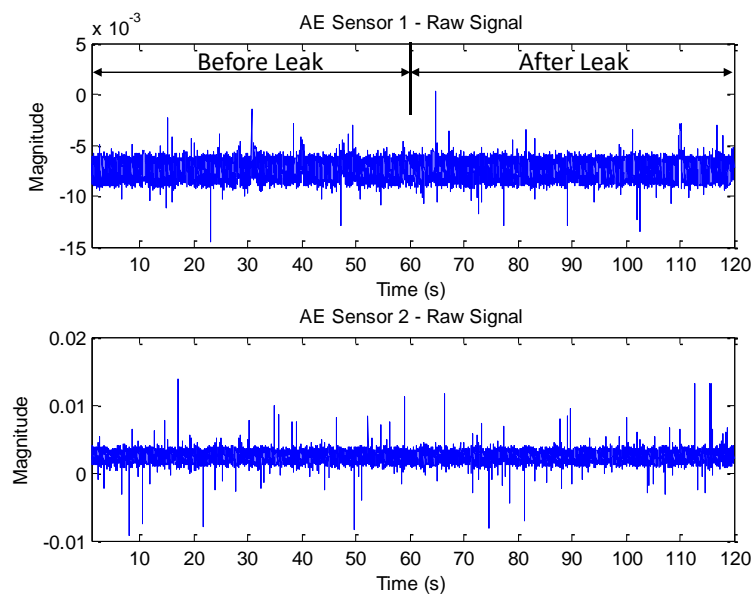
Figure 8.20: Raw signal of the two AE sensors

8.4.7.   The FFT for AE sensors.

For both AE sensors, the raw signals have been divided into two sections of the no-leak and the leak states (Before Leak and After Leak) and applied the FFT processing technique on each half. The result is shown in Figure 8.21. The initial visual assessment of the Fast Fourier Transform (FFT) signals illustrates that the two signals are identical in shape and have the same number of large peaks each. This means that both sensors are influencing in of the same manner with water flow characteristics and leaks. For better discrimination between the two situations of the leak and no-leak the two sections of the Fast Fourier Transform (FFT) signal for each sensor have been split into twelve small partitions. Figure 8.22 contains the full two sections of the signal on sensor no. 1 together in the same plot. The figure shows the twelve selected partitions to be analysed for each signal.
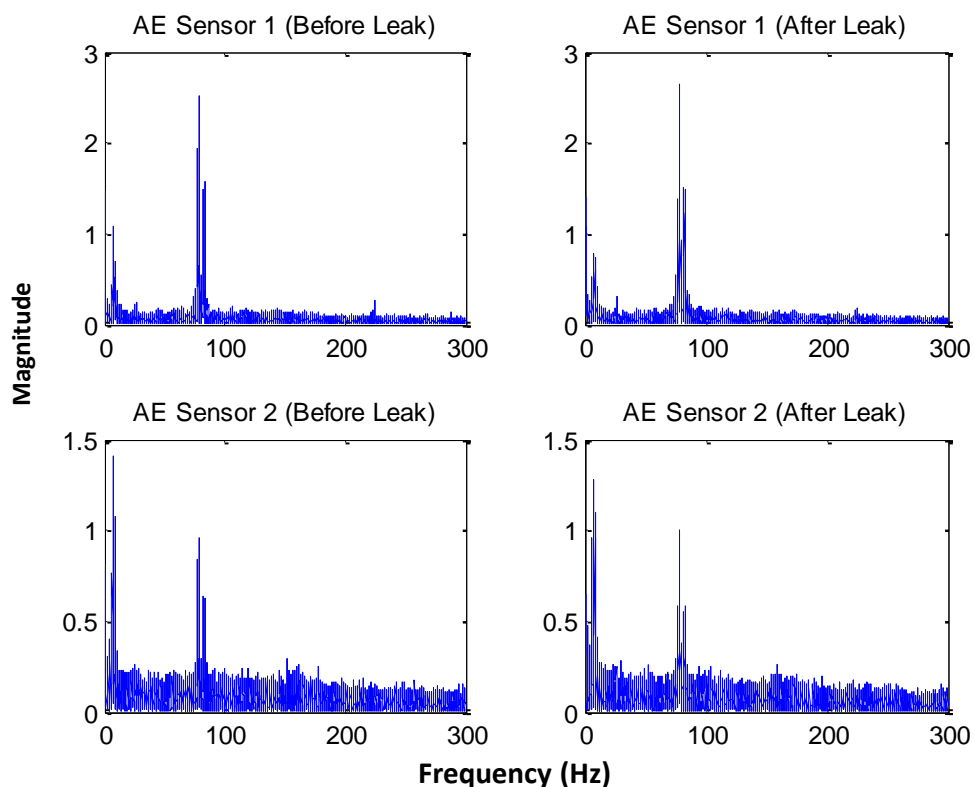
Figure 8.21: The FFT result of the two AE sensors (Before and after the leak)

8.4.8.   Extracting the SCFs using the displacement of the frequency for the AE sensor.

Similar to the process in the pressure sensor, as shown in Figure 8.22 the FFT signal of the AE sensor has been divided to twelve section to extract the maximum and minimum frequencies values in both conditions of the no-leak and leak for both sensors (the downstream and the upstream).

To extract the SCFs from the FFT signal partitions, first, the maximum and the minimum peaks in the signal are located with their position in x-axis which is the frequency in Hz. For example in Figure 8.23 the maximum peak of the no-leak (Before leak) condition is 7.78 Hz and for the leak (the After Leak) condition the maximum peak is at 8.18 Hz while for the minimums are 5.07 and 5.54 Hz consequently as shown in Figure 8.24.
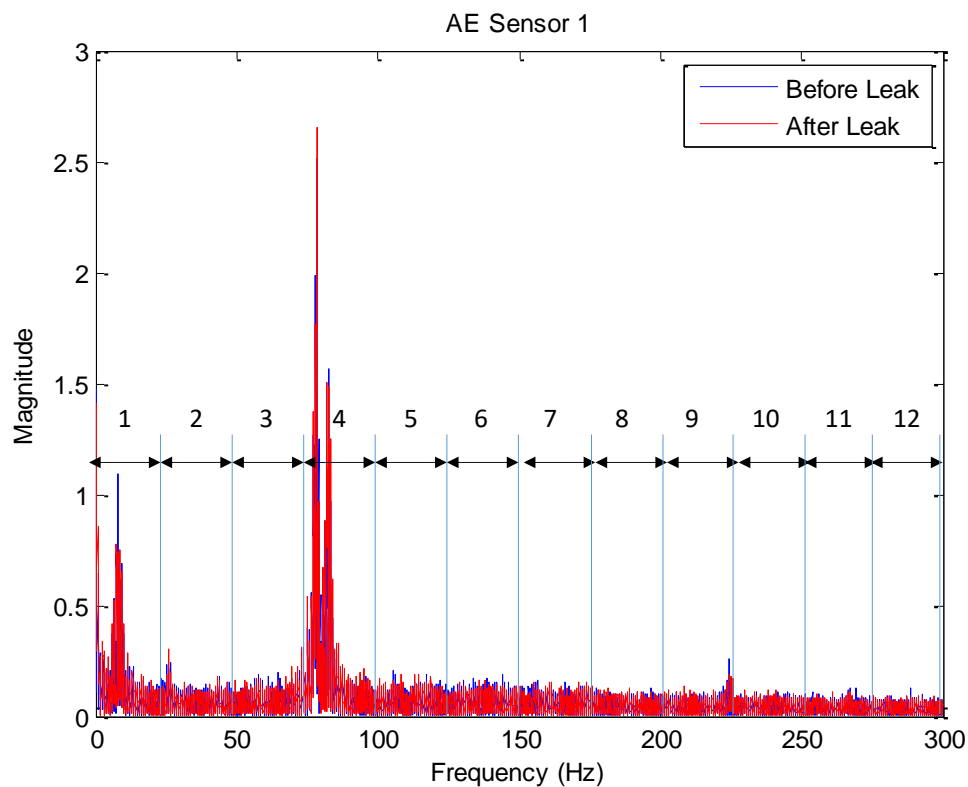
Figure 8.22: The two FFT signals in the two conditions of the leak and no-leak in one plot

The deviation in frequency has been extracted for all twelve section to be used as a feature for identification of the condition of the system. Partition no. 4 is selected as an example

for clarification. The values of the frequency at the maximum and the minimum have been traced and extracted.
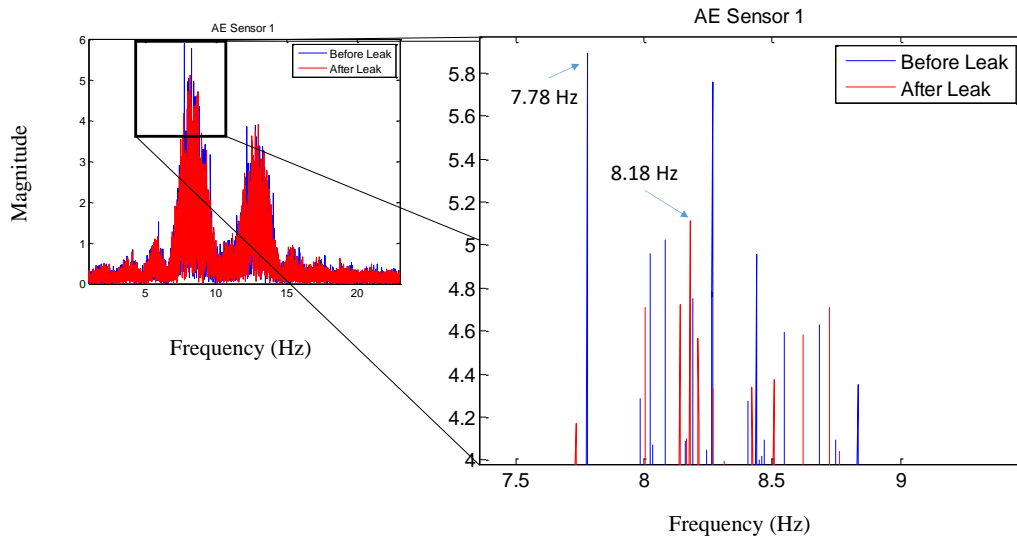
Figure 8.23: The partition no. 4 of the AE FFT signal (frequency of the minimum values)
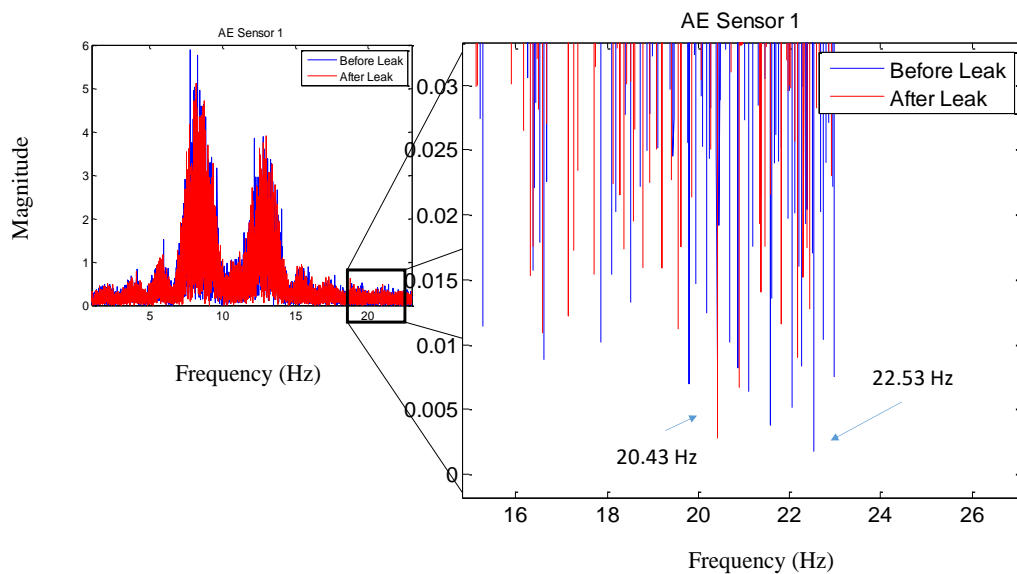
Figure 8.24: The partition no. 4 of the AE FFT signal (frequency of the minimum values)

8.4.9.   Discrete Wavelet Transform (DWT) for the AE sensor.

The DWT transform is also applied to the AE sensors. Two components of the signal have been created as shown in Figure 8.25. The two components are the approximation

component and the detail component. Both components have been subject to analysis using thirteen statistical functions.
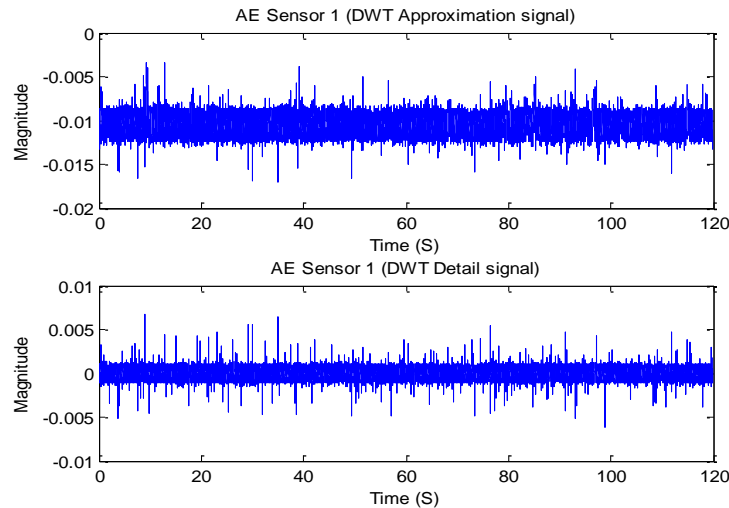
Figure 8.25: Wavelet transform signal for the AE signal.

8.4.10. Flow Sensor

The flow sensors raw signals do not show much information as it is in a form of pulses. To visualise any changes, the signal has to be converted from the pulses into a readable number (see 4.6.4 flow sensor for details). Figure 8.26 shows the raw signal for both upstream and downstream in pulses. The flow signal in its current form of a pulse is retaining hidden information more than when converted to streamline of flow indicator. The processing technique such the DWT and the FFT would extract that information better than in streamline flow data.
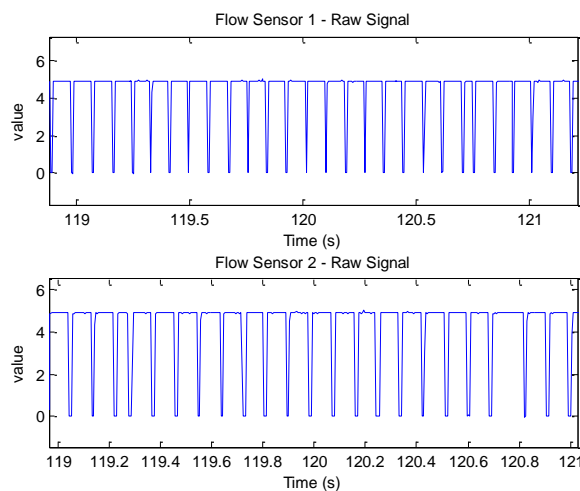
Figure 8.26: Raw signal of the two the flow sensors

8.4.11.   The FFT for flow sensors.

Figure 8.27 illustrates four plots for the flow sensor FFT signal. The plots are for sensor no. 1 the downstream sensor and the upstream sensor no. 2. Each sensor signal has been plotted in both cases of the no-leak and the leak. From the figure, the result of the FFT shows that the FFT signal is matching for both conditions of the no-leak and the leak with slight differences. The signal has been subjected to an analysis similar to the analysis work carried out with the two previous sensors (pressure and AE).
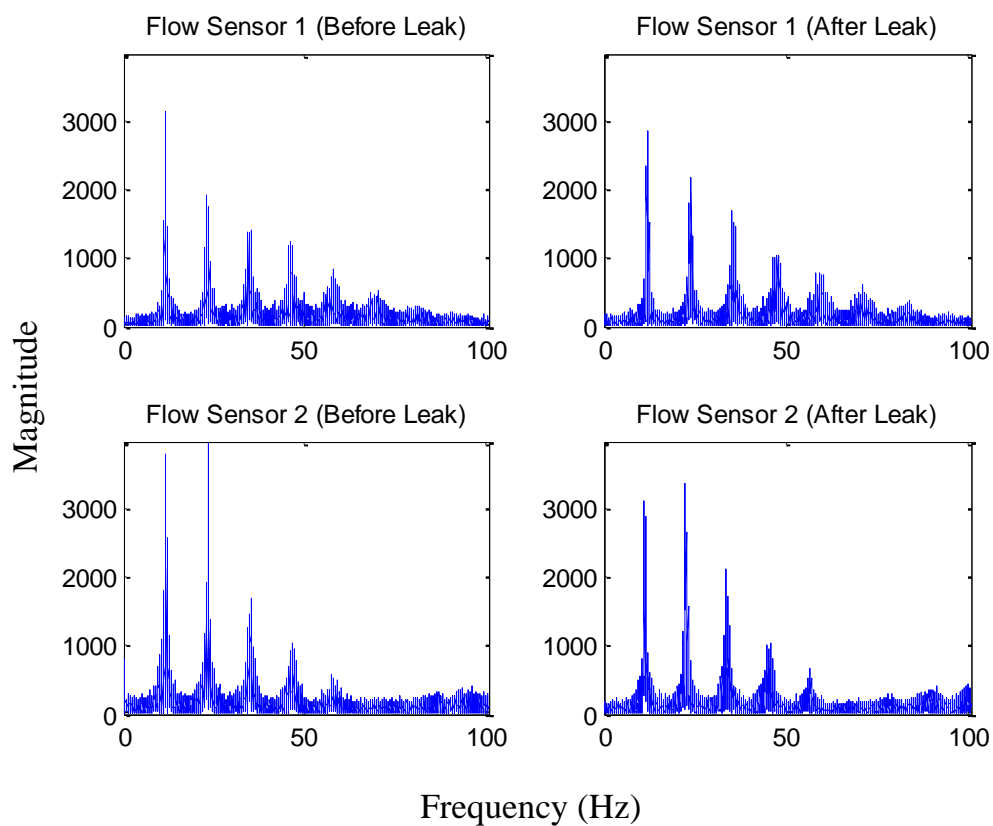
Figure 8.27: The FFT result of the two flow sensors (Before and after the leak)

8.4.12.   Extracting the SCFs using the displacement of the frequency for the AE sensor.

Again, similar to the work in the previous sensors, the flow sensor FFT signal has been divided into twelve small partitions to extract features from it. The process of reading the frequency at the maximum and minimum position is shown in Figure 8.29 and Figure 8.30.
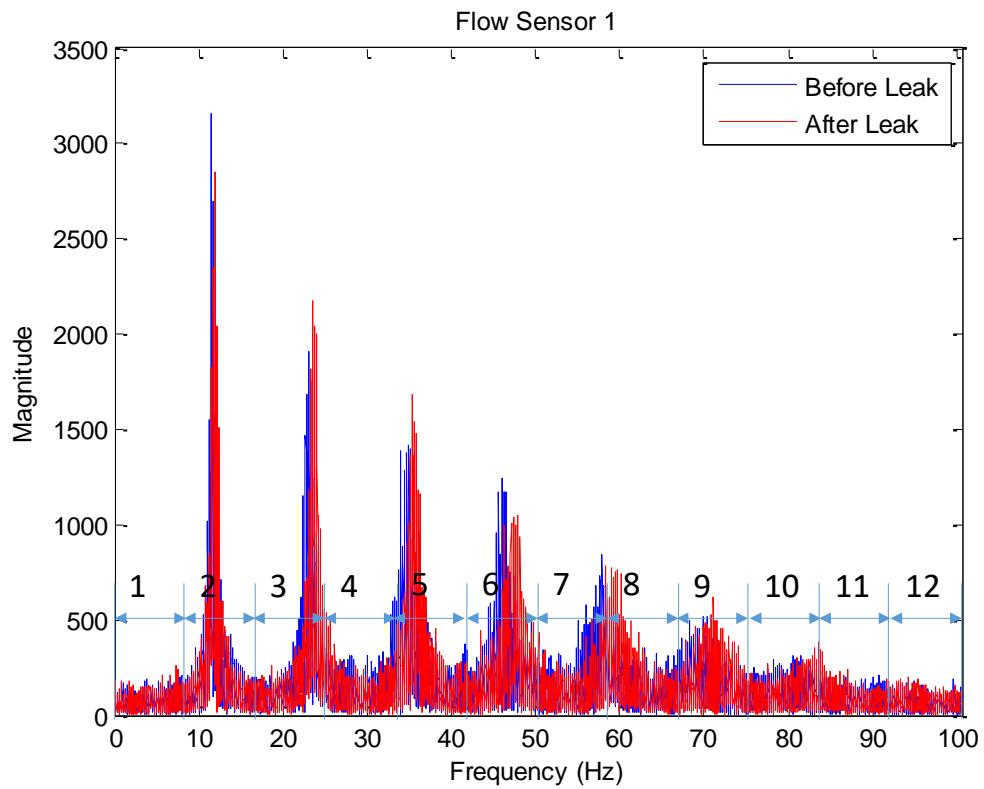
Figure 8.28: The two FFT signals in the two conditions of the leak and no-leak in one plot.
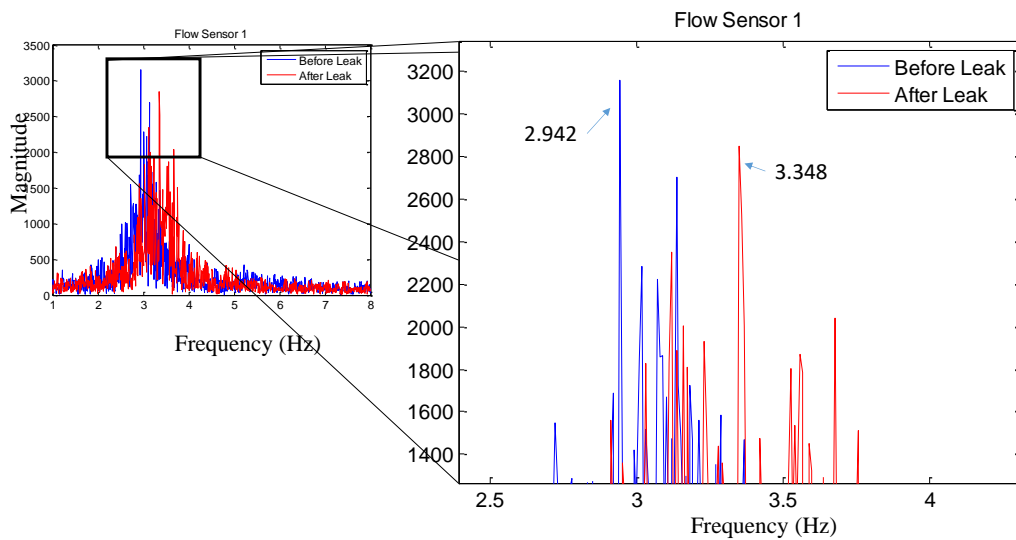
Figure 8.29: The partition no. 2 of the Flow Sensor FFT signal (frequency of the maximum values)
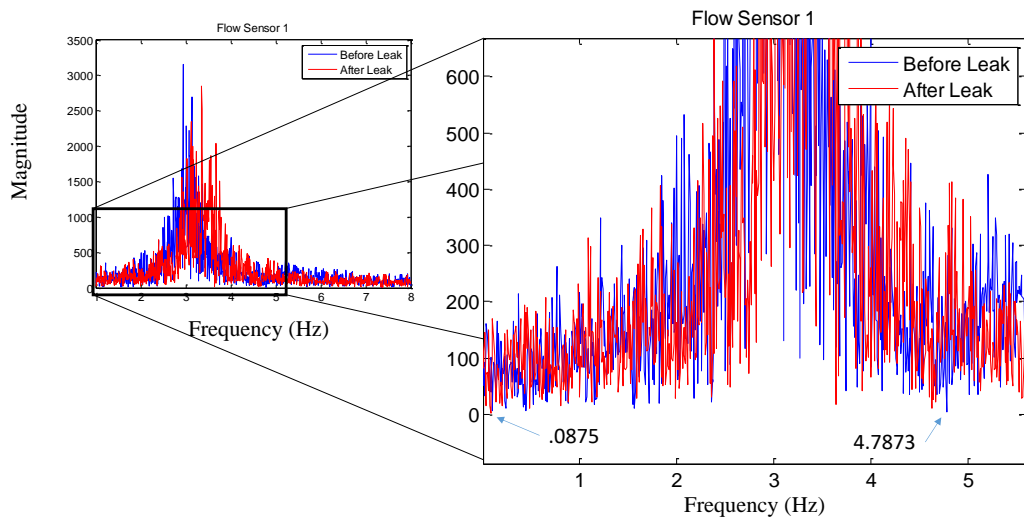
Figure 8.30: The partition no. 2 of the Flow Sensor FFT signal (frequency of the minimum values)

8.4.13. Discrete Wavelet Transform (DWT) for the flow sensor.

The DWT transform is applied to the flowmeter signals. The two components of approximation and detail components of the signal have been created as shown in Figure 8.31. Both components have been subject to analysis using thirteen statistical functions.
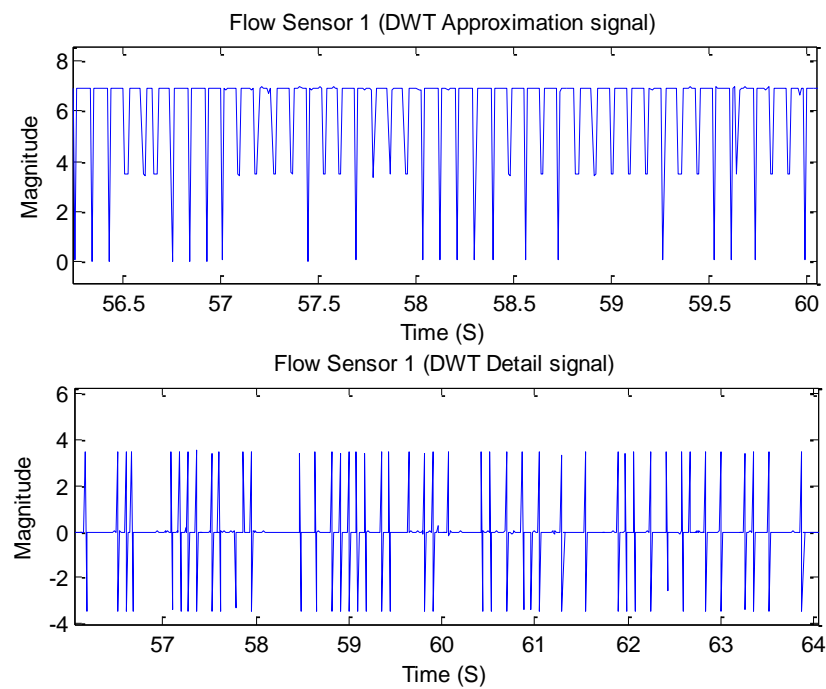
Figure 8.31: Wavelet transform signal for the flowmeter signal.

8.5. Results of signal processing.

On completion of the process of calculating the percentage of the difference, an Association Matrix ASM has been generated to give a visual presentation of the achieved results as in Figure 8.32. In the ASM, the colour map shows the value of the feature. The white colour is the highest value while the black is the lowest one. Higher value means higher sensitivity and a lower value means lower sensitivity. As shown in the associated matrix, the values of y-axis are the features and the x-axis are the sensors. The number of features produced are 600 (75 Features x 8 Sensors)
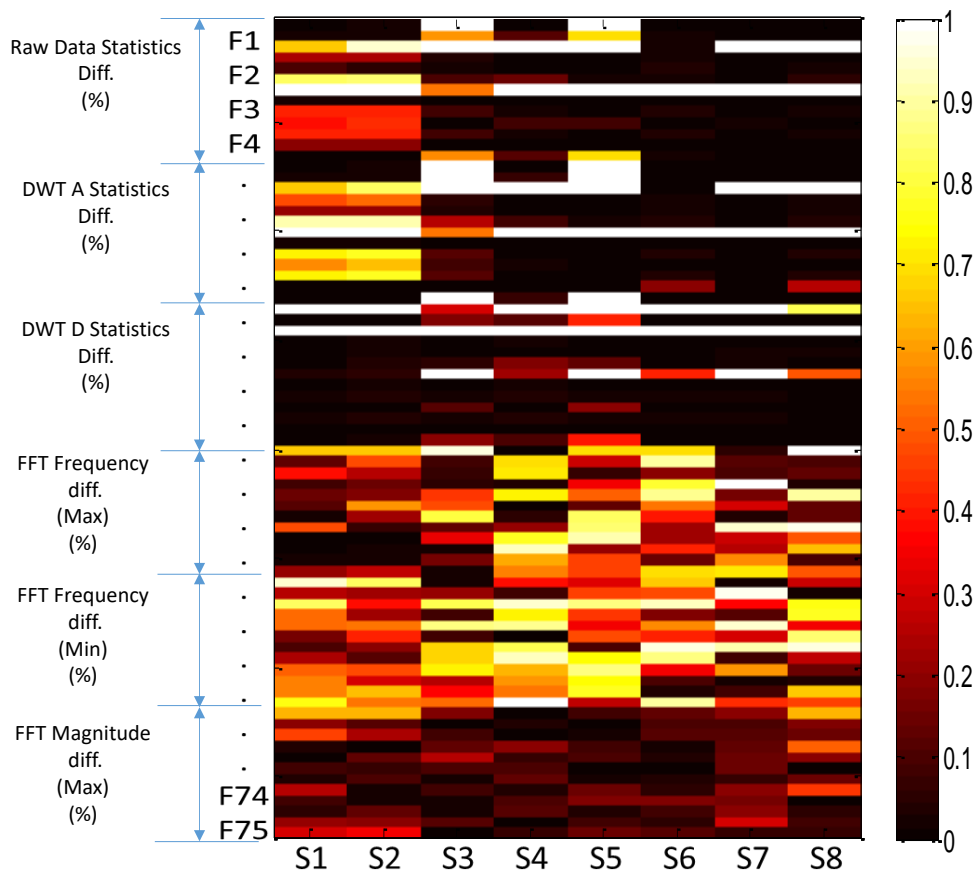
Figure 8.32: The ASM for the ID sensors (Pressure, AE, Flow).

8.6. Summary

A systematic process as a part of the ASPS approach has been carried out in this chapter to extract the best features from the 1D sensors. The chapter at the beginning has

explained the method of selecting the right signals for investigation purposes. Then explained the process of extracting features from those signals. The process carried out by applying a multiple advanced signal processing techniques on three pairs of the sensors that have been used on the test rig. The sensors are Pressure, AE, and Flow. Each type of the sensors has one downstream and one upstream. The signal processing techniques used in this systematic method are the FFT, the DWT, with the statistical analysis functions such as Mean, Max, Min, STD, MAD, Kurtosis, Skewness, RMS, Covariance, Range, Variance, IQR, and Crest Factor. The FFT used to extract details of the frequency content in all acquired signal from the six sensors. The result of this systematic process is a matrix named the Associated Matrix ASM contains all the features. The ASM for the 1D sensors is used to form the general ASM using the fusion system including the thermal camera.

Chapter 9.   ASPS approach for water leakage detection

9.1. Introduction

This chapter provides the concept and the implementation of the ASPS approach for water leak detection, describes the ability of the proposed approach in detecting water leaks using a fusion sensory and imager system, the ASM in detail as well as the stability matrix SM by which the consistency of the ASM is confirmed. The results gained from the previous two chapters were used in final step towards accomplishing the ASPS approach. The associated matrices resulted for both 1D and 2D sensors are joined together to shape the final associated matrix for the proposed ASPS approach. The neural network as an artificial intelligence is applied to the result of the ASPS approach in order to confirm the sensitivity of the approach in leaks detecting.

9.2. The Associated Matrix for the fusion system

The sensitivity of the selected features determines the sensitive sensors and signals. The ASM presents the result of the sensitive features process attained from the signal (1D) and image (2D) processing. The ASM contains 75 rows represent the features and 13 columns that represent the sensors. In total, there are 975 features. The sensitivity of the attained features is varying from 0 to 1. As it is shown in Figure 9.1, the features vary in colours. The bright ones are the most sensitive features while, the dark ones are the less sensitive features.

The ASM is built based on the number of signal and image processing methods used to extract the sensitive features and the number of the available sensors. As shown in Figure 9.1, the first thirteen rows, from the top, are for the application of the statistical analysis on the raw data. The second thirteen are for the statistical functions applied on component A of discrete wavelet transform (dwt). The third 13 rows are for the detail component of the discrete wavelet transform. The last group of the rows which are for the FFT are divided to twelve rows each. The first twelve are for the difference in the maximum frequencies between the two different states (before and after the leak). The second twelve are for the difference in the minimum of the frequencies. The last group is the difference in the maximum magnitude of the FFT signal in each state. The colour map shows the amplitude of each feature. The ASM provides a clear visual estimation of the sensitive

features and consequently the sensitive sensors and the appropriate signal processing methods to be used in differentiation between the states of the leak and no-leak. For more clarification, the ASM marked in the y-axis with F1 to F75 and in the x-axis with S1 to S13. The F1 to F75 are the number of the features extracted with the processing techniques explained earlier. The S1 to S2 are the number of sensors. For example F1 and S1 are selected as a sensitive feature and represent the thermal camera as a sensor with the application of the Mean as a processing method.
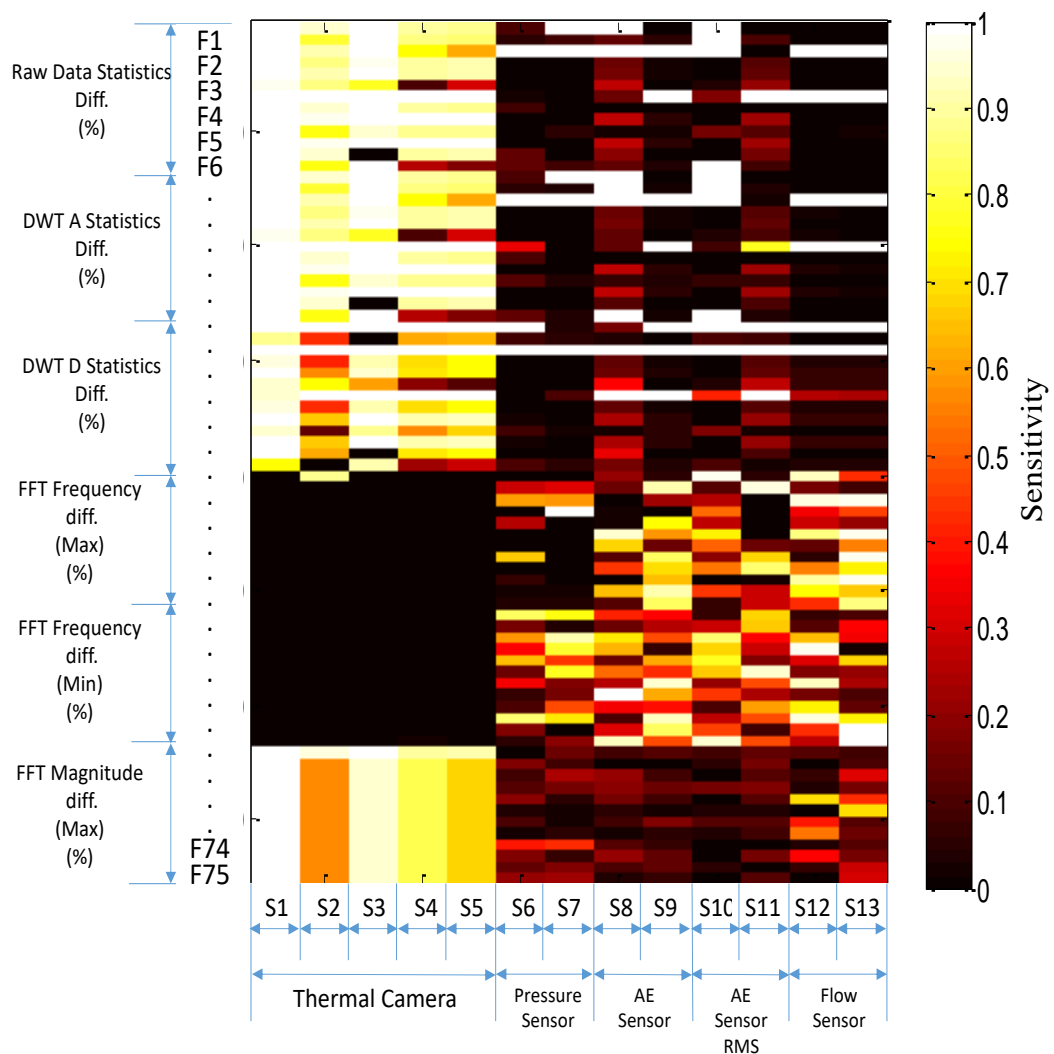
Figure 9.1: The ASM of the fusion system.

To test the best combination of the sensors and the processing techniques, the SCFs data is ranked in descending order from the higher sensitivity to the lowest one. The ranked data then has to be grouped into a certain number, each group is called a system. The

first group or system is the highest sensitivity while the last system contains the features of the lowest sensitivity.

To confirm the reliability of the ASPS in producing the ASM, further experiments with their systematic process for features extraction have been carried out. The method produced a number of ASM identical to the first one. In addition to the ASM shown in Figure 9.1, Figure 9.2 and Figure 9.3 show ASMs for other experiments.
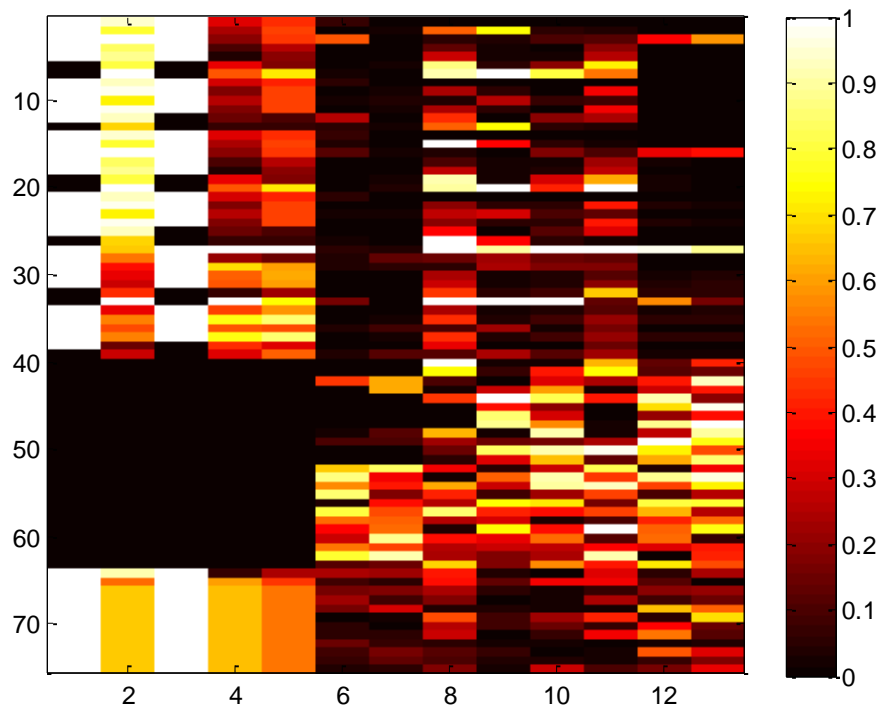
Figure 9.2: ASM from the second experiment.
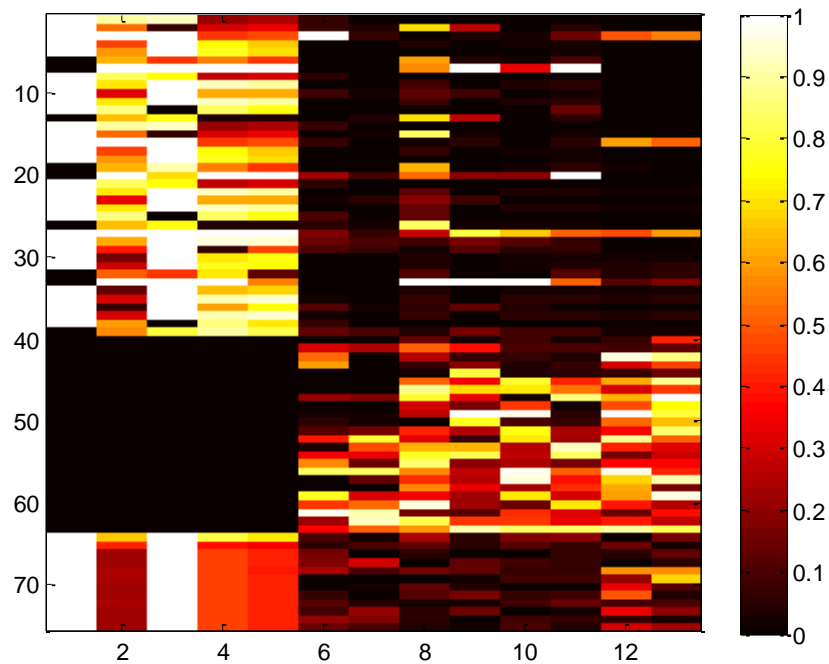
Figure 9.3: ASM from the third experiment.

The two ASMs in Figure 9.2 and Figure 9.3 are identical in shape and similar to the first ASM. All the ASMs show the same regions of strengths and weaknesses of the sensitivity of the features. However, to check the consistency and stability of each feature in the ASM separately another systematic process is required to produce another matrix named Stability Matrix (SM).

9.3. The Stability Matrix

The stability is the quality of something that does not change easily. The purpose of the stability matrix is to test the ability of every feature in the ASM to remain unchanged or changes within the acceptable range that do not affect its sensitivity. To calculate the stability matrix, the standard deviation (SD) is used. The standard deviation is one of the powerful statistical tools to check the spread of the data. The standard deviation tells how the data is strong or weak by checking its spread out from the mean. The lower value of standard deviation means the data is close to the average and within the required range and consequently is stable. While the large value of standard deviation means the data is instable.

9.3.1.   Calculation of the Stability Matrix (SM)

The stability matrix is calculated using the original data used in producing the ASMs. The original data contains the real value of the no-leak and the leak conditions of each feature. From the original data, the absolute delta value (the difference) of the two conditions is calculated for all the available data from multiple experiments. This requires to build a 3D matrix contains the original data. Therefore, in addition to the x-axis and y-axis, z-axis is added. The data from z-axis is used to calculate the stability matrix using the standard deviation (Figure 9.4).
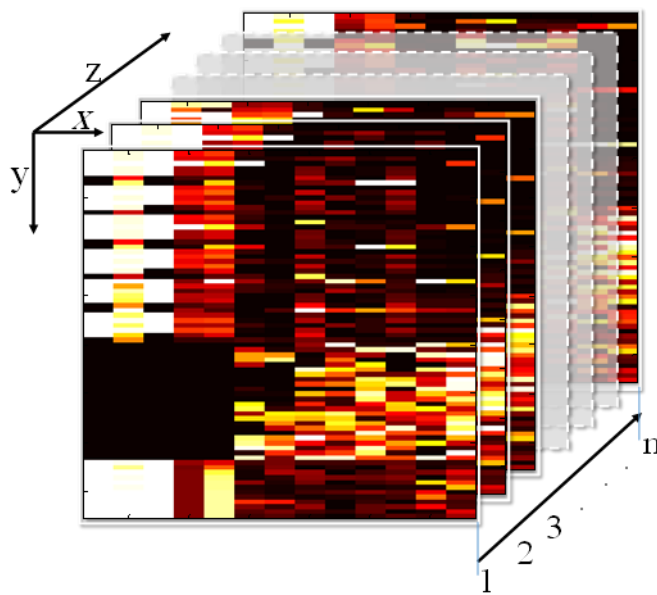
Figure 9.4: 3D matrix

The 3D matrix in Figure 9.4 constructed from the ASMs. The ASM is the index of the sensitivity of the original data. The calculation of the stability carried out using the original data. Equation (9-1) is used first to calculate the delta between each two elements of the no-leak and leak data then the stability matrix is calculated using the standard deviation of the delta along the z-axis for each resulted delta.

$$\Delta M = |m_1 - m_2| \tag{9-1}$$

Where:

ΔM: is the resulted matrix from delta values along z-axis.

m_1: is matrix of the no-leak data.

m_2: is the matrix of the leak data.

$$SM = \sigma(\Delta M_1, \Delta M_2, \Delta M_3, \ldots, \Delta M_n) \qquad \textbf{(9-2)}$$

Where:

SM: the Stability Matrix

σ: the standard deviation

The generated stability matrix SM is shown in Figure 9.5. Unlike the sensitivity matrix ASM in which the highest values mean greater sensitivity, the highest values in the SM mean the lowest stability because it has been built on the standard deviation. The area shown in black in the SM is the area that has a lower values and higher stability.
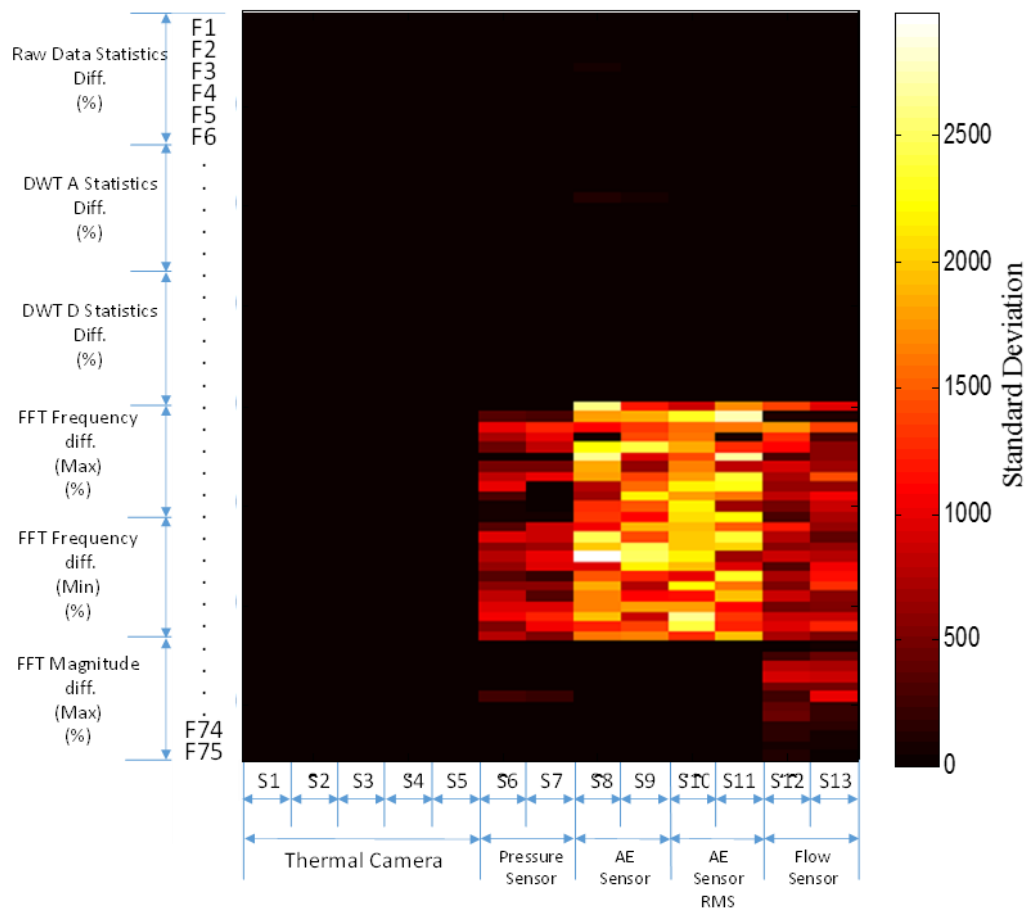
Figure 9.5: The stability matrix SM.

After getting the stability matrix using the standard deviation, a new sensitivity matrix named Resultant Associated Matrix RASM is calculated and generated by simply

subtracting the SM from the ASM. However, it has to be adjusted before using the SM. The SM has a high values due to the large deviation amount in some features. To adjust the SM, it has to be multiplied by a scale factor to create some balance without affecting its influence on producing reasonable RASM.

$$RASM = ASM - SM * k \qquad\qquad (9\text{-}3)$$

RASM: is the new associated matrix named Resultant ASM

k: is a factor.
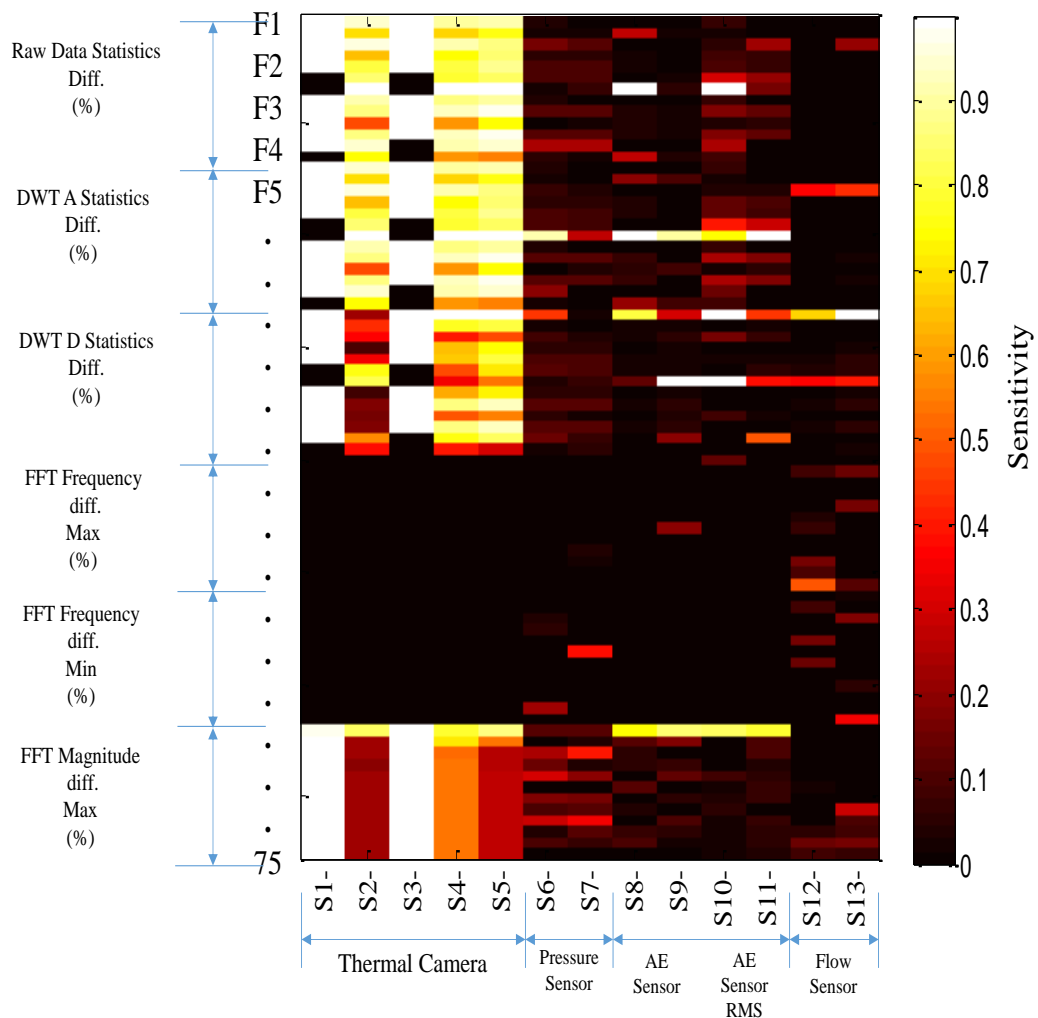
Figure 9.6: The Resultant Associated Matrix RASM.

The SCFs in the RASM are based on the sensitivity and the stability rather than the sensitivity only. The stability matrix SM actually improves the original ASMs and rearrange them in a new form (RASM) based on the sensitivity and the stability together.

The RASM is ranked in ascending order so the most sensitive and stable SCFs values are at the top and the less sensitive are at the bottom. The ranked SCFs divided to groups named 'systems'. Each system contains the selected SCFs based on the best combination of sensors and image/signal processing method.

As the RASM has columns and rows, it shows the average sensitivity of the sensors as well as the features with the image/signal processing. The average sensitivity of the sensors is calculated from the average of the columns in the ASM (Figure 9.7). The average sensitivity of the features is calculated using the average of the rows in the ASM (Figure 9.8).
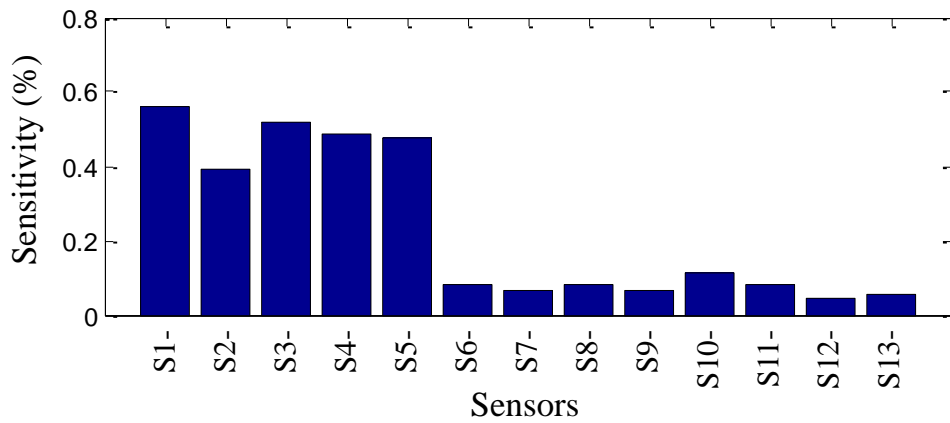
Figure 9.7: Average sensitivity of the sensors.
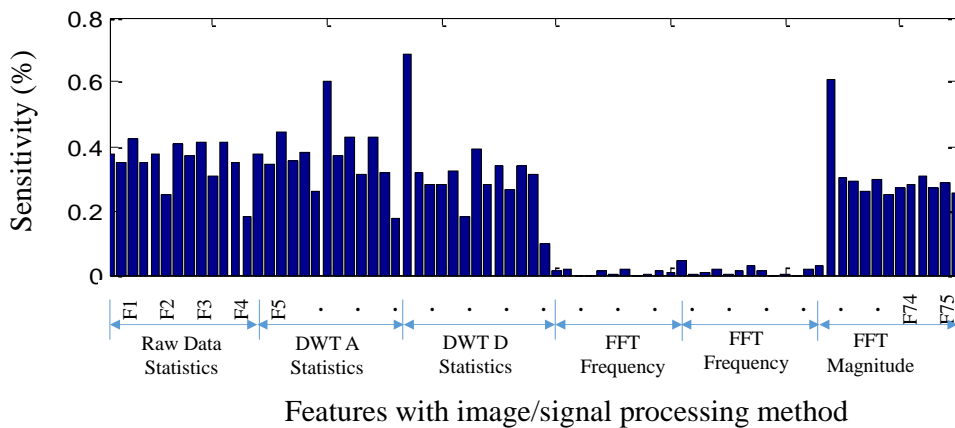
Figure 9.8: Average sensitivity of each feature with image/signal processing method.

9.4. Selection of the sensitive and stable features.

Selection of the sensitive and stable features is a cardinal stage in the ASPS approach. After creating the associated matrix ASM based on the sensitivity and the stability, the sensitive features to create systems containing these features are selected.

The total number of SCFs are 975 features as a result of multiplying the number of features (75) and the number of sensors (13). The total number of features is divided into group of systems. There is no standard to select a certain number of features in each system but the number that gives a reliable identification of the state. The total number (975) of the achieved SCFs divided into 25 systems. Each system contains 39 features. The systems from different experiments have been assessed for their reliability using neural network.

9.5. Neural Network

The neural network provides a good assessment test for the sensitivity of the selected SCFs. Two neural networks utilized to evaluate the systems; the Learning Vector Quantisation LVQ and the newff-BP which creates a feed-forward backpropagation network.

As each system has 39 features, the data of all systems (25) have been prepared in sets from different experiments for each system. The neural network prepared to receive 39 inputs each time. The available data for training and testing are from six experiments. Each experiment provides 2 sets of data (no-leak & leak) for each system. This means there are 12 sets of data for each system. The data of the three first experiments selected for training and validating the neural network. The rest assigned for testing the network. Multiple runs for both neural networks on each system have been carried out. The network parameters such as the number of epochs, iteration and the transfer equations were adjusted several times for learning purposes. The learning accuracy was high for both networks but the testing error results were higher in the newff network than the LVQ. Figure 9.9 shows the error classification for all the 25 systems using the two neural networks. The figure clearly shows how the sensitive system has less average error classification while the less sensitive has more error classification.
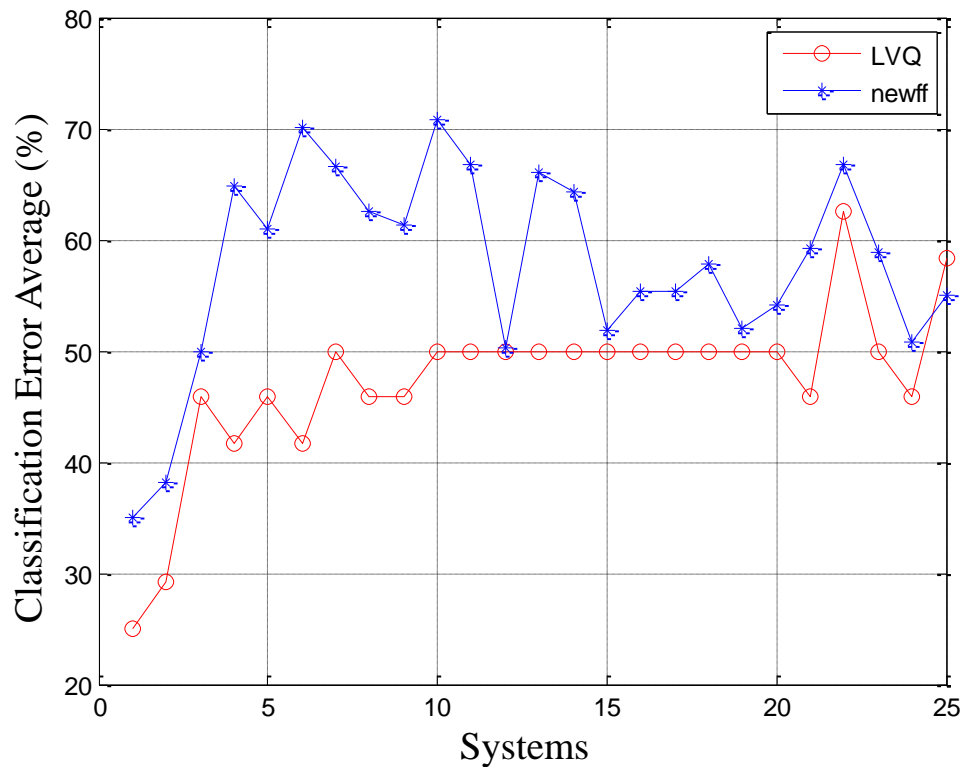
Figure 9.9: Classification error average for both neural networks.

9.6. Summary

The work in this chapter and previous chapters have shown that the ASPS approach which is a very systematic technique are able to select the sensitive sensors and the proper image/signal processing method. In this chapter, the ASPS approach led to creating the ASM and the SM and then the RASM in a systematic way. The two ASMs for both images and signals joined together in this chapter to form a general ASM for the proposed system. Multiple general ASMs have been produced from several experiments. Those ASMs are used to produce a new matrix called Stability Matrix SM. The stability matrix tells how stable each feature in the ASMs. A function with adjusted factor has been created to calculate and to generate RASMs contains the stable features. The RASMs is more robust than the ASMs because it is based on the sensitivity and the stability together. The RASM is able to determine exactly the sensitive sensor and the sensitive image/signal processing technique. Newer groups of systems are created from the RASMs. To test the created systems and to confirm their sensitivity, algorithms based on the neural network

is used. Two types of the neural networks are used to test the systems. Results of the neural network presented in Figure 9.9 which has classified the sensitive system based on the average of the number of errors for each system. The graph shows that the most sensitive the system, the less number of errors.

Chapter 10. Conclusion

The need for International sustainable water supply systems is on the increase with monetary and ecological incentives available for the conservation of water and reducing leaks and waste of water. We need to ensure that our systems of water supply remain sustainable as they use water as a renewable resource. Water resources are under pressure and water costs are on the increase, therefore conserving water makes sense on many levels. With time, all water delivery systems (international) will deteriorate which makes maintaining system efficiency virtually impossible unless there are monitoring systems strategically installed to highlight changes in flow and consumption.

Water leakage is one of the penitent factors when considering one of the most life altering precious resources on earth, with considerable impacts upon economic progression, environmental disasters and eventually life in general. The decrease in the availability of water over-time, especially in an era of increased global warming, has led international researchers all over the world looking to address this major problem. Identification for searching a cost-effective, automated intelligent monitoring system to combat this problem.

Strategically installing water leaking detection systems will monitor water consumption, highlight deterioration in efficiency and stop water flow in the event of a leakage. The efficient use of water and immediate response to burst and leaking water is one of the effective and efficient methods of conserving water and protecting the environment. This study has demonstrated that stopping or even reducing leaks can help with schools, colleges, universities, business and domestic supply, see a delivered savings approach of 30% of annual usage, (OFWAT, 2012) meeting most international benchmark for reducing water waste and with new strict budgets will also save money on water and any repairs necessary due to the damaged caused by a burst or leaking water.

This study has investigated water leakage detection in buried pipelines using an automated fusion system. The study has also investigated, discussed and concluded the implementation of the novel ASPS approach [32] as an advanced and systematic tool for designing automated intelligent monitoring systems. The ASPS approach is adapted to work in water leakage detection within buried pipeline system for the first time in this

study. The work also investigated the use of the thermal technology in water leakage detection within a live environment and lab. The study has focused on the use of low-resolution thermal camera in comparison to a high-resolution thermal camera when conducting water leakage detection in a dry environment area. The outcome of the study has demonstrated that the thermal technology can be used in water leakage detection in dryer environments, with the low-resolution thermal camera is just as competent as compared to the high-resolution thermal camera when detecting water leakage. The study has unequivocally demonstrated that the best period to detect water leakage is at night, however, leaks can be detected in the day time as well, when the leaks are running for a sustained period of time with its moisture reaching the sub-surface or the surface of the inspected area.

In this study, a combination of multiple sensors such as pressure, flow, and Acoustic emission have been intergraded with thermal cameras for the design of a precision monitoring system for leaks in buried water pipeline systems. The designed system has been created based on the ASPS approach, in which a wide range of sensitive sensor characteristics have been selected using multiple processing methods for both signals and images. As a result, an automated and processing novel approach has been developed to select the required sensitive characteristics for a water leakage detection in buried pipeline system.

The thesis is divided into 10 chapters, starting with an introduction to the leakage detection systems then literature review, methodology, experimental work setup, experimental work, field work, thermal image processing, signal processing, ASPS approach, and finally the conclusion chapter.

Firstly, the thesis presented a general view of the associated problems of water leakages and highlighted their impacts upon the environment, people and the economy. Water leakage has been defined with the percentage of lost water due to associated leaks around the world also presented. The percentage of water lost around the world is found to be respectively high and is estimated around 30%. In addition, the problem of current water leakage detection systems with their limitations have been also presented in the chapter.

The aim of the study is to overcome the existing problems in water leakage detection systems by developing an efficient, low-cost leakage detection system, based on

automated fusion system with an artificial intelligence. The objectives was to investigate and select the right sensors and image/signal processing techniques that can detect the leakage correctly. Together with the development of a software and the creation of a water test rig to investigate the thermal technology and thermal cameras for use in water leakage detection in warmer climates. Furthermore, to also investigate the artificial intelligence techniques presented in the first chapter.

A wide range of literature has been carried out for some of the recent methods used in the monitoring of water distribution systems and leakage detection. The thesis has presented some of the common used techniques in water leakage detection, such as transient pressure, acoustic emission and their principles of use. The thesis also introduced the thermal imaging as a technique for water leakage detection and explained the principal of the thermal imaging in water leakage detection. A number of factors that might affect the signal and image have been highlighted. The thesis presented the ASPS approach which has been developed by Prof. Amin Al-Habaibeh and addressed and emphasized the state of the art, in designing a reliable and cost effective fusion system. It has been demonstrated that there is a lack in designing fusion systems for water leakage detection and monitoring of the water distribution systems.

The methodology used in this study has been explained in details. The thesis has presented the framework for implementing the proposed system for water leakage detection and justified the use of the test rig comparing to an actual water project. The implementation of ASPS approach, as well as data processing techniques for the images and the signals with the calculated method of the sensitivity have been presented. The method of advanced processing techniques of images and signals are clearly presented and explained in the thesis. The neural network and the structure of the neural network and its use is also explained with illustrations.

Within the experimental rig setup section, the thesis presented in details, the steps of the test rig constructed at the university laboratory. It has presented the in-house software which describes how each sensor has been wired, connected and linked to the software. The test rig designed to match a 'live' environment, therefore, an infrared light is used to heat up the test area to simulate the sun. Also, a cooling machine is used to cool the source

water in order to create a difference in temperature between the water and the surface of the tested area.

The utilization of the thermal technology in water leakage detection has been discussed extensively and applied in this work. The results have showed that the thermal technology is successful in detecting water leakages using a low-resolution thermal camera as well as the high resolution camera. The low-resolution thermal camera was found to be able to detect the leakage, especially at night which is the recommended time to detect the leakage, as much as the thermal camera. The thermal camera can detect the leakage in the day time if the leak is running for a sustained period. The leak appears in the thermal camera images before it appears on the surface to be seen by bare eye. In addition, the experimental work showed that the thermal camera can detect the pipeline pathway. The outcome of the experimental work has demonstrated that before sunrise the thermal camera can detect the leak earlier than when the leak starts during the day time. The heat of the sun will delay the leakage detection but, once the leak reaches the subsurface, the thermal camera will obviously detect. The best time for water leakage detection is found to be at night but the leak can be detected during the day time as explained earlier. The use of cold water accelerated the detection process but its effectivity decreased once the surface is hot as the heat flowing from the surface prevents the cooling process from expediting the detection process. Selecting the best time and the correct image processing method leads to better detection. Other objects in the thermal image cooler than the leak point affecting the detection, therefore, the selecting of the exact region of interest is important in processing the image. In summary chapter 5, thermal technology has been found able to detect leakage and the low-resolution thermal camera can perform similar to a high-resolution thermal camera when the recommended time with the appropriate processing method is selected.

A field work has been carried in Benghazi city in Libya on October 2013. The details of the thermal camera, the software, the test area and the pipeline and all other tools used in the study as well as the weather at the time of the experiment has been presented. The experiment has been conducted over two complete days and the leak started mid-day of the second day. The acquired images have been subject to extensive analysis. The outcome of the fieldwork was as close as the laboratory experimental work results presented in chapter 5, where the heating process of the surface has delayed the detection

process. The leak in the fieldwork did not appear until the ground cooled down. The leak did appear for a limited time before the sunset and then disappeared until the night time when it became evident and consistent for a while. The next day the leak continued to become more evident even after the sunrise. The fieldwork has proved that the thermal technology is successful in detecting the leakage in warmer climates as well as the low-resolution thermal camera is able to detect leakage when the correct timing and correct image processing methods were selected.

Within the thesis the image processing and analysis of the images collected from the experimental work, have been clarified in details. The systematic steps of the best features extraction from the thermal image to identify the status of the no-leak and leak is presented. The selected five features are processed to inform the state of the image. The analysis showed that the features are successful in determining the state of the image. Following the features extraction, the systematic process ASPS approach is used with those selected five features to extract the best features with the best processing method in order to build up the automated system using a thermal image. Thirteen statistical analysis functions in addition to advanced image processing techniques have been applied. The result of this processing is an associated matrix ASM contains the utmost useful features which indicates the sensitive sensors with the best processing methods. The results are used to build the general ASM of the fusion system presented in Chapter 9. An artificial neural network is used to classify the thermal images. Based on the selected features, the network successfully learnt to identify each image correctly.

A systematic process of signal processing method has been carried out to extract features for the 1D sensors. There are three pairs of sensors; AE, Pressure, and Flow sensors. The signal acquired from the sensors subjected to processing, use the thirteen statistical functions and the advanced signal processing techniques. The result of this processing is another association matrix ASM which contains the utmost useful features for the 1D sensors. The ASM is also used to build the general ASM of the fusion system presented in Chapter 9.

The final step in building up the fusion system using the systematic approach the ASPS, the results presented in Chapters 7 and 8 have been used in creating a unified ASM. Additionally, another new matrix called Stability Matrix SM is created from multiple

ASMs from different experiments. The SM used to select the required stable feature among the sensitive features selected previously. The SM enhancing the reliability of the ASM by selecting the best stable features. The process is carried out by subtracting the SM from the old ASM for each experiment, a newer ASM named Resultant Associated Matrix RASM is produced. The features in the RASM are more reliable, more stable in stating the state the system (no-leak or leak). The RASM is used to produce new systems (groups of the best features) to be used later to identify the pipeline system condition. The systems are created by ranking all the features in ascending order so the first system contains the best-selected features and the last system contains the less sensitive features. The number of features in one system is decided based on the result from the neural network. The number is either increased or decreased until a good result is reached.

As a final step, a neural network algorithm is created to test the systems sensitivity. Two advanced neural networks (LVQ-BP and newff-BP) are selected to create the algorithm. The results show that SCFs with high sensitivity show relatively lower error when using ANN

Finally, this study has investigated the thermal technology for water leakage detection using both low and high-resolution thermal cameras. The study has showed how the low-resolution thermal cameras can be used to detect water leakage similar to high-resolution. The selection of the accurate image processing method enables the low-resolution thermal camera to detect the leak. Even though the best time for water leakage detection by using the thermal cameras is recommended at night time in warmer weather, the leakage can be detected in the day time as well, when it runs for a sustained period.

A systematic and simplified way of collecting data from the 1D and 2D sensors and processing them for defining the state of pipeline system (no-leak or leak) has been achieved in this study. The images and signals are processed skilfully using multiple advanced image/signal processing techniques and analysed competently using a statistical method in order to extract the best combination of the sensors and image/signal processing method.

The proposed ASPS approach has been used proficiently to generate ASMs, SM, and RASMs. The RASMs are an index for the best combination of the sensors and processing methods. The SCFs contained in the RASMs have been arranged in descending order to

select the best features, consequently the best combination of sensor and image/signal processing techniques. The higher sensitivity sensors with the best processing method with stable sensitive 'features' are at the top of the selected features. The less sensitive sensors are ignored and rejected in order to reduce the cost of the automated system merely. Successfully, the ASPS approach led to the creation of leak detection systems based on the feature sensitivity.

This thesis has proved that the systematic ASPS approach can also be used to design condition monitoring system of water leakage detection system. The approach has helped in designing a novel condition monitoring system based on the change in the condition rather than on a predefined values and thresholds. This means the system can be applied in varies location without the need of setting and resetting the threshold values. It also helped in designing the novel system using the available sensors by utilizing its most useful features.

10.1.   Contribution to knowledge and contribution to project

The contribution to knowledge and contribution to project have included significant technical and theoretical aspects as follows:

10.1.1.   Conceptual Contribution

1. The use of infrared thermography and the associated algorithms to detect water leakage in buried pipes.

2. Determining the best time for water leak detection in warmer and dry environmental conditions.

3. A comparison between the high and low-resolution infrared cameras.

4. The use of a combination of infrared technology and sensors in a sensory fusion system.

5. Creating a novel monitoring system based on the differences in condition rather than predefined values and thresholds.

6. Designing a monitoring system which uses the available sensors by utilizing the useful features in every single sensor.

10.1.2. Project Contribution (Technical)

1. Developing image processing methods to differentiate between the images with a leak and the images without a leak.

2. Estimating the amount of leakage from the infrared images.

3. The application of the ASPS approach in water leakage detection.

4. Producing reliable, a low-cost automated system for water leakage detection.

5. Developing artificial intelligence algorithm for water leakage detection.

6. Developing the feature selecting method by creating Stability Matrix and producing a Resultant Associated Matrix.

7. Developing a water system test rig.

8. Use of infrared light with test rig to resemble the sun in a real environment.

9. Use of multiple sensors such as AE, Pressure and Flow sensors in the test rig.

10.2. Future work

Use of additional sensors such as vibration sensor, torque sensor on the water pump shaft, and power meters to test the effect of the leak on pump and its power consumption.

Carrying out practical work for water leakage detection using the flying drones as proposed in the methodology chapter.

Carrying out additional fieldwork in Libya for the GMRP once situation in the country permits. See appendix G for a brief about the GMRP.

References:

[1] L. Michel and T. Lindhqvist, "Opportunities for Change in the Water Supply System of Chișinău , Moldova A case study on actor behavior for sustainable water supply system management in a transition economy," no. September, 2011.

[2] A. F. Colombo, P. Lee, and B. W. Karney, "A selective literature review of transient-based leak detection methods," *J. Hydro-environment Res.*, vol. 2, no. 4, pp. 212–227, Apr. 2009.

[3] A. Lay-Ekuakille, G. Vendramin, and A. Trotta, "Spectral analysis of leak detection in a zigzag pipeline: A filter diagonalization method-based algorithm application," *Measurement*, vol. 42, no. 3, pp. 358–367, Apr. 2009.

[4] M. Ahadi and M. S. Bakhtiar, "Leak detection in water-filled plastic pipes through the application of tuned wavelet transforms to Acoustic Emission signals," *Appl. Acoust.*, vol. 71, no. 7, pp. 634–639, Jul. 2010.

[5] S. Renzetti and D. Dupont, "Buried Treasure: The Economics of Leak Detection and Water Loss Prevention in Ontario," Ontario, ESRC-2013-001, 2013.

[6] R. Ben-Mansour, M. a. Habib, a. Khalifa, K. Youcef-Toumi, and D. Chatzigeorgiou, "Computational fluid dynamic simulation of small leaks in water pipelines for direct leak pressure transduction," *Comput. Fluids*, vol. 57, pp. 110–123, 2012.

[7] D. Sala and P. Kolakowski, "Detection of leaks in a small-scale water distribution network based on pressure data - Experimental verification," *Procedia Eng.*, vol. 70, pp. 1460–1469, 2014.

[8] G. R. Anjana, K. R. S. Kumar, M. S. M. Kumar, and B. Amrutur, "A Particle Filter Based Leak Detection Technique for Water Distribution Systems," *Procedia Eng.*, vol. 119, pp. 28–34, 2015.

[9] S. Fox, W. Shepherd, R. Collins, and J. Boxall, "Experimental proof of contaminant ingress into a leaking pipe during a transient event," *Procedia Eng.*, vol. 70, pp. 668–677, 2014.

[10] A. Santos, "Faculty Of Engineering Of The University Of Porto A Sensor Network For An Early And Efficient Leak Detection In Long Pipelines," no. January, 2011.

[11] Z. Liu and Y. Kleiner, "State of the art review of inspection technologies for condition assessment of water pipes," *Measurement*, vol. 46, no. 1, pp. 1–15, Jan. 2013.

[12] S. Sreepathi, D. Brill, R. Ranjithan, and G. (Kumar) Mahinthakumar, "Parallel Multi-Swarm Optimization Framework for Search Problems in Water Distribution Systems," *World Environ. Water Resour. Congr. 2012*, pp. 3217–3224, 2012.

[13] J. Sousa, L. Ribeiro, J. Muranho, and A. S. Marques, "Locating Leaks in Water Distribution Networks with Simulated Annealing and Graph Theory," *Procedia Eng.*, vol. 119, pp. 63–71, 2015.

[14] S. K. Mandal, F. T. S. Chan, and M. K. Tiwari, "Leak detection of pipeline: An integrated approach of rough set theory and artificial bee colony trained SVM,"

References:

Expert Syst. Appl., vol. 39, no. 3, pp. 3071–3080, Feb. 2012.

[15]   "How much does your water company leak?," *BBC news*, 2012. [Online]. Available: http://www.bbc.co.uk/news/uk-17622837.

[16]   D. Laucelli and S. Meniconi, "Water distribution network analysis accounting for different background leakage models," *Procedia Eng.*, vol. 119, pp. 680–689, 2015.

[17]   W. Tylman, J. Kolczyński, and G. J. Anders, "Fully automatic AI-based leak detection system," *Energy*, vol. 35, no. 9, pp. 3838–3848, Sep. 2010.

[18]   EPD, "Water Leak Detection And Repair Program," *Georgia Environmental Protection Division Watershed Protection Branch*, 2007. [Online]. Available: http://www1.gadnr.org/cws/Documents/Leak_Detection_and_Repair.pdf. [Accessed: 24-Apr-2014].

[19]   Z. Poulakis, D. Valougeorgis, and C. Papadimitriou, "Leakage detection in water pipe networks using a Bayesian probabilistic framework," *Probabilistic Eng. Mech.*, vol. 18, no. 4, pp. 315–327, 2003.

[20]   T. El-Shiekh, "Leak Detection Methods In Transmission Pipelines And Error Sources," *icfd11.org*, pp. 1–12, 2010.

[21]   J. Xu, Z. Nie, F. Shan, J. Li, and Y. Luo, "Leak Detection Methods Overview and Summary," *asce.org*, no. 146, 2012.

[22]   O. Hunaidi, W. Chu, A. Wang, and W. Guan, "Detecting leaks in plastic pipes," *J. Am. Water Work. Assoc. Century Treat. Distrib.*, vol. 92, no. 2, pp. 82–94, 2000.

[23]   M. Ferrante and B. Brunone, "Pipe system diagnosis and leak detection by unsteady-state tests. 1. Harmonic analysis," *Adv. Water Resour.*, vol. 26, no. 1, pp. 107–116, Jan. 2003.

[24]   P. Ostapkowicz, "Leak detection in liquid transmission pipelines using simplified pressure analysis techniques employing a minimum of standard and non-standard measuring devices," *Eng. Struct.*, vol. 113, pp. 194–205, Apr. 2016.

[25]   W. Li *et al.*, "Development of systems for detection, early warning, and control of pipeline leakage in drinking water distribution: A case study," *J. Environ. Sci.*, vol. 23, no. 11, pp. 1816–1822, Nov. 2011.

[26]   H. L. Zhao, J. K. Wang, and X. Jiang, "A Real-time Monitoring System for the Pipeline Network of Coalmine," *J. Phys. Conf. Ser.*, vol. 364, p. 012107, May 2012.

[27]   S. Dudić, I. Ignjatović, D. Šešlija, V. Blagojević, and M. Stojiljković, "Leakage quantification of compressed air using ultrasound and infrared thermography," *Measurement*, vol. 45, no. 7, pp. 1689–1694, Aug. 2012.

[28]   Z. Sun, P. Wang, M. C. Vuran, M. a. Al-Rodhaan, A. M. Al-Dhelaan, and I. F. Akyildiz, "MISE-PIPE: Magnetic induction-based wireless sensor networks for underground pipeline monitoring," *Ad Hoc Networks*, vol. 9, no. 3, pp. 218–227, May 2011.

[29]   J. M. Muggleton, M. J. Brennan, and R. J. Pinnington, "Wavenumber Prediction of Waves in Buried Pipes for Water Leak Detection," *J. Sound Vib.*, vol. 249, no.

References:

5, pp. 939–954, Jan. 2002.

[30] S. Kim, "Extensive development of leak detection algorithm by impulse response method," *J. Hydraul. Eng.*, no. March, 2005.

[31] N. Ge, G. Peng, and M. Jiang, "Fuzzy clustering of infrared images applied in air leak localization," *Proc. SPIE*, vol. 7383, p. 73830U–73830U–8, 2009.

[32] a. Al-Habaibeh and N. Gindy, "A new approach for systematic design of condition monitoring systems for milling processes," *J. Mater. Process. Technol.*, vol. 107, no. 1–3, pp. 243–251, Nov. 2000.

[33] A. Al-Habaibeh and N. Gindy, "Self-learning algorithm for automated design of condition monitoring systems for milling operations," *Int. J. Adv. Manuf. Technol.*, vol. 18, no. 6, pp. 448–459, 2001.

[34] A. Al-Habaibeh, F. Zorriassatine, and N. Gindy, "Comprehensive experimental evaluation of a systematic approach for cost effective and rapid design of condition monitoring systems using Taguchi's method," *J. Mater. Process. Technol.*, vol. 124, no. 3, pp. 372–383, Jun. 2002.

[35] J. Abbas, A. Al-Habaibeh, and D. Su, "The effect of tool fixturing quality on the design of condition monitoring systems for detecting tool conditions," *Jordan J. Mech. Ind. Eng.*, vol. 5, no. 1, pp. 17–22, 2011.

[36] H. Alkhadafe, a Al-Habaibeh, S. Daihzong, and a Lotfi, "Optimising Sensor Location for an Enhanced Gearbox Condition Monitoring System," *J. Phys. Conf. Ser.*, vol. 364, p. 012077, May 2012.

[37] M. Fahmy, O. Moselhi, P. Eng, A. M. Asce, and F. Asce, "Automated Detection and Location of Leaks in Water Mains Using Infrared Photography," *J. Perform. Constr.*, no. June, pp. 242–248, 2010.

[38] B. Y. C. Jones and K. Laven, "Leak Detection," vol. 133, no. 11, pp. 0–3, 2009.

[39] Y. Bai and Q. Bai, "Leak Detection Systems," *Subsea Pipeline Integr. Risk Manag.*, pp. 125–143, 2014.

[40] M. (Texas a & M. U. Scott, S; Barrufet, "Worldwide Assessment of Industry Leak Detection Capabilities for Single & Multiphase Pipelines Project Report Prepared for the Minerals Management Service Under the MMS / OTRC Cooperative Research Agreement Task Order 18133," p. 125, 2003.

[41] S. Bagavathiappan, B. B. Lahiri, T. Saravanan, J. Philip, and T. Jayakumar, "Infrared thermography for condition monitoring – A review," *Infrared Phys. Technol.*, vol. 60, pp. 35–55, Sep. 2013.

[42] A. Of, "The Testing of Harmful Gases Using Passive Infrared Thermography Ispitivanje Štetnih Gasova Primenom Pasivne," *Undergr. Min. Eng.*, vol. 22, pp. 99–109, 2013.

[43] N. Jalali, B. Saghafian, F. Imanov, and M. Museyyibov, "Recognition of shallow karst water resources and cave potentials using thermal infrared image and terrain characteristics in semi-arid regions of Iran," *Int. J. Appl. Earth Obs. Geoinf.*, vol. 11, no. 6, pp. 439–447, Dec. 2009.

[44] Q. Chen, C. Zhang, J. Zhao, and Q. Ouyang, "Recent advances in emerging

References:

imaging techniques for non-destructive detection of food quality and safety," *TrAC Trends Anal. Chem.*, vol. 52, pp. 261–274, Dec. 2013.

[45] Ashish and Aijay, "Review on thermal image processing techniques for machine condition monitoring," *Int. J. Wirel. Commun. Netw. Technol.*, vol. 3, no. 3, pp. 49–53, 2014.

[46] A. Al-Habaibeh and R. Parkin, "An autonomous low-Cost infrared system for the on-line monitoring of manufacturing processes using novelty detection," *Int. J. Adv. Manuf. Technol.*, vol. 22, no. 3–4, pp. 249–258, Sep. 2003.

[47] T. Inagaki and Y. Okamoto, "Diagnosis of the leakage point on a structure surface using infrared thermography in near ambient conditions," *Science (80-.).*, vol. 30, no. 3, pp. 135–142, 1997.

[48] S. Soldan, G. Bonow, and A. Kroll, "RoboGas Inspector – A Mobile Robotic System for Remote Leak Sensing and Localization in Large Industrial Environments : Overview and First Results," pp. 33–38, 2012.

[49] T. Inagaki and T. Ishii, "On the proposal of quantitative temperature measurement by using three-color technique combined with several infrared sensors having di € erent detection wavelength bands," vol. 41, 2000.

[50] a. Kroll, W. Baetz, and D. Peretzki, "On autonomous detection of pressured air and gas leaks using passive IR-thermography for mobile robot application," *2009 IEEE Int. Conf. Robot. Autom.*, pp. 921–926, May 2009.

[51] M. J. Suriani, A. Ali, a Khalina, S. M. Sapuan, and S. Abdullah, "Detection of defects of Kenaf/Epoxy by Thermography Analyses," *IOP Conf. Ser. Mater. Sci. Eng.*, vol. 36, p. 012013, Sep. 2012.

[52] A. Safitri, X. Gao, and M. S. Mannan, "Dispersion modeling approach for quantification of methane emission rates from natural gas fugitive leaks detected by infrared imaging technique," *J. Loss Prev. Process Ind.*, vol. 24, no. 2, pp. 138–145, Mar. 2011.

[53] J. Vlachopoulos and D. Strutt, "Basic Heat Transfer and Some Applications in Polymer," vol. 2, pp. 21–33, 2002.

[54] J. E. Patterson, D. Ph, R. J. Miers, and N. Carolina, "The Thermal Conductivity of Common Tubing Materials Applied in a Solar Water Heater Collector," 2009.

[55] G. Holst, *Common sense approach to thermal imaging*. 2000.

[56] S. Taib and M. Jadin, "Thermal Imaging for Enhancing Inspection Reliability: Detection and Characterization," *InTech, Rijeka, Croat.*, 2012.

[57] J. Snell and M. Stuart, *Introduction to Thermography Principles*. 2009.

[58] Q. Xu, R. Liu, Q. Chen, and R. Li, "Review on water leakage control in distribution networks and the associated environmental benefits.," *J. Environ. Sci. (China)*, vol. 26, no. 5, pp. 955–61, May 2014.

[59] B. Brunone, "Transient test-based technique for leak detection in outfall pipes," *J. water Resour. Plan. Manag.*, no. October, pp. 302–306, 1999.

[60] P. J. Lee, J. P. Vítkovský, M. F. Lambert, A. R. Simpson, and J. a. Liggett, "Leak location using the pattern of the frequency response diagram in pipelines: a

References:

numerical study," *J. Sound Vib.*, vol. 284, no. 3–5, pp. 1051–1073, Jun. 2005.

[61] D. Covas and H. Ramos, "Hydraulic Transients used for Leakage Detection in Water Distribution Systems," *Water*, pp. 227–241, 2001.

[62] K. E. Abhulimen and A. a. Susu, "Liquid pipeline leak detection system: model development and numerical simulation," *Chem. Eng. J.*, vol. 97, no. 1, pp. 47–67, Jan. 2004.

[63] X. Wang, M. Lambert, and J. Liggett, "Leak detection in pipelines using the damping of fluid transients," *J. Hydraul. Eng.*, vol. 128, no. 7, pp. 697–711, 2002.

[64] J. Vítkovský, "Leak detection and calibration using transients and genetic algorithms," *J. Water ...*, no. August, pp. 262–265, 2000.

[65] H.-F. Duan, P. J. Lee, M. S. Ghidaoui, and Y.-K. Tung, "Leak detection in complex series pipelines by using the system frequency response method," *J. Hydraul. Res.*, vol. 49, no. 2, pp. 213–221, 2011.

[66] A. Agapiou *et al.*, "Investigation of Ground Remote Sensing Techniques for Supporting an Early Warning Water-Leakage System," no. 1999, 1991.

[67] D. Ozevin and H. Yalcinkaya, "Reliable monitoring of leak in gas pipelines using acoustic emission method," *CHSM-4 Civ. Struct. Heal. Monit. ...*, 2012.

[68] A. Anastasopoulos, D. Kourousis, and K. Bollas, "Acoustic Emission Leak Detection Of Liquid Filled Buried Pipeline," *J. Acoust. Emiss.*, vol. 27, pp. 27–39, 2009.

[69] M. Pal, N. Dixon, and J. Flint, "Detecting & Locating Leaks in Water Distribution Polyethylene Pipes," *Engineering*, vol. II, 2010.

[70] C. U. Grosse and E. Ohtsu, Masayasu, "Acoustic emission testing," 2008. [Online]. Available: https://www.nde-ed.org/EducationResources/CommunityCollege/Other Methods/AE/AE_Intro.php.

[71] "Capgo - Acoustic Emissions." [Online]. Available: http://www.capgo.com/Resources/ConditionMonitoring/Acoustic.html.

[72] O. Hunaidi, W. W. Chu, A. Wang, and W. Guan, "LEAK DETECTION METHODS FOR PLASTIC WATER DISTRIBUTION PIPES," *Spring*, no. February, pp. 18–19, 1999.

[73] M. Bimpas, A. Amditis, and N. Uzunoglu, "Detection of water leaks in supply pipes using continuous wave sensor operating at 2.45GHz," *J. Appl. Geophys.*, vol. 70, no. 3, pp. 226–236, 2010.

[74] "SmartBall ® Inspection Report," 2011. [Online]. Available: http://your.kingcounty.gov/dnrp/library/wastewater/wtd/construction/NorthBeach FM/1108_NorthBeachForceMainInspectionReport.pdf.

[75] D.-L. Xu *et al.*, "Inference and learning methodology of belief-rule-based expert system for pipeline leak detection," *Expert Syst. Appl.*, vol. 32, no. 1, pp. 103–113, Jan. 2007.

[76] C. Guo, Y. Wen, P. Li, and J. Wen, "Adaptive noise cancellation based on EMD in water-supply pipeline leak detection," *Measurement*, vol. 79, pp. 188–197, Feb.

References:

2016.

[77] W. Wassef, M. Bassim, and M. Houssny-Emam, "Acoustic emission spectra due to leaks from circular holes and rectangular slits," *J. Acoust.*, pp. 916–923, 1985.

[78] O. Hunaidi, "Acoustical characteristics of leak signals in plastic water distribution pipes," *Appl. Acoust.*, vol. 58, pp. 235–254, 1999.

[79] R. Miller, A. Pollock, and D. Watts, "A reference standard for the development of acoustic emission pipeline leak detection techniques," *NDT E ...*, vol. 32, pp. 1–8, 1999.

[80] O. Hunaidi, "CONSTRUCTION Acoustic Leak Detection Survey Strategies for," no. 79, pp. 1–5, 2012.

[81] J. M. Muggleton and M. J. Brennan, "Leak noise propagation and attenuation in submerged plastic water pipes," *J. Sound Vib.*, vol. 278, no. 3, pp. 527–537, Dec. 2004.

[82] H. V. Fuchs and R. Riehle, "Ten years of experience with leak detection by acoustic signal analysis," *Appl. Acoust.*, vol. 33, no. 1, pp. 1–19, Jan. 1991.

[83] A. Baghdadi and H. Mansy, "A mathematical model for leak location in pipelines," *Appl. Math. Model.*, vol. 12, no. March 1987, pp. 25–30, 1988.

[84] P. G. Angaitkar, K. Saxena, N. Gupta, and A. Sinhal, "Enhancement of infrared image for roof leakage detection," *2013 IEEE Int. Conf. Emerg. Trends Comput. Commun. Nanotechnol.*, no. Iceccn, pp. 580–585, Mar. 2013.

[85] A. Atef, T. Zayed, A. Hawari, M. Khader, and O. Moselhi, "Multi-tier method using infrared photography and GPR to detect and locate water leaks," *Autom. Constr.*, vol. 61, pp. 162–170, Jan. 2016.

[86] A. Al-Habaibeh and R. M. Parkin, "A Generic Approach Towards Intelligent Condition Monitoring Systems of Machining Operations," pp. 1–8, 2004.

[87] W. H. Yang and Y. S. Tarng, "Design optimization of cutting parameters for turning operations based on the Taguchi method," *J. Mater. Process. Technol.*, vol. 84, no. 1–3, pp. 122–129, Dec. 1998.

[88] J. . Lin and C. . Lin, "The use of the orthogonal array with grey relational analysis to optimize the electrical discharge machining process with multiple performance characteristics," *Int. J. Mach. Tools Manuf.*, vol. 42, no. 2, pp. 237–244, Jan. 2002.

[89] P.-S. S. Murvay and I. Silea, "A survey on gas leak detection and localization techniques," *J. Loss Prev. Process Ind.*, vol. 25, no. 6, pp. 966–973, May 2012.

[90] S. Tian, J. Du, S. Shao, H. Xu, and C. Tian, "A study on a real-time leak detection method for pressurized liquid refrigerant pipeline based on pressure and flow rate," *Appl. Therm. Eng.*, vol. 95, pp. 462–470, Feb. 2016.

[91] M. H. Ranginkaman, A. Haghighi, and H. M. V. Samani, "Inverse Frequency Response Analysis For Pipelines Leak Detection Using The Particle Swarm Optimization," *Int. J. Optim. Civ. Eng.*, vol. 6, no. May 2015, pp. 1–12, 2016.

[92] A. Martini, M. Troncossi, and A. Rivola, "Automatic Leak Detection in Buried Plastic Pipes of Water Supply Networks by Means of Vibration Measurements," *Shock Vib.*, vol. 2015, pp. 11–15, 2015.

References:

[93] B. Brunone, S. Meniconi, P. J. Lee, A. Kashima, and M. Ferrante, "Impulse response function and wavelet analysis of transient pressure signals for leak detection in pipes," in *Conference on Computing and Control for the Water Industry*, 2011, pp. 2–7.

[94] J. Wan, Y. Yu, Y. Wu, R. Feng, and N. Yu, "Hierarchical leak detection and localization method in natural gas pipeline monitoring sensor networks.," *Sensors (Basel).*, vol. 12, no. 1, pp. 189–214, Jan. 2012.

[95] G. Moser, S. German Paal, and I. F. C. Smith, "Performance Comparison Of Reduced Models For Leak Detection In Water Distribution Networks," *Adv. Eng. Informatics*, vol. 29, no. 3, pp. 714–726, Aug. 2015.

[96] F. Nejjari, R. Sarrate, and J. Blesa, "Optimal Pressure Sensor Placement in Water Distribution Networks Minimizing Leak Location Uncertainty," *Procedia Eng.*, vol. 119, pp. 953–962, 2015.

[97] J. Meseguer, J. M. Mirats-Tur, G. Cembrano, and V. Puig, "Model-based Monitoring Techniques for Leakage Localization in Distribution Water Networks," *Procedia Eng.*, vol. 119, pp. 1399–1408, 2015.

[98] S. Adachi, S. Takahashi, H. Kurisu, and H. Tadokoro, "Estimating Area Leakage in Water Networks Based on Hydraulic Model and Asset Information," *Procedia Eng.*, vol. 89, pp. 278–285, 2014.

[99] E. Creaco and G. Pezzinga, "Embedding Linear Programming In Multi Objective Genetic Algorithms For Reducing The Size Of The Search Space With Application To Leakage Minimization In Water Distribution Networks," *Environ. Model. Softw.*, vol. 69, pp. 308–318, Nov. 2014.

[100] S. Demirci, E. Yigit, I. H. Eskidemir, and C. Ozdemir, "Ground Penetrating Radar Imaging Of Water Leaks From Buried Pipes Based On Back-Projection Method," *NDT E Int.*, vol. 47, pp. 35–42, Apr. 2012.

[101] J. Gao *et al.*, "Study on Leakage Rate in Water Distribution Network Using Fast Independent Component Analysis," *Procedia Eng.*, vol. 89, pp. 934–941, 2014.

[102] W. W. L. Lai, R. K. W. Chang, J. F. C. Sham, and K. Pang, "Perturbation Mapping Of Water Leak In Buried Water Pipes Via Laboratory Validation Experiments With High-Frequency Ground Penetrating Radar (GPR)," *Tunn. Undergr. Sp. Technol.*, vol. 52, pp. 157–167, Feb. 2016.

[103] D. Ayala-Cabrera, E. Campbell, E. P. Carreño-Alvarado, J. Izquierdo, and R. Pérez-García, "Water Leakage Evolution Based on GPR Interpretations," *Procedia Eng.*, vol. 89, pp. 304–310, 2014.

[104] J. Gao, S. Qi, W. Wu, a. Han, C. Chen, and T. Ruan, "Leakage Control of Multi-source Water Distribution System by Optimal Pump Schedule," *Procedia Eng.*, vol. 70, pp. 698–706, 2014.

[105] A. Agapiou, D. D. Alexakis, K. Themistocleous, and D. G. Hadjimitsis, "Water Leakage Detection Using Remote Sensing, Field Spectroscopy And GIS In Semiarid Areas Of Cyprus," *Urban Water J.*, vol. 9006, no. January 2015, pp. 1–11, 2014.

[106] A. M. Ghazali and M. A. Abounahia, "An Optimum Approach For The Utilization

References:

Of The Great Man-Made River Water In Libya," *Ninth Int. Water Technol. Conf. IWTC9 2005, Sharm El-Sheikh, Egypt*, 2005.

[107] M. F. Ghazali and P. S. B. M. B. and P. W. J. Staszewski, "Leak Detection Using Instantaneous Frequency Analysis," The University of Sheffield, 2012.

[108] A. Aherwar and S. Khalid, "Vibration Analysis Techniques For Gearbox Diagnostic: A Review," *Int. J. Adv. Eng. Technol.*, vol. 3, no. 2, pp. 4–12, 2012.

[109] P. Heckbert, "Fourier Transforms and the Fast Fourier Transform (FFT) Algorithm," in *Computer Graphics*, 1998, pp. 1–13.

[110] X. Wang, M. Zhao, and S. Li, "An Improved Cross-correlation Algorithm Based on Wavelet Transform and Energy Feature Extraction for Pipeline Leak Detection," *... Int. Conf. Pipelines ...*, no. 1239, 2013.

[111] M. Weeks and M. Bayoumi, "Discrete Wavelet Transform : Architectures , Design and Performance Issues," *J. VLSI Signal Process.*, vol. 35, pp. 155–178, 2003.

[112] A. Martin and S. Tosunoglu, "Image Processing Techniques For Machine Vision," *Miami, Florida*, pp. 1–9, 2000.

[113] S. Rege and R. Memane, "2D Geometric Shape And Color Recognition Using Digital Image Processing," *Int. J. ...*, vol. 2, no. 6, pp. 2479–2487, 2013.

[114] R. Gonzalez and R. Woods, *Digital image processing*. 2002.

[115] J.-L. Starck, F. D. Murtagh, and A. Bijaoui, "Image Processing and Data Analysis," *Image Process. Data Anal.*, 1998.

[116] D. Shiffman, *The Nature of Code*, 5th ed. 2012.

[117] N. N. Prince, "Real – World Applications of Neural Network," vol. 20, pp. 192–197, 2011.

[118] W. Gerstner, "Supervised Learning for Neural Networks: A Tutorial with JAVA Exercises," *Intelligent Systems*, 2000. [Online]. Available: http://lcn.epfl.ch/tutorial/docs/supervised.pdf.

[119] S. Dolinšek, J. Kopac, Z. J. J. Viharos, L. Monostori, and S. Dolinsek, "An intelligent AE sensor for the monitoring of finish machining process," *Proc. Second Int. Conf. Intell. Process. Manuf. Mater. IPMM'99 (Cat. No.99EX296)*, pp. 847–853 vol.2, 1999.

[120] D. Fadare, "Artificial neural network model for prediction of friction factor in pipe flow," *J. Appl. Sci. Res.*, vol. 5, no. 6, pp. 662–670, 2009.

[121] B. Bhattacharya and D. P. Solomatine, "Application of artificial neural network in stage-discharge relationship," in *Proc. 4th International Conference on Hydroinformatics, Iowa City, USA*, 2000, no. July, pp. 1–7.

[122] D. Svozil, V. Kvasnicka, and J. Pospichal, "Introduction to multi-layer feed-forward neural networks," *Chemom. Intell. Lab. Syst.*, vol. 39, no. 1, pp. 43–62, 1997.

[123] R. M. Cesar and L. da Fontoura Costa, "An introduction to neural networks," *Neurocomputing*, vol. 14, no. 1, p. 104, 1997.

[124] W. Duch and N. Jankowski, "Transfer functions: hidden possibilities for better

References:

neural networks," *9th Eur. Symp. Artif. Neural Networks*, pp. 81–94, 2001.

[125] D. Ventura, M. Bruno, G. J. Lasinio, A. Belluscio, and G. Ardizzone, "A low-cost drone based application for identifying and mapping of coastal fish nursery grounds," *Estuar. Coast. Shelf Sci.*, vol. 171, pp. 85–98, Jan. 2016.

[126] R. Kind, "Image Processing Techniques." [Online]. Available: http://www.ncsa.illinois.edu/People/kindr/phd/PART1.PDF.

[127] UNHCR, "Libyan Arab Jamahiriya," *Capacity Building for Drainage in North*. pp. 2006–2007, 2009.

Appendix A: Leak Detection progress from multiple experiments

Results examples from four different experiments

Experiment 1:
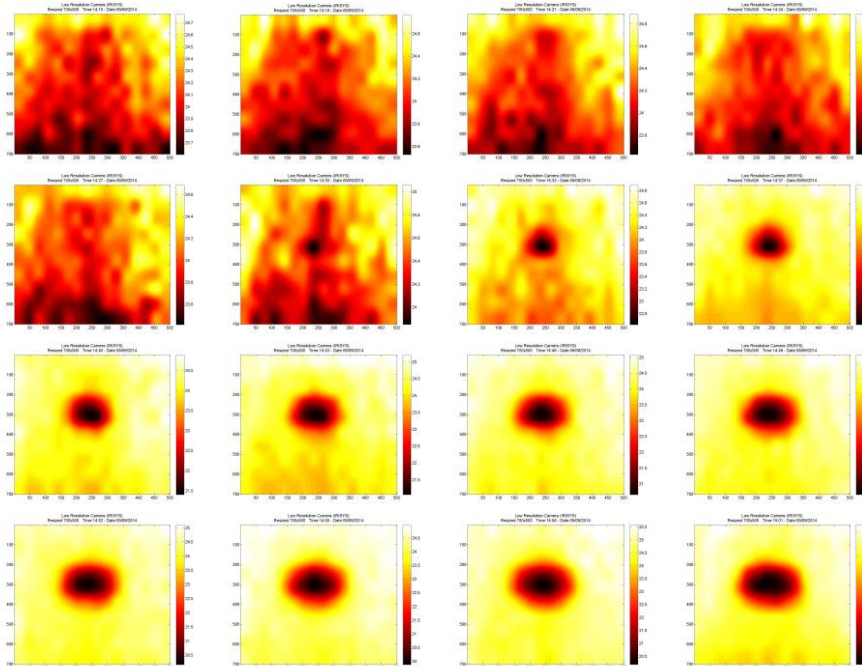
Experiment 2:
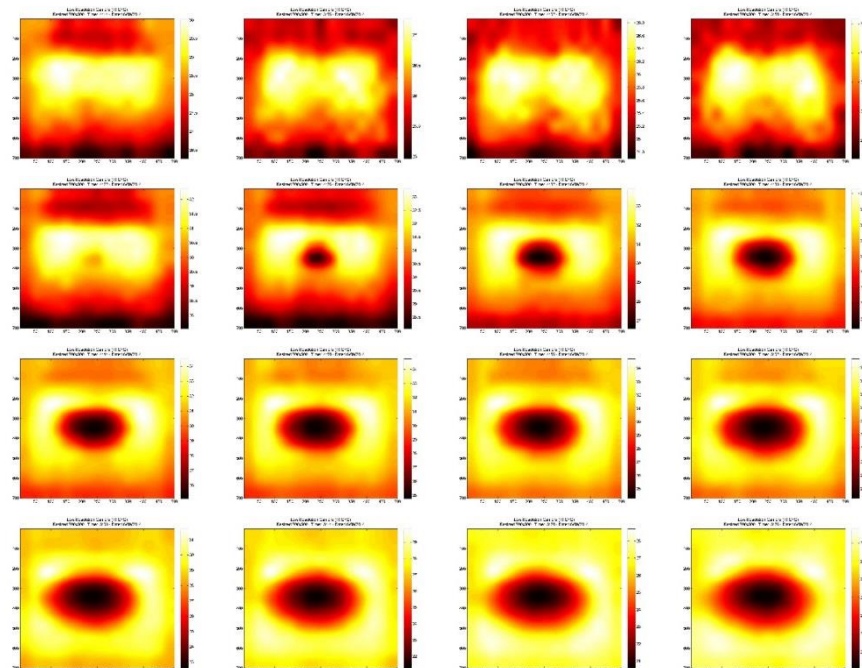
Experiment 3:
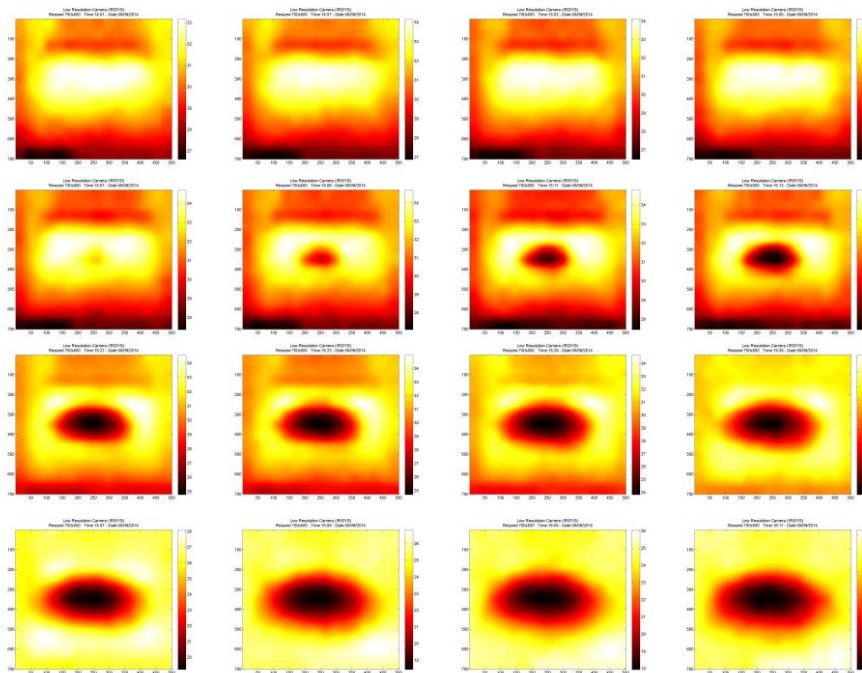
Experiment 4:
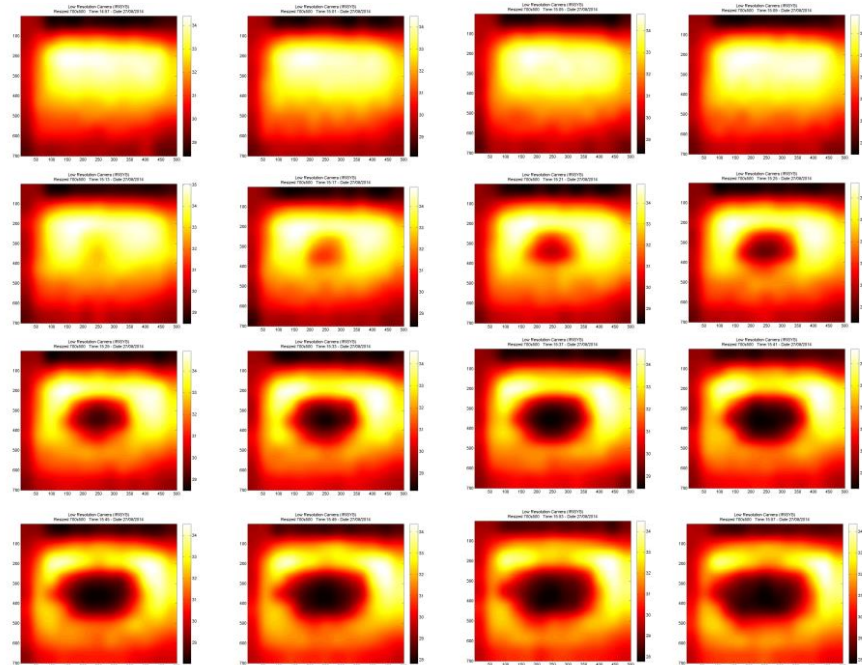
Appendix B: Results of Image processing

Sample of the results of the thermal image processing for two experiments (Round Shape).
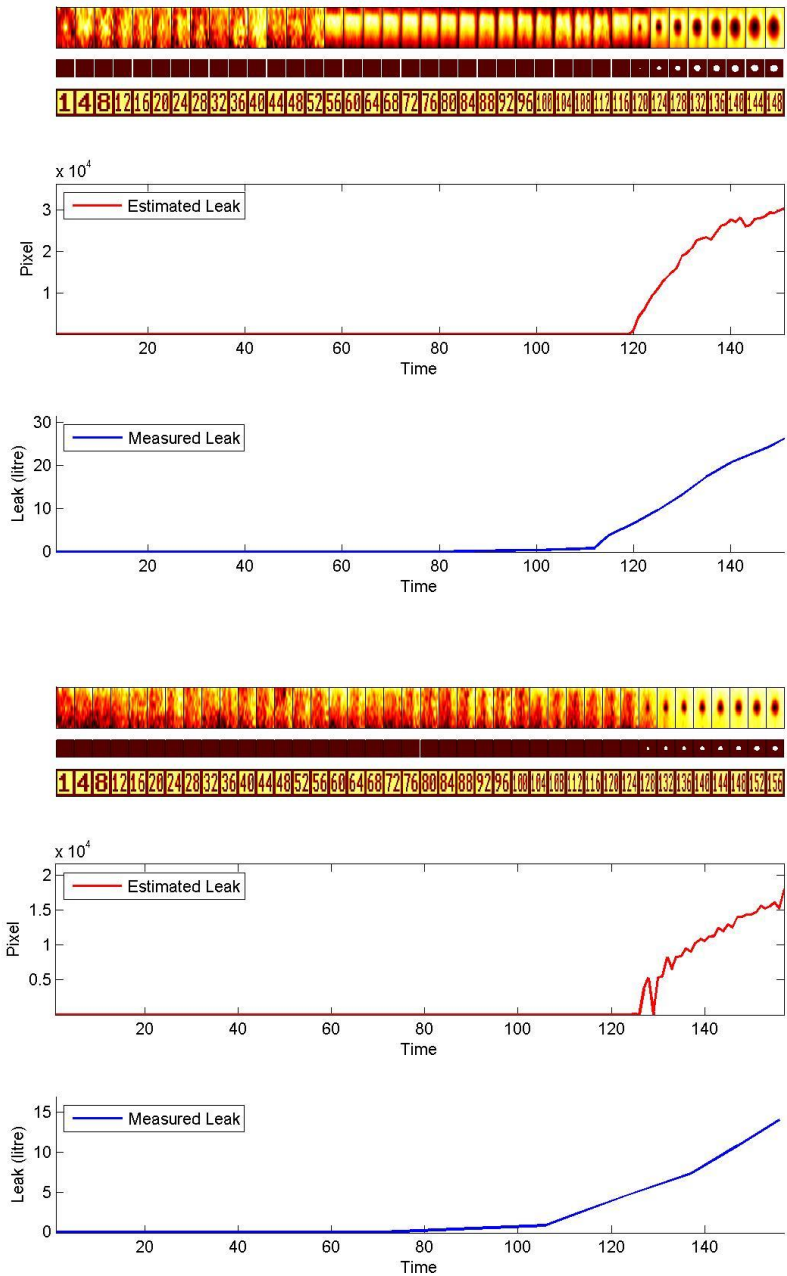
Sample of the results of thermal image processing for two experiments (d-Value).
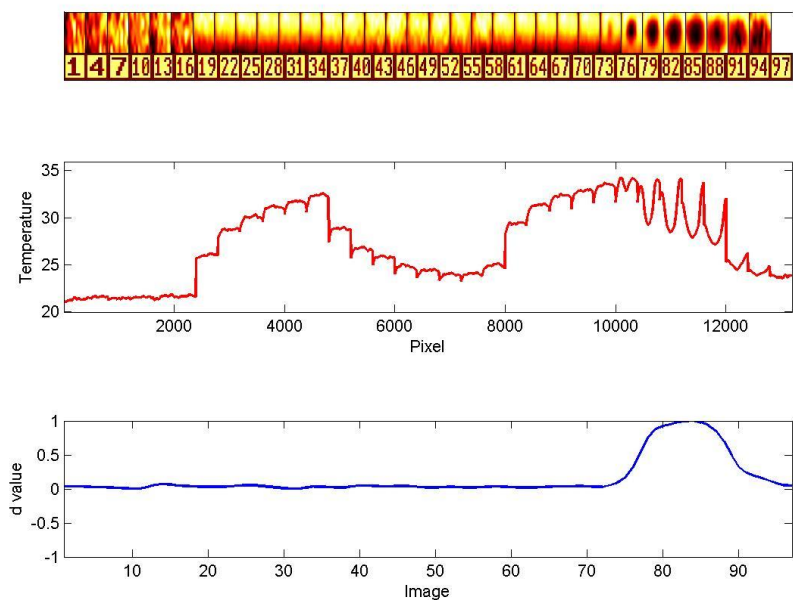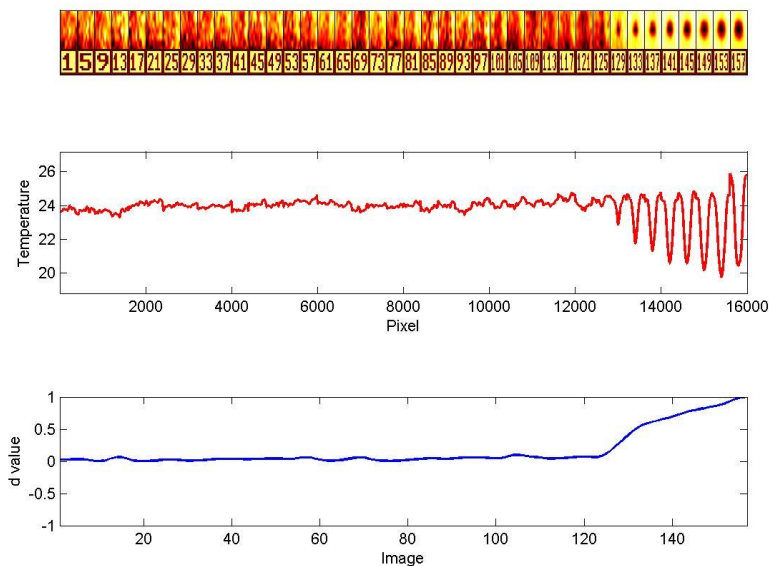
Sample of the results of thermal image processing for two experiments (Symmetricity).
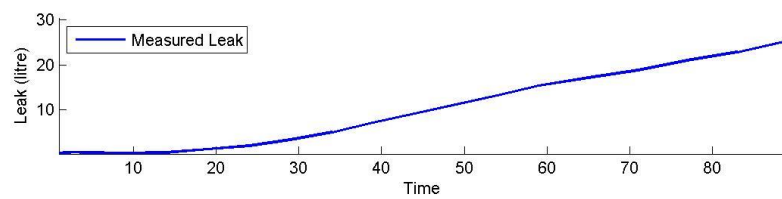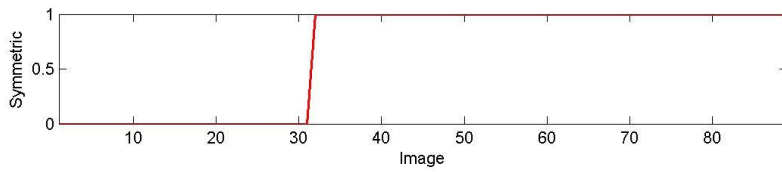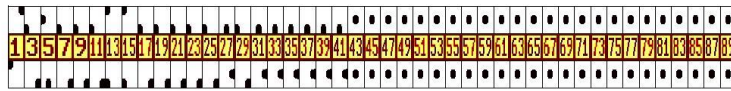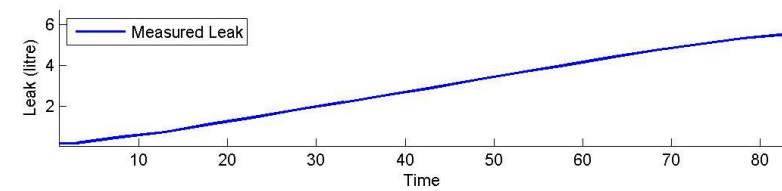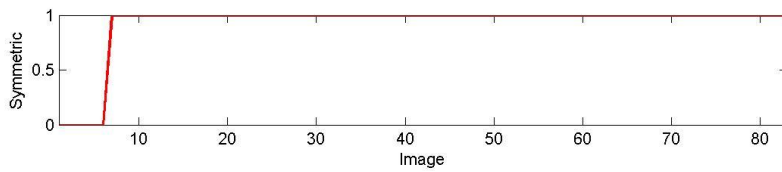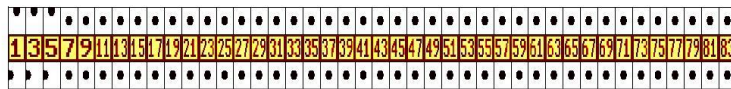
Sample of the results of thermal image processing for two experiments (Standard Deviation).
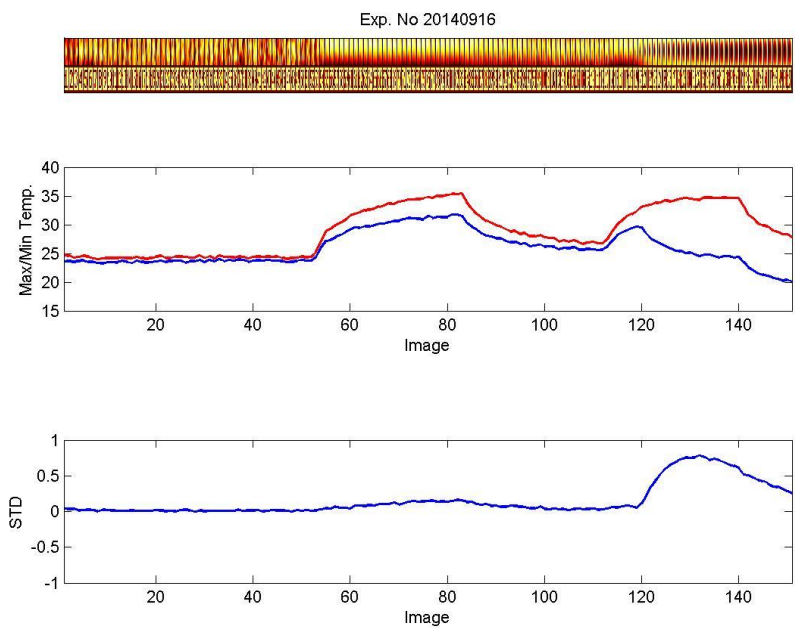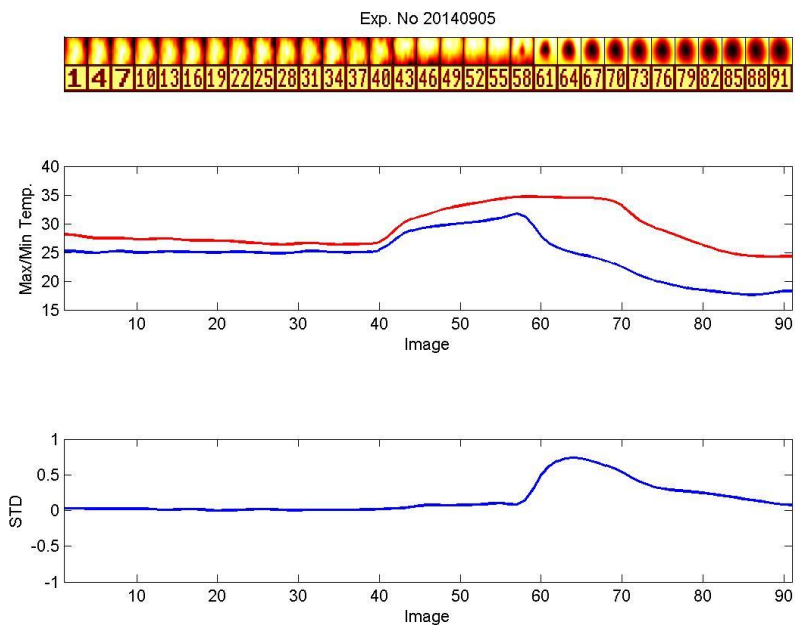
Sample of the results of thermal image processing using the five features for three experiments.
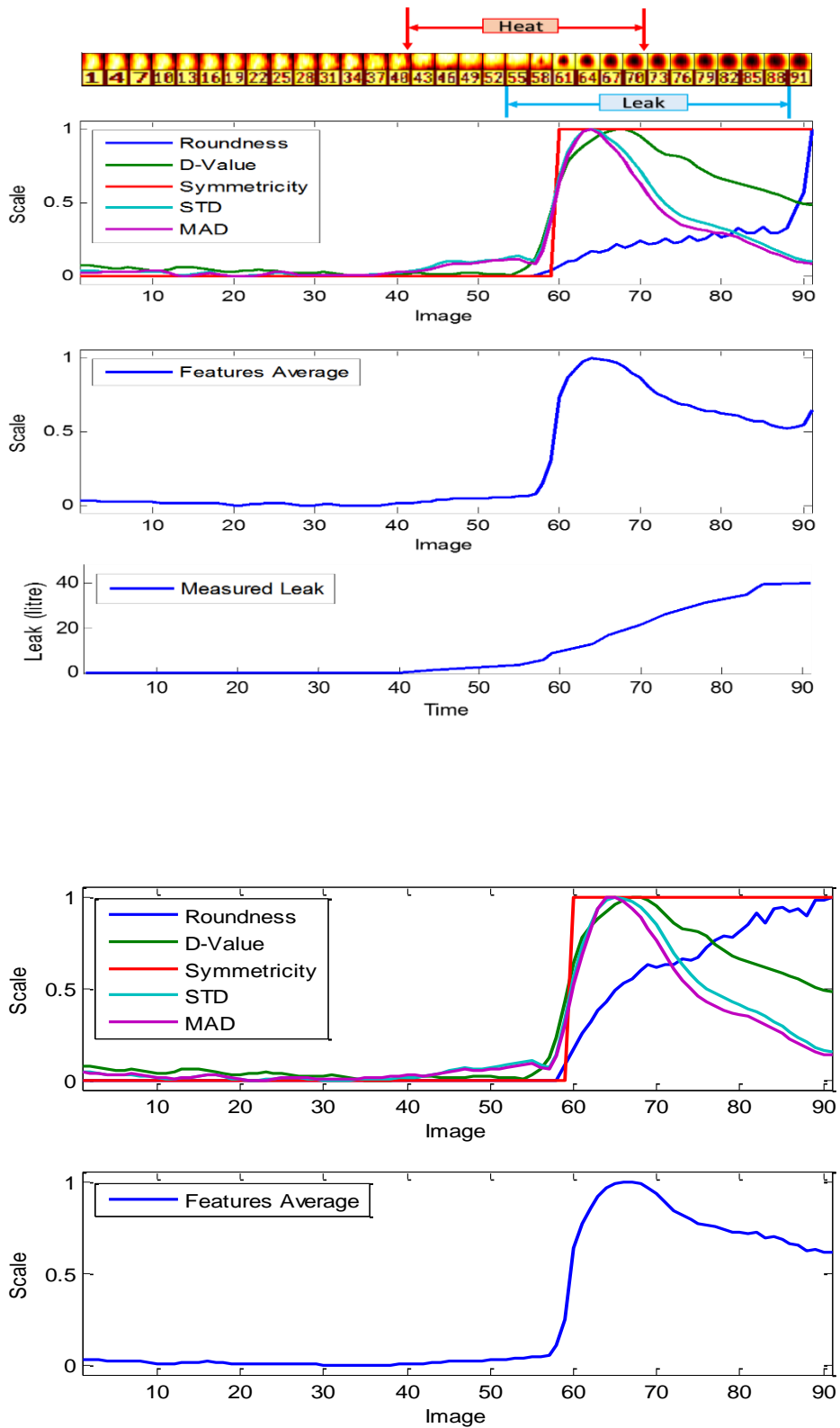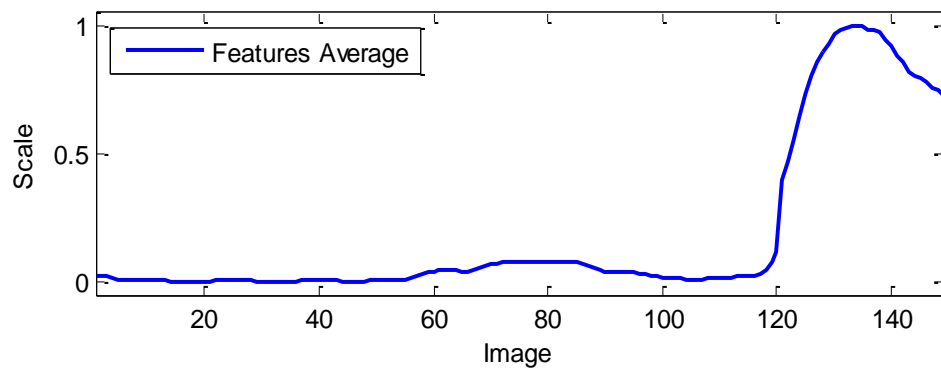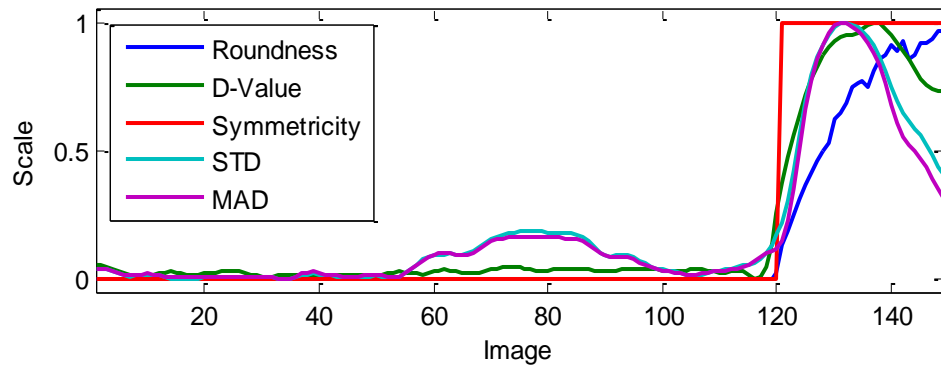
Appendix C: Results of ASMs

Results of ASMs from different experiments (six experiments).
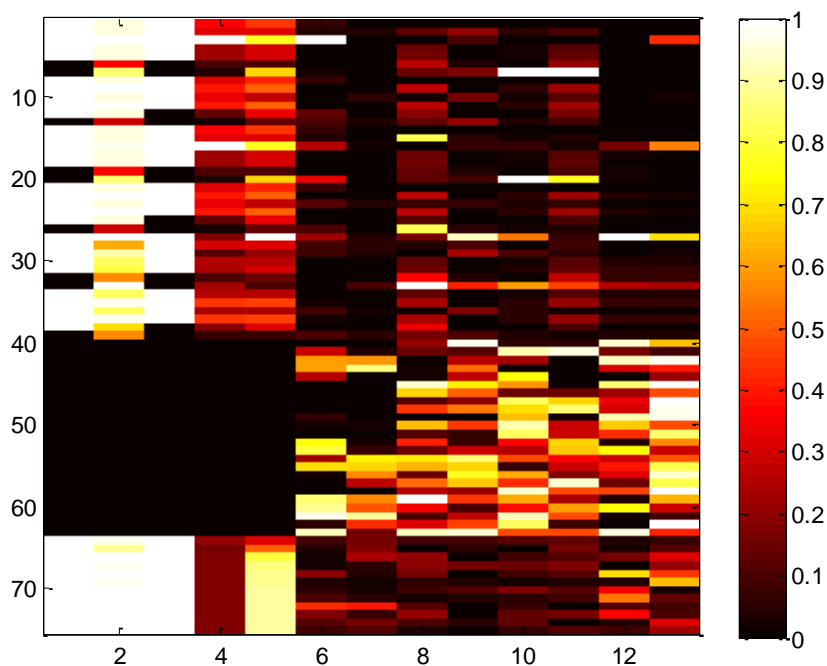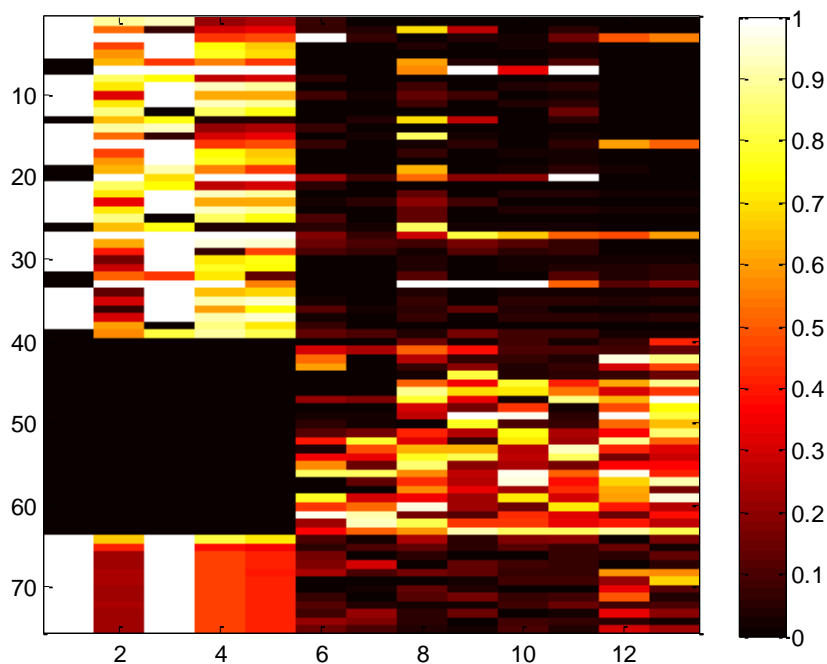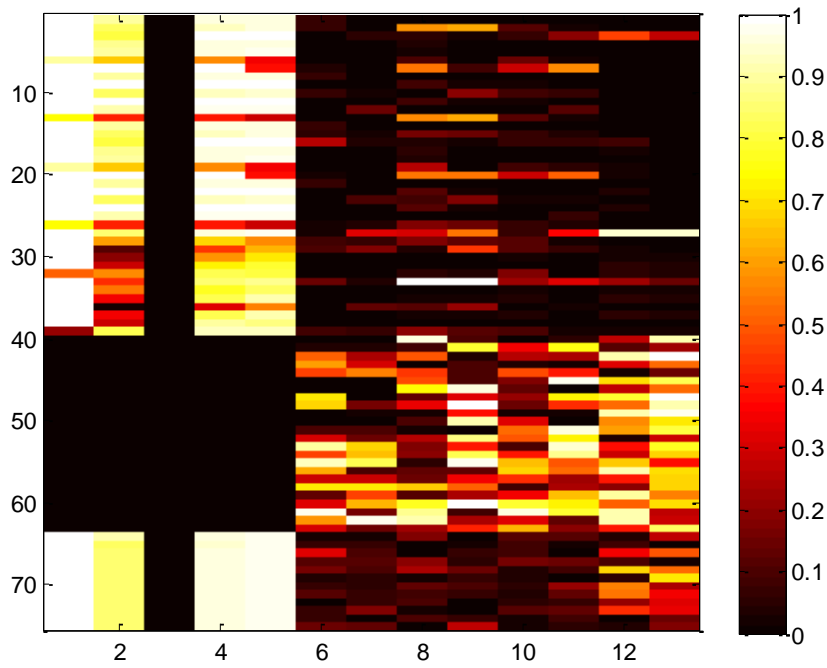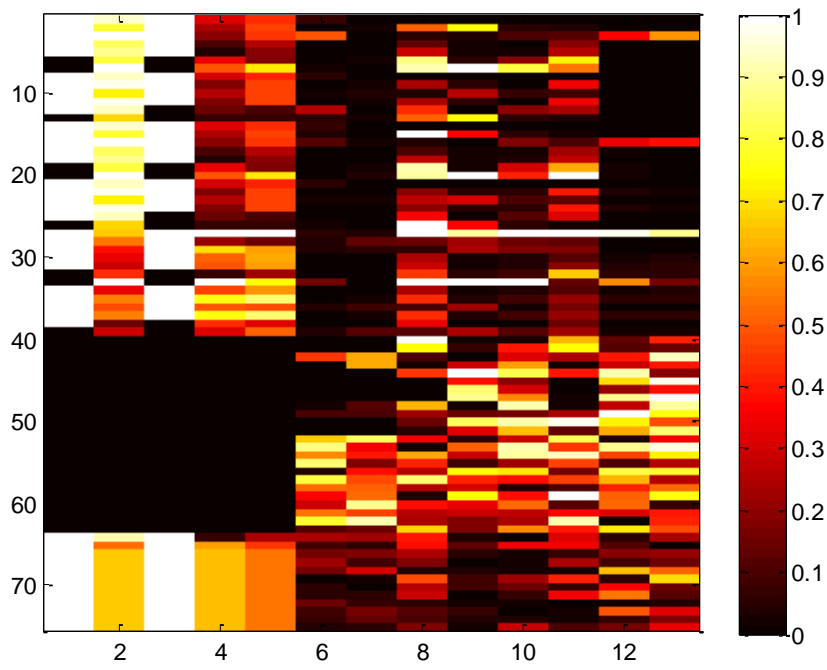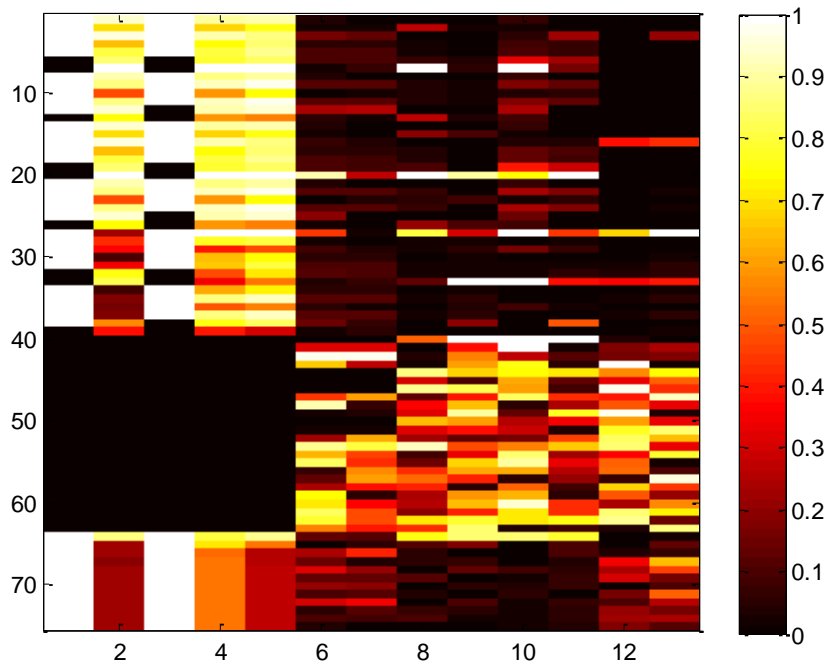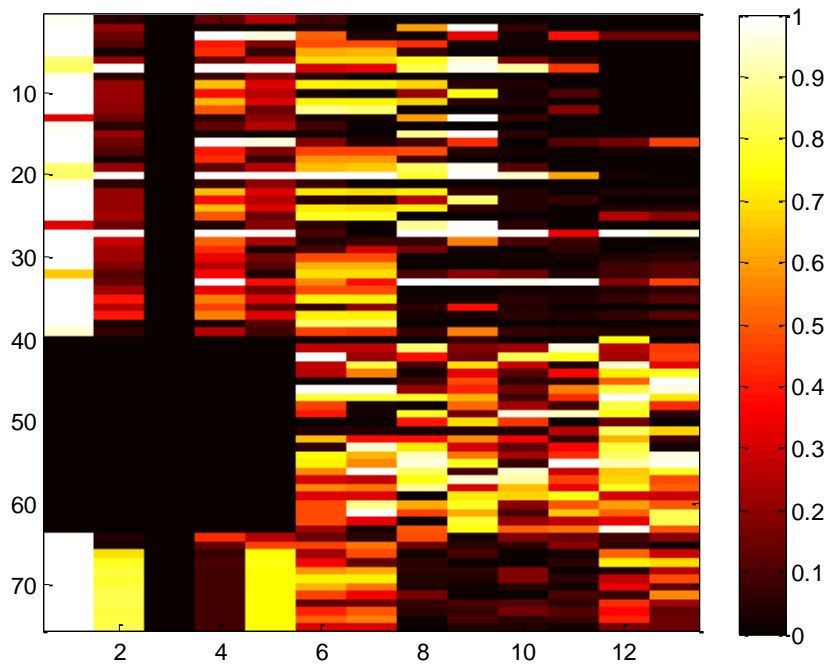
Appendix D: Results of Neural Network for APAS results

LVQ neural network.

Training Data for system 1
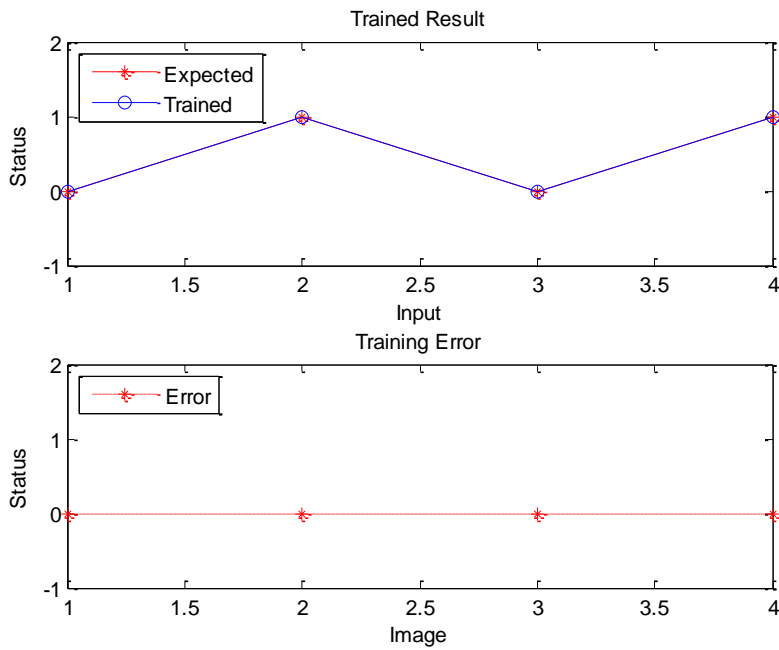
Testing Data
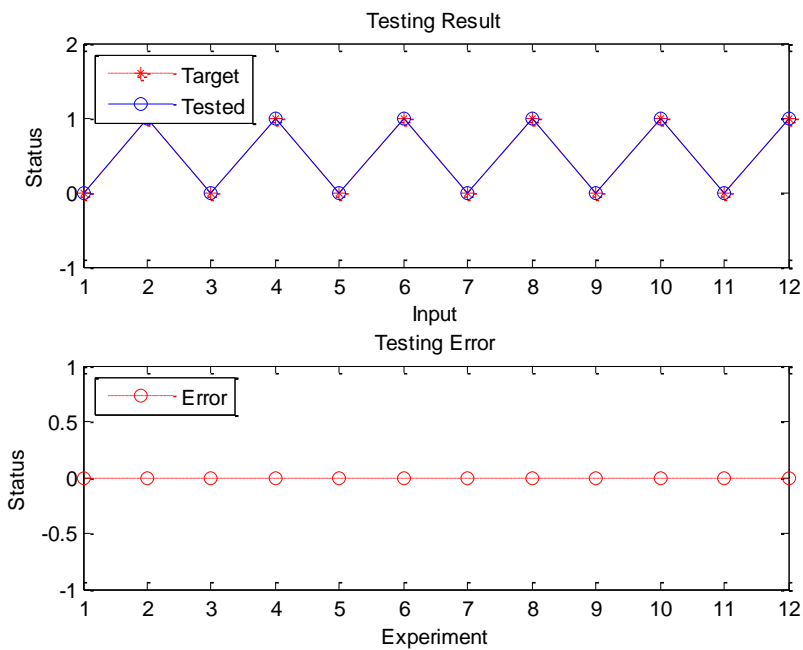
Training Data for system 5
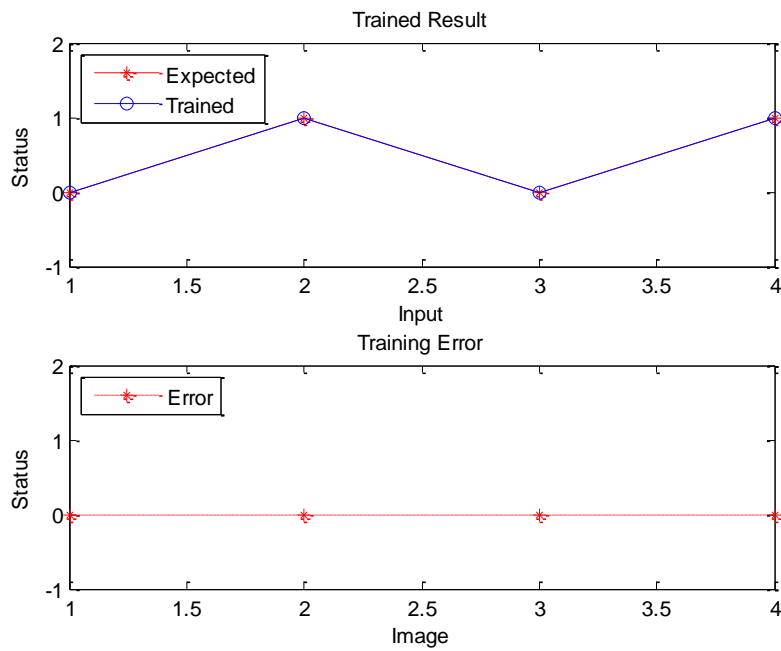
Testing data
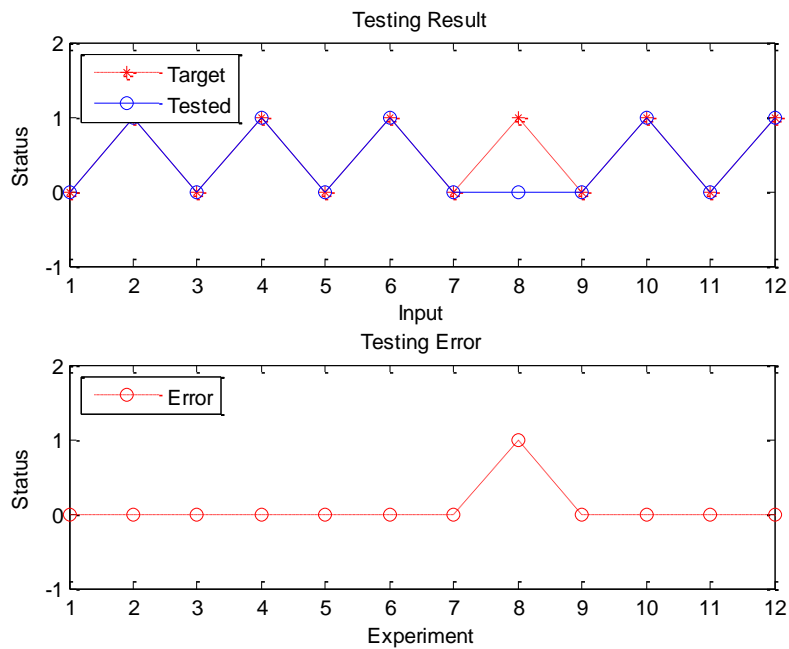
Appendix E: The conference paper:

2015 IEEE Jordan Conference on Applied Electrical Engineering and Computing Technologies (AEECT).

Detection of Water Leakage in Buried Pipes Using Infrared Technology;

A Comparative Study of Using High and Low Resolution Infrared Cameras For Evaluating Distant Remote Detection

Bubaker Shakmak
Innovative and Sustainable Built Environment Technologies
Research Group (iSBET)
School of Architecture, Design and Built Environment
Nottingham Trent University, Nottingham, NG1 4BU, UK
abubaker.shakmak2008@my.ntu.ac.uk

Amin Al-Habaibeh
Innovative and Sustainable Built Environment Technologies
Research Group (iSBET)
School of Architecture, Design and Built Environment
Nottingham Trent University, Nottingham, NG1 4BU, UK
amin.al-habaibeh@ntu.ac.uk

Abstract:

Water is one of the most precious commodities around the world. However, significant amount of water is lost daily in many countries through broken and leaking pipes. This paper investigates the use of low and high resolution infrared systems to detect water leakage in relatively dry countries. The overall aim is to develop a non-contact and high speed system that could be used to detect leakage in pipes remotely via the effect of the change in humidity on the temperature of the ground due to evaporation. A small scale experimental test rig has been constructed to simulate water leakage in The Great Man-Made River Project in Libya, taking into consideration the dryness level of the desert sand and the scaled dimensions of the system. The results show that the infrared technology is an effective technology in detecting water leakage in pipes. The low resolution system has been found as valuable as the high resolution system in detecting water leakage. The results indicate the possibility of distant remote detection of leakage in water systems using infrared technologies which could be mobilised using drones, helium balloons, aeroplanes or other similar technologies.

Keywords: Water leakage detection, thermal images, infrared cameras, sensors, monitoring systems, remote detection, drones.

I. INTRODUCTION

No doubt, water resources are limited around the world and a high standard of water management is extremely required in most countries. Economically, leaks are costing where in addition to wasting water; it consumes significant power to treat water or to transfer it from one point to another [1]. Some global studies have shown that the losses are ranging from 10% to 40% around the world [2]. Early detection of leaks improves operational efficiency, lowers operational costs, reduces potential for contamination, extends the life of the facilities, reduces potential property damage and water system liability and reduces water outage events [3]. Several research projects have been presented in the literature to detect water leakage using different leakage detection techniques such as acoustic emission, pressure sensors and infrared [2, 4, 5]. Different sensors are found to have different capabilities, for example when water is pumped at relatively high pressure, it could be difficult to detect the pressure drop caused by a leakage; hence pressure sensors could fail to detect that. Also, some sensors could be expensive and would require distributed installation around the water system.

As the water leakage causes temperature differences in the area nearby, infrared thermal cameras can detect the leak by visualising the leakage points upon the change in temperature on the surface above the pipeline. This paper addresses the use of infrared technology in order to detected water leakage from buried pipes. The goal is to detect and locate the leakage in pipes effectively with low cost and low resolution technology [6]. This paper compares between a low resolution camera and a high resolution camera in respect to leakage and location detection with support of image processing techniques. This to assess the potential of using distant remote detection of leakage in water systems using infrared technologies which could be mobilised using drones, helium balloons and aeroplanes.

When solar radiation falls on any surface of material, part of this radiation will be reflected from the surface and the rest will be absorbed. The energy generated by the absorbed radiation will increase the temperature of the surface of the material. The difference in temperature between the surface and the material underneath will create heat flow from hot part to the cold part. The rate of heat flow will depend on the conductivity of the material and the amount of temperature difference. It is well known that heat transfers between bodies by conduction, convection and radiation. Heat is the energy that flows from the hotter body to the cooler one [7]. In our case of buried water pipe system, heat transfers from the surface above the pipe to the pipe and vice versa based on which is cold and which is hot. The pipeline system will work as heat exchanger whereas heat from the surface flows to the pipe.

In some cases, the temperature difference might not be detected using infrared technology as some of the thermography cameras have limited sensitivity within 0.2 °C [8] or because the levels of temperature of the pipeline and the surrounding areas are similar. To avoid this situation, it is proposed to use the technology in real life within a specific time of the day when the difference is maximised.

1

The pipeline system itself causes difference in temperature on the surface above it. However, leaks could significantly influence the difference in temperature more than what the pipeline can do. In this simulated experiment, the water in the pipe was at a lower temperature than the surrounding backfill material in order to simulate real scenarios, especially in summer times in hot areas, when the temperature of the water will be at significantly lower temperatures.

For the buried pipeline, the heat flows from the surface to the pipeline if the pipeline is cooler than surrounding areas even if there is no leak and vice versa if the pipeline is hotter. The direction of the heat transfer depends on the temperature of the fluid transported and some other factors such as the conductivity of the material of the pipe, diameter, and the thickness of the pipe wall, etc. However, when the leak happens, the nearby area will be cooler than the surrounding and this causes remarkable change in the surface temperature above it. In this project the used pipe material was plastic which known to be a less conductive material [9].

II. THE GREAT MAN-MADE RIVER PROJECT (GMRP)

The Great Man-Man Made River project is the largest water transfer scheme built on earth to date. The project is divided to five stages. The total length of the pipeline exceeds 6000 km of 4 m diameter pipes. For Example, just the first phase of the project (Sarir/Sirt Tazerbo/Benghazi System) requires approximately 250,000 pipes of 7.5 meter long and 4 meter diameter [10].
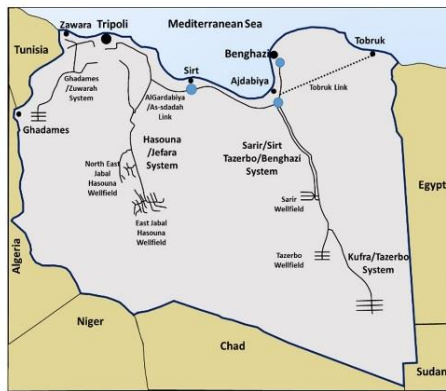
Fig. 1. The Great Man-Made River Project Map in Libya.

The GMRP transfers more than six Million Cubic Metres per Day (MCMD) from the south to the north of Libya. The initial design of first phase transfers 2.68 MCMD and will reach 3.68 MCMD [11]. The water is extracted from beneath the Sahara and either pumped, or allowed to flow by gravity, to the coastal side where the majority of the Libyans live. In addition to the 6000 km of pipeline, the project includes many water well-fields composes of a great net of pipelines and hundreds of wells of about 500 meters deep each. Many huge pump station complexes and many more huge water reservoirs of more than 50 million cubic meter of water storage capacity are also included.

As a water transfer system, the Great Man Made River Project will be definitely subjected to water leaks similar to any other water projects. The conveyance pipeline in is the most vulnerable section of the project than other sections such as the wells. It represents a major risk [10]. One of the project's high management priorities is to have a good early leakage detection system that can identify the leaks at their very first stages. Fig. 1 shows the map of the Great Man-Made River Project in Libya.

The sand temperature in the desert where the project has been constructed exceeds 50 °c in the day time [10]. The temperature of water is normally between 25-30 °c because it is pumped from deep water wells.

III. THE EXPERIMENTAL WORK:

A. The test rig

Fig. 2 shows the experimental test rig implemented to monitor the test section of the buried pipeline using two infrared cameras (the high and low resolution thermal cameras). The rig consists of a pipeline with inlet/outlet water tank, water pump and valves to control water flow. The test area consists of a box filled with soil in which part of the pipeline is passing through it to simulate actual buried pipeline. The test area is surrounded by polystyrene pieces to avert the heat effect of the surroundings in order to get clear thermal image for the tested area.

The pipeline is buried 110 mm deep under the surface. That is bigger than 5 times of the pipe diameter which is 20mm. The type of pipe material is plastic, which is known with less heat conductivity.
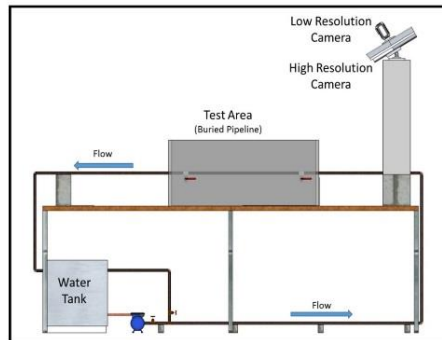
Fig. 2. The experimental test rig with the high and low-resolution cameras.

B. Thermal Imaging cameras utilised in this work

The thermal imaging is a non-destructive technique (NDT) for sensing infrared radiated from the surface of an object [12].

2

The thermal image of an object is the result of infrared radiation of the surface of the object, which can be sensed using the thermal infrared camera. The thermal image is a visible image from which tested objects can be assessed based on their heat emission [13]. The used cameras in this work are a low resolution camera (IRISYS) and the high resolution camera (Flir A310f).

Flir A310f is a relatively high cost, high resolution infrared camera with network connectivity. The camera is normally used in monitoring properties, process monitoring, quality control, fire detection in hazardous areas as well as a security camera.

The used IRISYS camera in this project is a low resolution and low cost infrared imager that can be easily used as a measuring device for measuring temperatures. Despite its low resolution and low cost, it is still beneficial in bringing the advantages of thermal imaging techniques. The IRISYS is producing a 16x16 low resolution image which can be enhanced using interpolation method to improve it visibility [6].

Fig. 3. The IRISYS system (a) and the Flir Camera (b) (images not to scale) .

The following figures (Fig. 4 and Fig. 5) show the original images and the processed imaged from both low resolution and high resolution cameras.
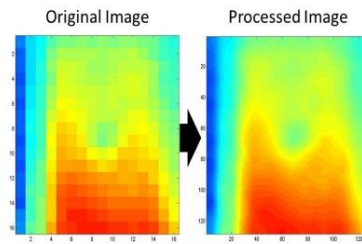
Fig. 4. A low resolution original image and the associated processed image.
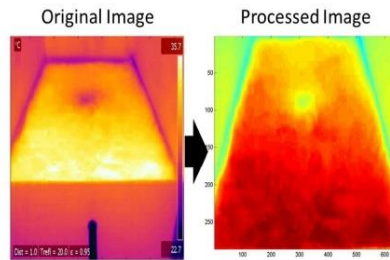
Fig. 5. A high resolution original image and the associated processed image.

IV. LEAKAGE DETECTION

A. Leak Detection comparison using both low and high resolution cameras:

Fig. 6 (A to F) is a series of processed images for both the low resolution camera (IRISYS) and the high resolution camera (Flir) taken simultaneously from the same experiment. The figures represent the progress of the leak detection throughout the experiment. The surface of the test area has been subjected to heating using infrared light to simulate surface heating during daytime by the sun. The leak is this case has started at the beginning of the experiment.

In Fig. 6, the leak is not detectable visually in the first images (A and B) while it becomes more detectable later during the day or early evening (D and E) where the leak is so evident and both cameras have given almost the same results.

3
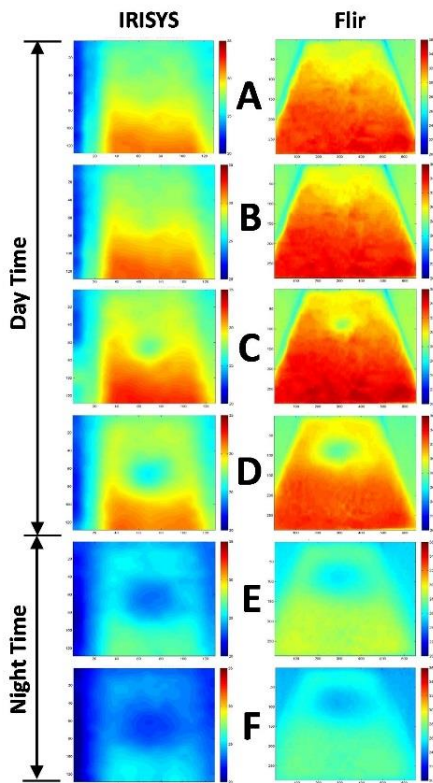
Fig. 6. Progress of leakage detection (A to II) for both Flir and IRISYS in daytime and night-time

B. Finding the leak location in both low and high resolution cameras:

Fig. 7 and Fig. 8 are selected images for both Flir and IRISYS cameras respectively. Analysis to the image is done via a chart using cross-section lines drawn on it along the pipeline direction or perpendicular to it.

In the chart, the cross section line which crosses the pipeline above the leak point outlines a different shape from the other two lines and will show the leak, as the temperature in the suspected leak point was clearly less than the preceding and succeeding points. Both cameras, the high resolution and the low resolution, have shown the leak with similar capabilities.
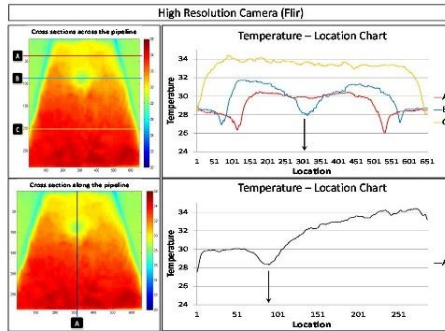
Fig. 7. A high resolution infrared image and the assciated temperature profiles.
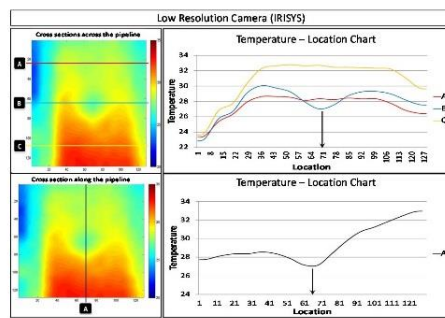
Fig. 8. A low resolution infarred image and the assciated temperature profiles.

C. Differentiation between leak and no-leak condition using 3D image.

The thermal image shows the leak as a spot on the suspected leak point while it shows the path of the pipeline in case there is no leak. The 3D mesh image as in Fig. 9 shows the leak as a 'sinkhole' in the middle of the suspected area while it shows the path of the pipeline as a trench along the pipeline length.
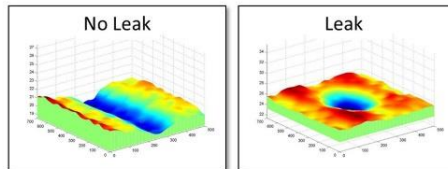
Fig. 9. Examples of 3D images showing the difference in detecting leakage and detecting the pipe path itself.

4

D. Differentiation between leak and no-leak condition using the temperature profile:

A chart for three selected cross-section lines across the image can clearly show how the pipeline is affecting the surface temperature above it.
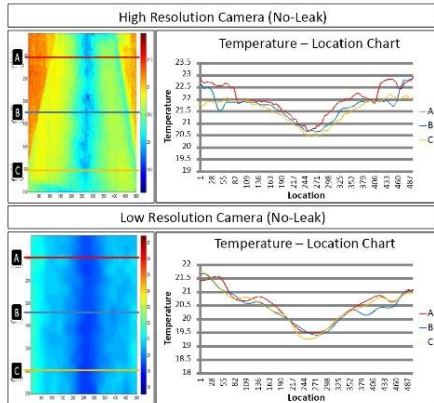
Fig. 10. No-leak condition for both Flir and IRISYS cameras.
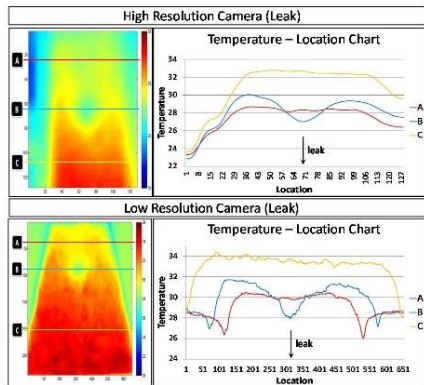
Fig. 11. Water leakage condition for both Flir and IRISYS cameras.

The lines will have a lower (or higher based on the temperature of the water) temperature on the area above the pipeline than the two other sides. In case of the no-leak condition, the three lines drawn for the three selected cross sections have shown a lower temperature at the middle point. While, in the leak condition only the line located above the leak point have shown a lower values in the middle than the other two cross section lines, see Fig. 10 and Fig. 11

E. Proposal for the use of the thermal cameras for pipeline inspection:

The thermal cameras could be fixed in certain point for continuous monitoring especially for critical points of the pipeline where leaks are most expected. It also can be used as a mobile camera in routine inspection for the pipeline especially in large projects such GMRA or where it cannot be fitted in open areas. It is suggested that the camera would be better used as a part of a sensor fusion system to confirm whether the leak exists or not.

The use of mobile cameras can be done using several techniques. In this paper it is suggested that the camera can be fitted with either quadcopter drone or a helium balloon so the images can be taken from higher and better point of sight. This might require to be jointed with GPS system in order to record the location of the image taken, see Fig. 13 and Fig. 14.

1) The thermal camera with a helium balloon:

For larger projects with longer distances pipeline in open areas the camera can be fitted to a helium balloon. The balloon could be secured to a vehicle as shown in Fig. 12.
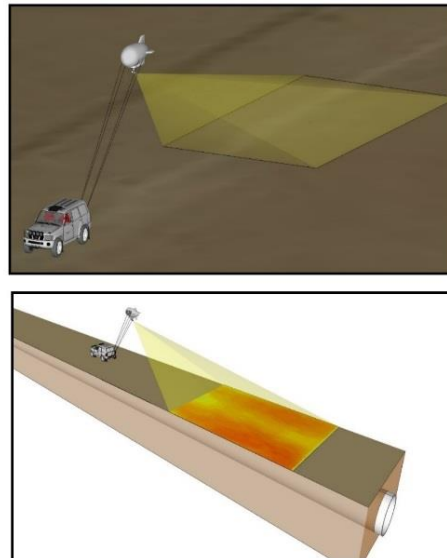
Fig. 12. An infared camera and a GPS system can be attached to a helium balloon to be used for pipeline inspection for long distances.

2) The thermal camera with quadcopter drone:

For shorter distances pipeline, the quadcopter drone can be used to hold the camera and fly over the pipeline or the suspected area of leak for inspection, see Fig. 13.

5
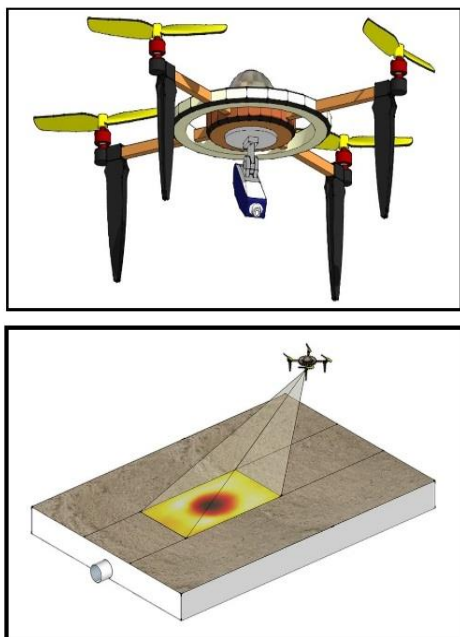
Figure 13: An artistic impression of the quadcopter drone with infrared camera and a GPS system.

CONCLUSION

Detection of water leakage in pipes is becoming extremely important to save water and energy. This paper has suggested the use of low and high resolution cameras to test the detection of water leakage using a small scale simulator. It has been found that when leakage occurs, a specific thermal profile will be generated that could be easily detected by both types of cameras (particularly late afternoon or early evening). The cameras are able to visualise the leak despite the leak itself is not being evident on the surface by visual inspection. The difference in the temperature generated on the surface has clearly been detected by both, the high resolution thermal camera (Flir A310f) and the low resolution thermal camera (IRISYS). However, the resulted images from both cameras have needed additional processing to confirm the leakage and its location.

The low resolution camera is found as successful as the high resolution camera in detecting and locating the leakage. As the cost of producing water leakage detection system using thermal cameras is an important factor, the result of this research will assist in the design of a low cost water leakage detection system. The produced systems could be mobile or use fixed cameras, depending on the importance of the inspected point. One other important outcome of the findings, is that the high resolution camera could be used to detect leakage in large areas from high altitudes since the pixel density of the images will still be effective as evident from test conducted using the low resolution infrared camera.

REFERENCES:

[1] H. L. Zhao, J. K. Wang, and X. Jiang, "A Real-time Monitoring System for the Pipeline Network of Coalmine," *J. Phys. Conf. Ser.*, vol. 364, p. 012107, May 2012.

[2] A. F. Colombo, P. Lee, and B. W. Karney, "A selective literature review of transient-based leak detection methods," *J. Hydro-environment Res.*, vol. 2, no. 4, pp. 212–227, Apr. 2009.

[3] EPD, "WATER LEAK DETECTION AND REPAIR PROGRAM," 2007.

[4] H. V. Fuchs and R. Riehle, "Ten years of experience with leak detection by acoustic signal analysis," *Appl. Acoust.*, vol. 33, no. 1, pp. 1–19, Jan. 1991.

[5] R. Pérez, V. Puig, J. Pascual, J. Quevedo, E. Landeros, and A. Peralta, "Methodology for leakage isolation using pressure sensitivity analysis in water distribution networks," *Control Eng. Pract.*, vol. 19, no. 10, pp. 1157–1167, Jul. 2011.

[6] A. Al-Habaibeh and R. Parkin, "An autonomous low-Cost infrared system for the on-line monitoring of manufacturing processes using novelty detection," *Int. J. Adv. Manuf. Technol.*, vol. 22, no. 3–4, pp. 249–258, Sep. 2003.

[7] J. Vlachopoulos and D. Strutt, "BASIC HEAT TRANSFER AND SOME APPLICATIONS IN POLYMER," vol. 2, pp. 21–33, 2002.

[8] T. Inagaki and Y. Okamoto, "Diagnosis of the leakage point on a structure surface using infrared thermography in near ambient conditions," *Science (80-.)*, vol. 30, no. 3, pp. 135–142, 1997.

[9] J. E. Patterson, D. Ph, R. J. Miers, and N. Carolina, "The Thermal Conductivity of Common Tubing Materials Applied in a Solar Water Heater Collector," 2009.

[10] D. P. Loucks, "The Third Annual D. R. F. Harleman Honorary Lecture in Environmental Fluid Mechanics The Great Man-Made River in Libya : Does it Make Sense ? by," 2004.

[11] A. El Geriani and O. Essamin, "Cost-effectiveness analyses of Libya's water supply system," *J. water ...*, 1998.

[12] N. Jalali, B. Saghafian, F. Imanov, and M. Museyyibov, "Recognition of shallow karst water resources and cave potentials using thermal infrared image and terrain characteristics in semi-arid regions of Iran," *Int. J. Appl. Earth Obs. Geoinf.*, vol. 11, no. 6, pp. 439–447, Dec. 2009.

[13] Z. Liu and Y. Kleiner, "State of the art review of inspection technologies for condition assessment of water pipes," *Measurement*, vol. 46, no. 1, pp. 1–15, Jan. 2013.

6

Appendix F: NTU Conference 2013

The Investigation of Water Leakage Detection and Defects in Pipes Using Sensor Fusion Systems

Detecting leaks as soon as they happen will save significant wasted costs by saving water, power consumption and the environment. A sensory fusion system is expected to be more accurate in detecting and identifying leaks more than any individual method and should be able to overcome the limitations associated with each individual sensor separately. A successful system can protect major water projects like the GMRP shown above which transfers at least 6 million cubic meter per day across vast country like Libya.

How big the problem of water leakage? (UK)

If one person uses 150 litres of water per day on average, How much each company loses per day. (Just a sample)

•Thames Water loses 664.6 million litres of water per day. That's enough to supply 4,430,400 people or 50% of their domestic users.

•Severn Trent Water loses 497 million litres of water per day. That's enough to supply 3,313,400 people or 40% of their domestic users.

•United Utilities Water loses 464.2 million litres of water per day. That's enough to supply 3,094,933 people or 44% of their domestic users.

The Project:

The Project Aim:
The project aims to address current problems in leakage detection systems by developing a more efficient and low-cost leak detection system.

The Project Methodology:
The project will attempt to identify and quantify any leaks that may occur in a pipeline using sensor fusion systems by managing the process as follows:
   1Detecting the leakage using the most suitable sensor or a combination of sensors.

2Determining the location of the leakage

3Confirming the existence of the leakage

4Identifying the leakage characteristics (e.g. size)

The Experimental Rig:
The pipeline system will be of an experimental scale inside the laboratory as shown in figure at the left. Part of pipeline will be buried under soil to represent actual situation. The pipeline system will consist of inlet and outlet water tank and water pump plus several sensors and data acquire device. The buried section of the pipe will contain some openings to represent the leak points. Multiple sensors such as pressure, acoustic emission, moisture, vibration and temperature plus thermal and digital cameras will be used to monitor the pipeline for any leaks.
The buried section will be covered by slabs contains holes. The holes will be used as a guide for located the leak using thermal camera.

Advanced Design and Manufacturing Engineering Centre
School of Architecture, Design and the Built Environment

Student Name: Bubaker Shakmak
Supervisors: Dr. Amin Al-Habaibeh, Daizhong Su

Appendix G: Great Man-Made River Project (GMRP)

The Great Man-Man Made River Project (GMRP) is the largest water transfer scheme built in the world to date. The project pipeline total length is more than 6000 km of 4 m diameter pipes. It transfers more than six million cubic meters per day from the south to the north of Libya [106]. The water is extracted from beneath the Sahara and either pumped or allows gravity to facilitate the flow to the coastal area where the majority of the Libyan people live. In addition to the 6000 km of pipeline, in this project there are many water wellfields composes of a great net of pipelines and hundreds of wells of about 500 meters deep each, many enormous pump station complexes and many more huge water reservoirs of more than 50 million cubic meter of water storage capacity [127].

As a water transfer system, the Great Man-Made River Project will be definitely subjected to water leaks similar to any other water projects. One of the project's high management priorities is to have a good early leak detection system that can discover the leaks at its earliest stages and before it turns to a disaster. Figure G-1 shows the map of the Great Man-Made River Project in Libya.
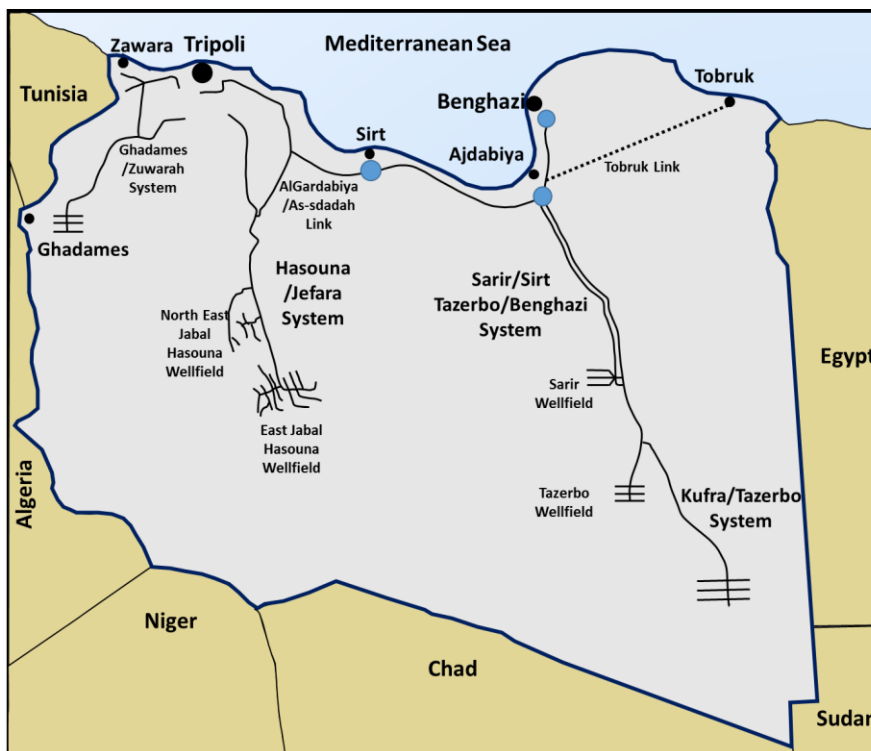
Figure G-1: Libyan Map showing the River Project

Figure G-2 shows some photos related to GMRP such as the pipeline construction and laying, water reservoir, overflow station and control room. Figure G-3 shows one of the pump stations and the one of the groups of the surge vessels constructed in the project. Figure G-4 shows the layout of one of the pump stations complexes in the project. This complex is a bidirectional pump station complex where the water passes through it in both directions depend on the demand.
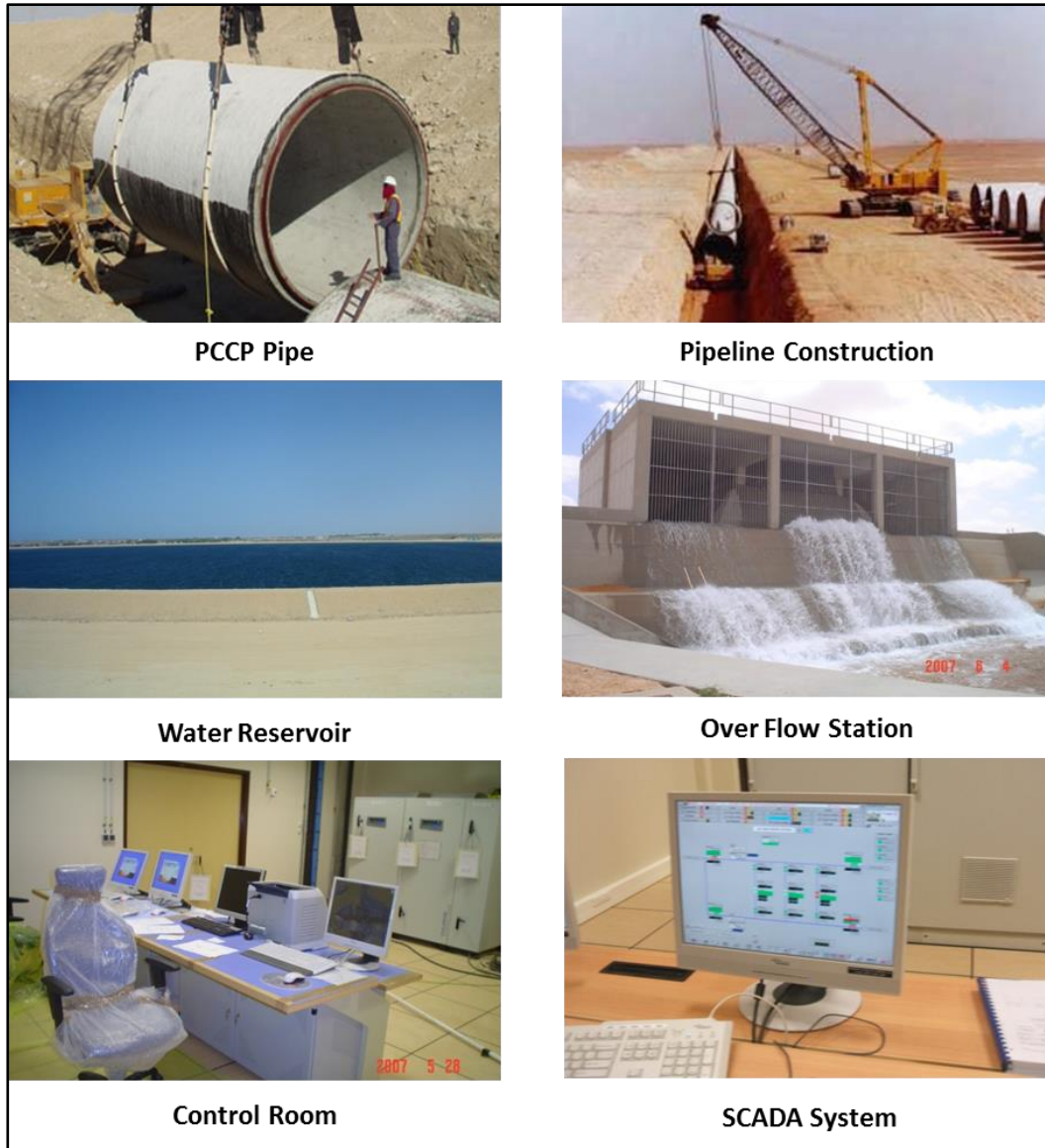
Figure G-2: Photos related to GMRP

Figure G-3: Pump stations and Surge Vessels

Figure G-4: Layout of the Bi-directional Pump Station Complex (this is one of multiple pump station complexes in the project)

Appendix H: Technical Details of Sensors and Data Acquisition Devices

1. Acoustic Emission Sensor:

Acceleration

KISTLER
measure. analyze. innovate.

Piezotron® Sensor

Type 8152B...

Acoustic Emission Sensor

Piezotron Acoustic Emission Sensor with an integral impedance converter for measuring acoustic emission (AE) above 50 kHz in machine structures. With its small size it mounts easily near the source of emission to optimally capture the signal. The sensor has a ver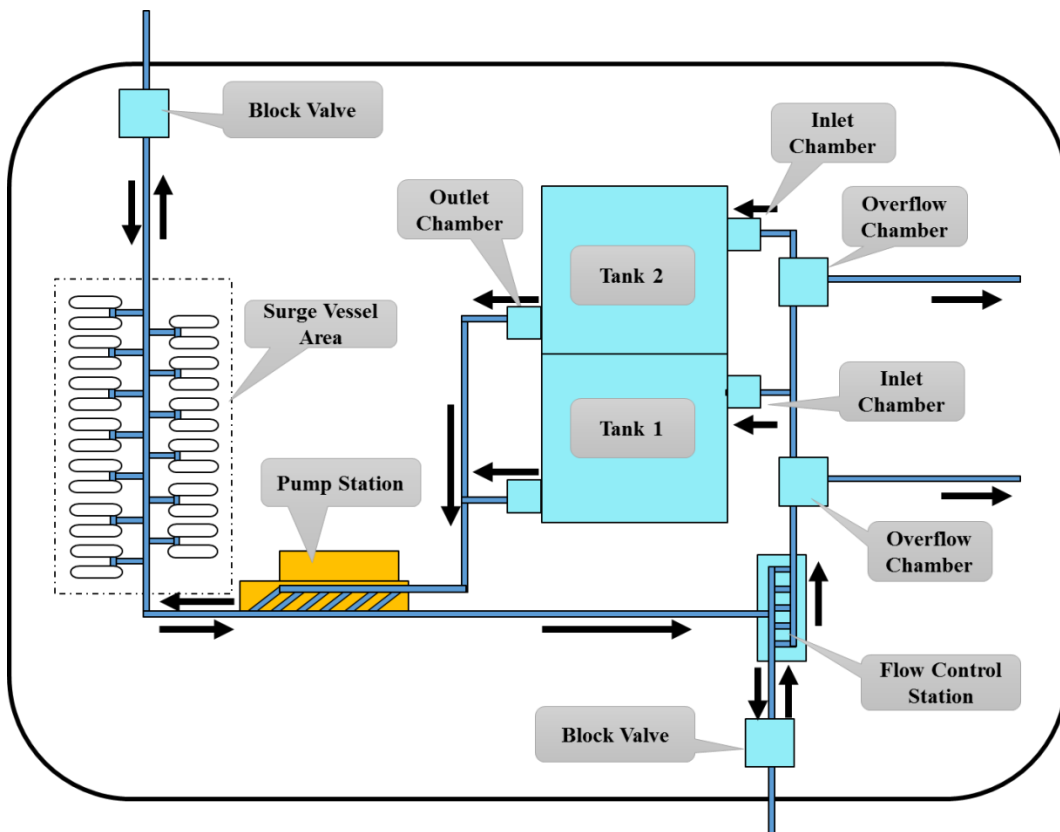y rugged welded housing (degree of protection IP 65 PUR or IP 67 Viton). The small sensor is easily mounted nearly everywhere; an M6 or 1/4-28 bolt is all that is needed.

- High sensitivity and wide frequency range
- Inherent highpass-characteristic
- Insensitive to electric and magnetic noise fields
- Robust, for industrial use (IP65 (PUR), IP67 (Viton))
- Ground isolated: Prevents ground loops
- Conforming to CE

Description

The Piezotron AE Sensor consists of the sensor housing, the piezoelectric sensing element and the built-in impedance converter. The sensing element, made of piezoelectric ceramic, is mounted on a thin steel diaphragm. Its construction determines the sensitivity and frequency response of the sensor. The coupling surface of the diaphragm welded into the housing is slightly protruding to measure the AE signals. Thus a precisely defined coupling force results when mounting. This assures a constant and reproducible coupling for the AE transmission. The sensing element is acoustically isolated from the housing by design and therefore well protected against external noise. The Kistler AE sensors feature a very high sensitivity for surface (Rayleigh) and longitudinal waves over a broad frequency range. Type 8152B1… covers 50 ... 400kHz and Type 8152B2… covers 100 ... 900 kHz. A miniature impedance converter is built into the Piezotron AE Sensor, giving an output low-impedance voltage signal. The AE Piezotron Coupler Type 5125B1, is used to supply power to the sensor and for signal processing. Special highly insulating and low noise connecting cables are not required.

8152B_000-204a-01.07

258

Acoustic Emission Sensor, Type 8152B...

KISTLER
measure. analyze. Innovate.
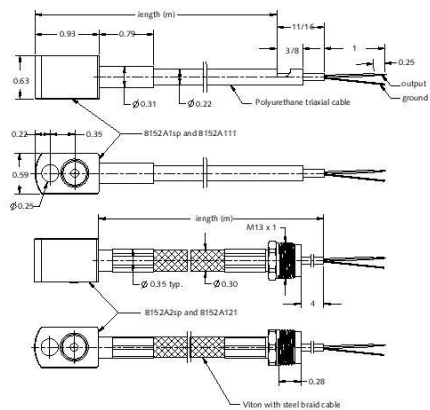
Technical Data

Type	Unit	8152B111/121	8152B11/12sp	8152B211/221	8152B21/22sp
Sensitivity	dBref 1V/(m/s)	57	57	48	48
Frequency Range ±10dB	kHz	50 ... 400	50 ... 400	100 ... 900	100 ... 900
Ground Isolation	MΩ	>1	>1	>1	>1
Environmental:					
Shock Limit (0.5ms pulse)	gpk	2000	2000	2000	2000
Temperature Range Operating	°F	-40 ... 140	-40 ... 140	-40 ... 140	-40 ... 140
Output:					
Bias nom.	VDC	2.2	2.2	2.5	2.5
Impedance	Ω	<10	<10	<10	<10
Voltage full scale	V	±2	±2	±2	±2
Current	mA	2	2	4	4
Source:					
Voltage (Coupler)	VDC	5 ... 36	5 ... 36	5 ... 36	5 ... 36
Constant Current	mA	3 ... 6	3 ... 6	3 ... 6	3 ... 6
Construction:					
Sensing Element	type	ceramic	ceramic	ceramic	ceramic
Housing/Base	material	stainless steel	stainless steel	stainless steel	stainless steel
Sealing-housing/connector	type	hermetic	hermetic	hermetic	hermetic
Viton Cable Bend Radius, max.	in	0.6	0.6	0.6	0.6
Weight (without cable)	grams	29	29	29	29
Mounting Torque	lbf-in	80±10	80±10	80±10	80±10

1 g = 9.80665 m/s², 1 inch = 25.4 mm, 1 gram = 0.03527 oz, 1 lbf-in = 0.1129 Nm

Application

The AE Sensor is especially well suited for measuring AE above 50 kHz in the surface of metallic components or structures. Such AE results from plastic deformation of materials, crack formation and growth, fracturing or friction. Application examples are monitoring of processes, tools and machines in metal cutting as well as forming operations. Thanks to its rugged construction and the tightly welded housing this sensor can operate under severe environmental conditions.

Accessories Included	Type
• Mounting screw, 1/4-28 x 1in	431-0500-001
• Mounting screw, M6 x 25mm	431-0497-001

Optional Accessories	Type
• Magnetic clamp	8443B
• Piezotron AE coupler	5125B

8152B_000-204a-01.07

Page 2/4

Acoustic Emission Sensor, Type 8152B...

KISTLER
measure. analyze. Innovate.

Mounting

The AE Sensor is simply mounted with an M6-1/4 screw or a magnetic clamp Type 8443B onto the surface of the structure. A minimum tightening torque is sufficient for a reproducible and constant coupling. The smoother the mounting surface, the better the result. The use of a highly viscous grease (e.g. silicone grease) between the coupling surfaces is recommended.
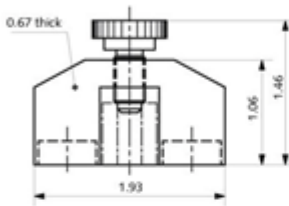
Type 8443B Magnetic clamp
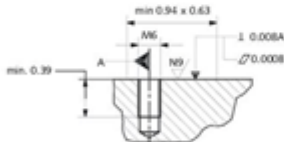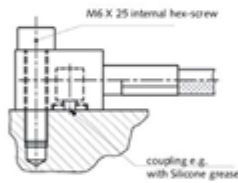
Ordering Key

Variants		8152B ☐
PUR, 5m (50 ... 400kHz)	111	
PUR, 0.3 ... 10m (50 ... 400kHz)	11sp	
PUR, 5m (100 ... 900kHz)	211	
PUR, 0.3 ... 10m (100 ... 900kHz)	21sp	
Viton, 2m (50 ... 400kHz)	121	
Viton, 0.3 ... 3m (50 ... 400kHz)	12sp	
Viton, 2m (100 ... 900kHz)	221	
Viton, 0.3 ... 3m (100 ... 900kHz)	22sp	

Measuring Chain

		Type
1	Acoustic emission sensor	8152B...
2	Piezotron AE Coupler	5125B...
3	Output cable, made by customer	

Mounting AE-Sensor

Page 3/4

Acoustic Emission Sensor, Type 8152B...

Frequency Response

Type 8152B1

Type 8152B2

Kistler Calibration

Kistler accelerometers are calibrated in the factory and delivered with a calibration certificate. The reference sensors are cross-referenced to national standards. Kistler operates a NIST traceable calibration center and the calibration laboratory No. 049 of the Swiss Calibration Service for the measurands: force, pressure, acceleration and electric charge.

Kistler and some of its group companies offer a recalibration service and the company records in its archives the details of when and how often a particular sensor was calibrated.
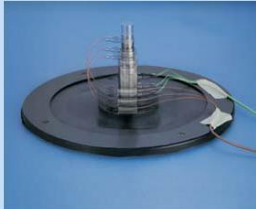
Kistler offers an onsite service for recalibrating built-in sensors, thereby minimizing downtimes. In addition, Kistler offers a wide range of instruments for use in calibration laboratories.

Our calibration service receives the highest marks. The calibration of your instruments, manufactured by Kistler or someone else, is performed with quality care and precision. Our standard prompt service is exceptional. Kistler operates numerous calibration laboratories accredited to ISO/IEC 17025.

Calibration

Onsite, traceable calibration systems

National referenced calibration services available
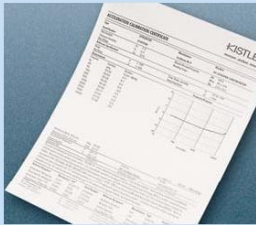
Kistler Cailbration Service Description by Type Number

Type	Calibration Service Description
9953AnM	Recalibration: n-axis accelerometers, Swept sine excitation, calibration at intermediate frequencies
9950AnM	Accredited calibration: n-axis accelerometers, Swept sine excitation, calibration at intermediate frequencies, calibration certificate conforms to ISO 17025
9953AnL	Recalibration: n-axis accelerometers, Swept sine excitation, calibration at low frequencies
9950AnL	Accredited calibration: n-axis accelerometers, Swept sine exciation, calibration at low frequencies, calibration certificate conforms to ISO 17025
9953AnX	Recalibration: n-axis accelerometers, shock calibration

2. **Flow Sensor/Switch:**

RS

Search by keyword, manufacturer part no. or RS part no.　　Log In | Register

Branch Network　Solutions　Help

0 　£0.00

All Products　　Our Brands　　New Products　　My Account　　Services

Home > Automation & Control Gear > Fluid Control Systems > Flow Sensors, Switches & Indicators

RS Pro Acetal Copolymer Liquid Sensor/Switch without Indicator, 0.25 → 6.5 L/min, 4.5 → 16 V dc

RS Stock No. 257-149
Brand RS Pro

124 in stock for FREE next working day delivery

£26.21
Price Each

Units	Per unit
1 +	£26.21

Quantity 1 　　Units

Add to basket

Check stock levels　　Add to a parts list

Technical Reference

RoHS Status: Not Applicable

Datasheet

Statement of conformity

Product Details

Liquid Flow Sensors

Two flow transducers manufactured in acetal copolymer with brass compression fittings at both ends to fit 15mm diameter pipe connections.

- Provides a pulsed output proportional to flow rate
- LED and photodetector are separated by a turbine mounted on sapphire bearings
- LED requires an external current limiting resistor (dependent on supply voltage)
- Suitable for use with mains and heating system waters etc.
- Rise/fall times 80/8ns
- Output voltage 200mV (low), V_{CC} (high)
- Diode: Forward current 10mA, Power dissipation 100mW

Note

Not suitable for use with strong mineral acids/solutions, strong or searching solvents.
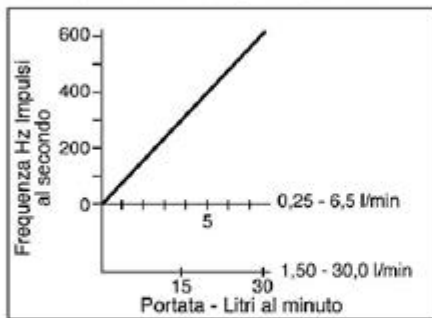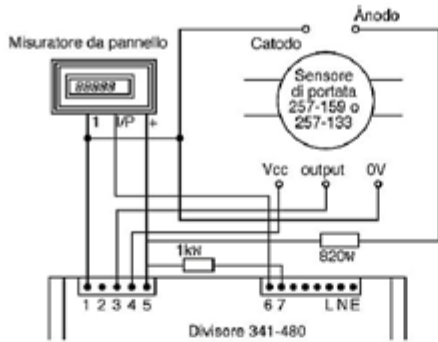
Inline Flow Transducers

☐ Add product to Compare

Specifications

Not what you're looking for? Select the attributes you require, then click the button below

☐	Media Monitored	Liquid
☑	Device Type	Sensor/Switch without Indicator
☐	Minimum Flow Rate	0.25 L/min
☐	Maximum Flow Rate	6.5 L/min
☐	Supply Voltage	4.5 → 16 V dc
☐	Pipe Diameter Range	15 mm
☐	Maximum Pressure	20bar
☐	Material	Acetal Copolymer
☐	Minimum Operating Temperature	-40°C
☐	Maximum Operating Temperature	+70°C
☐	Current Rating	10 mA
☐	Select all	

Find alternative products

Customer reviews

Add a review - Log In

Similar Products

View Similar Products

Alternative for RS Pro Acetal Copolymer Liquid Sensor/Switch without Indicator, 0.25 → 6.5 L/min, 4.5 → 16 V dc

RS Pro Liquid Sensor/Switch
without Indicator, 0.5 → 15
L/min, 4.5 → 24 V dc
£35.14

Compare All Alternatives

3. Pressure Transducer:

PRESSURE
Product Data Sheet

HPS-A Series Voltage Output Pressure Transducer

Three wire, amplified voltage output transducer offering superb chemical and corrosion resistance. Gauge or Absolute pressure is detected using a four active arm strain gauge bridge sensor, fused to a high-purity ceramic diaphragm. Available in three classes of accuracy and stability specified below, with ranges from 100mbar to 600 bar or scaled to customer requirements.

- Stainless Steel housing
- Rugged construction
- Excellent linearity
- Excellent long term stability
- Wide temperature range

CLASS A
HIGH SPECIFICATION TRANSDUCER

Output Span	4V ±0.5%
Output Zero	1V ±0.5% of span
Non Linearity, Hysteresis & Repeatability (NLH)	±0.1% of span (best fit straight line)
Compensated Temp Range	-20°C to 125°C
Operating Temp Range	-20°C to 125°C
Thermal Zero Shift	0 to 100°C, ±0.01% of span / °C <0°C & >100°C, ±0.015% of span / °C
Thermal Span Shift	±0.015% reading/ °C typical
Long Term Stability	0.1% / 12 months typical
Power Supply	10 to 32Vdc

CLASS B
INDUSTRIAL TRANSDUCER

Output Span	4V ±1%
Output Zero	1V ±1% of span
Non Linearity, Hysteresis & Repeatability (NLH)	±0.15% of span (best fit straight line)
Compensated Temp Range	0°C to 100°C
Operating Temp Range	-20°C to 125°C
Thermal Zero Shift	±0.015% of span / °C
Thermal Span Shift	±0.015% reading / °C typical
Long Term Stability	0.1% / 12 months typical
Power Supply	10 to 32Vdc

CLASS C
GENERAL PURPOSE/OEM TRANSDUCER

Output Span	4V ±1%
Output Zero	1V ±1% of span
Non Linearity, Hysteresis & Repeatability (NLH)	±0.25% of span (best fit straight line)
Compensated Temp Range	0°C to 80°C
Operating Temp Range	-20°C to 125°C
Thermal Zero Shift	±0.04% of span / °C
Thermal Span Shift	±0.015% reading/ °C typical
Long Term Stability	0.1% / 12 months typical
Power Supply	10 to 32Vdc

OPTIONS

Pressure Connection
1/4"BSP male or female
1/2"BSP male
1/4"NPT male or female
1/2"NPT male
Others available on request

Electrical Connection
IP65 mini plug & socket
IP65 large plug & socket
IP65 cable & ferrule
IP68 glanded cable
Others available on request

Housing Material
316L Stainless Steel
Others available on request

Electrical Output
0 - 10V*, 0 - 5V
Others available on request
* minimum supply: 13V

DIMENSIONS

IP68 GLANDED CABLE

IP65 CABLE & FERRULE

DIN 40050 PLUG & SOCKET

DIN 43650 PLUG & SOCKET

Note: >200 bar, Hexagon 27 A/F and diameter 27

SENSIT pressure transducers are also available with the following outputs:

- Voltage : 0-5V, 0-10V or 1-5V
- Active mV : 0-100mV or 0-200mV
- mA : 4-20mA

MECHANICAL SPECIFICATION

Safe Over-range Pressure	1.5 x rated range
Burst Pressure	3 x rated range minimum
Wetted Materials	Stainless steel, alumina ceramic, Viton (other O ring materials available)

For level or depth measurement, use the **NEW TRIDENT Series of submersible pressure transducers**, or if your application requires something special, contact sales. If we do not already have the solution our OEM design team are ready to help.

Operating & installation instructions

RS TYPE 461 PRESSURE TRANSDUCERS

APPROVALS
PED: ALL RM&C Pressure transducers are designed & manufactured in accordance with 'Sound Engineering Practice' as defined by the Pressure Equipment directive 97/23/EC, article 1, Paragraph 2.1.3. The CE mark on the unit does not relate to the Pressure Equipment Directive
EMC: Type 461 Pressure transducers & transmitters with the CE mark conform with the essential protection requirements of the EMC Directive 89/33/EEC amended by certified type testing to BS EN 61000 6-2 and BS EN 6100 6-3
RoHS: Type 461 Pressure transducers & transmitters with the CE mark conform with the essential requirements of the RoHS Directive 2002/95/CE

GENERAL
Transducers must not be subjected to mechanical impact.
Maximum pressure range being measured must not exceed the transducer pressure range
Pressure media must be compatible with the transducers wetted parts listed below.
Liquid must not be allowed to freeze in the pressure port.
The gasket must be fitted under the electrical connector

WETTED PARTS
96 % alumina; 316L Stainless steel; Fluorocarbon (Viton) O ring

ELECTRICAL INSTALLATION
Conformity with the requirements of the CE mark only applies when connection is made with **RM&C approved cable** (see approved cable section). If a 'Ground Loop' problem is encountered when the body of the unit is grounded by the piping then it is permissible to remove the cable shield from the instrumentation ground.

APPROVED CABLE
RM&C uses cable comprising of 2,3 & 4 core to standard DEF61-12PT4 with an outer jacket of black PVC with an overall diameter approximately 0.17 in or 4.3mm

OPERATION
Having installed the transducers as instructed, they are ready for use. The transducer should not be removed while the system is at pressure. Always ensure, before applying power, that the correct polarity & excitation levels are being applied

mV	Connections	0-5 Volt	Connections	4-20mA	Connections
461-290		461-389		461-294	
461-301	Pin 1 : +ve supply	461-373	Pin 1 : Output	461-335	Pin 1 : -ve supply
461-307	Pin 2 : -ve supply	461-323	Pin 2 : -ve supply	461-351	Pin 2 : N/C
461-256	Pin 3 : +ve Output	461-363	Pin 3 : +ve supply	461-345	Pin 3 :+-ve supply
461-395	Pin 4 : -ve Output	461-288	Pin 4 : N/C	461-357	Pin 4 : Earth
461-385		461-367		461-341	
461-284	Excitation:	461-278	Excitation:	461-262	Excitation:
461-317	10 Volts	461-379	10 - 32 Volts	461-339	10 - 32 Volts
461-329		461-266		461-313	
		461-272		461-250	

MECHANICAL INSTALLATION
Use either a 19mm or 24mm AF wrench on the hexagon provided to a maximum torque of 15Nm. The customer must ensure that the pressure seal is suitable for the application, if in doubt contact RM&C.

LOAD CHARACTERISTICS (4-20mA current output)
The total resistive load in the loop (to include all cable resistance) can be from zero to 50* (supply volts -10) ohms e.g. with a 24Volt supply the permissible load is from zero up to 700 ohms.

WARRANTY
We guarantee this product as designed & manufactured by RM&C to be free from defects in material & workmanship for a period of one year after the date of despatch or otherwise agreed in writing. This warranty shall not apply if the product has been disassembled, tampered with, repaired, modified outside of the factory, subject to misuse, neglect or accident.

MAINTENANCE & REPAIR
Routine periodic inspection of the cable & connector is required to ensure integrity of parts.
The instrument contains no user serviceable parts & cannot be repaired in the field. It must be returned, fully decontaminated, to RM&C:
PERIODIC CALIBRATION
A UKAS calibration is available on this transducer.

S2027 Issue 01

4. Flir A310f Thermal Camera:

FLIR A310 f

Fixed Mount Thermal Imaging Camera for Condition Monitoring and Fire Prevention

FLIR A310 f thermal cameras can be installed almost anywhere to monitor the condition of your critical equipment and other valuable assets. Designed to help safeguard your plant and measure temperature differences, they allow you to see problems before they become costly failures -- preventing downtime and enhancing worker safety.

FLIR A310 f is ideal for various applications that require temperature measurement capabilities including: substation, transformer, waste bunker, and coal pile monitoring.

EXCELLENT IMAGE QUALITY

FLIR A310 f contains an uncooled Vanadium Oxide (VOx) microbolometer detector, producing crisp, 320 x 240 resolution thermal images and making small temperature differences clearly visible. The camera features a built-in lens with motorized focus, the ability to stream video over Ethernet to view live images on a PC, communication and power over Ethernet cable, and can be controlled remotely over the Web and TCP/IP protocol.

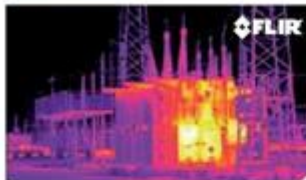### BUILT-IN ANALYSIS AND ALARM FUNCTIONS

FLIR A310 f comes standard with built-in analysis functions like spot, area measurement, and temperature difference. Alarms can be set to go off as function of analysis, internal temperature or digital input. The camera automatically sends analysis results, IR images, and more as an e-mail on schedule or at alarm. Autonomous dispatch of files or e-mails, acting as an FTP- or SMTP-client is possible. Since FLIR A310 f is Ethernet/IP and Modbus TCP compliant, analysis and alarm results can easily be shared to a PLC. Digital inputs/outputs lare available for alarms and control of external equipment. An image masking function allows you to select only the relevant part of the image for your analysis.

DESIGNED FOR USE IN HARSH ENVIRONMENTS

A310 f is an extremely rugged system that meets IP66 requirements, protecting the camera from dust and water.
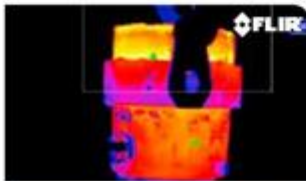
Thermal imaging cameras can detect hot spots on the ladle.

A transformer showing an excessive temperature.

www.flir.com

FLIR | The World's Sixth Sense

Imaging Specifications

System Overview	FLIR A310 f
IR resolution	320 × 240 pixels
Thermal sensitivity/NETD	< 0.05°C @ +30°C (+86°F) / 50 mK
Field of view (FOV)	FLIR A310f 15°: 15° × 11.25° FLIR A310f 25°: 25° × 18.8° FLIR A310f 45°: 45° × 33.8° FLIR A310f 6°: 6° × 4.5° FLIR A310f 90°: 90° × 73°
Minimum focus distance	FLIR A310f 15°: 1.2 m (3.93 ft.) FLIR A310f 25°: 0.4 m (1.31 ft.) FLIR A310f 45°: 0.20 m (0.66 ft.) FLIR A310f 6°: 6° × 4.5° FLIR A310f 90°: 20 mm (0.79 in.)
Focal length	FLIR A310f 15°: 30.38 mm (1.2 in.) FLIR A310f 25°: 18 mm (0.7 in.) FLIR A310f 45°: 9.66 mm (0.38 in.) FLIR A310f 6°: 76 mm (3.0 in.) FLIR A310f 90°: 4 mm (0.157 in.)
Spatial resolution (IFOV)	FLIR A310f 15°: 0.82 mrad FLIR A310f 25°: 1.36 mrad FLIR A310f 45°: 2.45 mrad FLIR A310f 6°: 0.33 mrad FLIR A310f 90°: 6.3 mrad
Lens identification	Automatic
F-number	1.3

Imaging and optical data	
Image frequency	30 Hz
Focus	Automatic or manual (built in motor)
Zoom	1–8× continuous, digital, interpolating zooming on images

Detector data	
Detector type	Focal Plane Array (FPA), uncooled microbolometer
Spectral range	7.5–13 µm
Detector pitch	25 µm
Detector time constant	Typical 12 ms

Measurement	
Object temperature range	−20 to +120°C (−4 to +248°F) 0 to +350°C (+32 to +662°F)
Accuracy	±4°C (±7.2°F) or ±4% of reading

Measurement analysis	
Spotmeter	10
Area	10 boxes with max./min./average/position
Isotherm	1 with above/below/interval
Measurement option	Measurement Mask / Filter Schedule response: File sending (ftp), email (SMTP)
Difference temperature	Delta temperature between measurement functions or reference temperature
Reference temperature	Manually set or captured from any measurement function
Atmospheric transmission correction	Automatic, based on inputs for distance, atmospheric temperature and relative humidity
Optics transmission correction	Automatic, based on signals from internal sensors
Emissivity correction	Variable from 0.01 to 1.0
Reflected apparent temperature correction	Automatic, based on input of reflected temperature
External optics/windows correction	Automatic, based on input of optics/window transmission and temperature
Measurement corrections	Global and individual object parameters

Alarm	
Alarm functions	6 automatic alarms on any selected measurement function, Digital In, Camera temperature, timer
Alarm output	Digital Out, log, store image, file sending (ftp), email (SMTP), notification

Ethernet	
Ethernet	Control, result and image
Ethernet, type	100 Mbps
Ethernet, standard	IEEE 802.3
Ethernet, connector type	RJ-45
Ethernet, communication	TCP/IP socket-based FLIR proprietary
Ethernet, video streaming	MPEG-4, ISO/IEC 14496-1 MPEG-4 ASP@L5
Ethernet, image streaming	16-bit 320 × 240 pixels @ 7-8 Hz- Radiometric
Ethernet, power	Power over Ethernet, PoE IEEE 802.3af class 0
Ethernet, protocols	Ethernet/IP, Modbus TCP, TCP, UDP, SNTP, RTSP, RTP, HTTP, ICMP, IGMP, ftp, SMTP, SMB (CIFS), DHCP, MDNS (Bonjour), uPnP

Set-up	
Color palettes	Color palettes (BW, BW inv, Icon, Rain)
Set-up commands	Date/time, Temperature°C/°F

Storage of images	
Storage media	Built-in memory for image storage
File formats	Standard JPEG, 16-bit measurement data included

Digital input/output	
Digital input, purpose	Image tag (start/stop/general), Input ext. device (programmatically read)
Digital input	2 opto-isolated, 10–30 VDC
Digital output, purpose	As function of ALARM, Output to ext. device (programmatically set)
Digital output	2 opto-isolated, 10–30 VDC, max 100 mA
Digital I/O, isolation voltage	500 VRMS
Digital I/O, supply voltage	12/24 VDC, max 200 mA
Digital I/O, connector type	6-pole jackable screw terminal

Power system	
External power operation	The camera operates on 12/24 VDC, 9 W max. (allowed range: 10-30 VDC) and heaters on 24 VDC, 25 W max. In total: 34 W.
External power, connector type	2-pole jackable screw terminal
Voltage	Allowed range 10–30 VDC

Environmental data	
Operating temperature range	−25°C to +50°C (−13°F to +122°F)
Storage temperature range	−40°C to +70°C (−40°F to +158°F)
Humidity (operating and storage)	IEC 60068-2-30/24 h 95% relative humidity +25°C to +40°C (+77°F to +104°F)
EMC	• EN 61000-6-2 (Immunity) • EN 61000-6-3 (Emission) • FCC 47 CFR Part 15 Class B (Emission)
Encapsulation	IP 66 (IEC 60529)
Bump	5 g, 11 ms (IEC 60068-2-27)
Vibration	2 g (IEC 60068-2-6)

Physical data	
Weight	5 kg (11.0 lb.)
Size (L × W × H)	460 × 140 × 159 mm (18.1 × 5.5 × 6.3 in.)
Base mounting	TBA
Housing material	Aluminum

System features	
External power operation (heater)	24 VDC, 25 W max.
External power, connector type (heater)	2-pole jackable screw terminal
Voltage (heater)	Allowed range 21-30 VDC
Automatic heaters	Clears window from ice

Shipping information	
List of contents	Cardboard box, Infrared camera with lens and environmental, housing, FLIR Sensors Manager download card, FLIR Tools & Utilities CD-ROM, Lens cap, Printed documentation, Small accessories kit, User documentation CD-ROM

5. IRISYS IRI 1011 Thermal Infrared Camera:

Low cost Thermal Infrared Imager - IR Irisys IRI 1011 IR camera

What you get included in the price from PTS:

1. IRI 1011 IRISYS universal infrared thermal imager
2. Software for Pocket PC & PC
3. 2m RS232 connection cable (imager to PC)
4. AC Power Supply
5. Instruction manual
6. Pocket PC HP iPAQ RX1950 with 64MB ROM (Option 2 and 3 only)
7. Lanyard and hand strap
8. Foam lined protective carry case

Other popular items ordered with this Irisys IRI 1011 Thermal Imaging Camera kit:

Ultrasonic Distance Meter	Light Meter TM201	4 in 1 Environment meter	Gaussmeter C.A. 40	
£ 95 + VAT	£ 59 + VAT	£ 89.95 + VAT	£ 175 + VAT	▲ TOP

* Prices excludes delivery carriage @ £10 and VAT @ 20%

http://www.pat-training.co.uk/irisys_iri_1011_thermal.htm

6. M Series Multifunction DAQ for USB:

Last Revised: 2014-11-06 07:14:36.0

M Series Multifunction DAQ for USB - 16-Bit, 250 kS/s, up to 80 Analog Inputs

- Up to 80 analog inputs at 16 bits, 250 kS/s
- Up to 4 analog outputs at 16 bits, 833 kS/s
- Up to 48 TTL/CMOS digital I/O lines (up to 32 hardware-timed at up to 1 MHz)
- Two 32-bit, 80 MHz counter/timers

- Digital triggering supported; power supply included
  - NI-PGIA 2 and NI-MCal calibration technology for improved measurement accuracy
- NI signal streaming for 4 high-speed data streams on USB
- NI-DAQmx driver software and LabVIEW SignalExpress LE included

Overview

With recent bandwidth improvements and new innovations from National Instruments, USB has evolved into a core bus of choice for measurement and automation applications. NI M Series devices for USB deliver high-performance data acquisition in an easy-to-use and portable form factor through USB ports on laptop computers and other portable computing platforms. NI created NI signal streaming, an innovative patent-pending technology that enables sustained bidirectional high-speed data streams on USB. The new technology, combined with advanced external synchronization, helps engineers and scientists achieve high-performance applications on USB.

M Series multifunction data acquisition (DAQ) modules for USB are optimized for superior accuracy at fast sampling rates. They provide an onboard NI-PGIA 2 amplifier designed for fast settling times at high scanning rates, ensuring 16-bit accuracy even when measuring all available channels at maximum speed. All externally powered M Series devices have a minimum of 16 analog inputs, 24 digital I/O lines, digital triggering, and two counter/timers. USB M Series devices are ideal for test, control, and design applications including portable data logging, field monitoring, embedded OEM, in-vehicle data acquisition, and academic. NI USB-622x M Series devices have a one-year calibration interval.

Calibration

NI measurement hardware is calibrated to ensure measurement accuracy and verify that the device meets its published specifications. To ensure the ongoing accuracy of your measurement hardware, NI offers basic or detailed recalibration service that provides ongoing ISO 9001 audit compliance and confidence in your measurements. To learn more about NI calibration services or to locate a qualified service center near you, contact your local sales office or visit ni.com/calibration.

Detailed Specifications

Specifications listed below are typical at 25 °C unless otherwise noted. Refer to the *M Series User Manual* for more information about NI 622x devices.

Analog Input	
Number of channels	
NI 6220/6221	8 differential or 16 single ended
NI 6224/6229	16 differential or 32 single ended
NI 6225	40 differential or 80 single ended
ADC resolution	16 bits
DNL	No missing codes guaranteed

INL	Refer to the *AI Absolute Accuracy Table*
Sampling rate	
Maximum	250 kS/s single channel, 250 kS/s multi-channel (aggregate)
Minimum	No minimum
Timing accuracy	50 ppm of sample rate
Timing resolution	50 ns
Input coupling	DC
Input range	±10 V, ±5 V, ±1 V, ±0.2 V
Maximum working voltage for analog inputs (signal + common mode)	±11 V of AI GND
CMRR (DC to 60 Hz)	92 dB
Input impedance	
Device on	
AI+ to AI GND	>10 GΩ in parallel with 100 pF
AI- to AI GND	>10 GΩ in parallel with 100 pF
Device off	
AI+ to AI GND	820 Ω
AI- to AI GND	820 Ω
Input bias current	±100 pA
Crosstalk (at 100 kHz)	
Adjacent channels	-75 dB
Non-adjacent channels	-90 dB[1]
Small signal bandwidth (-3 dB)	700 kHz
Input FIFO size	4,095 samples
Scan list memory	4,095 entries
Data transfers	
PCI/PXI devices	DMA (scatter-gather), interrupts, programmed I/O
USB devices	USB Signal Stream, programmed I/O
Overvoltage protection (AI <0..79>, AI SENSE, AI SENSE 2)	
Device on	±25 V for up to two AI pins
Device off	±15 V for up to two AI pins
Input current during overvoltage condition	±20 mA max/AI pin

[1] For USB-6225 devices, channel AI <0..15> crosstalk to channel AI <64..79> is -71 dB; applies to channels with 64-channel separation, for example, AI (x) and AI (x + 64).

Settling Time for Multichannel Measurements

Accuracy, full scale step, all ranges	
±90 ppm of step (±6 LSB)	4 µs convert interval
±30 ppm of step (±2 LSB)	5 µs convert interval

±15 ppm of step (±1 LSB) | 7 µs convert interval

Analog Output

Number of channels	
NI 6220/6224	0
NI 6221/6225	2
NI 6229	4
DAC resolution	16 bits
DNL	±1 LSB
Monotonicity	16 bit guaranteed
Maximum update rate	
1 channel	833 kS/s
2 channels	740 kS/s per channel
3 channels	666 kS/s per channel
4 channels	625 kS/s per channel
Timing accuracy	50 ppm of sample rate
Timing resolution	50 ns
Output range	±10 V
Output coupling	DC
Output impedance	0.2 Ω
Output current drive	±5 mA
Overdrive protection	±25 V
Overdrive current	10 mA
Power-on state	±20 mV1
Power-on glitch	400 mV for 200 ms
Output FIFO size	8,191 samples shared among channels used
Data transfers	
PCI/PXI devices	DMA (scatter-gather), interrupts, programmed I/O
USB devices	USB Signal Stream, programmed I/O

1. Labjack U12:

A. LabJack U12 Specifications V1.04 (11/5/2002)

Parameter	Conditions	Min	Typical	Max	Units
General					
USB Cable Length				3	meters
User Connection(s) Length	CE compliance			3	meters
Supply Current (1)			20		mA
Operating Temperature		-40		85	°C
Clock Error	~ 25 °C			±30	ppm
	0 to 70 °C			±50	ppm
	-40 to 85 °C			±100	ppm
+5 Volt Power Supply (+5V)					
Voltage (Vs) (2)	Self-Powered	4.5		5.25	volts
	Bus-Powered	4.1		5.25	volts
Output Current (2) (3)	Self-Powered	450		500	mA
	Bus-Powered	50		100	mA
Analog Inputs (AI0 - AI7)					
Input Range For Linear Operation	Alx to GND, SE	-10		10	volts
	Aix to GND, Diff.	-10		20	volts
Maximum Input Range	Alx to GND	-40		40	volts
Input Current (4)	Vin = +10 volts		70.1		μA
	Vin = 0 volts		-11.7		μA
	Vin = -10 volts		-93.5		μA
Resolution (No Missing Codes)	C/R and Stream		12		bits
	Burst Diff. (5)		12		bits
	Burst SE (5)		11		bits
Offset	G = 1 to 20		±1 * G		bits
Absolute Accuracy	SE		±1		% FS
	Diff.		±0.2		% FS
Noise	C/R and Stream		±1		bits
Integral Linearity Error			±1		bits
Differential Linearity Error			±0.5		bits
Repeatability			±1		bits
CAL Accuracy	CAL = 2.5 volts		±0.05	±0.25	%
CAL Current	Source			5	mA
	Sink	20	200		μA
Trigger Latency	Burst	25		50	μs
Trigger Pulse Width	Burst	40			μs
Analog Outputs (AO0 & AO1)					
Maximum Voltage (6)	No Load		Vs		volts
	At 1 mA		0.99 * Vs		volts
	At 5 mA		0.98 * Vs		volts
Output Current	Each AO			30	mA

Parameter	Conditions	Min	Typical	Max	Units
IO					
Low Level Input Voltage				0.8	volts
High Level Input Voltage		3		15	volts
Input Leakage Current			±1		μA
Output Short-Circuit Current (7)	Output High		3.3		mA
Output Voltage (7)	No Load	Vs - 0.4	Vs		volts
	At 1 mA		Vs - 1.5		volts
D					
Low Level Input Voltage (8)	D0 - D12			0.8	volts
	D13 - D15			1	volts
High Level Input Voltage (8)	D0 - D12	2		Vs + 0.3	volts
	D13 - D15	4		Vs + 0.3	volts
Input Leakage Current			±1		μA
Output Current (8)	Per Line			25	mA
	Total D0 - D15			200	mA
Output Low Voltage				0.6	volts
Output High Voltage		Vs - 0.7			volts
CNT					
Low Voltage (9)		GND		1	volts
High Voltage (9)		4		15	volts
Schmitt Trigger Hysteresis			20-100		mV
Input Leakage Current			±1		μA
Minimum High Time				500	ns
Minimum Low Time				500	ns
Maximum Input Frequency		1			MHz

(1) Current drawn by the LabJack through the USB. The status LED is responsible for 4-5 mA of this current.

(2) Self-powered would apply to USB hubs with a power supply, all known desktop computer USB hosts, and some notebook computer USB hosts. Bus-powered would apply to USB hubs without a power supply and some notebook computer USB hosts.

(3) This is the total current that can be sourced by +5V, analog outputs, and digital outputs.

(4) The input current at each analog input is a function of the voltage at that input (Vin) with respect to ground and can be calculated as: $(8.181 * Vin - 11.67)$ μA.

(5) Single-ended burst mode only returns even binary codes, and thus has a net resolution of 11 bits. In addition, extra noise in burst mode can reduce the effective resolution.

(6) Maximum analog output voltage is equal to the supply voltage at no load.

(7) The IO lines each have a 1500 ohm series resistor.

(8) These lines have no series resistor. It is up to the user to make sure the maximum voltages and currents are not exceeded.

(9) CNT is a Schmitt Trigger input.

Appendix I: Emissivity Table

Electronic Temperature Instruments

emissivity table

The accuracy of the following figures is almost impossible to guarantee as the emissivity of a surface will not only alter with regard to texture and colour but also with its actual temperature at the time of measurement. We would recommend, in the first instance, comparing measurements found, with an accurate surface probe or wire probe, and then the infrared thermometer can be adjusted to match the correct emissivity and used for subsequent measurements.

No responsibility can be assumed by ETI Ltd for the accuracy or otherwise of the following figures.

Material	Emissivity
Aluminium: anodised	0.77
Aluminium: polished	0.05
Asbestos: board	0.96
Asbestos: fabric	0.78
Asbestos: paper	0.93
Asbestos: slate	0.96
Brass: highly polished	0.03
Brass: oxidized	0.61
Brick: common	.81-.86
Brick: common, red	0.90
Brick: facing, red	0.92
Brick: fireclay	0.75
Brick: masonry	0.94
Brick: red	0.90

Carbon: candle soot	0.95
Carbon: graphite, filed surface	0.98
Carbon: purified	0.80
Cement:	0.54
Charcoal: powder	0.96
Chipboard: untreated	0.90
Chromium: polished	0.10
Clay: fired	0.91
Concrete	0.92
Concrete: dry	0.95
Concrete: rough	.92-.97
Copper: polished	0.05
Copper: oxidized	0.65
Enamel: lacquer	0.90
Fabric: Hessian, green	0.88
Fabric: Hessian, uncoloured	0.87
Fibreglass	0.75
Fibre board: porous, untreated	0.85
Fibre board: hard, untreated	0.85
Filler: white	0.88

Redwood: unwrought, untreated	0.84
Rubber	0.95
Rubber: stopper, black	0.97
Sand	0.90
Skin, human	0.98
Snow	0.80
Soil: dry	0.92
Soil: frozen	0.93
Soil: saturated with water	0.95
Stainless Steel	0.59
Stainless Plate	0.34
Steel: galvanized	0.28
Steel: rolled freshly	0.24
Styrofoam: insulation	0.60
Tape: electrical, insulating, black	0.97
Tape: masking	0.92
Tile: floor, asbestos	0.94
Tile: glazed	0.94
Tin: burnished	0.05
Tin: commercial tin-plated sheet iron	0.06